Institut für Hydrologie
Albert-Ludwigs-Universität Freiburg i. Br.

Markus Konz

Development of a glacier module for the process-oriented catchment model TAC^d and application to the Langtang Khola catchment, Nepal

Diplomarbeit unter Leitung von Prof. Dr. S. Demuth

Freiburg i. Br., Juli 2005

Institut für Hydrologie
Albert-Ludwigs-Universität Freiburg i. Br.

Markus Konz

Development of a glacier module for the process-oriented catchment model TAC^{d} and application to the Langtang Khola catchment, Nepal

Referent: Prof. Dr. S. Demuth
Koreferent: Prof. Dr. S. Uhlenbrook

Diplomarbeit unter Leitung von Prof. Dr. S. Demuth

Freiburg i. Br., Juli 2005

Acknowledgements

Numerous people have contributed to the successful completion of this thesis in different ways. I would like to express my gratitude to each of them.

I would like to thank my lector Prof. Dr. Siegfried Demuth for supporting this interesting topic.

Prof. Dr. Stefan Uhlenbrook took over the co-lecture, encouraged me to undertake this thesis and provided scientific advice.

Sincere thanks goes to Dr. Ludwig Braun who accompanied my studies since 2001 when I worked as “Gletscherknecht” on the Vernagtferner, Austria. He provided continuous support during all stages of this work. His constructive and challenging comments in numerous discussions during my stay in Munich and via e-mail are very much appreciated. Thank you for everything!

Dr. Arun Shrestha and his colleagues were cooperative partners in Nepal who provided hydrometeorological data from the Langtang Khola catchment.

My thanks are given also extended to Dr. Markus Weber and Dr. Heidi Escher-Vetter for numerous discussions on meteorological questions and the mathematical aspects of hydrological modeling.

Dipl. Hyd. Laurin Wissmeier, Dipl. Hyd. Andreas Steinbrich, Sebastian Wrede and Dipl. Ing. Volker Abraham gave great computer support. Thank you very much for your patience.

Special thanks go to Susan Braun-Clarke for proofreading this thesis.

I wish to express my thanks to my parents. They encouraged my interest in natural phenomena and enabled me to study such a fascinating subject. They further supported all my interests, whether they were related to my studies or to my spare-time activities.

Last but not least, a thank you to Nadine, for sharing all my joys and frustration.

Markus Konz

Contents

List of figures

List of tables

Notations

*_box	Water content of storage (general)	(mm)
*_H	Limit of storage capacity (general)	(mm)
*_K	Storage coefficient (general)	(1/time step)
*_P	Percolation capacity (general)	(mm/time step)
α	Surface albedo	(-)
ΔH_l	Change in snowpack latent heat content (i.e. snowmelt or sublimation)	(W/m²)
ΔH_s	Change in snowpack sensible heat content (i.e. snow temperature)	(W/m²)
ΔS	Changes in storages, here primarily in form of snow accumulation which feeds the glaciers	(mm/a)
Δz	Altitude difference	(m)
a	year	
a(t)	Ablation rate over time t	(m/day)
A,B,C	Coefficients	(-)
a.s.l.	Above sea level	
a_a	Annual ablation	(m)
ActET	Actual evaporation	(mm/time step)
a_i	Ablation rate of bare ice	(mm/day)
AltDiff	Vertical distance between target cell and climatic station	(m)
a_m	Ablation rate under the debris layer	(mm/day)
b_a	Specific annual mass balance at a given point	(m)
B_a	Total annual mass balance of the glacier	(m³)
Balance	Internal water balance of simulation period	(mm)
BETA	Empirical parameter	(-)
c(i)	Weight	(-)
c(t)	Accumulation rate over time t	(m/day)
c_a	Annual accumulation	(m)
Cfmax	Degree-day factor	(mm/°C day)
CFR	Coefficient of refreezing	(-)
CounterDay	Day (starting from 1st October = day 272)	
CPERC	Percolation capacity into lower zone	(mm/day)
CWH	Water holding capacity of snow	(-)
DAV	German Alpine Club	
DEM	Digital elevation model	
DHM	Department of Hydrology and Meteorology	
DistToClim	Horizontal distance between target cell and climatic station	(km)
dt	Time derivative	
du	Time derivative	
EML	Environmental modelling language	
ETGrad	Vertical evapotranspiration gradient	((%/100m)/100)

ETH	Eidgenössische Technische Hochschule	
ETmax	Maximum of potential evapotranspiration	(mm/day)
FC	Maximum soil moisture storage (field capacity)	(mm)
$F_{r,m}$	Mean ratio of amount of precipitation between station r and SGHU station of the month m	(-)
GIS	Geographic information system	
GlacierLS_box	Water content of glacier storage	(mm)
GlacierLS_H	Limit of glacier storage	(mm)
GlacierLS_K	Storage coefficient of glacier storage	(1/time step)
GlacierQ_LS	Outflow of glacier storage	(mm/time step)
GLOF	Glacier lake outburst flood	
G_{melt}	Glaciermelt	(mm/a)
grad	Vertical temperature gradient	(K/100m)
GTZ	German Agency for Technical Cooperation	
h	Moraine-cover thickness	(cm)
h	Gauge height	(m)
h	hour	
HQ	Highest flow in observation period	(m^3/s)
HRU	Hydrological response unit	
i	Time step	
ICIMOD	International Center for Integrated Mountain Development	
$Input_{i,j}$	Input of water fluxes at actual time step	(mm)
InSoil	Output from snow and glacier routine	(mm/time step)
j	Raster cell	(-)
k	Number of grid cells	(-)
k	Storage coefficient	(1/time step)
K	Kelvin	
l	Day of maximum potential evapotranspiration	
ldd	Local drainage direction	
$\overline{\log(Q_{obs})}$	Mean logarithmic observed runoff for the whole observation period	(mm/time step)
LP	Reduction parameter of field capacity	(-)
LS_box	Water content of lower storage	(mm)
LS_K	Storage coefficient of lower storage	(1/time step)
Q_LS	Outflow of lower storage	(mm/time step)
m	Month	
MassBalance	Annual glacier mass balance	(mm)
MaxBas	Empirical parameter	(-)
MaxDay	Maximum days of the year (365 or 366)	
MaxShade	Maximum potential sunshine duration	(h/day)
MeltWaterGlacierClean	Meltwater of the debris-free glaciers	(mm/time step)
MeltWaterGlacierDebris	Meltwater of the debris-covered glaciers	(mm/time step)
MeltWaterGlacierforBalance	Annual meltwater of glaciers	(mm)
MeltWaterSnow	Amount of snow melt	(mm/time step)

MeltWaterSnowPack	Meltwater of the snowpack	(mm/time step)
MeltWaterSnowpackforBalance	Annual meltwater of snow	(mm)
MHQ	Mean high flow	(m^3/s)
MinShade	Minimum potential sunshine duration	(h/day)
MNQ	Mean low flow	(m^3/s)
MQ	Mean flow (arithmetic mean)	(m^3/s)
N	Number of reference stations	
n	Duration of simulation period	(-)
NQ	Lowest flow in observation period	(m^3/s)
nRGType	Runoff generation type units	
$Output_{i,j}$	Output of water fluxes at actual time step	(mm)
Overflow	Overflow of the storage	(mm/time step)
P	Precipitation	(mm)
P_b	Basin precipitation	(mm/a)
PCF	Precipitation correction factor for rain	(-)
PGrad	Vertical precipitation gradient	((%/100m)/100)
PHorizGrad	Horizontal precipitation gradient	((%/1000m)/100)
PotET	Potential evaporation	(mm/time step)
PotETAltitude	Altitude-corrected potential evapotranspiration	(mm/time step)
POTRAD 5	Potential Radiation Equator Model	
P_r	Measured precipitation at reference station r	(mm/day)
Prec	Corrected solid precipitation	(mm/time step)
PrecAltitude	Altitude-corrected precipitation	(mm/time step)
PrecCor	Corrected liquid precipitation	(mm/time step)
PrecHorizontal	Horizontally corrected precipitation	(mm/time step)
PrecStation	Measured precipitation	(mm/time step)
P_{SGHU}	Precipitation at SGHU station	(mm/day)
Q	Discharge	(m^3/s)
Q_*	Runoff of storage (general)	(mm/time step)
Q_{adv}	Heat flux advected by precipitation across the snowpack surface	(W/m^2)
$Q_{beforerouting}$	Simulated discharge before routing	(m^3/s)
Q_{gnd}	Ground heat flux across the snowpack base	(W/m^2)
$Q_{i,obs}$	Observed runoff at time step i	(mm/time step)
$Q_{i,sim}$	Simulated runoff at time step i	(mm/time step)
Q_{il}	Incoming long-wave radiation	(W/m^2)
Q_{is}	Incoming short-wave radiation	(W/m^2)
Q_{lat}	Latent heat flux across the snowpack surface	(W/m^2)
$\overline{Q_{obs}}$	Mean observed runoff for the whole observation period	(mm/time step)
Q_{ol}	Outgoing long-wave radiation	(W/m^2)
Q_{rad}	Net all-wave radiation flux across the snowpack surface	(W/m^2)
Q_{sen}	Sensible heat flux across the snowpack surface	(W/m^2)
$\overline{Q_{sim}}$	Mean simulated discharge for the whole	(mm/time step)

	observation period	
$Q_{sim}(t)$	Simulated discharge	(m^3/s)
r	Reference station	
R^2	Coefficient of determination	(-)
R_{eff}	Model efficiency	(-)
Refreeze	Refreezing water in snowpack	(mm/time step)
Rexp	Correction factor for cells with maximum potential sunshine duration	(-)
RexpMap	Correction factor for degree-day method	(-)
R_{logeff}	Logarithmic model efficiency	
Rmult	Multiplicative factor to account for accelerated melt over ice as compared to snow	(-)
Rmultd	Reduction factor of glaciermelt over debris-covered parts of the glacier	(-)
s_{ab}	Ablation area of the glacier	(m^2)
s_{ac}	Accumulation area of the glacier	(m^2)
SFCF	Snowfall correction factor	(-)
s_g	Area of the glacier	(m^2)
SGHU	Snow and Glacier Hydrology Unit	(m)
Shade	Potential sunshine durations	(h/day)
SMHI	Swedish Meteorological and Hydrological Institute	
SnowPack	Snowpack storage	(mm snow water equivalent)
SnowpackforBalance	Annual snow accumulation	(mm)
SoilMoisture	Soil moisture storage	(mm)
$Storages_{1,j}$	Sum of storage levels at first time step of simulation period	(mm)
$Storages_{i,j}$	Sum of storage levels of all storages at actual time step	(mm)
t	Time step	(time step)
T	Temperature	(°C)
t_0	First day of the measurement year (usually 1st October)	
t_1	Last of measurement year (usually 30th September the following year)	
TAC^d	Tracer-aided catchment model, distributed	
Temp	Altitude-corrected air temperature	(°C)
TempStation	Measured air temperature at climatic station	(°C)
TGrad	Vertical temperature gradient	(°C/100m)
TIN	Triangular irregular network	
ToRunoffGeneration	Infiltration into runoff generation routine as fraction of the actual soil moisture	(mm/time step)
T_{Ref}	Temperature at reference station	(°C)
T_{SGHU}	Temperature at SGHU station	(°C)
TT	Threshold value of temperature for	(°C)

	snowfall also general temperature correction	
u	Time step	(day)
UNEP	United Nations Environmental Program	
US_box	Water content of upper storage	(mm)
US_H	Limit of upper storage	(mm)
US_K	Storage coefficient of upper storage	(1/time step)
US_P	Percolation capacity	(mm/time step)
Q_US	Outflow of upper storage	(mm/time step)
V	Storage level	(mm)
V(t)	Storage level at time t	(mm)
V_0	Storage level at time t = 0	(mm)
ValleyLS_box	Water content of valley storage	(mm)
ValleyLS_H	Limit of valley storage	(mm)
ValleyLS_K	Storage coefficient of valley storage	(1/time step)
ValleyQ_LS	Outflow of valley storage	(mm/time step)
VE	Volume error	(mm/a)
WaterContent	Water content of snow cover	(mm)
$W_{i,m}$	Weighting of station i according to the joint occurrence probability of precipitation at target station and reference stations for the month m	(-)

Summary

The objective of this work was the development of a glacier routine for the distributed process-oriented catchment model TAC^d (Tracer Added Catchment Model, distributed) and the modification of the model routines for the application to the remote, highly glacierized Langtang Khola catchment in the Nepal Himalayas. In addition, statistical methods to compute complete time series of climatic input data are applied.

The distributed process-oriented catchment model TAC^d was developed in the Brugga catchment (Black Forest, Germany) and has a modular structure. Experimental results were the basis for the development of the runoff generation routine which is the core piece of the model. Laterally and vertically connected simple linear storages simulate the runoff generation processes of the hydrological response units (HRUs). Sophisticated approaches are used in the model to calculate the sections of the land phase hydrological circle, for instance, potential evapotranspiration based on the data-intensive method of Penman-Monteith. For regionalization of climatic input data the inverse distance weighting method is implemented which requires a dense observation network.

The 360 km² Langtang Khola catchment is located in the Nepalese Himalayas with an altitude range from 3600 to 7234 m a.s.l. About 46 % of the catchment area is covered by glaciers. There is one climatological station at 3920 m a.s.l. where air temperature and precipitation is measured. Climatic and hydrologic data are available in daily resolution.

Fundamental modifications were necessary for the application of TAC^d to the Langtang Khola catchment. The modification and development work was carried out using the dynamic GIS PCRaster. This programming environment achieves a high-level linkage of the spatial data base with the dynamic modeling which is a prerequisite for effective distributed hydrological modeling.

Vertical gradients for regionalization of air temperature and potential evapotranspiration are implemented in conjunctions with an additional horizontal gradient for regionalization of precipitation. Evapotranspiration plays a minor role in the annual water balance of a high alpine catchment and is calculated using a simple sinusoidal function with a fixed calibrated maximum on 1st August and the minimum of 0.0 mm/day on 1st February.

Ice- and snowmelt are calculated with the classical temperature-index method using the degree-day factor as proportionality coefficient that determines melt rates on the basis of air temperature. Incoming short-wave radiation expressed as potential sunshine duration per day per raster cell is used to distribute the meltwater calculation. This regionalization approach enables a temporal and spatial distributed meltwater calculation based on topographic and astronomic information. Differences in melt conditions between ice and snow as well as between debris-free and debris-covered glaciers are considered based on empirical factors.

The delineation of hydrological response units is achieved using topographic and physiographic information. Four units are determined for conceptualization of the runoff generation processes. The glacier and non-glacier areas are the dominating units whose runoff generation processes are simulated on the basis of two vertically connected simple linear storages. Two other units are delineated and are considered to store water during the monsoon season for the maintenance of winter runoff. These units are the glacier tongues with an inclination of less than 3° and debris cover, and the valley bottom with an inclination of less than 8°. They account for only 2 % of the catchment area but are designed as large storage.

In the preprocessing section, extrapolation methods were applied to bridge gaps in the time series of air temperature and precipitation data. Further, cumulated precipitation sums were redistributed over the previous days if necessary.
The spatial resolution of the raster maps of 200 x 200 m^2 is necessary for the realistic calculation of meltwater, but it is in conflict with the temporal resolution of daily time steps. A reduction of the delay of the onset of the simulated discharge at the beginning of the monsoon season caused by the disadvantageous ratio between temporal and spatial resolution was achieved by extending the river network to include the glacier-covered parts. This accounts further for the subglacial drainage networks which were not included in the original river network.

The model was calibrated using glacier mass balance data as additional calibration criteria to adjust the parameters of the snow and glacier routine. The simulation results are generally satisfying but a drop in performance in the verification period can be observed. This can be attributed partly to changes in the glacier area during the simulation period, which are not considered in the model. The comparison with the semi-distributed HBV-ETH model revealed that the main advantages of TAC^d are the distributed treatment of runoff components and storages of the catchment. As the output of the snow and glacier routine shows no significant differences between both models the runoff generation routine of TAC^d is able to store the water during the monsoon season for the maintenance of winter discharge.

Weak spots of the model application were revealed in the calculation of ablation in high altitudes and in the simulation of discharge at the beginning of the monsoon season. Ablation is calculated by the temperature-index method if air temperature is above a threshold value. This leads to an unrealistic snow cover in high altitudes where air temperature is below the threshold value and sublimation plays a significant role for ablation. Further, distribution of snow by avalanches is not considered as an ablation process in the model. This among other reasons also affects the simulation of the onset of discharge at the beginning of the monsoon season, since snow in lower altitudes starts melting earlier and thus contributes to the runoff generation of the early monsoon season.

The presented version of TAC^d is seen as the framework for further investigations and developments. The subjectively conceptualized runoff generation routine and the dimensions of the assumed storages need to be checked by experimental investigations in the catchment. An energy balance approach could simulate sublimation processes of the high altitudes and further knowledge of the redistribution of snow is necessary for an exact description of the hydrological cycle with a numerical model.

The results of this study encourage continuing investigations of this climatically highly sensitive region. Interdisciplinary approaches are necessary to determine the impacts of climate change in this region from both the hydrological and the socio-economic point of view.

Keywords:

Distributed process-oriented modelling
Distributed snow- and icemelt modelling
Langtang Khola catchment
Storage concepts

Zusammenfassung

Ziel dieser Arbeit war die Entwicklung einer Gletscherroutine für das flächendetaillierte Einzugsgebietsmodell TAC^d (Tracer Added Catchment Model, distributed). Das bestehende Modell sollte auf seine Anwendbarkeit für den Einsatz in entlegenen Einzugsgebieten des Himalajas überprüft und gegebenenfalls modifiziert werden. Darüber hinaus musste man Extrapolationsverfahren anwenden um Lücken in den vorhandenen Temperatur- und Niederschlags-Messreihen zu schließen.

Das flächendetaillierte, prozess-orientierte Modell TAC^d wurde im Brugga Einzugsgebiet (gelegen im Schwarzwald in Deutschland) entwickelt und hat eine modulare Struktur. Die „runoff generation routine" ist das Herzstück des Modells und wurde mit Hilfe experimenteller Untersuchungen entwickelt. Lateral und vertikal verknüpfte Einzellinearspeicher simulieren die Abflussbildungsprozesse der einzelnen Raumgliederungsklassen. Die einzelnen Teile des hydrologischen Kreislaufes werden mit Methoden berechnet, die sehr datenintensiv sind oder ein dichtes Messnetz benötigen, wie z.B. die Berechnung der potentiellen Verdunstung nach Penman-Monteith oder die Regionalisierung der klimatologischen Inputdaten mit der „inverse distance weighting" Methode.

Das 360 km² große Langtang Khola Einzugsgebiet ist im Himalaja (Nepal) gelegen und hat eine vertikale Erstreckung von 3600 bis 7234 m über NN. 46 % der Gebietsfläche sind mit Gletschern bedeckt. Temperatur und Niederschlagswerte werden an einer Station in 3920 m über NN gemessen und als Tagesmittelwerte bzw. –summen angegeben.

Das TAC^d Model musste umfassend modifiziert werden um es im Langtang Khola Einzugsgebiet anwenden zu können. Dies wurde in der Entwicklungsumgebung des Programmpaketes PCRaster durchgeführt. PCRaster verknüpft ein geographisches Informationssystem mit dynamischer Modellierung, was die Voraussetzung für eine effektive flächendetaillierte Modellierung ist.
Zur Regionalisierung der Temperatur und zur potentiellen Verdunstung verwendet man höhenabhängige Gradienten, Niederschlagswerte werden darüber hinaus durch einen horizontalen Gradienten regionalisiert. Die potentielle Verdunstung wird mit einem einfachen Sinusansatz berechnet, dessen durch Kalibrierung bestimmtes Maximum auf den ersten August festgelegt ist. Das Minimum der potentiellen Verdunstung von 0.0 mm/Tag ist auf den ersten Februar gelegt. Der klassische Temperatur-Index Ansatz berechnet die Schnee- und Eisschmelze unter Verwendung des Grad-Tag Faktors als Proportionalitätskoeffizient, der die Schmelze auf der Basis der Temperatur bestimmt. Die Schmelze wird mit Hilfe der direkten Sonnenstrahlung flächendetailliert berechnet unter Berücksichtigung der saisonalen Variabilität der Schmelzbedingungen. Zur Berechnung der direkten Sonnenstrahlung werden topographische und astronomische Gegebenheiten berücksichtigt und als potentielle Sonnenscheindauer pro Tag und pro Zelle ausgedrückt. Unterschiedliche Schmelzbedingungen von Eis und Schnee sowie von schuttbedeckten und freien Gletschern sind durch empirische Faktoren berücksichtigt.
Die Raumgliederung anhand dominanter Abflussbildungsmechanismen wird aufgrund physiographischer und topographischer Gegebenheiten durchgeführt. Vier physiographische Einheiten werden zur Konzeptionalisierung der Abflussbildungsprozesse bestimmt. Die vergletscherten und nicht vergletscherten Gebiete sind die dominierenden Einheiten, deren Abflussbildungsprozesse über zwei vertikal verknüpfte Einzellinearspeicher simuliert werden. Zwei weitere Einheiten, die während der Monsunzeit das Wasser aufnehmen und es in der Trockenzeit wieder abgeben, sind definiert. Dies sind die schuttbedeckten Gletscherzungen

mit einer Steigung von weniger als 3° und die Talböden mit einer Steigung von weniger als 8°.Auf das gesamte Einzugsgebiet bezogen machen diese Gebiete nur 2 % der Fläche aus, sind aber als große Speicher konzipiert.

Im Preprocessing werden Extrapolationsmethoden zum Schließen der Datenlücken in den gemessenen Temperatur- und Niederschlags-Zeitreihen angewendet. Darüber hinaus werden kumulierte Niederschlagswerte auf die vorausgehenden Tage verteilt.
Die räumliche Auflösung von 200 x 200 m² ist notwendig für eine realistische Berechnung der Schmelze, sie steht jedoch in Konflikt zu der geringen zeitlichen Auflösung von Tagesschritten. Die Verzögerung des Einsetzens des simulierten Abflusses zu Beginn der Monsunzeit aufgrund des ungünstigen Verhältnisses zwischen räumlicher und zeitlicher Auflösung konnte durch die Erweiterung des Gerinnenetzes unter Einbezug der vergletscherten Flächen verringert werden. Dies berücksichtigt darüber hinaus auch die subglazialen Entwässerungsnetze, die in dem originalen Gerinnenetz nicht enthalten sind.

Zur Kalibrierung des Modells werden Gletschermassenbilanzen als zusätzliches Kalibrierungskriterium verwendet um die Parameter der Schnee- und Gletscherroutine anzupassen. Die Simulationsergebnisse sind grundsätzlich zufriedenstellend, wobei ein Rückgang der Güte in der Validierungsphase beobachtet werde kann. Dies wird teilweise durch die Änderung der Gletscherflächen während der Simulationsperiode verursacht. Der Vergleich mit dem semi-distribuierten HBV-ETH Modell zeigt, dass der Vorteil des TAC^d Modells in der flächendetaillierten Behandlung der Abflusskomponenten und Speicher des Einzugsgebietes liegt. Die berechneten Ausflüsse aus der Schnee- und Gletscherroutine der beiden Modelle unterscheiden sich kaum, das TAC^d Model ist allerdings in der Lage dieses Wasser besser zeitlich zu verteilen, d.h. es während der Monsunzeit zu speichern um damit den Winterabfluss aufrecht zu erhalten.

Während der Modellanwendung zeigen sich die Schwachstellen des Modells bei der Berechnung der Ablation in großen Höhen und bei der Simulation des Abflusses zu Beginn der Monsunzeit. Die Ablation wird mit dem Temperatur-Index Verfahren als Schmelze berechnet, wenn die Temperatur über einem Schwellenwert liegt. Dies führt zu einer unrealistischen Schneedecke in großen Höhen, wo die Temperatur geringer als dieser Schwellenwert ist und die Sublimation eine wichtige Rolle bei der Ablation spielt. Darüber hinaus wird die Umverteilung des Schnees durch Lawinen als Ablationsprozess nicht berücksichtigt. Dies wird als einer von mehreren Gründen für die verzögerte Simulation des Abflusses zu Beginn der Monsunzeit betrachtet, da Schnee in tieferen Regionen schneller schmilzt und somit zu der Abflussbildung zu Beginn der Monsunzeit beiträgt.

Die vorliegende Version von TAC^d wird als Grundlage für weitere Untersuchungen und Entwicklungen angesehen. Experimentelle Untersuchungen müssen die subjektiv konzeptionalisierte Abflussbildungsroutine und die Dimensionen der angenommenen Speicher überprüfen. Sublimation könnte mit einem Energiebilanzansatz berechnet werden. Detailliertes Wissen über die Umverteilung des Schnees ist wichtig für die exakte Beschreibung des hydrologischen Kreislaufes mit numerischen Modellen.

Die Ergebnisse dieser Studie ermutigen zu weiteren Untersuchungen dieser klimatisch hochsensitiven Region. Interdisziplinäre Ansätze sind notwendig um die Auswirkungen des Klimawandels in dieser Region umfassend zu bestimmen.

1 Introduction

Runoff from glaciermelt plays a significant role in most parts of the world's high mountain regions (e.g. Chen et al. 1990, Messerli 1997). Glaciermelt characterizes the seasonal variation of runoff in the respective catchments. Melting snow and ice supply water to much of the Himalayan region in the dry months before the summer monsoon (Kattelmann 1993).
The seven most important rivers in Southern and Eastern Asia are fed by glaciers during dry season: Indus, Ganges, Brahmaputra, Salween, Mekong, Yangtze and the Yellow River. Snow- and icemelt comprises about 70 % of the annual discharge of the Indus and its tributaries (Tarar 1982). It is questionable how long the ice masses of the Himalayan head watersheds will be able to maintain these compensating effects. 500 million people depend on river water in the Ganges basin alone (Jauk 2003). There is clearly an urgent need for further knowledge of the climatic and hydrologic conditions of mountainous regions as they relate to water and energy resources.

Although it is known that the hydrological models have certain limitations, they nevertheless contribute largely to the development of Nepal's hydro-electricity and water resources management. Hydrological models are tools for water resources management which can bridge the gap in a reliable way between the available data base and the demand for information about hydrological processes, such as snow accumulation and ablation, runoff production from rain and snowmelt and runoff from glaciers. In view of the effects of global change, it is, however, not sufficient to get a good fit between simulated and measured hydrographs by optimal calibration of model parameters, especially when calculating the impact of climate change scenarios. In order to cope with these crucial issues, the experiences gained from the application of sophisticated, distributed, process-oriented hydrological models to thoroughly investigated research catchments must be transformed into hydrological models which run with a minimum of input data but account for most of the hydrological processes in as detailed a way as possible.

The target area of this thesis is a highly glacierized head watershed in the Nepalese Himalayas where continuous climatological and hydrological observations began in 1987, initiated by the German Agency for Technical Cooperation (GTZ). First simulations with a conceptual precipitation-runoff model were conducted by Braun et al. (1993) in the Langtang Khola catchment. Their findings are the basis for the model development of this thesis.

This thesis is integrated in the FRIEND HKH Project, which is supported by the German IHP/HWRP secretariat.

1.1 Objectives

Many models of different complexity have been developed to simulate the dynamics of snow accumulation and ablation phenomena (e.g., Cazorzi et al. 1996, Verbunt et al. 2003, Zappa et al. 2003). Model complexity strongly depends on the available data base. A main objective of this thesis was to incorporate the knowledge about high alpine hydrological processes and about the modeling of these processes, gained from highly sophisticated hydrological models and "laboratory-like" research catchments, into a conceptual hydrological model which is able to simulate the most important sequences of the land-phase hydrological cycle of a high alpine catchment with limited data availability. Since data scarcity is the most common limitation factor in the application of hydrological models, the underlying modeling philosophy is that the model should require only input data with high availability, even in remote regions of the Nepalese Himalayas. These data include daily mean air temperature and daily sums of precipitation, while topographic and physiographic information has to be implemented for the regionalization of, for instance, the simulation of snow- and icemelt. The objectives of this study can be translated into the following key tasks:

- Statistical extrapolation methods for filling the gaps in the time series of air temperature and precipitation have to be applied in order to provide a reliable data base for hydrological modeling.

- Glaciermelt has to be implemented into the snow and glacier routine of the process-oriented catchment model TAC^d. Potential sunshine duration is used for a distributed simulation of snow- and glaciermelt. Since data availability of the Langtang Khola catchment is limited to air temperature and precipitation, the routines of TAC^d have to be simplified or replaced.

- Inner annual distribution of water has to be simulated with an adequate conceptualization of the runoff generation routine. Therefore, hydrological response units are determined from available topographic and land use maps as well as from observations during field visits. Storage concepts and hydrological response units must account for the hydrological situation of the catchment; however, they have to be adapted to the limited knowledge about the runoff generation processes of the catchment. Thus, the most obvious runoff generation processes which are related to physiographic and topographic characteristics of the catchment must be discerned.

1.2 Procedure

An intensive literature study was necessary to describe the Langtang Khola catchment and to determine the most important hydrologic and climatic characteristics which have to be accounted for in the hydrological model. Further, it was necessary to study the principles of the geographic information system PCRaster.

The model version of TAC^d which was developed by Roser (2001), Ott (2002) and revised by Wissmeier (2005) was reviewed for its applicability to the conditions of a high alpine glacierized catchment. It became apparent that most of the routines or regionalization methods cannot be adopted. Following existing hydrological models, appropriate regionalization methods for climatic input data and the simplified calculation of potential evapotranspiration were incorporated into the model script. The development work focuses on the distributed calculation of ice- and snowmelt. Concepts proposed in the literature were verified for their applicability to the available data base. The methods suggested by Braun et al. (1993), Hottelet et al. (1993) and Hock (1998) are those which mainly influenced the approach developed in this thesis.
The literature provides only very few studies about the runoff generation processes of the Langtang Khola catchment. Results from these studies were evaluated and, together with the experience gained during field trips, used to design the runoff generation routine.
Modifications of the model script were tested in a virtual test site in order to achieve deeper insight into the simulated processes. The internal water balance was used as an indicator for the soundness of the code.

In the following, the model was applied to the Langtang Khola catchment. For this purpose an intensive reliability check of the climatic and hydrologic data was necessary, revealing significant inconsistencies which had to be corrected with statistical methods. Gaps in the time series of precipitation and air temperature were filled using the extrapolation methods suggested by Weber (1997). Additional glacier mass balance data were taken from the literature and used for model calibration. The applicability and the quality of the model were further evaluated by comparing TAC^d with the well-proven HBV-ETH model.

2 Methodology and modeling theory

2.1 Modeling of hydrological systems

A hydrological model is a simplified representation of a complex natural system. A natural system summarizes elements, which define temporal relations between input (material and energy) and output (material and energy) of the system. Hydrological systems are part of natural systems. The hydrological simulation describes mathematically the response of a hydrological system on a sequence of events during the defined simulation period (Viessmann et al. 1996). Figure 2.1 gives an overview of the main principles of hydrological models.

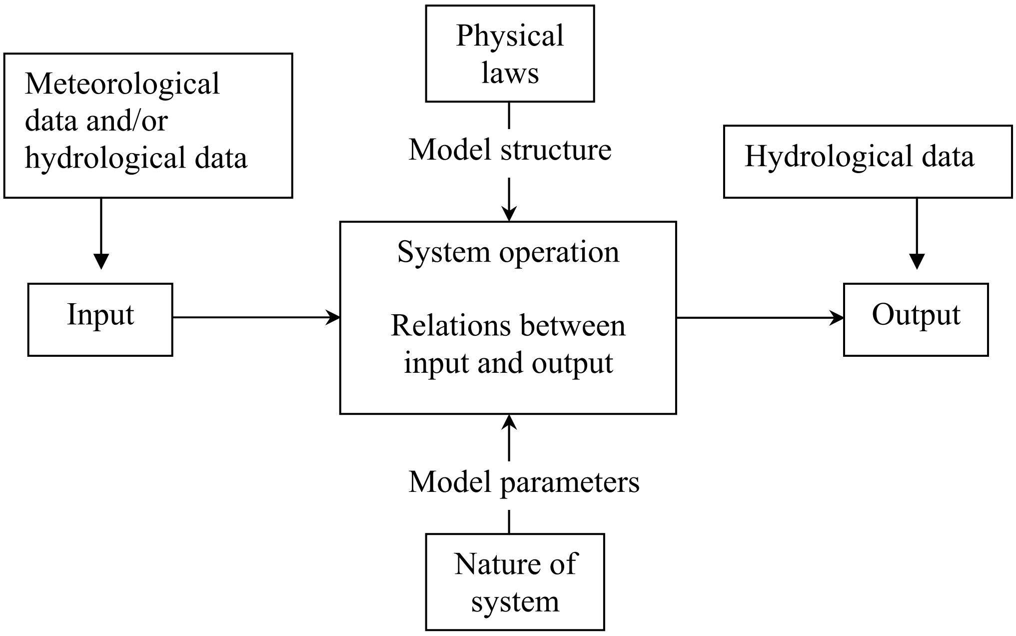

Figure 2.1: Principal components of hydrological models (after Dyck & Peschke 1995)

Different approaches are used to simulate the relation between input and output of a hydrological system (Figure 2.2). Uhlenbrook 1999 gives a review of the different approaches the following is taken from this study. A black-box model simulates the natural system without considering single physical processes within the catchment. These models are based on analyses of time series of input and output. In contrast to black-box models physical based models (white-box) describe the natural system based on the laws of physics considering mass- and energy balances of the system. In the ideal case all integrated equations have a direct physical meaning and the parameters can be derived by external measurements. In the spectrum between the black-box and the white-box models are the conceptual models, or gray-box models. Gray-box models describe the physical processes with simplified, mathematical, semi-empirical equations. The parameters used in these mathematical equations are primarily derived by calibration or can be confined in intervals by measurements such as air temperature gradients, precipitation gradients, etc. .

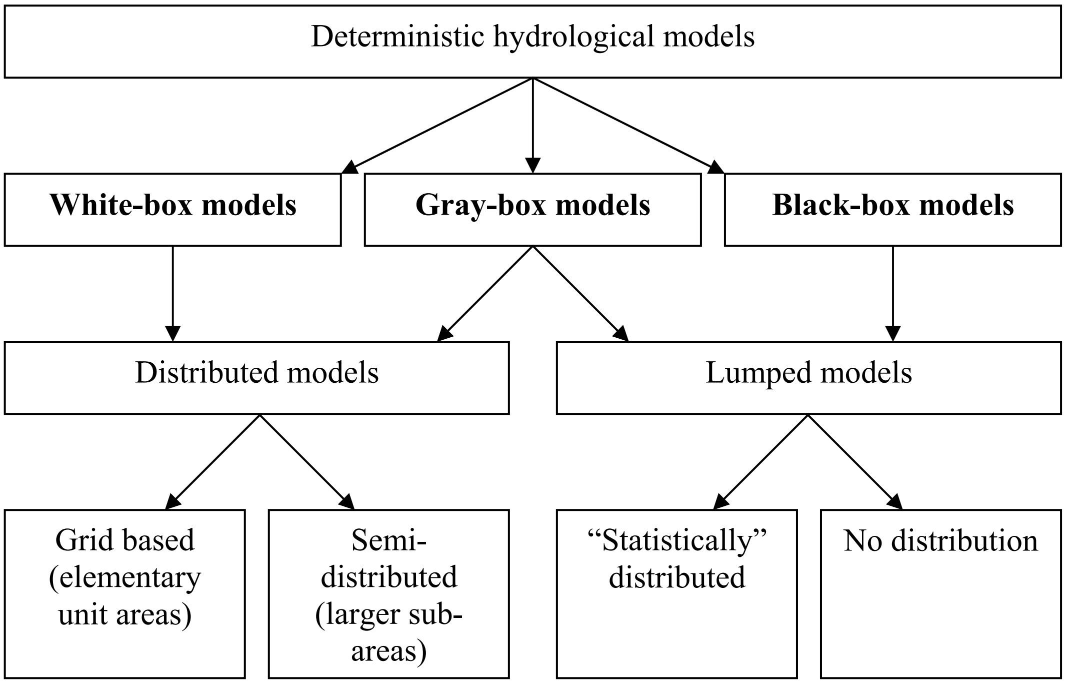

Figure 2.2: Different types of hydrological models and their spatial distribution (after Demuth 2001, revised)

Hydrological models can further be distinguished by their spatial discretization. Lumped models consider the entire natural system as one unit. Distributed models allow spatial variation of all parameters and model variables. The catchment area is sub-divided into grid cells and the simulation of system flows (e.g. runoff) is realized by neighborhood relations of these cells. Parameters or variables vary for larger sub-areas like altitude belts or homogeneous land use types (e.g. glaciers) in semi-distributed models.

2.2 Modeling of snow- and icemelt

There are a number of comprehensive reviews of modeling snow processes (Braun 1985, Morris 1985, Ferguson 1999, Melloh 1999). In this thesis only a brief overview of the different modeling approaches will be given and it is referred to literature for detailed discussion of the approaches.

2.2.1 Energy balance models

Physically based models calculate energy input into the snowpack by considering the components of the surface energy balance and they simulate the resultant changes in snowpack heat and mass balance (e.g. in Hock 1998, Escher-Vetter 2000). The principal and most influential terms of the energy balance are as follows:

$$\Delta H_s + \Delta H_l = Q_{rad} + Q_{sen} + Q_{lat} + Q_{adv} + Q_{gnd} \qquad \text{(Eq. 2.1)}$$

ΔH_s: Change in snowpack sensible heat content (i.e. snow temperature) (W/m²)
ΔH_l: Change in snowpack latent heat content (i.e. snowmelt or sublimation) (W/m²)
Q_{rad}: Net all-wave radiation flux across the snowpack surface (W/m²)
Q_{sen}: Sensible heat flux across the snowpack surface (W/m²)
Q_{lat}: Latent heat flux across the snowpack surface (W/m²)

Q_{adv}: Heat flux advected by precipitation across the snowpack surface (W/m²)
Q_{gnd}: Ground heat flux across the snowpack base (W/m²)

with

$$Q_{rad} = Q_{is}\,(1\text{-}\alpha) + Q_{il} + Q_{ol} \qquad \text{(Eq. 2.2)}$$

Q_{is}: Incoming short-wave radiation (W/m²)
α: Surface albedo (-)
Q_{il}: Incoming long-wave radiation (W/m²)
Q_{ol}: Outgoing long-wave radiation (W/m²)

The energy conducted by solid or liquid precipitation and the soil heat flux can also be taken into account even if their contribution is rather small (Zappa et al. 2003). The snow albedo is treated with more or less complex approaches usually using a function considering the age of surface snow and the surface temperature of the snowpack (Rohrer et al 1994).
The primary advantage of using physically based models is that they have applicability in a wide range of conditions and environments. Their big disadvantage is the large amount of input data which are necessary to run the model (Fox 2003).

2.2.2 Temperature-index models

These models lump all components of the surface energy balance discussed in Chapter 2.2.1, into a degree day factor, which is a proportionality coefficient that calculates melt rates on the basis of air temperature (normally in excess of some threshold value). Air temperature is considered to be representative for the main terms of the energy balance. A recent overview of this approach is given by Hock (2003).

2.2.3 Hybrid models

These types of snow- and icemelt models attempt to keep the simplicity of the degree day approach, but also explicitly represent other important components of the surface energy balance, in particular by solar radiation (Fox 2003). The most common addition to temperature-index-type models has been the incorporation of measured short-wave radiation or net radiation (Martinec 1989, Brubaker et al. 1996, Cazorzi et al. 1996). Hock (1999) proposed the extension of the temperature-index approach under consideration of the daily potential direct radiation variations. This approach was found to considerably improve simulations of spatial and temporal variations in melt rates compared with a model using a single degree-day melt factor, and only little additional improvement in model performance was achieved using a fully distributed energy balance model (Fox 2003, Zappa 2003).

2.3 PCRaster

PCRaster is a geographic information system (GIS), which combines classical GIS applications with dynamic modelling. The programme package was developed at the Institute of physical geography at the University of Utrecht, Netherlands (PCRaster 2005). PCRaster provides a variety of tools to store, manipulate and analyse spatial and temporal information. PCRaster is used as programming environment for the modification of TAC^d.

2.3.1 Concepts of PCRaster

PCRaster provides a high level linkage between GIS and the dynamic section of a modelling system. Hence PCRaster is called a dynamic GIS (van Deursen 1995) and different ways of combining GIS and dynamic modelling are shown in Figure 2.3.

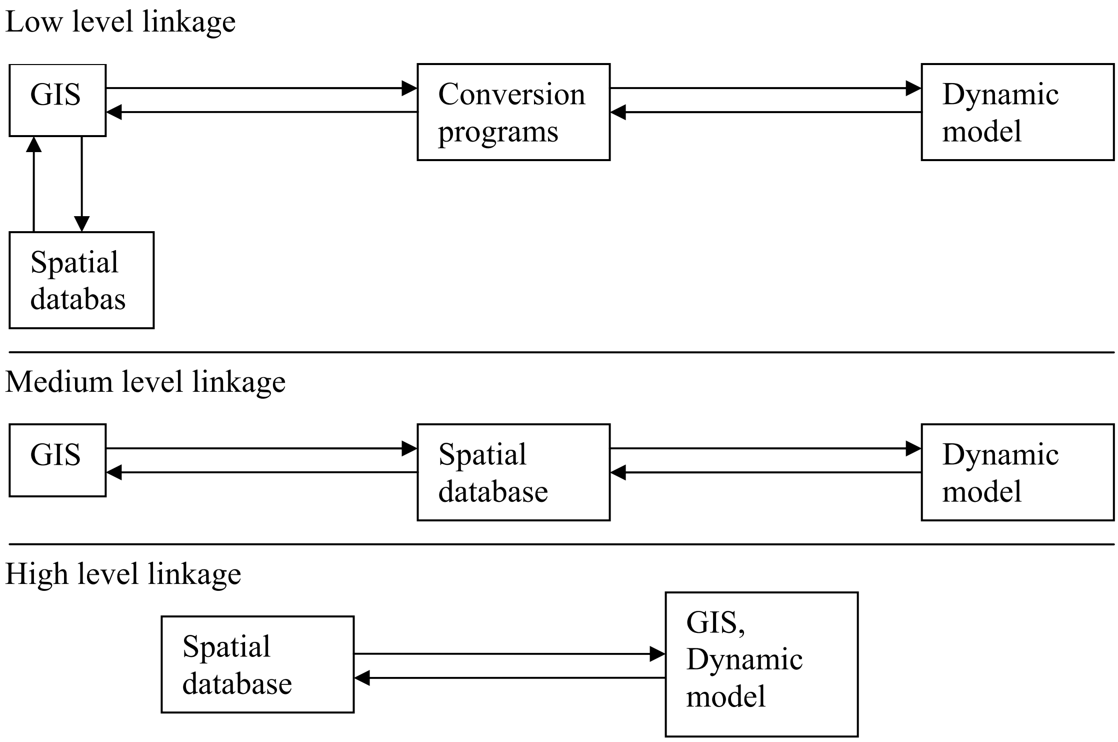

Figure 2.3: Level of linkage between GIS and dynamic modelling (taken from Ott 2002, after van Deursen 1995)

The high level linkage of PCRaster makes the use of an external data conversion program unnecessary. Here the dynamic model is one of several tools within the development environment of PCRaster, which is directly linked to the spatial GIS database. This approach enables the spatial distributed treatment of temporal variable data, like time series. Other approaches like low- or medium level linkage consider the dynamic model as a separate tool with spatial input data provided by an external GIS. Data exchange usually happens manually or by an automatic external conversion programme. The PCRaster environmental modelling language (EML) is specially designed for the tasks of modelling dynamic environmental systems in spatial and temporal resolutions. Therefore, a function library provides operators and functions from which many are especially designed for hydrological modelling. Further, it is possible to develop functions in Delphi or C++. These functions can be implemented into the model script in form of a dynamic link library. Thus, PCRaster allows a flexible treatment of individual questions.
The handling of data types is very strict to avoid forbidden map operations. Typical data types of maps, tables or time series are boolean, scalar, nominal or ordinal.
The spatio-temporal conceptionalization of PCRaster is shown in Figure 2.4. Rectangular cells are used to describe the natural system. Attributes like storage levels or altitudes are assigned to each cell of a raster map. Lateral information exchange between cells is realised by neighbourhood relations, which are also expressed in raster maps or can be calculated via GIS operations. Neighbourhood relations enable the simulation of lateral and vertical fluxes, e.g. of water, within a catchment. In Figure 2.4 time dependent attributes (variables) are

assigned to the vertically arranged cells. Depending on the number of vertically layered maps a 3 dimensional structure can be simulated via 2 dimensional map stacks. The information exchange conditions are saved in each cell as attributes. This approach is referred to as 2.5 dimensional (PCRaster 2004).
Input respectively output of a PCRaster model can be single raster maps or time series. Input raster maps or time series are read in for each time step, whereas specific time steps (e.g. monthly values) can be chosen for the creation of output files (maps, time series). Output files can be used in other programmes for further treatment.

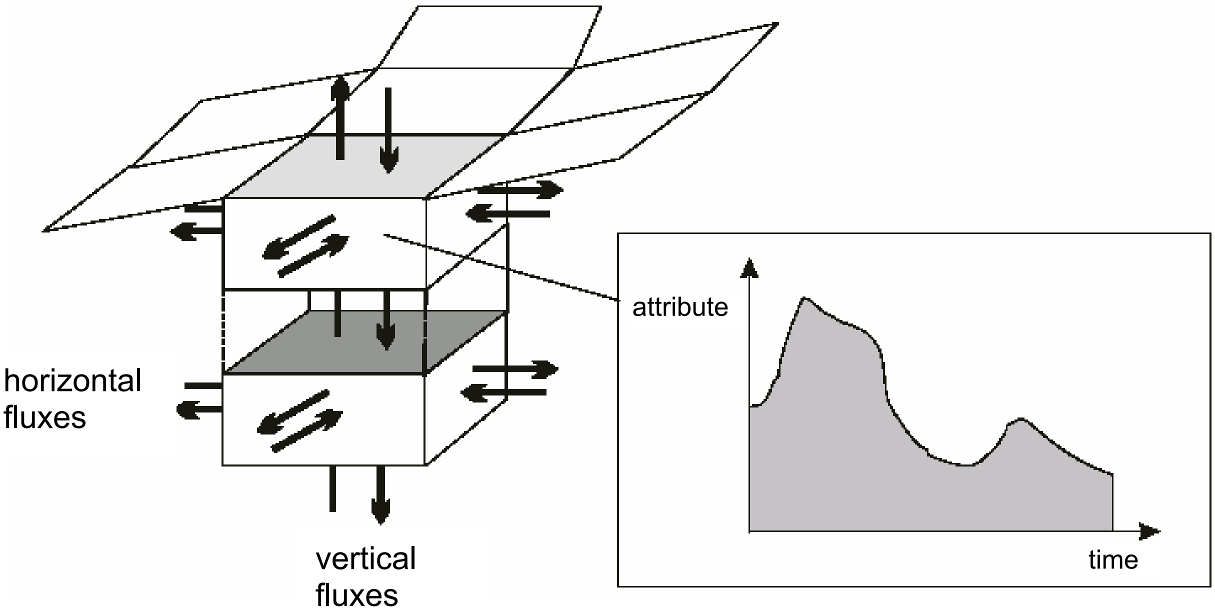

Figure 2.4: Spatial fluxes and time-variable cell attributes (taken from Roser 2001, after van Deursen 1995)

2.3.2 Dynamic modelling with PCRaster

PCRaster operations can be executed in a DOS shell. The model script summarizes single operations and can be called with a batch file. The script consists of five major sections with different responsibilities towards data management within the model. The first section is the **binding** section. Here variables are defined and assigned to the respective data type (boolean, scalar, nominal, ordinal). In this section external time series are read in as well as raster maps like the digital elevation model (DEM). The **areamap** section contains the name of the clone map, which consists of the information about the spatial discretization for all maps produced in the model. Further all input maps have to correspond with the information of the clone map. The **timer** section defines the time step discretization and the number of time steps in a model run. The initial values of the variables are assigned in the **initial** section. This section might contain functions to calculate the initial values or specific values e.g. for initial storage levels. The **dynamic** section is the core of the model where the sequential definition of model operations for each time-step is realised. At time-step i variable values are used, which were calculated in time-step i-1 and at the end of time-step i the values of variables for the time-step i+1 are available. All variables and their values are saved as raster maps.
The dynamic modelling language enables mathematical and analytical map operations and provides conditional structures (if…else) and an iterative section (repeat…until). PCRaster (2004) provides an excellent documentation of the dynamic GIS with comments and explanations of all functions and operators. Thus, the description of PCRaster in this work is limited to the main ideas and concepts of the development environment, which are necessary to understand the further descriptions of model development.

2.4 Methodology of model modification

2.4.1 The internal water balance

As stressed in Wissmeier (2005) the main criterion for the soundness of a catchment model is the internal water balance. Input and output fluxes as well as stored water are calculated for each time step and than cumulated over the simulation period. The internal water balance summarizes the storages and fluxes. Thus, input fluxes are added while output fluxes are subtracted. Due to the integral structure of the internal water balance fundamental errors in the model script result in a continuously rising or declining water balance. Water is “produced” in the model if the balance is negative, whereas a positive balance indicates that water “disappears” during simulation. The internal water balance is a calculation of the internal mass conservation of the model and must therefore be balanced out. This can be seen as the fundament of a precipitation-runoff model (Wissmeier, 2005).

$$Balance = \sum_{i=1}^{n}\left(\sum_{j=1}^{k} Input_{i,j} - \sum_{j=1}^{k} Output_{i,j} + \sum_{j=1}^{k} Storages_{1,j} - \sum_{j=1}^{k} Storages_{i,j}\right) \qquad \text{(Eq. 2.3)}$$

Balance:	Internal water balance of simulation period (mm)
$Input_{i,j}$:	Input of water fluxes at actual time step (mm)
$Output_{i,j}$:	Output of water fluxes at actual time step (mm)
$Storages_{1,j}$:	Sum of storage levels of all storages at first time step of simulation period (mm)
$Storages_{i,j}$:	Sum of storage levels of all storages at actual time step (mm)
n:	Number of time steps (-)
k:	Number of grid cells (-)
i:	Time step (-)
j:	Raster cell (-)

Glaciermelt water and precipitation is considered as input into the model. Output fluxes are calculated for water that is entering the river network or losses due to evaporation. Storages are snowpack, water content of snowpack, soil moisture, upper and lower storage, storage of water in flat parts of the glaciers and valley bottom storage (Chapter 5.5).

One needs to keep in mind that numerical models always suffer from inaccuracies related to time and spatial discretization and rounding. Minimal fluctuations of the internal balance are therefore expected even if the script is fully debugged. Earlier applications of the internal water balance as diagnostic tool (e.g. Wissmeier 2005) have shown that the internal water balance can be considered sufficiently accurate if the value stays within millionth of the input amount. Further, no systematic decline or increase should be evident.

2.4.2 The virtual test site

Virtual test sites are synthetic small catchments with the same topographical features as the real catchment the model should be applied to. In this study it is necessary to create a test site with an altitude range of several 1000 meters and a significant glacier cover. The test site is used for testing the new developed subroutines. Figure 2.5 shows the virtual test site of 10 x 10 grid cells with glacier covered parts and the local drainage direction (ldd).

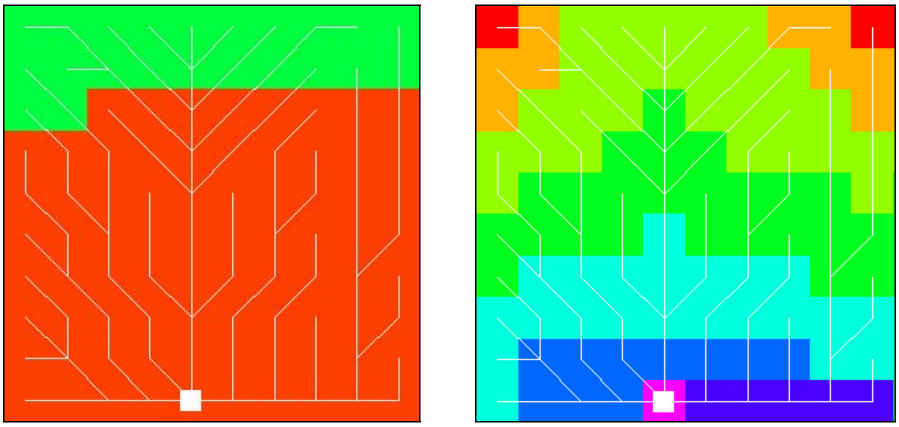

Figure 2.5: Virtual test site. Glacier map with ldd (left) and digital elevation model with ldd (right)

With a virtual test site interconnected effects are manageable in order to observe specific catchment reactions. Processes can be observed with only short computation times. Thus, parameter tuning becomes clearer and the effects of changes in catchment characteristics and climatic input data become more obvious.

2.5 Conclusions

PCRaster combines GIS with dynamic modelling which avoids intensive data conversion between both systems. The GIS provides classical tools for spatial analyses. In the dynamic section spatial and temporal input data can be processed with the help of special hydrological tools. Output files of all attributes can be created at any time step as a map or time series. The dynamic modelling language is easy to understand and to learn and therefore no specialist knowledge in computer sciences is necessary. A limitation for model application is the guideline that a model run has to start at time step ”1”. Therefore new formatting of input data is necessary if the modelling time is supposed to be changed.
The internal water balance is used as a diagnostic variable to evaluate the soundness of the model code which is tested in a virtual test site.

3 Area of investigation

The Langtang Valley is located about 60 km north of Kathmandu in the central region of the Nepal Himalayas (Figure 3.1). With a total area of 360 km² the catchment belongs to the upper meso-scale (Becker, 1992).

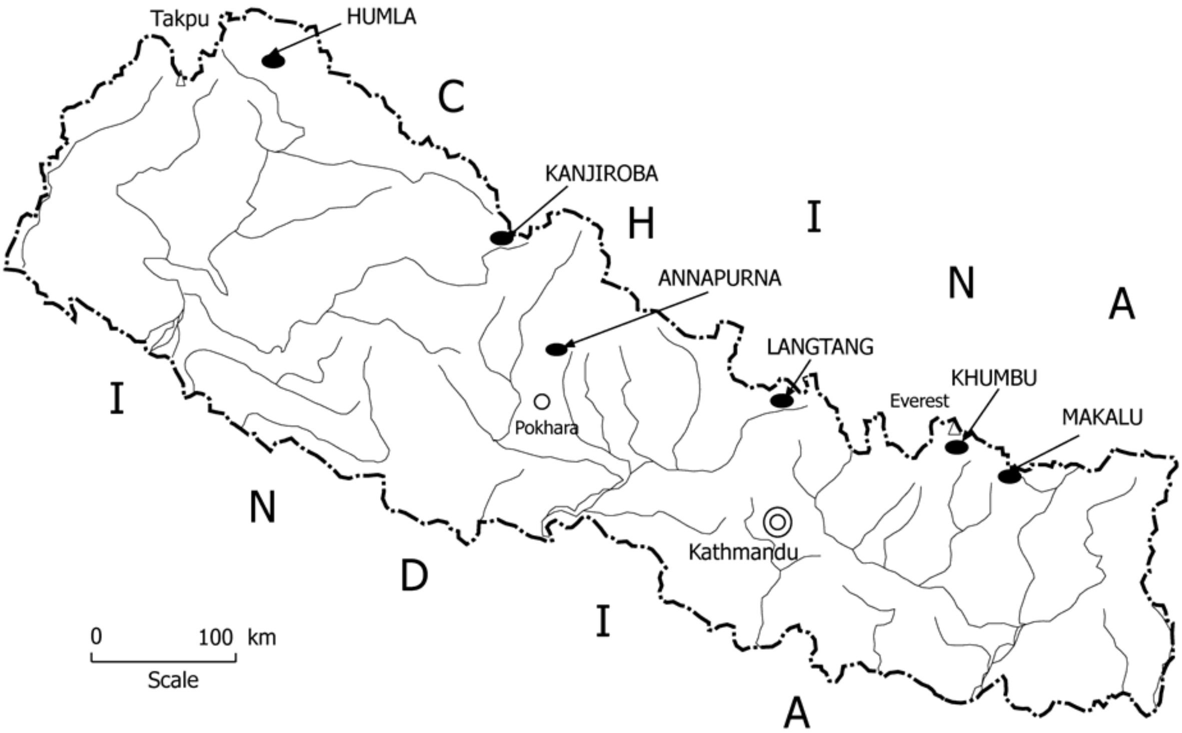

Figure 3.1: Map of Nepal with the hydro- meteorological stations (map produced by SGHU, Kathmandu, Nepal)

The Langtang National Park is one of Nepal's most popular tourist regions with infrastructure like lodges and trails. In the investigated catchment the lodges are located in Kyangjing and there are no further housing estates. There is one meteorological station located in Kyangjing which is operated by the Snow and Glacier Hydrology Unit (SGHU) of the Department of Hydrology and Meteorology (DHM).
The description of the catchment is the result of an intensive literature study as well as further statistical analyses of the meteorological and hydrological time series and topographic information.

3.1 Morphology, topography and land cover

The catchment reaches from 3600 m a.s.l. up to the Langtang Lirung at 7234 m a.s.l.. Two further peaks reach above 7000 m. The maximum altitude range is 3634 m with an average altitude of 5158 m a.s.l.. An average steepness of the slopes of 27° reflects the high potential relief energy of the catchment (Figure 3.2). The valley is dissected by the Langtang Khola and it is typically U-shaped. Table 3.1 summarizes the main characteristics of the investigation area. The data base for these analyses is described in Chapter 6.5.1.

Table 3.1: Main characteristics of the investigated catchment

Area		
Total	(km²)	360.0
Glacierized	(km²/%)	164.4/45.7
Debris-covered glacier	(km²/%)	32.1/19.5*[1]
Altitudes		
Range	(m a.s.l.)	3600-7234
Average	(m a.s.l.)	5158
Exposition		
North	(%)	21.4*[2]
South	(%)	26.8*[3]
East, West, Horizontal	(%)	51.9*[4]
Land cover		
Glacier	(km²/%)	166.3/46.2
Barren land	(km²/%)	185.5/51.5
Forest	(km²/%)	2.1/0.6
Others	(km²/%)	8.0/2.2

*[1] in percent of glacier-covered area
*[2] 315° - 45°
*[3] 135° - 225°
*[4] 45° - 135° and 225° - 315°

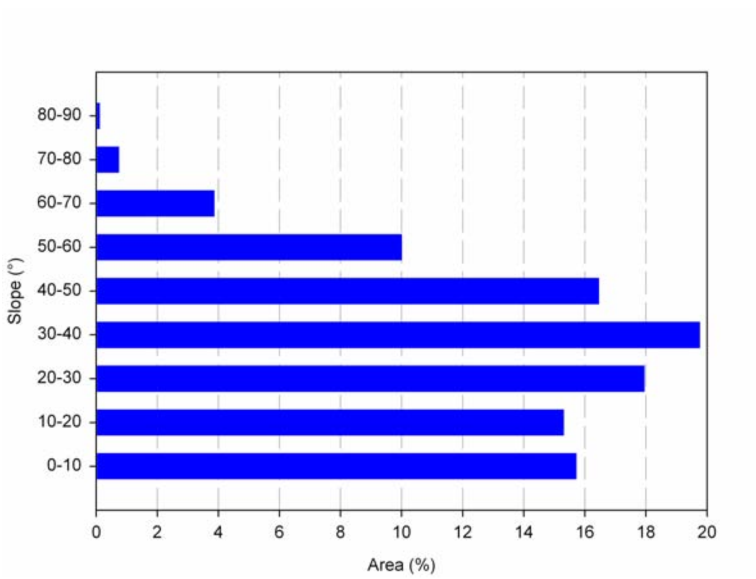

Figure 3.2: Inclinations of slope as proportion of the entire catchment area

Several sets of moraines occupy the valley bottom, which have been correlated to the Little Ice Age, Neoglacial, Late glacial younger and older and the advance older than Late glacial (Heuberger et al. 1984; Ono 1986 quoted in Watanabe et al. 1989). Boulders and scree cover the steep slopes and high plateaus, while the occurrence of forest and grass land in the lower altitudes with no steep inclination along the river is limited to 2.3 % of the entire catchment

area. The river bed consists of sand and gravel. The geology of this area is part of the Main Central Thrust Zone, which consists of granite, gneiss and schist.
Himalayan glaciers are summer accumulation type glaciers, which means that both accumulation and ablation occur primarily during summer monsoon season. The glaciers are categorized into two types, according to the surface conditions of the ablation zone: debris-free glaciers and debris-covered glaciers (Moribayashi 1974). 166 km² of the 360 km² catchment area are occupied by glaciers from which 32 km² (19 %) are covered by debris, especially the glacier tongues below 5200 m. Figure 3.3 shows the glaciers of the Langtang Khola catchment and the main characteristics are summarized in Table 3.2. A 3D-visualization is given in Figure 3.5.

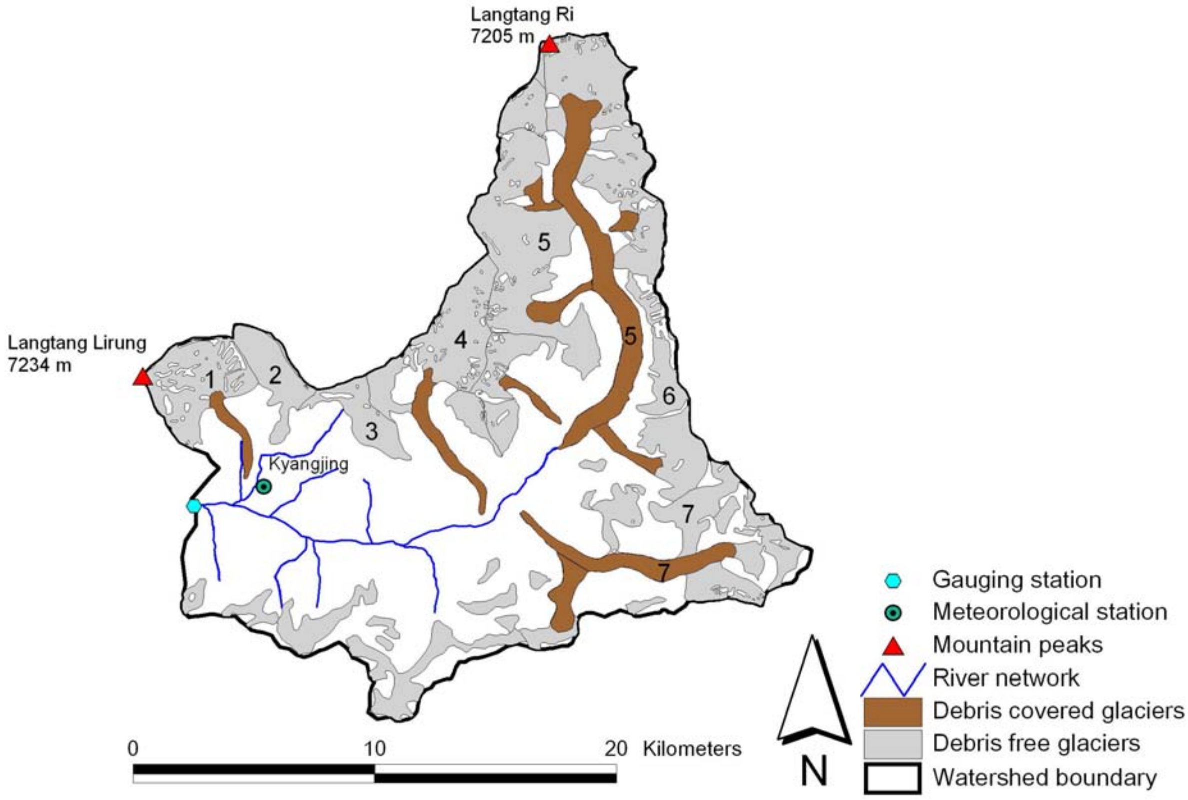

Figure 3.3: Langtang Khola catchment with meteorological station and the gauging station. Glaciers with numbers are described in Table 3.2

Table 3.2: Characteristics of the glaciers in the Langtang Khola catchment (ICIMOD 2002)

Glaciers Map No.	Name of the glacier	Area (km²)	Mean length (m)	Mean elevation (m)	Orientation of ablation area	Orientation of accumulation area
1	Lirung	12	6580	5522	S	SE
2	-	6	5830	5136	SW	SW
3	Yala	5	1520	5841	SW	SW
4	-	16	11590	4991	SE	SE
5	Langtang	68	17740	5833	S	S
6	-	4	2150	5737	SW	SW
7	-	26	1580	5243	SW	SW

Glaciers reach down to 4000 m a.s.l., and the proportion of glacier covered area increases with altitude (Figure 3.4).

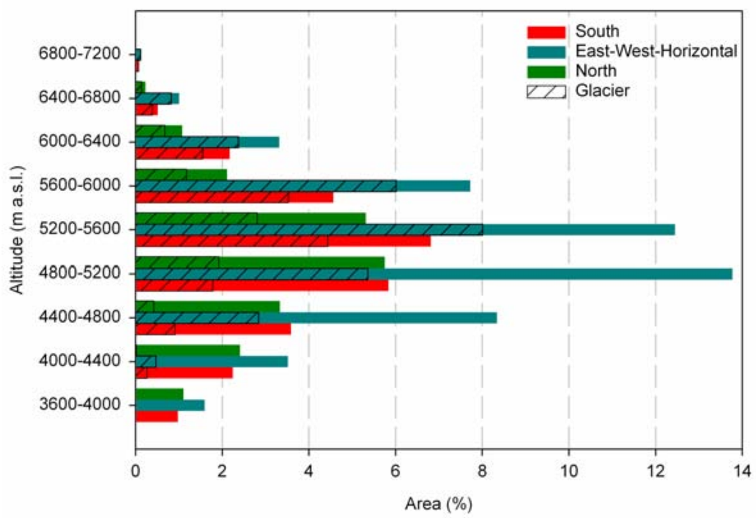

Figure 3.4: Area-altitude distribution in exposition classes north (315° - 45°), south (135° - 225°) and east-west-horizontal (45° - 135° and 225° - 315°) with information about glacier covered parts as proportion of the entire catchment area

Yala glacier and Lirung glacier have been studied in detail in terms of glacier fluctuations. Fujita et al. (1998) conducted a survey of Yala glacier terminus in September 1994, May and October 1996 and found that the retreat rate and surface lowering has accelerated in recent years. Repeated surveys of transverse surface profiles of Lirung glacier from 1987 to 1999 revealed that the glacier surface has lowered from 1996 to 1999 (Naito et al. 2002). Photographs taken at different times show clear retreat of the glacier and there is an indicator that the upper steep part and the lower flatter part of Lirung glacier will separate in near future (Shrestha et al. 2004).

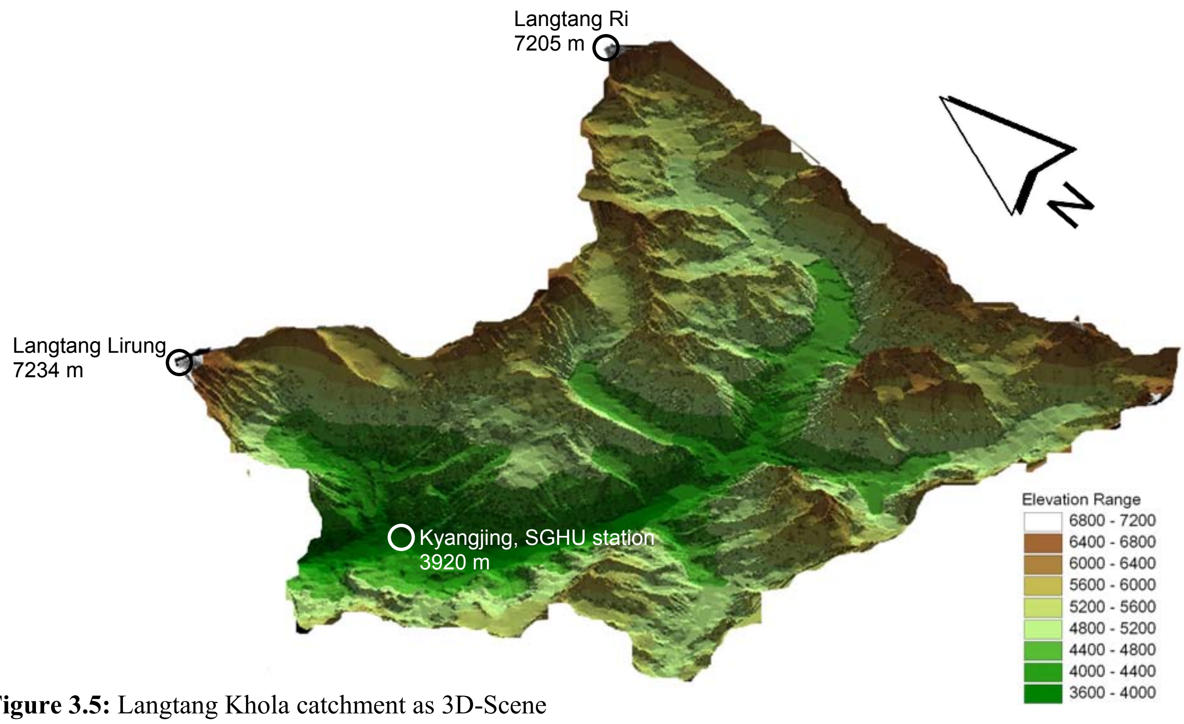

Figure 3.5: Langtang Khola catchment as 3D-Scene

3.2 Climate

The characteristical mark of the climate of Nepal is the monsoon circulation with predominant easterly-winds in the summer and westerly-winds from October to May. The summer monsoon with large precipitation sums from June to September does not break out at once. A gradual change from the dry winter season to the summer monsoon results from the pre-monsoonal convective precipitations which are often accompanied by thunderstorms (Ueno et al. 1993). Every summer, between June and July, the sun moves northwards and heats up the mountains creating a massive convection cell. The subsequent rising air produces a vacuum that draws the moisture-laden air of the Bay of Bengal. This air runs into the Himalayan barriers, cools as it rises and condenses in the form of rain. This is the start of the monsoon season, which brings three to four months of high humidity with overcast skies and gentle rain. About 70–80 % of annual precipitation falls during this period.
The eastern Himalayas receive the brunt of the monsoon, which loses its effect as it moves west along the mountains. Consequently, there is a distinct moisture gradient from east to west (Kraus 1966).
In winter, western Nepal experiences a reverse monsoon caused by a shift in the jet stream. This phenomenon, which drags weather patterns from the west of the Arabian Sea, brings moisture to the region in the form of snow. The oscillation of the jet stream lasts between November and March (ICIMOD 2002).

3.2.1 Air temperature

Seasonal variation of daily air temperature is shown in Figure 3.6 as average values of the period from 1988 to 1998 at the SGHU station (3920 m a.s.l.). The pre-monsoon season, from March to mid-June, is characterized by gradual increase of air temperature. The monsoon season, from mid-June to the end of September, is dominated by positive values of air temperature. In this season, diurnal variation of the air temperature is generally very small due to a thick cloud cover (Shiraiwa et al. 1992). The monsoon season ends in the end of September and is followed by the post-monsoon season, from October to December, which is characterized by fine weather. The air temperature decreases in this period, and the winter season begins in January. Mean daily air temperature was estimated in this study as 0.2 °C in the dry season from October to June and 8.4 °C in the monsoon season at SGHU station. Shiraiwa et al. (1992) reported a mean monthly air temperature of approximately -10 °C during winter period at three stations in the valley at an altitude between 5090 m a.s.l. and 5180 m a.s.l. and different expositions during their investigation period from June 1989 to March 1991. Air temperature shows distinctive altitude dependence with a mean annual air temperature of 1.9 °C at SGHU station and -3.5 °C in 5090 m a.s.l.. Based on the measurements conducted by Shiraiwa et al. (1992) a mean annual gradient can be calculated as -0.46 °C/100 m. Sakai et al. (2004) give a lapse rate of 0.5 °C/100 m for the monsoon season 1996. Figure 3.7 shows the mean monthly air temperature at the SGHU station and in 5090 m a.s.l. as reported by Shiraiwa et al. (1992) for the year 1990. Spatial variation of air temperature of around 1 °C was found at their three stations (5090 m a.s.l. to 5180 m a.s.l.) particularly from the pre-monsoon to the monsoon season. This variation is not related to exposition of slopes. Regional characteristics of the cloud amount and related sensible heating from the ground surface contribute to these characteristics (Shiraiwa et al. 1992). Diurnal variations of air temperature can be expressed as the difference between minimum and maximum temperature as shown in Figure 3.6. Diurnal amplitudes of 5 °C were found in this study at the SGHU station in the monsoon season and amplitudes larger than 10 °C in post-monsoon and pre-monsoon season. Shrestha et al. (2004) estimated an annual temperature rising rate of 0.27 °C/a. This high rate, however, could be caused by a systematic error in air temperature measurement as described in Chapter 6.3.1.

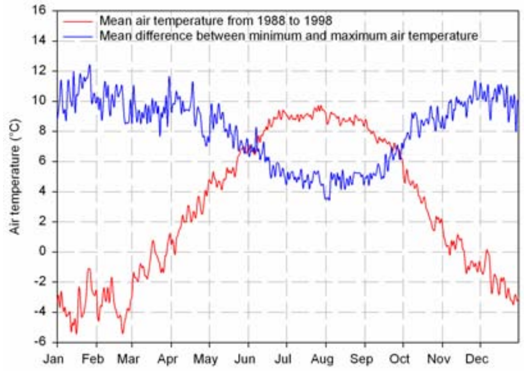

Figure 3.6: Seasonal variation of air temperature and of diurnal differences between minimum and maximum air temperature at SGHU station (3920 m a.s.l.) as mean values from 1988 to 1998

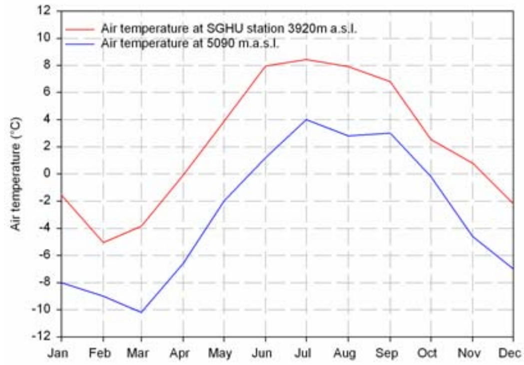

Figure 3.7: Mean monthly air temperature at SGHU station (3920 m a.s.l.) and at a station in 5090 m a.s.l., 1990

3.2.2 Precipitation

Precipitation is ruled by the impact of monsoon as shown in Figure 3.8 for the year 1996. 74 % of annual precipitation falls during monsoon season in the period from 1988 to 1998 (Figure 3.9). Figure 3.10 shows the seasonal variation of daily occurrence probability of precipitation. Mean annual precipitation can be estimated as 615 mm at SGHU station. The SGHU station is located at the bottom of the valley at an altitude of 3920 m a.s.l., where less precipitation falls from the cumulus clouds as compared to stations along the mountain slopes as reported by Seko (1987) and Ueno et al. (1990). Precipitation in the summer monsoon period is caused mainly by convective clouds. In the pre-monsoon season (April to May), the maximum daily amount of precipitation becomes smaller compared to winter season, while the number of days with precipitation increases month by month. From June to August total precipitation is large and occurs almost every day. However, the daily amount generally does not exceed 20 mm. In the later part of the monsoon season (September to October) the maximum daily amount is considerably greater, while the number of rainy days decreases gradually from previous months. In winter, precipitation is produced by the occasional passage of westerly troughs, which are called ‘western disturbances’ (Ramage 1971) and the amount increases with altitude (Seko 1987). Precipitation occurs on only a few days. However, the maximum daily precipitation is rather large. The altitudinal dependence of precipitation is strongly controlled by the characteristics of cumulus clouds and mountain-valley circulation. Only few studies exists, which examine the seasonal variation of altitudinal dependence of precipitation. Seko (1987) and Shiraiwa et al. (1992) observed that the amount of precipitation in an altitude of 5090 m a.s.l. is almost 1.5 times higher than at the SGHU station (3920 m a.s.l) during the monsoon periods of 1986 and 1990. From June to September precipitation amounted to around 820 mm at 5090 m and to 540 mm at SGHU station in 1990. From December to March the amount of precipitation at 5090 m is twice as high as at 3920 m in 1986. Based on these findings a linear precipitation gradient can be estimated as 4.4 %/100 m (related to the amount at 3920 m a.s.l.) as an annual mean (Ueno et al. 1993). Precipitation amounts generally decrease from the west to the upper parts of the valley in the north-east. The upper parts of the valley at an altitude of 5300 m a.s.l. receive almost the same amount of precipitation as the SGHU station. This is because less moist air is conveyed to the upper part of the valley by monsoonal circulations prevailing from the south. A mountain barrier running west-east in the southern side of the valley prevents moisture from penetrating into the uppermost reaches of the valley. The upper part of the valley receives approximately two third of the precipitation of the middle reaches (Shiraiwa et al. 1992). On the contrary, relatively small differences of the amount of precipitation are reported for the south- and north-facing slopes of the valley. The described altitudinal and spatial distribution of precipitation is valid for liquid as well as for solid precipitation. Further statistical analyses of the precipitation patterns can be found in Chapter 6.4.2.

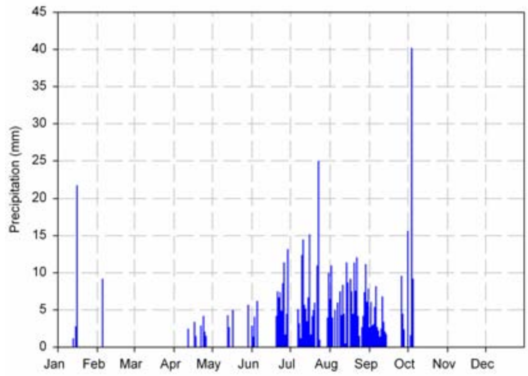

Figure 3.8: Seasonal variation of daily sums of precipitation at SGHU station (3920 m a.s.l), 1996

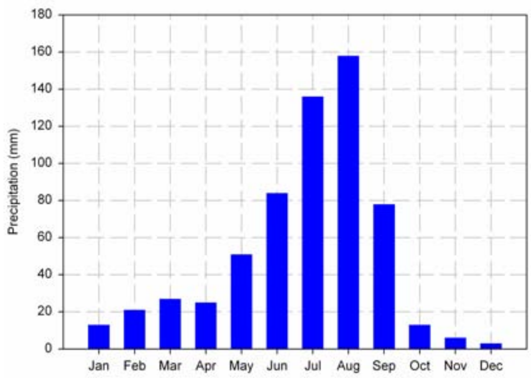

Figure 3.9: Mean monthly sums of precipitation at SGHU station (3920 m a.s.l.), 1988-1998

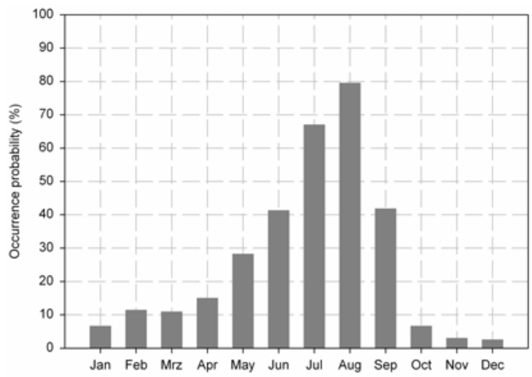

Figure 3.10: Seasonal variation of the occurrence probability of daily precipitation at the SGHU station (3920 m a.s.l.), 1988-1998

3.2.3 Evapotranspiration

Evapotranspiration was measured at Lirung glacier and at the SGHU station in altitudes of 4190 m a.s.l. and 3920 m a.s.l., respectively. Sakai et al. (2004) observed average daily actual evaporation of 4.5 mm/day at SGHU station and 1.99 mm/day at Lirung glacier from July to August 1996. Observations were carried out with lysimeters, which were plastic cylinders 10 cm in depth and 16.7 cm in diameter. The edge was set to be the same level as the ground surface. It was filled with debris or soil. Evaporation was obtained from precipitation and percolated water, which was collected in another cylinder below the lysimeter. During the observation period 59 % of precipitation evaporated at the SGHU station while evapotranspirated water accounted for 25 % at Lirung glacier. However, only 14.6 % of the entire catchment area is below 4500 m and as evaporation generally decreases with elevation and with the presence of snow and ice covers, this term plays a minor role in the water balance (Lang 1981).

3.3 Hydrology

The Snow and Glacier Hydrology Unit (SGHU) has collected discharge data of the Langtang Khola catchment from 1987 to 2000. Discharge is estimated from gauge height and rating curves as described in Chapter 6.2. Table 3.3 summarizes the discharge characteristics of Langtang Khola.

Table 3.3: Runoff characteristics of Langtang Khola for the period 1987-1998

		Langtang Khola
Easting *		85 33 00
Northing *		28 13 00
Altitude *	(m a.s.l.)	3600
HQ	(m^3/s)	22.94
MHQ	(m^3/s)	18.95
MQ	(m^3/s)	6.98
MNQ	(m^3/s)	2.13
NQ	(m^3/s)	1.00

* of gauging station

Several instantaneous floods occurred during the period 1987-1998. The most conspicuous flood arose in 1995 (Figure 3.11). It had a typical flash flood characteristic with fast rise and decline. There was no corresponding precipitation event causing the flood.

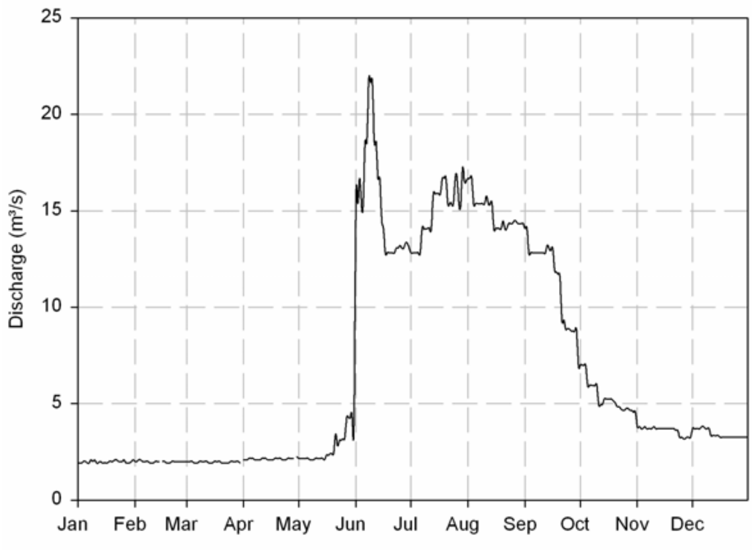

Figure 3.11: Discharge of the year 1995 with a flood event in June

This event could be a glacier lake outburst flood (GLOF). In the last half century, several glacial lakes have developed in the Hindu Kush-Himalayas and the Tibetan Himalayas. This may be attributed to the effect of recent global warming. The glacial lakes are formed on the glacier terminus due to the recent retreat of glaciers. The majority of these glacial lakes are dammed by unstable moraines, which were formed by the glaciation of the Little Ice Age. Occasionally a lake bursts releasing large amounts of its stored water, which causes serious floods downstream along the river channel. This phenomenon is recognized to be a common problem in Hindu Kush-Himalayan countries such as Nepal, India, Pakistan, Bhutan, and China (Tibet) (ICIMOD 2002). The sudden break of a moraine may generate the discharge of large volumes of water and debris causing floods.

In order to distinguish the hydrological seasons from full year's discharge, accumulated values of mean discharge (m³/s) from 1987 to 1998 are plotted against time as shown in Figure 3.12. The figure shows a rapid increasing rate of the accumulated values in the monsoon season and a comparatively slow increasing rate in winter. The discharge regime can be classified as glacial with maximum discharge from July to August and minimal discharge in winter (Figure 3.13).

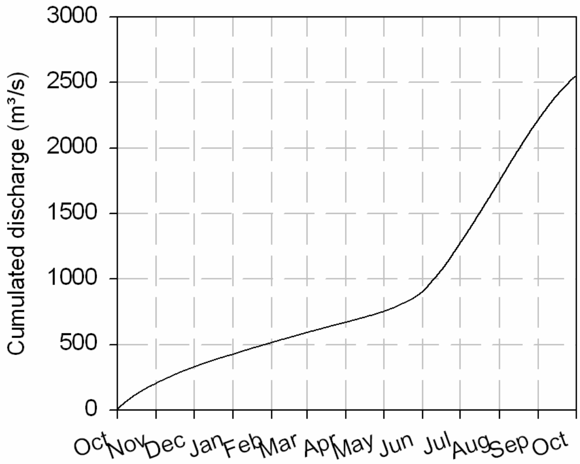

Figure 3.12: Accumulated mean discharge values of the period form 1987 to 1998

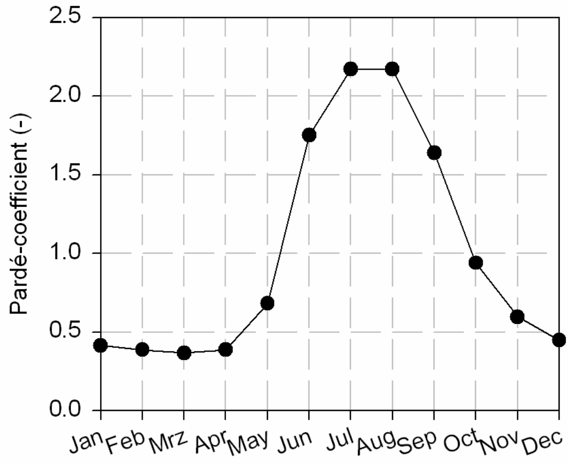

Figure 3.13: Runoff regimes of Langtang Khola (1987-1998) after Pardé (MQ_{month}/MQ_{year})

During the winter season precipitation falls as snow, and therefore it is stored until melting starts, usually in March. From the beginning of June to the end of September 65 % of annual discharge is observed, while in July and August it is 37 %. This is quite low compared to glaciarized catchments in the European Alps and can be explained with the high winter runoff. At the Rofenache catchment (Austria) 56 % of discharge occurs in July and August (Schulz 1999). Both catchments have nearly the same extent of glacier cover, 46 % and 41 %, respectively. For the same reason the Pardé-coefficients for July and August are relatively low for a glacierized catchment. Motoyama et al. (1987) determined a constant decreasing rate of the winter recession curve, with a recession rate of 0.01 day^{-1}. The half-value period of decreasing discharge is 67 days, from late December to late March, when the catchment is covered by snow. The constant rate implies that runoff processes are maintained throughout the winter. Consequently, winter runoff is characterized by a constant recession rate with no inflow of rainwater and meltwater under the condition of air temperature below the melting point. The mean discharge from December to the end of April is 2.8 m³/s. About 16.6 % of annual discharge occurs in this period. Motoyama et al. (1987) estimated the minimum runoff as 1.3 mm/day, referring to the glacier area in their observation period from July 1985 to July 1986. The winter discharge is attributed to the outflows of en-glacial water stored during monsoon season and to meltwater from the glacier bottom due to geothermal heat. Paterson (1969), however, determines maximum icemelt caused by geothermal heat as 6 mm per year. The generated runoff of the glacier area of the Langtang Khola catchment would amount to less than 0.007 mm/day (ice density = 0.91 g/cm³). This amount can be neglected compared to the minimum runoff of 1.3 mm/day. It is therefore reasonable to assume a rather significant water storage mechanism in glaciers as postulated by Tangborn et al. (2000). Drilling results during post-monsoon season in the ablation zone of Yala glacier revealed the existence of abundant water in the glacier body (Iida et al. 1984).

Based on the topographical map of the German Alpine Club (DAV) the drainage density can be estimated as 0.28 km/km² but the mapped river network does not include the subglacial drainage system. The real drainage density should therefore be higher.

3.4 Conclusions

The Langtang Khola catchment was chosen to apply the modified version of the TAC^d model because availability of climatological data on daily resolution is the most appropriate in the Nepal Himalayas. Detailed hydrogeological or geological maps are not available, thus the knowledge about the catchment is limited to topographical maps, field visits and catchment descriptions in literature which are mainly concentrated on climatological characteristics of the catchment. Main demands on model development must therefore be the integration of physiographic and topographic information in the mathematical description of the melt and runoff generation processes. The conceptualization of the runoff generation routine of TAC^d has to account for the inner-annual distribution of water because winter runoff is maintained by water stored during monsoon season. Limited knowledge about runoff generation processes of the Langtang Khola catchment implies the delineation of the hydrological response units based on topographical and land cover maps. Dominating land cover types are glaciers and barren land which are considered in the modification of TAC^d. Glaciers are covered by debris layers which affect meltwater production. Regionalisation of meteorological input data must be adapted to the altitude range of the Langtang Khola catchment.

4 The catchment model TAC^d

The catchment model TAC (tracer-aided catchment model) was developed by Uhlenbrook (1999) as a semi-distributed model. It belongs to the group of conceptual or grey box models. During the last years the model was developed further by Roser (2001), who introduced the raster-based distributed structure of the model (TAC^d). TAC^d was applied successfully to catchments in different climatic regions (Ott 2002; Johst 2003; Beek 2004). Wissmeier (2005) implemented solute transport to the model structure. In this section, the main model structure and conceptual ideas of the routines, which were taken from earlier model applications of TAC^d are described with parameter names as used in the model script. Modifications of routines and specific adaptations to conditions of Himalayan catchments are explained in Chapter 5.

4.1 Concepts and structure of TAC^d

The conceptual structure of TAC^d consists of individual routines (Figure 4.1). The sequentially linked routines represent the main parts of the land phase hydrological cycle and are mostly adopted from other conceptual models (WaSiM ETH: Schulla 1997; HBV: Bergström 1976, 1992).
The model consists of a snow routine to calculate snow accumulation and ablation and it contains a soil routine to determine soil moisture and actual evaporation. The runoff routine is the core of the model. It was developed based on tracer experiments and it attempts to simulate the dynamic of the runoff generation processes with simple linear storages. The routing routine simulates the wave propagation in the channel network. Apart from the main result, which is the simulated discharge, the model also yields intermediary results such as storage terms, soil moisture and snow cover.

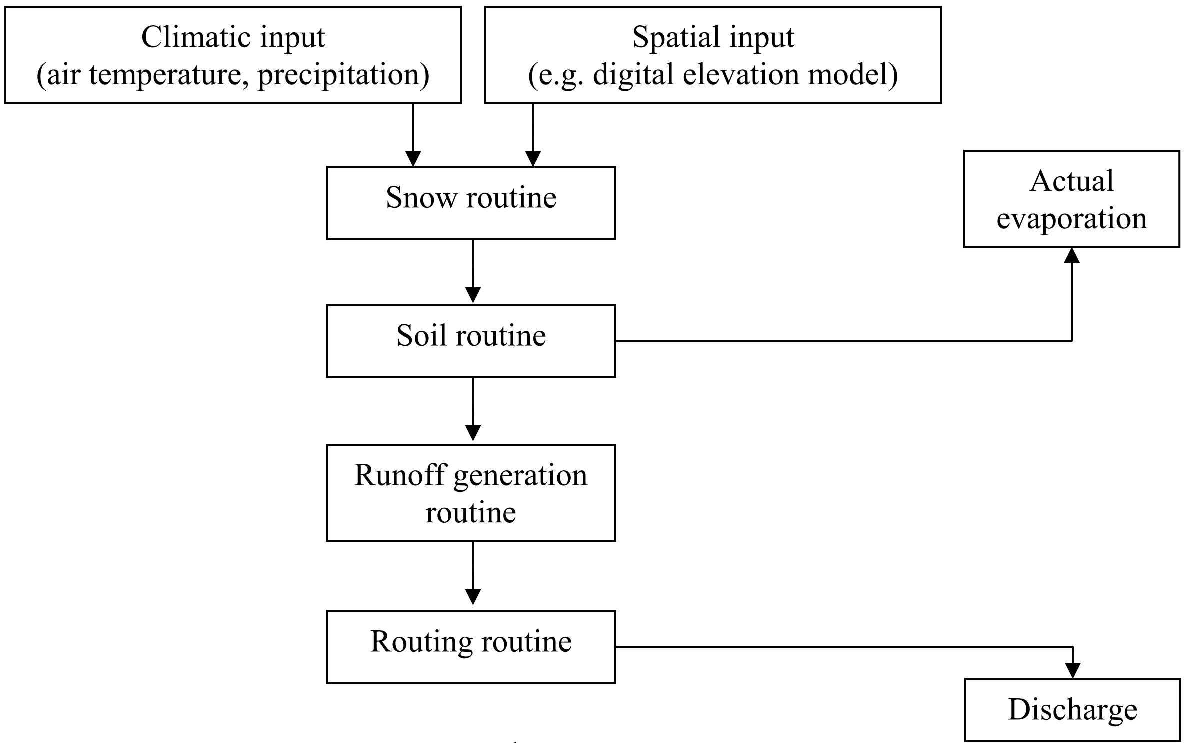

Figure 4.1: Schematic model structure of TAC^d

4.2 Routines of TAC^d

4.2.1 Snow routine

The snow routine was mainly adopted from the HBV model (Bergström 1976, 1992). The TAC^d model uses a temperature-index method to calculate the snowmelt. Input data are daily values of air temperature and precipitation. The output is the effective precipitation (InSoil), consisting of liquid precipitation and snowmelt. It is the input into the soil routine.

The following processes are considered:

a) Differentiation between liquid and solid precipitation
b) Correction of solid precipitation
c) Estimation of snowmelt
d) Estimation of storage and refreezing of liquid water in the snow cover.

a) Differentiation between liquid and solid precipitation

Precipitation is considered to be solid if air temperature is below the threshold value TT. TT is an empirical parameter which has to be determined by calibration. This parameter is also used in the degree-day method as a general temperature correction.

b) Correction of solid precipitation

The sum of solid precipitation of a day is corrected by the parameter SFCF. Systematic errors, such as unsatisfactory representativity of the climatic station or measuring errors of solid precipitation, can be corrected with the help of the precipitation correction factor (Sevruk 1985):

$$Prec = PrecStation \cdot SFCF \qquad \text{if air temperature} < \text{TT} \qquad \text{(Eq. 4.1)}$$

Prec: Corrected solid precipitation (mm/time step)
PrecStation: Measured precipitation (mm/time step)
SFCF: Snowfall correction factor (-)

Solid precipitation is added to the snowpack storage (SnowPack) in units of millimetre water equivalent.

c) Estimation of snowmelt

The TAC^d model uses a temperature-index method, the so called degree-day method (Zingg 1951), and the energy for snowmelt is derived directly from the air temperature. The required energy available for meltwater production, however, is best determined via the energy balance as approximately 60 to 80 % of the energy originates from radiation absorption (Paterson 1969). Energy balance methods to calculate snowmelt require data which are not available at the Langtang Khola catchment. The calculation of snow melt amount (MeltWaterSnow) is carried out as the product of the degree-day factor and the difference between air temperature and the threshold value TT, if the air temperature is above TT (Uhlenbrook 1999):

$$MeltWaterSnow = Cfmax\ (Temp - TT) \quad \text{(Eq. 4.2)}$$

MeltWaterSnow: Amount of snowmelt (mm/time step)
Cfmax: Degree-day factor (mm/(°C day))
Temp: Mean daily air temperature (°C)
TT: Threshold temperature or general temperature correction (°C)

d) Estimation of storage and refreezing of liquid water in the snow cover

The snow cover is able to store liquid water due to its porous structure. The water content of snow cover (WaterContent) is calculated with the parameter CWH (coefficient of water-retention capacity) as a fraction of the water equivalent of the actual snowpack (Uhlenbrook 1999):

$$WaterContent = CWH \cdot SnowPack \quad \text{(Eq. 4.3)}$$

WaterContent: Water content of snow cover (mm)
CWH: Coefficient of water-retention capacity (-)
SnowPack: Water equivalent of snowpack (mm)

The water content of snow cover is the second storage in the snow routine. In the case of the presence of a snow cover and air temperature above the threshold temperature, calculated meltwater and rain is added to the water content until the water-retention capacity is reached. Additional water, either as rain or meltwater, enters the following routine directly.
If the air temperature is below the threshold temperature, liquid water stored in the snow cover refreezes. Refreezing (Refreeze) is controlled by the parameter CFR (refreezing coefficient) and, together with meltwater (MeltWaterSnow), is the linkage between the two storage of the snow routine (Uhlenbrook 1999, Wiesmeier 2005):

$$Refreeze = CFR \cdot Cfmax \cdot (TT - Temp) \quad \text{(Eq. 4.4)}$$

Refreeze: Refreezing water in snowpack (mm/time step)
CFR: Refreezing coefficient (-)

4.2.2 Soil routine

The output of the snow routine is the input into the soil routine (InSoil) which was adopted from the HBV model (Bergström 1976, 1992).

The following processes are conceptualized:

a) Calculation of soil moisture storage, infiltration and percolation through the soil
b) Calculation of actual evaporation

a) Calculation of soil moisture storage, infiltration and percolation through the soil

The maximum storage capacity of the soil moisture storage is determined by the parameter FC (field capacity). Infiltration is calculated dependent on the ratio between actual soil moisture (SoilMoisture) and field capacity (FC) by a non-linear function. The parameter BETA accounts for different infiltration characteristics of soils. The smaller the BETA, the more water is sent to the next routine even when soil moisture is small compared to field capacity (Uhlenbrook 1999):

$$\frac{ToRunoffGeneration}{InSoil} = \left(\frac{SoilMoisture}{FC}\right)^{BETA} \qquad \text{(Eq. 4.5)}$$

ToRunoffGeneration: Infiltration into runoff generation routine as fraction of the actual soil moisture (mm/time step)
InSoil: Input into soil routine (mm/time step)
SoilMoisture: Soil moisture storage (mm)
FC: Maximum of soil moisture storage (mm)
BETA: Empirical parameter (-)

This conceptualization of the infiltration and percolation process is an important prerequisite for calculation of infiltration in high alpine soils where macro pores and preferential pathways are common. Due to the spatially variable parameterization of BETA and FC, different soil reactions can be simulated for each cell.

b.) Calculation of actual evaporation

Actual evaporation is calculated within the soil moisture routine dependent on the parameter LP. LP defines the fraction of FC above which actual evaporation is supposed to be equal to the potential evaporation. If the actual soil moisture (SoilMoisture) is below the product of LP and FC a linear reduction of potential evaporation is initialized (Figure 4.2) (Uhlenbrook 1999):

$$ActET = PotET \qquad \text{if SoilMoisture} \geq \text{LP} \bullet \text{FC} \qquad \text{(Eq. 4.6)}$$

$$ActET = PotET \cdot \frac{SoilMoisture}{LP \cdot FC} \qquad \text{if SoilMoisture} < \text{LP} \bullet \text{FC} \qquad \text{(Eq. 4.7)}$$

ActET: Actual evaporation (mm/time step)
PotET: Potential evaporation (mm/time step)
LP: Reduction parameter of field capacity (-)
FC: Field capacity (mm)

Actual evaporation is subtracted from the soil water storage (Equation 4.8).

$$SoilMoisture = SoilMoisture - ActET \qquad \text{(Eq. 4.8)}$$

There is no evaporation if a snow cover exists. This assumption is justified as over snow evaporation and condensation generally cancel each other out over longer time periods. Evaporation can be an important factor, energy-wise, over a short period, but as a mass balance component the amount of evaporation is small compared to, for instance, precipitation in high alpine areas (Lang 1981). The output of the soil routine (ToRunoffGeneration) is directed to the runoff generation routine.

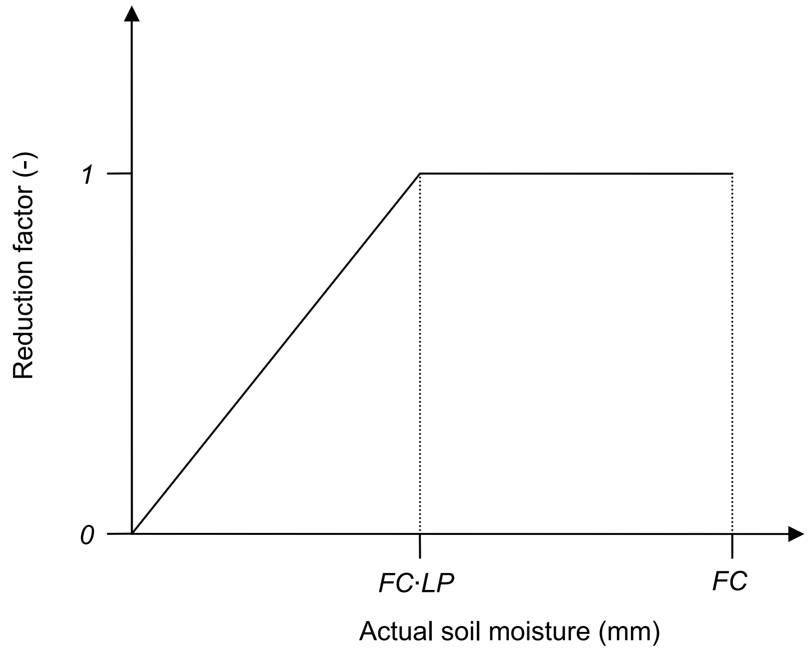

Figure 4.2: Reduction of potential evaporation in dependence on soil moisture (after Uhlenbrook 1999)

4.2.3 The runoff generation routine

In this chapter the general ideas behind the conceptualization of the runoff generation routine are explained, and generalized parameter names are used in the description and in the equations. Parameter names of the runoff generation routine consist of a specific part and a general part. The star (*) replaces the specific part of the parameter name.
The runoff generation routine of the TAC^d model refers to the hydrological classification of the catchment according to hydrogeologic and physiographic basin characteristics. This divides the catchment into different hydrological response units (HRU) and enables a process-oriented runoff simulation. The runoff generation processes of each HRU are conceptualized differently by linear storage concepts. Each cell consists of either a simple linear storage or a vertically arranged storage cascade, interconnected via vertical and lateral fluxes. The water content of each storage (*_box) is determined by the output of the soil routine (ToRunoffGeneration), lateral fluxes and by the storage characteristics. These are defined by an upper limit of storage capacity (*_H), by a storage coefficient (*_K) and in case of a storage cascade, vertical fluxes are controlled by a percolation parameter (*_P). The conceptual idea for storage outflow is the simple differential equation of a linear reservoir (Equation 4.9).

$$-\frac{dV}{dt} = k \cdot V = Q \qquad \text{(Eq. 4.9)}$$

V: Storage level (mm)
t: Time step (time step)
k: Storage coefficient (1/time step)
Q: Flux (mm/time step)

With the integral solution for an instantaneous Dirac impulse at time t = 0:

$$V(t) = V_0 \cdot e^{-kt} \qquad \text{(Eq. 4.10)}$$

V(t): Storage level at time t (mm)
V_0: Storage level at time t = 0 (mm)

Figure 4.3 shows a linear reservoir and the graphical visualization of its response function (Equation 4.10).

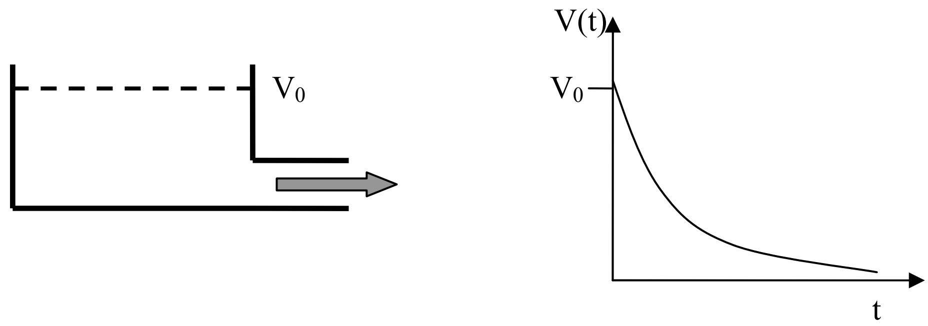

Figure 4.3: Linear reservoir and its response function to an instantaneous Dirac impulse (after Seibert 2002, revised)

These parameters and the arrangement of storage forms are assigned separately for the cells of each hydrological response unit. Runoff (Q_*) from these storages at time t is meant to be proportional to the water level of the respective storage (Equation 4.11).

$$Q\_* = *\_box \cdot *\_K \qquad \text{(Eq. 4.11)}$$

Q_*: Runoff of storage (mm/time step)
*_box: Water content of storage (mm)
*_K: Storage coefficient (1/time step)

If the upper limit of the storage is reached the additional water is added to Q_* (Equation 4.12). The process of saturated overland flow and the temporary extension of saturated zones can be simulated by an overflowing storage. This mainly happens at convergent cells like valley bottoms.

$$Q\_* = Q\_* + Overflow \qquad \text{(Eq. 4.12)}$$

Overflow: Overflow of the storage (mm/time step)

The direction of lateral flows is given by a local drain direction network (ldd). This drainage network can be created in PCRaster based on the digital elevation model. For the creation of the ldd a common D8 algorithm is used, where flows can be directed in eight different orthogonal and diagonal directions, depending on the steepest slope between the central cell (ldd code 5) and the neighbouring cells (ldd code 1 to ldd code 9) (PCRaster 2004).
Fluxes are redistributed into the storages according to the respective runoff generation type of the downstream cell. Thus, lateral fluxes are additional inputs to the storages (*_box) of each cell and therefore contribute to their filling.

4.3 Conclusions

The catchment model TAC^d is designed for process-oriented runoff simulation. Based on the distributed structure of TAC^d the catchment is discretized into cells of equal hydrological response, which are dominated by specific runoff generation processes. Storage analogies with different vertically and horizontally arranged and linked storages can be parameterized differently referring to the specific characteristics of the hydrological response unit. Lateral flow forms a storage cascade.

The modular structure of TAC^d enables an easy adaptation to regional catchment characteristics. Due to its complex distributed structure, especially of the runoff generation routine, thorough knowledge of runoff generation processes of a meso-scale catchment is a prerequisite for the application of TAC^d. Thus the reliable identification of runoff generation types via topographical, geological and pedological maps, aerial photography, remote sensing and personal user knowledge is essential (Wiesmeier 2005). Interaction between routines in the case of error compensation is a well-known problem (Braun et al. 1990) and must be considered in the calibration procedure. For this reason, sensitive parameters should be taken from the literature if available and ratios between storage parameters of the HRUs fixed before calibration. Over-parameterization is to be avoided as far as possible, and plausibility of parameters taken into account during the calibration procedure.

5 Modifications of TAC^d

The catchment model TAC^d was developed for lower alpine conditions of the Black Forest, Germany (Uhlenbrook 1999). The sophisticated routines for calculation of potential evaporation or for regionalization of climatic data require input data which are not available in the Nepal Himalayas. Therefore it was necessary to simplify or replace routines of TAC^d for the application to the Langtang Khola catchment. The development work focuses on incorporating as much physiographic information as possible to provide a physical base for process-oriented simulation of runoff generation as well as of snow and ice ablation or accumulation. In addition to Chapter 4, only the recent modifications of the TAC^d routines are explained in this chapter. The equations are written in PCRaster programming language with original variable names.

5.1 Regionalization of meteorological data

Daily data of air temperature and precipitation are available at one meteorological station in the Langtang Khola catchment (Chapter 3). For this reason, regionalization of these data is based on vertical and horizontal gradients taken from the literature.

5.1.1 Regionalization of precipitation

Measuring precipitation is a challenging task, especially in alpine regions. Nevertheless, precipitation data are a key element of runoff simulation as they are the main input to the model aside from glaciermelt. Systematic measurement errors occur and have to be corrected. The following components are responsible for these errors:

1. Deformation of wind field over the precipitation gauge orifice
2. Evaporation losses and splash losses
3. Interception losses of measuring instrument
4. Observer errors (e.g., variation in observation time)
5. Instrument errors (e.g., poor calibration, technical problems)

The list is not considered to be complete but shows the main sources of errors. Due to these errors precipitation is usually underestimated. Sevruk 1985 pointed out that in the case of the Hellmann precipitation gauge, points one and three are the most important. Various methods to correct these errors are discussed in the literature (Sevruk 1985, Richter 1995) and mainly depend on wind speed measurements. These data are not available at Langtang Khola catchment. Another problem is the representativity of the climatic station. In a high alpine catchment this might be the major problem in the determination of basin precipitation. As shown in Chapter 3.2.2, there are considerable differences in precipitation amounts in different parts of the catchment. In order to compensate for systematic errors and the lack of representativity of the climatic station, an empirical precipitation correction factor (PCF) similar to the snowfall correction factor (SFCF) was introduced:

$$PrecCor = PrecStation \cdot PCF \qquad \text{if air temperature} \geq \text{TT} \qquad \text{(Eq. 5.1)}$$

PrecCor: Corrected liquid precipitation (mm/time step)

PrecStation: Measured precipitation at climatic station (mm/time step)
PCF: Precipitation correction factor (-)

Shiraiwa et al. (1992) observed an increasing amount of precipitation with altitude. These observation results imply the application of an altitude dependent correction of precipitation via a vertical gradient for solid and liquid precipitation. This gradient reflects the increasing amount of precipitation in comparison to the measured value at an altitude of 3920 m (Equation 5.3). According to Shiraiwa et al. (1992) there is also a horizontal gradient. Thus, the measured amount of precipitation at the SGHU station is corrected for each cell depending on the horizontal distance between target cell and climatic station (Figure 5.1).

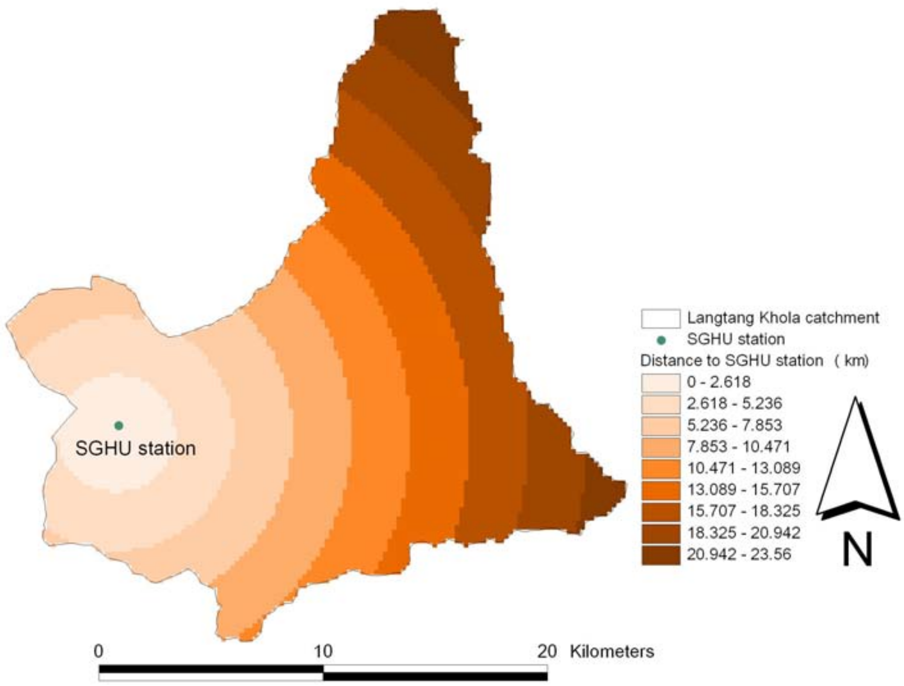

Figure 5.1: Horizontal distance between SGHU station and target cell

Precipitation declines towards the upper reaches of the catchment (Shiraiwa et al. 1992) with a negative horizontal gradient (PHorizGrad) in percent of the actually measured value at the climatic station per 1000 m distance (Equation 5.2).

$$PrecHorizontal = PrecCor \cdot (1 + (PHorizGrad \cdot DistToClim) \qquad \text{(Eq. 5.2)}$$

PrecHorizontal: Horizontally corrected precipitation (mm/time step)
PHorizGrad: Horizontal gradient ((%/1000m)/100)
DistToClim: Horizontal distance between target cell and climatic station (km)

Vertical correction is conducted after the horizontal correction.

$$PrecAltitude = PrecHorizontal \cdot (1 + (PGrad \cdot AltDiff) \qquad \text{(Eq. 5.3)}$$

PrecAltitude: Altitude-corrected precipitation (mm/time step)
PGrad: Vertical gradient ((%/100m)/100)
AltDiff: Vertical distance between target cell and climatic station (m)

PrecAltitude or PrecHorizontal is set at zero if Equations 5.3 and 5.2 become negative. Horizontal and vertical gradients are constant for the entire simulation period.
The amount of precipitation cannot increase constantly with altitude due to the declining water-retention capacity of the air caused by decreasing air temperature. Therefore, PrecAltitude is considered to be constant in altitudes above 5000 m.

5.1.2 Regionalization of air temperature

Air temperature is distributed with elevation by applying a fixed lapse rate (TGrad) as follows:

$$Temp = TempStation + (AltDiff \cdot TGrad) \quad \text{(Eq. 5.4)}$$

Temp: Altitude-corrected air temperature (°C)
TempStation: Measured air temperature at climatic station (°C)
TGrad: Vertical air temperature gradient (°C/100m)

5.2 Calculation and regionalization of potential evapotranspiration

Previous versions of TAC^d calculated potential evapotranspiration using approaches such as Penman-Monteith (Ott 2002) or Turc-Wendling (Roser 2001, Johst 2003). In the Langtang Khola catchment, neither method is applicable due to the absence of data. Braun (1985) applied a triangular function to calculate potential evapotranspiration. The parameter ETmax is considered a free parameter defining the maximum amount of potential evapotranspiration. A more realistic calculation of potential evapotranspiration can be achieved by a sinusoidal function (Hottelet et al. 1993). Maximum potential evapotranspiration is defined by the parameter (ETmax) peaking on August 1st (Figure 5.2). ETmax is the amplitude of the sinusoidal function with a minimum on February 1st.

$$PotET = (ETmax \cdot 0.5) \cdot (1 + \sin((l/MaxDay \cdot 360) - (360/MaxDay \cdot CounterDay))) \quad \text{(Eq. 5.5)}$$

PotET: Potential evapotranspiration (mm/time step)
ETmax: Maximum of potential evapotranspiration (mm/time step)
l: Day of maximum potential evapotranspiration (1st August = day 304 or 305)
MaxDay: Maximum days of the year (365 or 366)
CounterDay: Day (starting from 1st October = day 272)

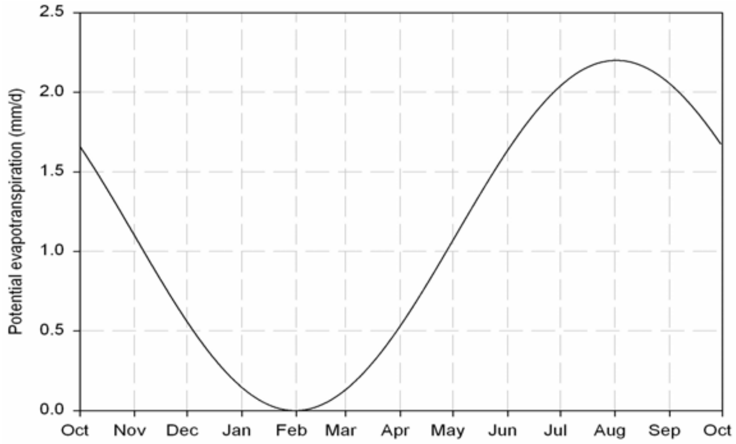

Figure 5.2: Potential evapotranspiration as a sinusoidal function

Detailed measurements of evapotranspiration reported in Gronowski (1992) justify the sinusoidal temporal distribution of potential evapotranspiration (Figure 5.3). Compared to Gronowski (1992), a shift of maximum potential evapotranspiration was necessary to adapt the function to high alpine climatic situations where a maximum of potential evapotranspiration usually occurs in August (Weber 2004). Evapotranspiration of grassland in particular shows a strong correlation to net radiation (Figure 5.3).

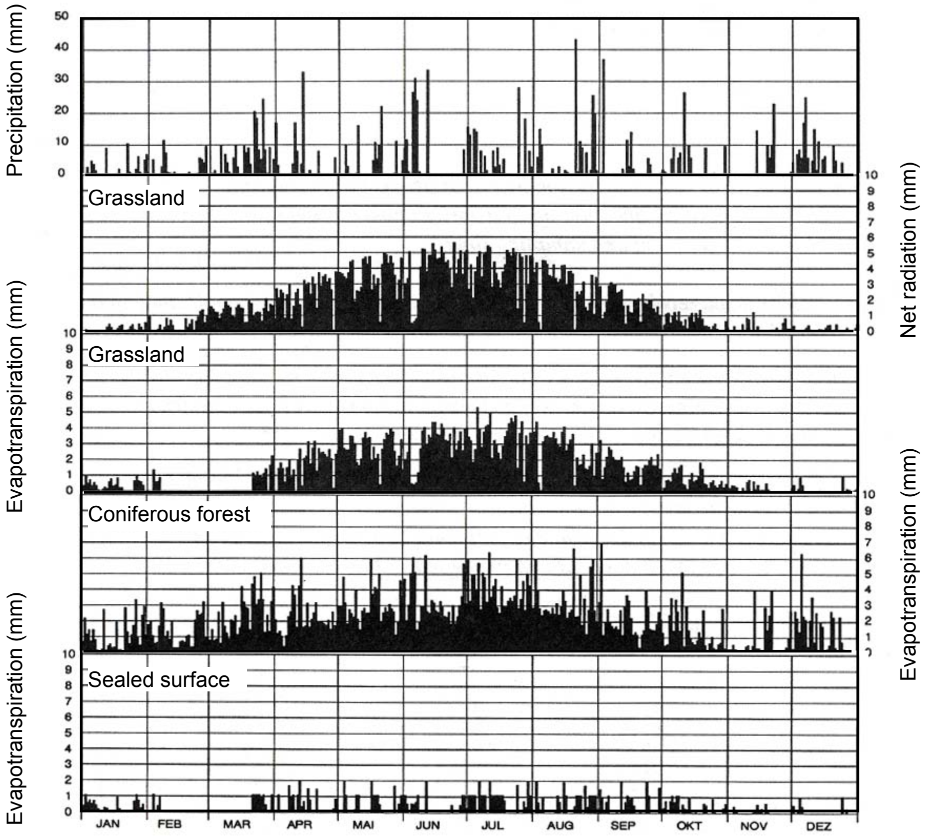

Figure 5.3: Comparison of daily evapotranspiration of different surfaces in the lower alpine region in Switzerland (Gronowski 1992)

Potential evapotranspiration is regionalized via an altitude gradient. This altitude-dependent correction of potential evapotranspiration takes the temperature dependence of evapotranspiration into account. As temperature decreases with altitude, less energy is generally available for evapotranspiration. This implies an altitude-dependent correction of potential evapotranspiration as well.

$$PotETAltitude = PotET \cdot (1 + ETGrad \cdot AltDiff) \quad \text{(Eq. 5.6)}$$

PotETAltitude:	Altitude-corrected potential evapotranspiration (mm/time step)
ETGrad:	Vertical gradient of potential evapotranspiration ((%/100m)/100)

5.3 The snow and glacier routine

5.3.1 Sunshine duration correction factor for temperature-index method

Glaciers are a form of long-term water storage. When snow does not melt completely, multi-year old snow or firn is formed which is eventually transformed into ice. The melting of ice during the summer months then contributes to runoff, especially during times when snow is already melted. The amount of snow- or icemeltwater is calculated here based on the temperature-index method. Computations using air temperature as the sole index of melt energy stem from to Zingg (1951), who introduced the degree-day factor. Air temperature measured at a station located downwards of the glacier provides more information about melting processes on the glacier surface than that which is measured at a station located directly on the glacier (Lang 1968, Ohmura 2001, Weber 2004). Temperature measurements on the glacier yield lower values due to the cooling effect of the melting ice surface. A station which lies within the catabetic wind system of the glacier but not on the glacier itself is not exposed to these energy losses and is therefore more representative of the energy actually available. This prerequisite for the application of the degree-day method is fulfilled in the Langtang Khola catchment.
Meltwater production in alpine regions, however, depends primarily on radiation as an energy source. Short-wave radiation balance over glaciers supplies up to 90 % of available melt energy on Vernagtferner, Austrian Alps (Weber 2004). Thus, short-wave radiation balance plays the most important role in meltwater production on alpine glaciers (Paterson 1969). Intensity of short-wave radiation input for a single cell in the raster-based distributed catchment is strongly influenced by astronomical and physiographic parameters such as the diurnal and annual course of the sun, the steepness and orientation of the slopes, and shadowing effects of surrounding mountains (Escher-Vetter 2000). Therefore, emphasis is placed, in this study on modelling the spatial distribution of meltwater production as a function of sunshine duration of a day per cell. Consequently, the degree-day factor needs to be diversified according to sunshine duration. Cazorzi et al. (1996) suggested a radiation index based on clear sky radiation as an approach to fully distributed snowmelt modelling. They produced maps of mean monthly energy indices and incorporated a so called “combined melt factor” to calculate snowmelt with air temperature as the only input variable. The “combined melt factor” is a modification of the classical degree-day factor. Hock (1999) proposed a further development of this idea, varying the melt factor on an hourly basis for each DEM cell according to temporal and spatial variation of clear sky direct radiation, calculated using standard solar algorithms. Braun (1993) applied a sinusoidal course of the degree-day factor in the HBV-ETH model defined by two parameters for the minimum and the maximum of the sinusoidal function. This approach accounts for the longer periods of sunshine duration during summer causing higher incoming short-wave radiation values; thus more energy for melting is available during summer-time. Hottelet (1993) introduced a parameter Rexp, which is applied to the results of the degree-day method as a multiplicative factor in order to simulate different meltwater production rates of the exposition classes: northern-, southern-, eastern- or western- oriented slopes or horizontal planes. Meltwater production usually increases on south-facing slopes whereas it decreases on north-facing slopes, as compared to eastern- and western- oriented slopes or horizontal planes. Thus, the parameter Rexp is larger than one to simulate the increased melting of south-facing slopes. For north-facing slopes, the inverse value of Rexp (1/Rexp) is used because this value is smaller than one and therefore diminishes the meltwater production. Meltwater production on eastern- and western- oriented slopes and horizontal planes is not modified by Rexp (Rexp = 1.0). In the semi-distributed HBV-ETH model, only the above-mentioned orientation classes

are used to modify the meltwater production. The distributed spatial discretization of TAC^d allows the specific manipulation of the degree-day method for each cell. The modification of the classical temperature-index method can be seen as the combination of the above mentioned approaches for distributed snowmelt modelling. Based on the digital elevation model (DEM), the potential sunshine duration is calculated by POTRAD 5 (Potential Radiation Equator Model; van Dam 2004) taking into account the aspect of cells and sun position as well as shading effects of mountains. Externally derived potential sunshine duration maps (Shade) are a further input to TAC^d and are used to derive cell-specific correction factors (RexpMap) for the degree-day method. Cells with long sunshine duration receive more short-wave radiation and thus can produce more meltwater than cells with less sunshine. Thirteen hours per day is the maximum sunshine duration in Langtang Khola catchment; by contrast, there are periods of the year during which northern-oriented cells at the bottom of the valley receive no direct sunlight at all due to shading effects.
The calibration parameter Rexp in TAC^d is used to define the range of the temporal and spatial variable RexpMap. Rexp is assigned to cells with maximum sunshine (13 h) and therefore defines the maximum possible value of RexpMap. The minimum of RexpMap is determined using the inverse value of Rexp (1/Rexp) which is assigned to cells with minimum sunshine duration (0 h). The inverse value of Rexp as the minimum of RexpMap is justified because this value is less than one and therefore diminishes the meltwater production and no further calibration parameter is necessary. A linear relation between Shade and RexpMap is assumed (Equation 5.7, Figure 5.4) for the calculation of the maps of the correction factor.

$$RexpMap = ((Rexp-(1/Rexp))/(MaxShade-MinShade))\cdot(Shade-MinShade)+(1/Rexp) \quad \text{(Eq. 5.7)}$$

RexpMap:	Map stack of correction factor for degree-day method (-)
Rexp:	Correction factor for cells with maximum potential sunshine duration (-)
MaxShade:	Maximum potential sunshine duration (h/day): 13 h in the Langtang Khola catchment
MinShade:	Minimum potential sunshine duration (h/day): 0 h in the Langtang Khola catchment
Shade:	Map stack of potential sunshine durations (h/day)

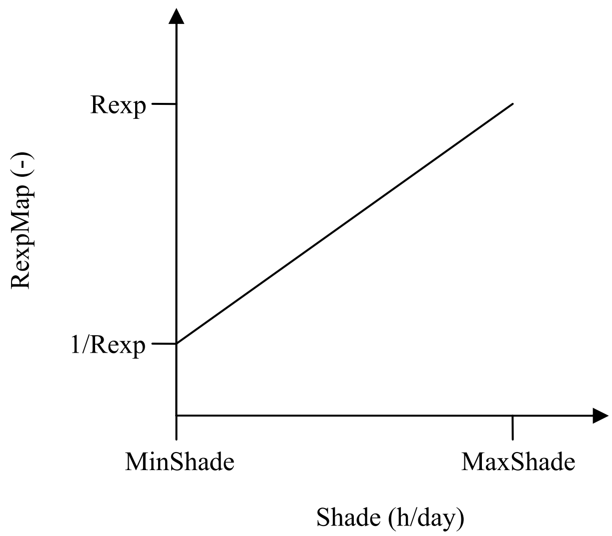

Figure 5.4: Linear relation between potential sunshine duration and the correction factor for the degree-day method

Maps of the correction factor are calculated for each day. This simple method enables a spatial and temporal discretized simulation of snow- and icemelt to be made.
The annual course of RexpMap of each cell equals a sinusoidal function and after Equation 5.8 this causes a sinusoidal annual course of the degree-day factor with its maximum at the end of June and its minimum at the end of December, as suggested by Braun (1993). The advantage compared to Braun (1993) is that the sinusoidal course of the degree-day factor is derived separately for each cell based on physiographic properties of the catchment. The approach combines the ideas of Braun (1993) and Hottelet (1993) based on a more physical background.

5.3.2 Accelerated melting of ice compared to snow

Ice shows an accelerated melting due to a reduced reflection compared to snow (Table 5.1). More short-wave radiation can be absorbed and therefore more energy for melting is available (Escher-Vetter 1980). Further, latent and sensible heat fluxes over snow are reduced due to lower roughness length of snow as compared to ice (Ambach 1972). For simulation of icemelt of snow-free parts of glaciers, the parameter Rmult (>1) is introduced to the degree-day method (Equation 5.9).

Table 5.1: Reflection of snow and ice surfaces (Paterson 1994)

	Range (%)	**Mean (%)**
Dry snow	80-97	84
Melting snow	66-88	74
Firn	43-69	53
Clean ice	34-51	40
Slightly dirty ice	26-33	29
Dirty ice	15-25	21
Debris-covered ice	10-15	12

5.3.3 Reduction of icemelt under debris layers

Melt conditions of ice under debris-covered parts of the glaciers must be considered separately from the conditions of clean glaciers. On the one hand, a rather thick debris cover protects the ice from direct solar and long-wave radiation, resulting in a reduction of melt as indexed by the current air temperature. On the other hand, the debris cover is darker than ice which increases absorption if the debris layer is thin (Table 5.1, dirty ice). Depending on the thickness of the debris cover, melting is decoupled from the current meteorological situation. This finding is reported by many researchers, but results vary as to the thickness required before ablation is accelerated or suppressed. Values of debris thickness required for an enhanced melting are typically 7-8 cm (Popovnin et al. 2002). Figure 5.5 shows a generalized spectrum of debris thicknesses and their impact on meltwater production.

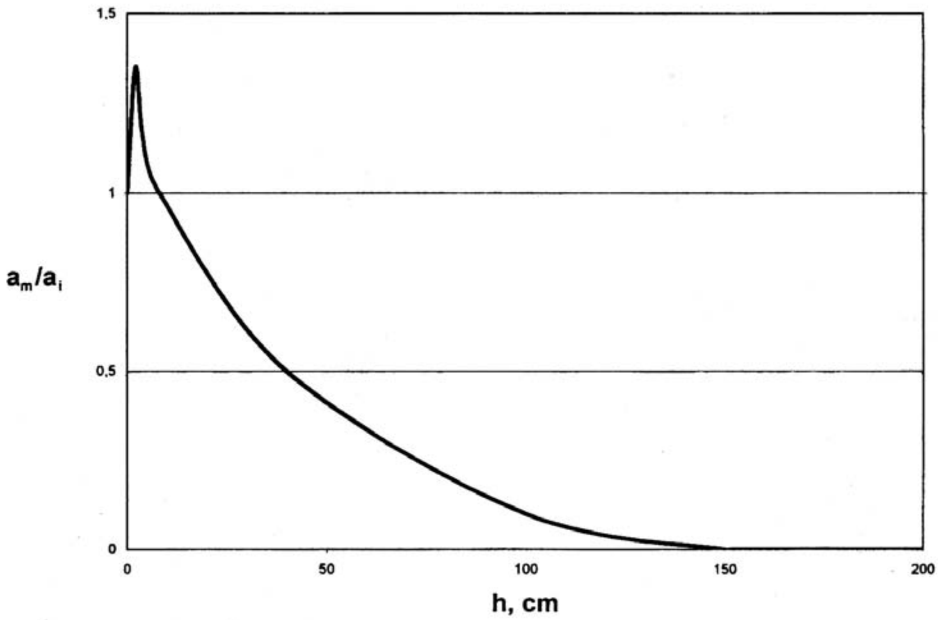

Figure 5.5: Non-dimensional ablation rate a_m/a_i dependence on moraine-cover thickness h (cm) for the Djankuat glacier. A_m is the ablation rate under the debris layer (mm/day) and a_i the ablation rate of bare ice (mm/day) (taken from Popovnin et al. 2002)

Nakawo et al. (1981) explained the discrepancies in the thicknesses required before ablation is accelerated or suppressed found by different researchers with different thermal properties of debris and different meteorological conditions when experiments were carried out. Thus, not only debris thickness has to be considered for examining ablation under a debris layer (Nakawo et al. 1982) but also the thermal properties of debris and the meteorological conditions. However, it is very difficult to measure debris distribution in the field partly because it varies between geographical areas, and partly because collecting such data is dangerous and it is sometimes impossible to assess the entire surface of debris-covered glaciers (Rana et al. 1997). Rana et al. (1996) suggested an average thickness of debris cover of 0,5 - 1 m for the ablation area of Lirung glacier and Langtang glacier. In the 1997 study, Rana et al. showed a considerable overestimation of ablation if debris-covered areas are treated the same way as debris-free glaciers, and an underestimation if no melt is assumed for these areas. The average thermal resistance of the debris cover has been estimated from surface temperature obtained from Landsat 5 (TM band 6) images. Their simulation results revealed that the debris cover of the Lirung glacier nearly halves the meltwater production compared to a virtual glacier tongue of Lirung glacier, which is assumed to be debris-free. Thus, the additional parameter Rmuld in Equation 5.10 was introduced following Braun et al. (1993). Rmultd is given a value below 1.0 in order to reduce the meltwater production under debris layers.

The revised equations for snow- and icemelt are as follows:

$$MeltWaterSnowPack = Cfmax \cdot (Temp - TT) \cdot RexpMap \qquad \text{(Eq. 5.8)}$$

MeltWaterSnowPack: Meltwater of the snowpack (mm/time step)

$$MeltWaterGlacierClean = Cfmax \cdot (Temp - TT) \cdot RexpMap \cdot Rmult \qquad \text{(Eq. 5.9)}$$

MeltWaterGlacierClean: Meltwater of the debris-free glaciers (mm/time step)
Rmult: Parameter for accelerated melt of ice compared to snow (-)

$$MeltWaterGlacierDebris = Cfmax \cdot (Temp - TT) \cdot RexpMap \cdot Rmult \cdot Rmultd \qquad \text{(Eq. 5.10)}$$

MeltWaterGlacierDebris: Meltwater of the debris-covered glaciers (mm/time step)
Rmultd: Parameter for reduced meltwater production under debris cover (-)

5.3.4 Annual mass balance of glaciers

The annual mass balance at a given point of a glacier is defined as the sum of water accumulation in the form of snow and ice and the corresponding ablation over the whole year (Paterson 1994):

$$b_a = a_a + c_a = \int_{t_0}^{t_1} [c(t) + a(t)]dt \qquad \text{(Eq. 5.11)}$$

b_a: Specific annual mass balance at a given point (m)
a_a: Annual ablation (m)
c_a: Annual accumulation (m)
c(t): Accumulation rate over time t, e.g. 1 day (m/day)
a(t): Ablation rate over time t, e.g. 1 day (m/day)
t_0: First day of the measurement year (usually 1st October)
t_1: Last of measurement year (usually 30th September the following year)

The annual mass balance of the glacier corresponds to the integration of the specific point balances b_a over the whole glacier area (Paterson 1994):

$$B_a = \int_{s_g} b_a ds = \int_{s_{ac}} b_a ds + \int_{s_{ab}} b_a ds \qquad \text{(Eq. 5.12)}$$

B_a: Total annual mass balance of the glacier (m^3)
s_g: Area of the glacier (m^2)
s_{ac}: Accumulation area of the glacier (m^2)
s_{ab}: Ablation area of the glacier (m^2)

Different methods exist to determine the annual mass balance at a set of points in the accumulation area and the ablation area (Paterson 1994). Total annual mass balance of the entire glacier is obtained via spatial interpolation. TAC[d] enables the estimation of the annual mass balance based on the hydrological simulation outputs. For each cell with glacier cover (nRGType 2, 3), the mass balance is calculated based on the simulated snow accumulation and the simulated snow- and icemelt (Schaefli et al. 2005):

$$MassBalance = SnowpackforBalance - MeltWaterGlacierforBalance - MeltWaterSnowpackforBalance \qquad \text{(Eq. 5.13)}$$

MassBalance: Annual glacier mass balance (mm)
SnowpackforBalance: Annual snow accumulation (mm)
MeltWaterGlacierforBalance: Annual meltwater of glaciers (mm)
MeltWaterSnowpackforBalance: Annual meltwater of snow (mm)

The annual mass balance of the entire glacier is the arithmetic mean of the mass balances of single cells belonging to the same glacier. Further, the equilibrium line altitude which is the altitude where accumulation and ablation balances out is calculated in the model.

5.4 Soil routine

The concepts of the soil routine (Chapter 4.2.2) were not revised in this study. However, different parameters can be used to simulate different hydrological response units (HRUs). Generally, soil is rare in the catchment thus the main function of the soil routine is to calculate actual evaporation before water reaches the runoff generation routine.

5.5 Runoff generation routine

The arrangement of the linear storages (Chapter 4.2.3) had to be adjusted to simulate the runoff generation processes of a high alpine catchment. In order to yield a more precise process simulation, four HRUs were defined according to their specific runoff generation types (nRGType). Each of the HRUs has a specific conceptual composition of the storages within a cell. The storage characteristics are defined by parameters such as storage coefficients, maximum storage levels and values for vertical fluxes (Chapter 4.2.3). The HRUs are as follows:

- Non-glacier area (nRGType 1)
- Glacier area (nRGType 2)
- Glacier area with an inclination of less than 3° and debris cover (nRGType 3)
- Valley bottom with an inclination of less than 8° (nRGType 4)

In partly glacierized catchments, runoff consists of liquid precipitation and meltwater (Menzies 2002). NRGType 1 represents the ice-free parts of the catchment except for the glacial gravel beds in the main valley of the catchment. Two form of storage are chosen to represent fast and slow runoff components. The fast components can be interpreted as preferential pathways like macro pore flow which is common in areas covered by gravel and boulders. Retardation of flow can be caused by depressions and by micro pores in the finer debris under the gravel or boulders. The slow runoff components can be attributed to drainage of water in fissures of the rocks which drain slowly.

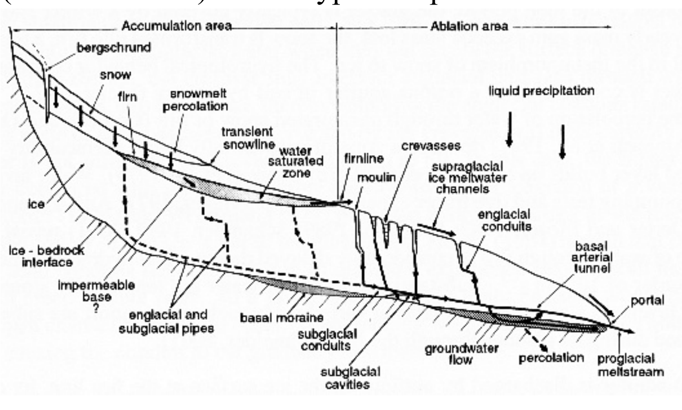

Figure 5.6: Schematic diagram of supraglacial, intraglacial and subglacial drainage pathways of a temperate glacier (after Röthlisberger and Lang (1987), taken from Schuler 2002)

Several runoff components in glaciers can be described (Moser et al. 1986). The drainage system of glaciers can be subdivided into supra-, intra-, subglacial drainage systems (Figure 5.6).

In the firn area water infiltrates the unsaturated porous snow and firn. Usually, snow and firn have a high storage capacity due to the connected pores (Colbeck 1972). Storage capacity is determined by the metamorphism of the snow (Male 1980). The ice represents the impermeable layer on which meltwater drains supraglacial on the ice surface. A supraglacial drainage network develops during the ablation period consisting of connected channels, ending in crevasses or moulins. The storage capacity of ice is lower than the storage capacity of snow and firn (Nesje et al. 2000). However, water can be stored in fissures (“water-veins”) and small pools (Mader 1992). Water is usually directed vertically through the intraglacial drainage system. The subglacial drainage system develops during ablation period to a channel network (Nye 1976). While doing so, meltwater extends the channels because of mechanical friction and friction heat causing thermal erosion (Röthlisberger 1972, Shreve 1972). Meltwater drainage through a glacier can be compared with runoff generation of a karst aquifer (Hooke 1989). According to Röthlisberger (1972) water fluxes concentrate in main channels due to decreasing pressure in the ice channels with increasing water drainage. Water pressure works against ice pressure and prevents the closing of the channels. As water pressure diminishes, ice pressure becomes more important and constricts the channels. These processes adjust the channels to the meltwater amount in time scales of weeks and months. Water leaves the glacier through the glacier terminus. Moser et al. (1986) subdivided runoff of glacierized catchments according to its origins: runoff from ice area and runoff from firn and snow areas (Figure 5.7).

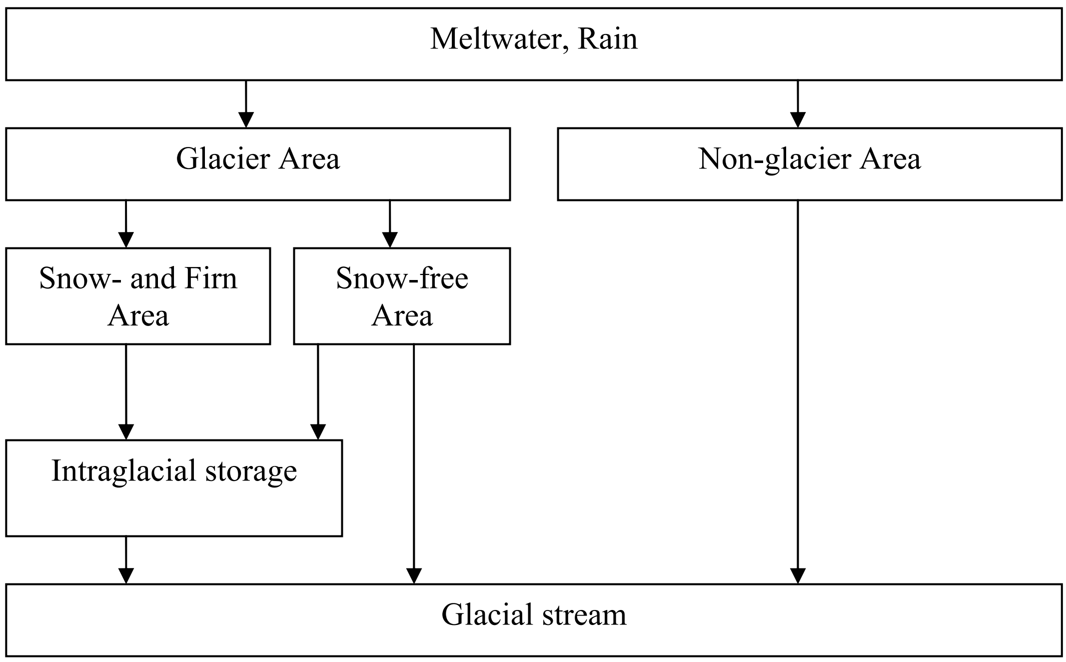

Figure 5.7: Runoff scheme of glacierized catchments (taken from Moser et al. 1986, revised)

In line with these considerations, glacier-covered parts of the catchment (nRGType 2), except for the valley glaciers with an inclination of less than 3° and debris cover, are treated with the same concepts as nRGType 1, but with different parameter values.

Input from the soil routine (ToRunoffGeneration) fills the upper storage box (US_box) and is controlled by the parameter US_P of the lower storage box (LS_box). Fast runoff components and interflow are simulated by the upper storage with limitation of storage capacity. If the upper limit of the upper storage (US_H) is reached, water flows directly to the next downstream cell without retardation. In this case, runoff from the upper storage is composed of the outflow of the storage, determined by the storage content (US_box) and the storage coefficient (US_K), and of the additional water which exceeds the storage capacity (US_box-US_H). Percolation into the lower storage occurs via a constant value (US_P). The outflow from the lower storage is also defined by the storage content (LS_box) and the storage coefficient (LS_K) and represents the slow baseflow component. There is no upper limit of this storage. Figure 5.8 shows the conceptualization of the runoff generation routine of nRGType 1 and 2.

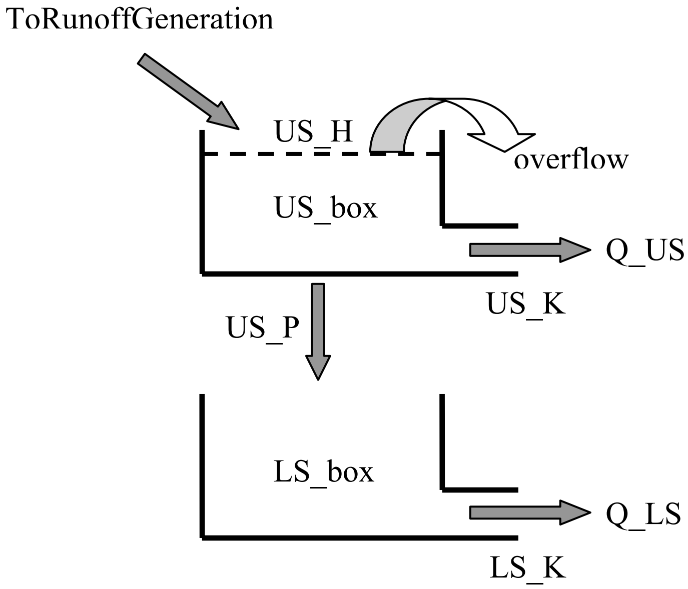

Figure 5.8: Conceptualization of the runoff generation routine of nRGType 1 and 2

The third HRU are the glacier tongues with an inclination of less than 3° and debris cover (nRGType 3). Glacier storage is a widely used term, applied to different processes and time scales by different disciplines in hydrology and glaciology (Jansson et al. 2002). Three time scales can be identified where storage occurs: Long-term storage concerns storage of ice and firn as glaciers on time scales of years to centuries and longer, intermediate-term storage is applicable to processes such as storage and release of snow and water, in and on a glacier on a seasonal time scale and the short-term storage concerning diurnal effects of drainage through the glacier (Jansson et al. 2002). Figure 5.9 summarizes the forms of glacier storage and the corresponding time scales.

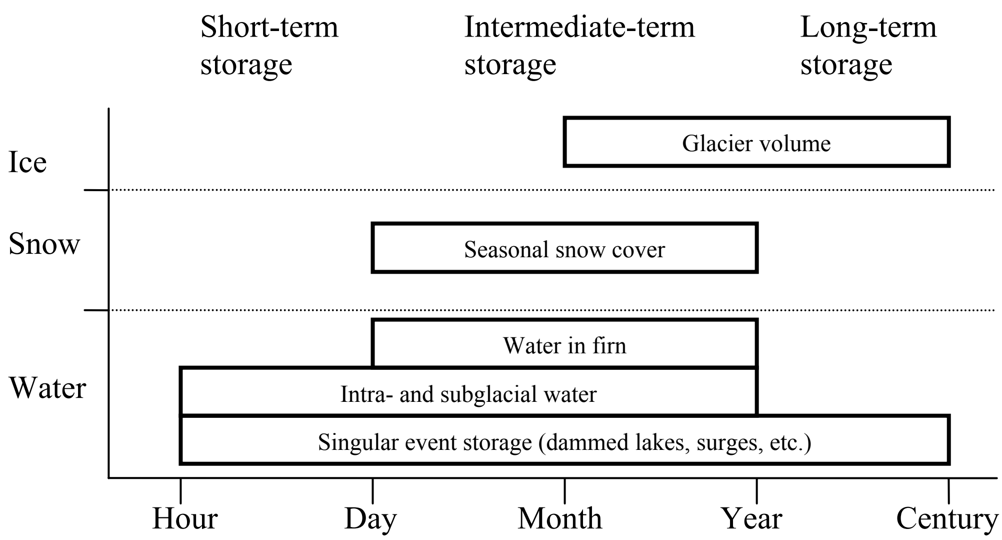

Figure 5.9: Forms of glacier storage and the corresponding time scales (taken from Jansson et al. 2002, revised)

Water can be stored in various ways: in surface snow and firn, surface pools, intraglacial pockets, subglacial cavities, crevasses, intraglacial and subglacial drainage networks and in basal sediments. As shown in Chapter 3.3, winter discharge is quite high in the Langtang Valley although there are neither liquid precipitation nor melting conditions from post-monsoon to pre-monsoon season. Motoyama et al. (1987) argued that winter discharge of the Langtang Khola is supplied from the outflow of englacial water and from bottom meltwater of the glaciers. This hypothesis is supported by drilling results on Yala glacier revealing the existence of abundant water in the glacier body which flowed in the post-monsoon season in the accumulation and ablation zone of Yala glacier (Iida et al. 1984). Winter discharge has been observed from many temperate glaciers (e.g. Vallon et al. 1976, Östling et al. 1986; Kohler 1995). For conceptualization of the runoff generation processes of the third HRU, only one storage is used. Storage capacity is limited by an upper limit (GlacierLS_H). Runoff of this storage (GlacierQ_LS) is computed by applying a storage coefficient (GlacierLS_K) with additional water if the storage content (GlacierLS_box) exceeds GlacierLS_H. This conceptualization is based on the assumption that the large valley glaciers can store a great amount of water in pools or small sub- and supraglacial lakes. Thus, GlacierLS_H is larger than the upper limits of the storages of nRGType 1, 2 or 4.

A fourth HRU (nRGType 4) was identified based on information acquired during field visits and on area photographs. The valley bottom with an inclination of less than 8° is considered to be an aquifer consisting of glacial gravel beds where water can be stored. The same structure of storage as in nRGType 3 is used to simulate the hydrological processes but with different parameterization for different flow dynamics. Figure 5.10 shows the conceptualization of nRGType 3 and 4. The threshold inclinations of 3° and 8° for delineation of nRGType 3 and 4 are used because hydraulic properties of glaciers with inclinations of more than 3° or glacial gravel beds with inclinations greater than 8° are considered to be inadequate to store large amounts of water. Due to the assumed well-developed subglacial drainage systems the threshold inclination of nRGType 3 must be smaller. Sub- or supraglacial pools or lakes cannot develop in steeper parts of the glacier tongues. Supraglacial lakes have only been observed on debris-covered glaciers in the Langtang valley.

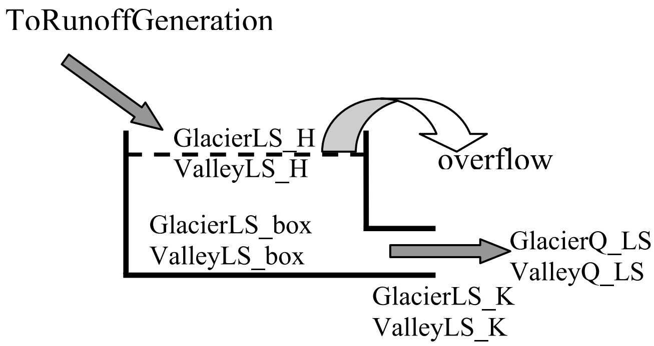

Figure 5.10: Conceptualization of the runoff generation routine of nRGType 3 (Glacier*) and 4 (Valley*)

5.6 Lateral flows

The distributed structure of TAC[d] enables the simulation of lateral flows from one cell to the next cell. Based on the local drain direction network (ldd), flow directions are determined according to the steepest slope between the cells (PCRaster 2004): Figure 5.11 gives an overview of the lateral connection of the HRUs. Within nRGType 1, 2 and between both nRGTypes, runoff from the upper storage is directed laterally to the US_box of the next downstream cell, whereas runoff from the lower storage is directed laterally to the LS_box of the corresponding cell. Runoff of US_box and LS_box of nRGType 1 or 2 is directed to GlacierLS_box of nRGType 3 and into ValleyLS_box of nRGType 4. Outflow of nRGType 3 flows into the upper storage of nRGType 1 or 2, or if the next downstream cell belongs to nRGType 4, into the ValleyLS_box. NRGType 4 drains into LS_box if nRGType 4 and 1 or 2 are neighbouring cells, or into GlacierLS_box of nRGType 3. All fluxes are directed to the river network if a cell is identified as a stream cell.

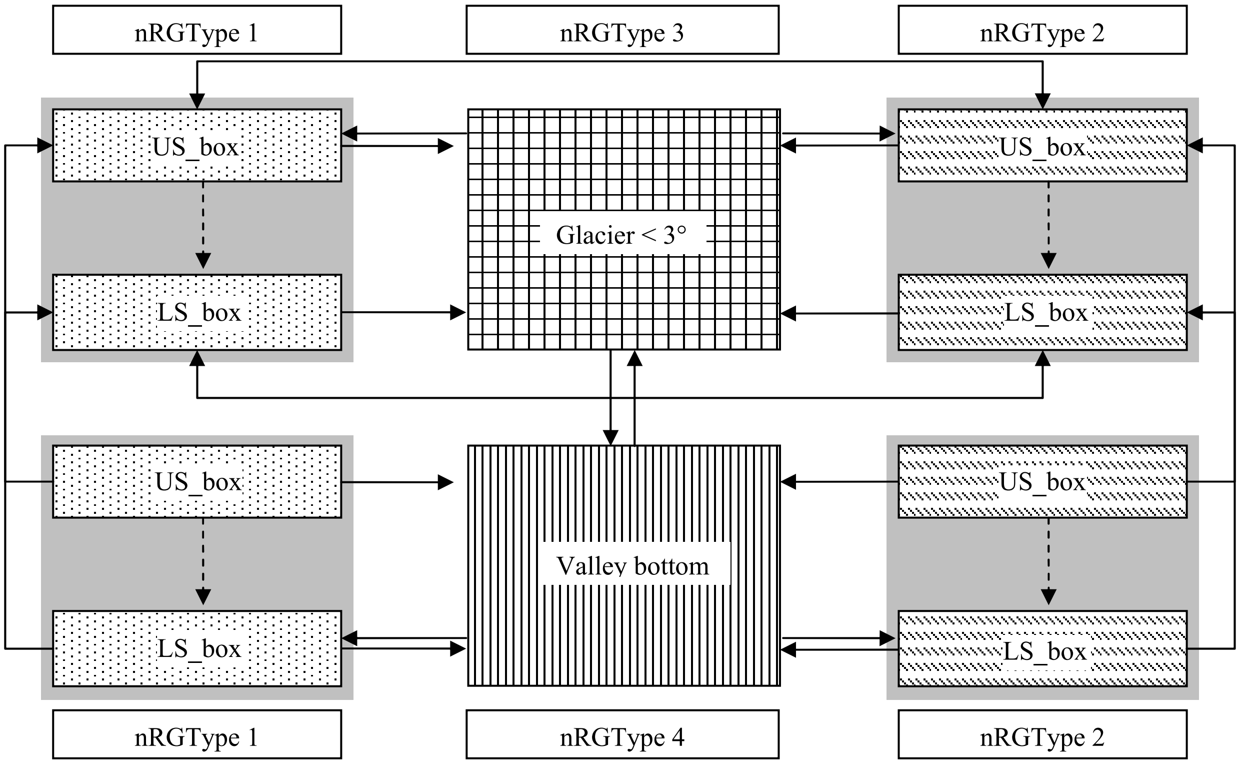

Figure 5.11: NRGTypes and their lateral connection. Solid arrows are lateral fluxes, dotted arrows are vertical fluxes between the storages

5.7 Routing routine

Once water fluxes have reached stream cells, the generated runoff from one time step is distributed on the following days using one free parameter (MaxBas), which determines the base in a equilateral triangular weighting function (Seibert, 2002):

$$Q_{sim}(t) = \sum_{i=1}^{MaxBas} c(i) \cdot Q_{beforerouting}(t - i + 1) \qquad \text{(Eq. 5.14)}$$

with the weighting function:

$$c(i) = \int_{i=1}^{i} \frac{2}{MaxBas} - \left| u - \frac{MaxBas}{2} \right| \cdot \frac{4}{MaxBas^2} du \qquad \text{(Eq. 5.15)}$$

$Q_{sim}(t)$:	Simulated discharge at time t (m³/s)
c(i):	Weight (-)
$Q_{beforerouting}$:	Simulated discharge before routing at time t (m³/s)
t:	Time (day)

i, u: Time steps (day)
MaxBas: Empirical parameter (-)

It is assumed that water remains in the river network for less than one day due to the high flow velocity of alpine rivers. Therefore the parameter MaxBas is set at 1.0 a priori.

5.8 Initialization of storages

Compared to previous applications of TAC^d, the Langtang Khola catchment has a permanent snow cover at high elevations. The two types of storage of the snow and glacier routine are the snowpack (SnowPack) and the water content of the snowpack (WaterContent). In previous versions of TAC^d these storage types were initialized as empty storages because there was no snow cover at the beginning of the hydrological year in the respective loweralpine catchments. If the storage types of the snow and glacier routine are initialized at zero the snow cover of the first simulated hydrological year consists only of solid precipitation having fallen during the winter season which precedes the first simulated monsoon season. This causes, on the one hand, a significant underestimation of snowmelt in the monsoon season and, on the other hand, overestimation of icemelt. If there is no snow cover on the glaciers and temperature is above the threshold temperature (TT), ice starts melting. Depending on the meteorological situation of the simulation period, this problem could affect more than just the first hydrological year. For this reason, additional initialization maps of SnowPack and WaterContent were introduced in this version of TAC^d.
Maps of the storage levels produced during initialization runs were used for initialization of the simulation period (Chapter 7.2).

The initialized storages are:

- Snowpack (SnowPack)
- Water content (WaterContent)
- Upper storage (US_box)
- Lower storage (LS_box)
- Glacier storage (GlacierLS_box)
- Valley bottom storage (ValleyLS_box)
- Soil moisture (SoilMoisture)

5.9 The internal water balance

Figure 5.12 shows the internal water balance of the modified TAC^d model for the Langtang Khola catchment for a simulation period of 2200 time steps. The cumulated precipitation input, as shown in the upper part of the graph, adds up to nearly 45 million millimeters. The maximum amplitude of the internal water balance, lower part of the graph, ranges from +31 mm to -17 mm. Neither an increasing nor a declining trend is evident. Therefore, the prerequisite described in Chapter 2.4.1 to consider the internal water balance as accurate is fulfilled. The increasing fluctuation with increasing time steps might be a result of rounding errors but the inaccuracies still stay within millionths of the amount of input.

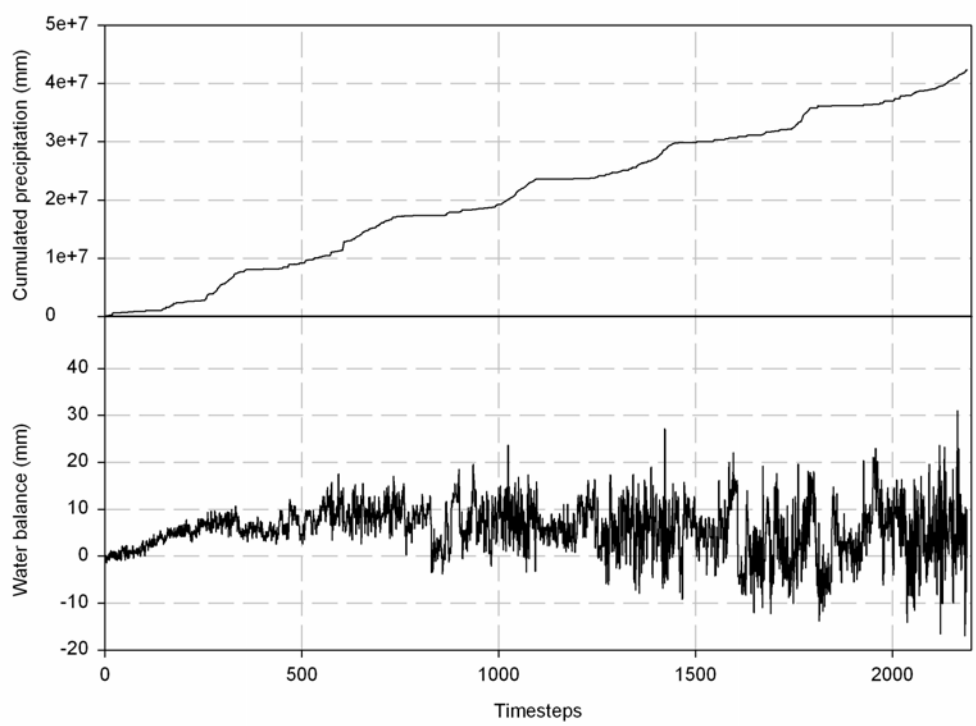

Figure 5.12: Internal water balance and cumulated precipitation input for 2200 time steps for the Langtang Khola catchment (here: 1 time step = 1 day)

5.10 Conclusions

Numerous modifications were carried out in order to adjust the model to climatologic and physiographic conditions of the Langtang Khola catchment. No significant violations of mass conservation of the modified TAC^d could be detected.

As far as possible the conceptual ideas behind the routines remained untouched. Implementation of glaciermelt was essential for simulations of the highly glacierized catchments such as the Langtang Khola catchment. Modifications of the temperature-index method allow a more realistic calculation of snow- and icemelt based on physiographic and topographic characteristics and astronomic parameters. Glacier mass balances can be simulated for each glacier, and these can be used for model evaluation or calibration if measured values are available.

A sinusoidal function is implemented for calculation of potential evapotranspiration, which seems to yield a realistic temporal distribution.

The runoff generation routine identifies the main hydrological response units and considers differences of runoff dynamics between them. The routing routine is quite rudimentary but adequate for this application as water leaves the catchment quickly once the river network is reached. Thus a complex wave routing is not necessary. Figure 5.13 gives an overview of the structure of TAC^d and the sequential order of routines either modified or taken from previous versions of TAC^d.

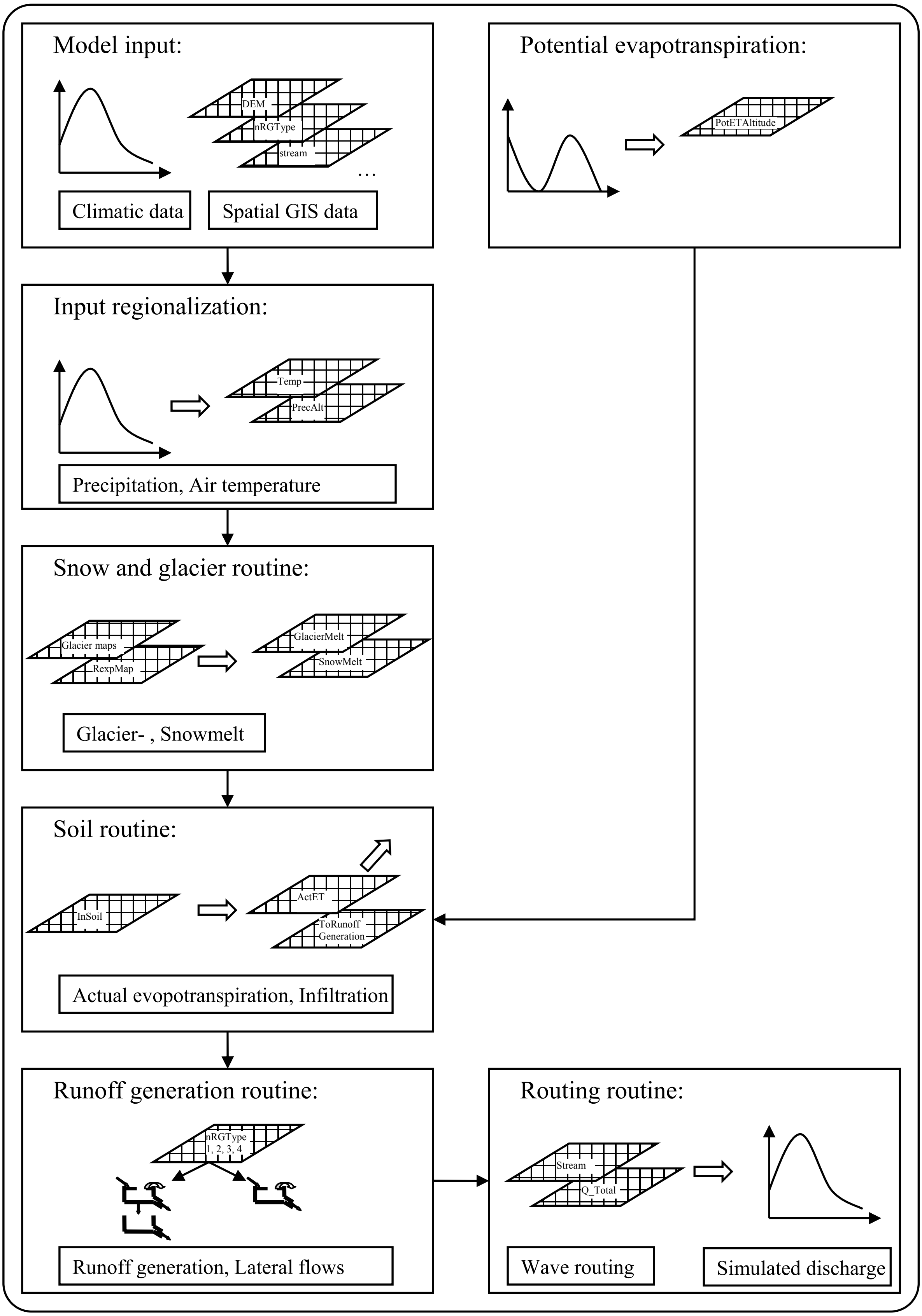

Figure 5.13: Structure of TAC[d] with the most important input and output maps or time series of each routine

6 Preprocessing: Data base and data processing

The preprocessing section in hydrological modeling contains the data processing of climatological input data and spatial data. In case of distributed modeling various digital maps need to be produced to provide spatial information in an adequate resolution and in the correct format demanded by the respective program environment used for the development of the model. Complete time series of meteorological input data are a prerequisite for the model application. This information has to be transformed into a specific format as well. In this study an intensive quality check of meteorological data was necessary, and gaps in time series of daily mean air temperature and daily sums of precipitation had to be bridged with appropriate methods.

6.1 Data collection at stations of the Snow and Glacier Hydrology Unit (SGHU)

Snow and glacier hydrological investigations have started in 1987 by the Department of Hydrology and Meteorology (DHM) in collaboration with the German Agency for Technical Cooperation (GTZ) within the framework of an expert fund provided by the government of Germany (Grabs et al. 1993). During this period three hydro meteorological stations were established in Annapurna, Langtang and Khumbu regions with the purpose of systematic collection of hydrological and meteorological data. Up to now 3 further stations were established and the project is undertaken by His Majesty's Government of Nepal, DHM.
Daily mean discharge is derived from 4-hourly gauge height measurements and stage-flow-relations. Rating curves are calculated using dilution techniques for discharge measurements. Air temperature is measured with Thermohydrographs and charts are evaluated in 6 h intervals and published as maximum, minimum and mean daily air temperature. Precipitation is read manually and published as daily total.
Data are published in yearbooks by His Majesty's Government of Nepal, Ministry of Science and Technology, Department of Hydrology and Meteorology, Snow and Glacier Hydrology Unit, Kathmandu, Nepal. Pictures in Figures 6.1 and 6.2 show the meteorological station of the Langtang Khola catchment and the position where gauge height is measured.
Most of the stations of the Snow and Glacier Hydrology Unit (SGHU) are situated in higher Himalayan regions. The access to these Himalayan catchments is rather difficult and it takes a long travel to reach the stations from Kathmandu. Due to this fact the data collection at SGHU stations has been outsourced to local staff living close to the station. These data observers are originally farmers or mountain guides and are often not familiar with the scientific demands for a reliable data basis. The environmental conditions in the high alpine Himalayas are rough, too. As a result, the time series of precipitation, air temperature and gauge height show data gaps caused by measurement errors, avalanches, hail, thunderstorms or heavy rainfall during monsoon season. These harsh weather conditions cause considerable damage to the stations and the instruments. Vandalism by local people and animals is also a reason for data loss. SGHU has made a lot of efforts to improve data collection and to keep the stations operational throughout the whole year. Emergency field visits in addition to regular field visits and training of local staff are some of these efforts to provide more reliable data. Despite of this, remoteness and inaccessibility of stations during monsoon and winter season sometimes delay the maintenance work of the stations. Figure 6.3 shows the availability of precipitation, air temperature and gauge height data of the Langtang Khola catchment. More details are summarized in Table A1 (Appendix) for each hydrological year.

Figure 6.1: Outlet of Langtang Khola catchment where water level is measured at 3600 m a.s.l.

Figure 6.2: Meteorological station of Langtang Khola catchment situated in Kyangjing at 3920 m a.s.l.

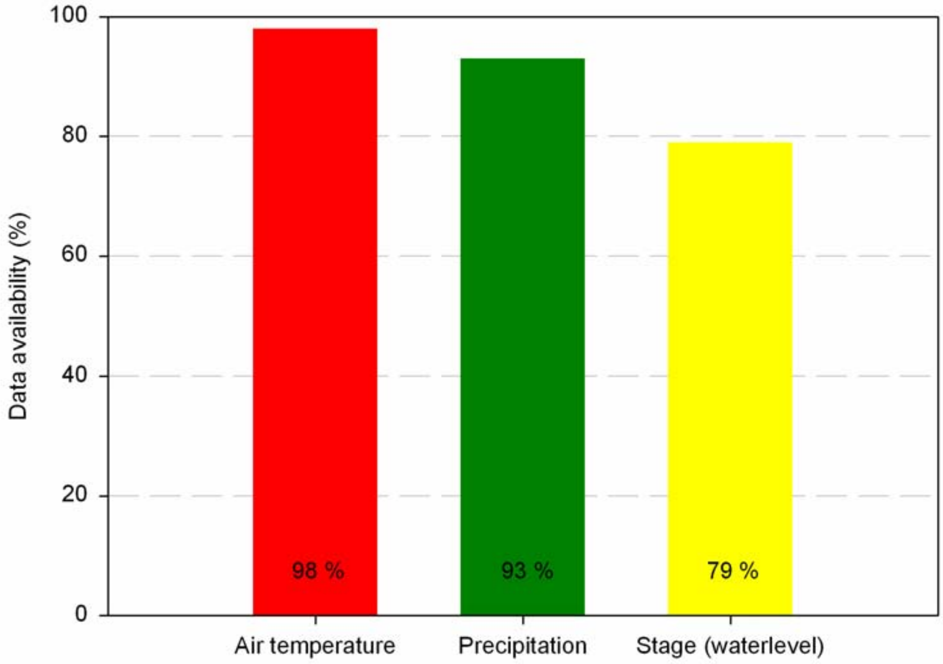

Figure 6.3: Data availability at Langtang Khola catchment

6.2 Daily discharge data

Discharge data are derived from gauge height readings and stage-discharge calibration measurements executed by SGHU staff during their field trips throughout the year. Tracer dilution methods are used to measure discharge as described by Spreafico et al. (1993). Based on these measurements SGHU derives rating curves to calculate daily discharge values. In this study additional stage-discharge-relations were calculated applying various regression functions like exponential-, potential- and linear regression functions and the calculated discharges were evaluated and corresponding R^2-values given. The potential function as proposed by SGHU (Equation 6.1) is considered to be the most reliable one to derive discharge data from gauge height measurements with $R^2 = 0.92$. Discharge measurements are available for water levels between 0.49 m and 1.72 m.

$$Q = 8.409\,(h - 0.078)^{1.334} \quad \text{(Eq. 6.1)}$$

Q: Discharge (m^3/s)
h: Gauge height (m)

Intensive data analysis was necessary to ensure the reliability of discharge data. For the investigation period of 1987 to 1998 daily gauge height data were plotted and checked for consistency. A typical error detected by this procedure is demonstrated in Figure 6.4. The bold orange line is the discharge calculated with original gauge height values as published in SGHU yearbooks, which is obviously inconsistent. Compared with other years it seems that the original values of gauge heights were recorded, where 1 m was erroneously subtracted (0.40 m instead of 1.40 m). In that case the original yearbook values were adjusted by adding 1.0 m to each daily value of the respective period in accordance with original staff gauge data sets (handwritten). The blue line shows the discharge calculated from revised gauge height. The revised discharge data are used for model evaluation and calibration.

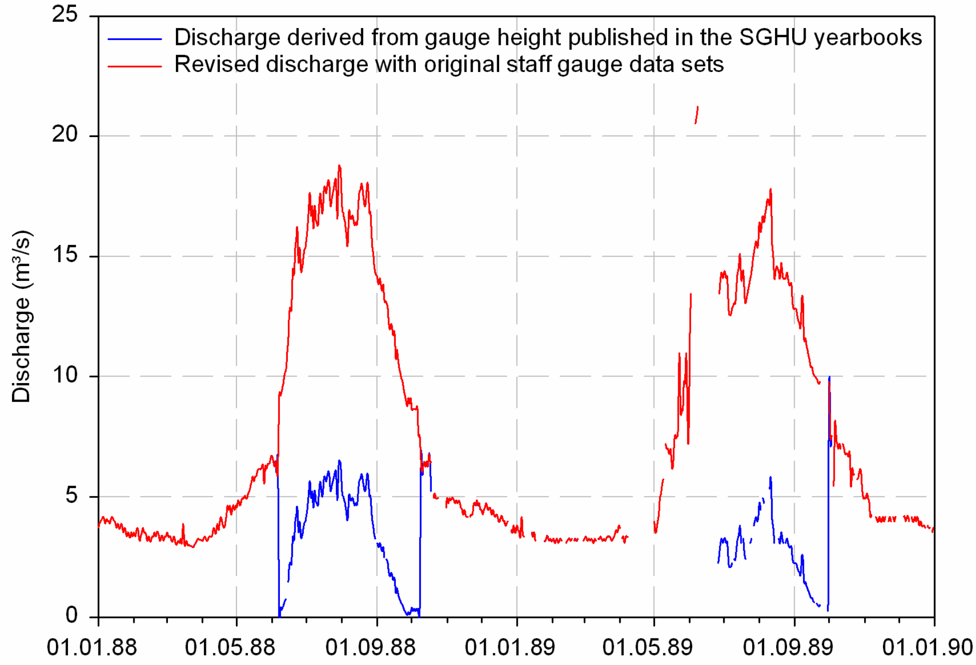

Figure 6.4: Typical error in discharge data calculated from gauge height as published by SGHU and the revised discharge data. In the erroneous discharge data stage level were recorded that were 1.0 m too low

Another inconsistency was detected for the hydrological year 1997/98 when the low flow period seems to show inaccurate values. Again, the original staff gauge data were used to revise the published data as shown in Figure 6.5.

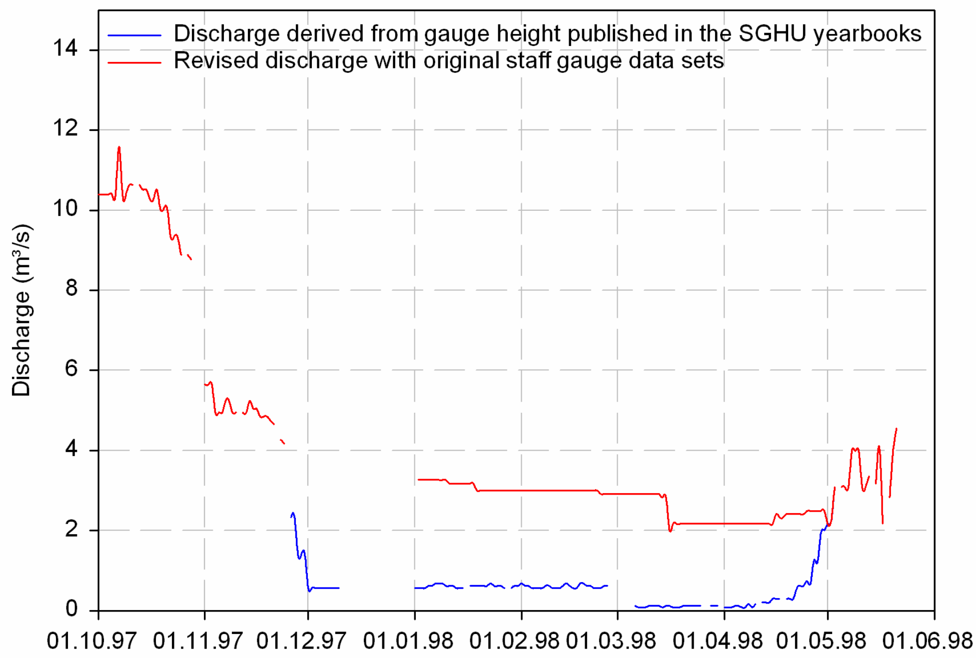

Figure 6.5: Original and revised discharge data of the low flow period of the hydrological year 1997/98

6.3 Daily air temperature data

Daily air temperature data are available for 98 % of the investigation period. This can compete with European standards. However, hydrological models require data sets without gaps. Thus, an appropriate procedure to bridge the gaps in air temperature time series had to be found based on air temperature data of reference stations of the Standard Data Meteorological Service Network of DHM in the vicinity of the Langtang valley. Table 6.1 summarizes the reference stations with elevation, conducted measurements and the schematic map in Figure 6.6 shows the location of the stations.

Table 6.1: Summary of DHM reference stations used for data processing (P: precipitation, T: temperature)

Region	Station	Elevation (m a.s.l.)	Measurements
Langtang	Timure	1900	P
Langtang	Sarmathang	2625	P
Langtang	Kathmandu Airport	1336	TP
Langtang	Thamachit	1847	P
Langtang	Paigutary	unknown	P
Langtang	Dhunche	1982	TP
Langtang	Tarke Ghyang	2480	P

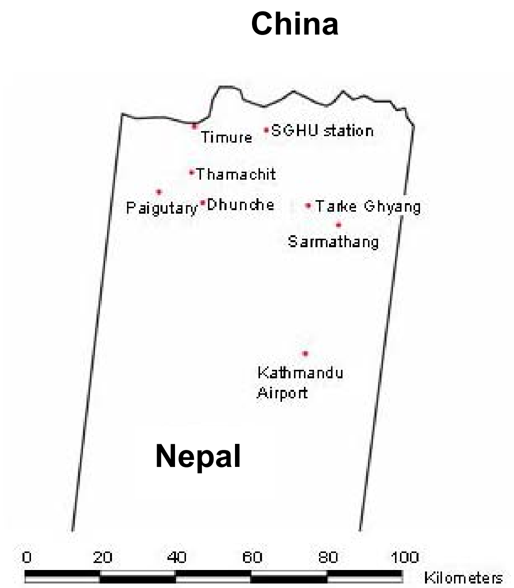

Figure 6.6: Schematic map of SGHU station and DHM reference stations in the Langtang region

6.3.1 Correction of inconsistencies in the measured air temperature time series

The time series of measured daily mean air temperature shows inconsistencies from January 1995 onwards (Figure 6.7). The mean air temperature from 1988 to 1995 is 1.79 °C, whereas it is 4.40 °C for the period from 1995 to 2000.

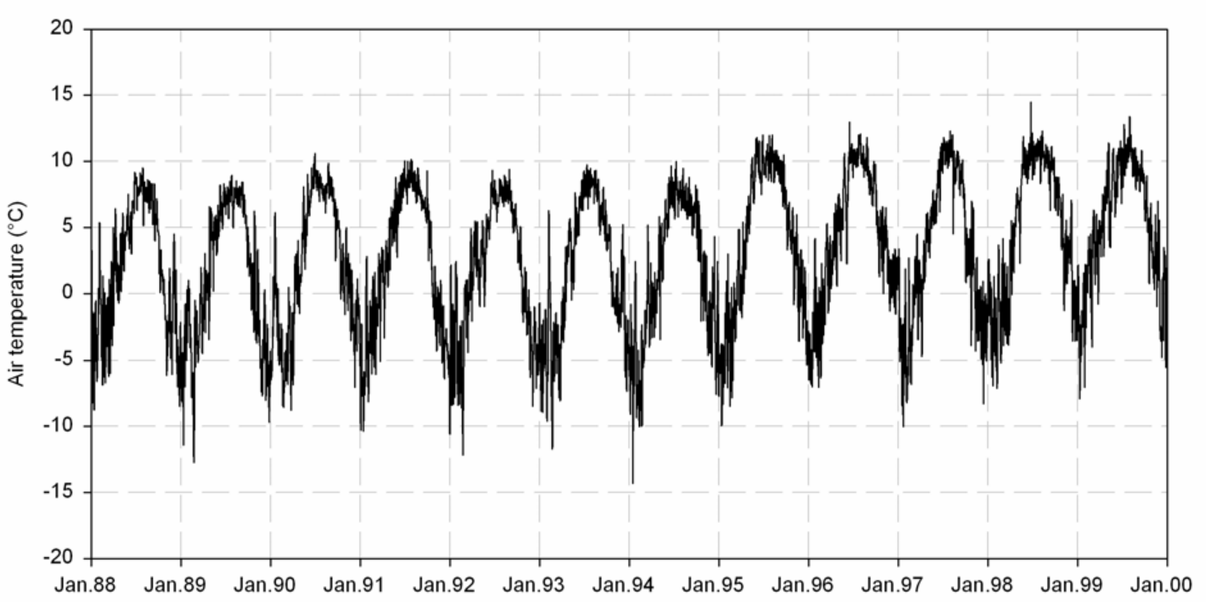

Figure 6.7: Inconsistencies in the time series of air temperature from 1988 to 2000. There is a shift from 1995 onwards

This shift has a significant impact on the discharge simulation and had to be corrected. It is assumed that the shift is caused by a systematical error in the measurement of the air temperature. Thus, the difference between both average air temperature values was subtracted from each daily value from 1995 onwards and the revised time series was taken for the simulation.

6.3.2 Extrapolation of air temperature data

The entire procedure of data processing in case of daily mean air temperature data shall be described with the example year 1997 and is based on Weber (1997). The method was applied to each year of the period from 1987 to 1998 where data gaps occur.

6.3.2.1 General remarks and data analyses

The current value of air temperature (generally measured 2 m above ground) does not only depend on the entire synoptic situation and the altitude above sea level but also on local vertical and horizontal exchange conditions. Horizontal processes can be all advective processes like local wind systems or passing fronts, vertical distribution of air temperature near the surface is connected to the surface energy balance.

Local air temperature measurements at different stations cannot be transferred directly from one station to the other due to the different specific micro climatic conditions at the meteorological station like albedo, heat conductivity of soil, water content of soil and vegetation as well as the surface roughness (Kraus 1966, Weber 1997). The mentioned impacts on local air temperature measurements are not complete but it can be clarified that even in a small area significant differences of micro climatic conditions occur. Air temperature graphs of different stations in Langtang region are given in Figure 6.8.

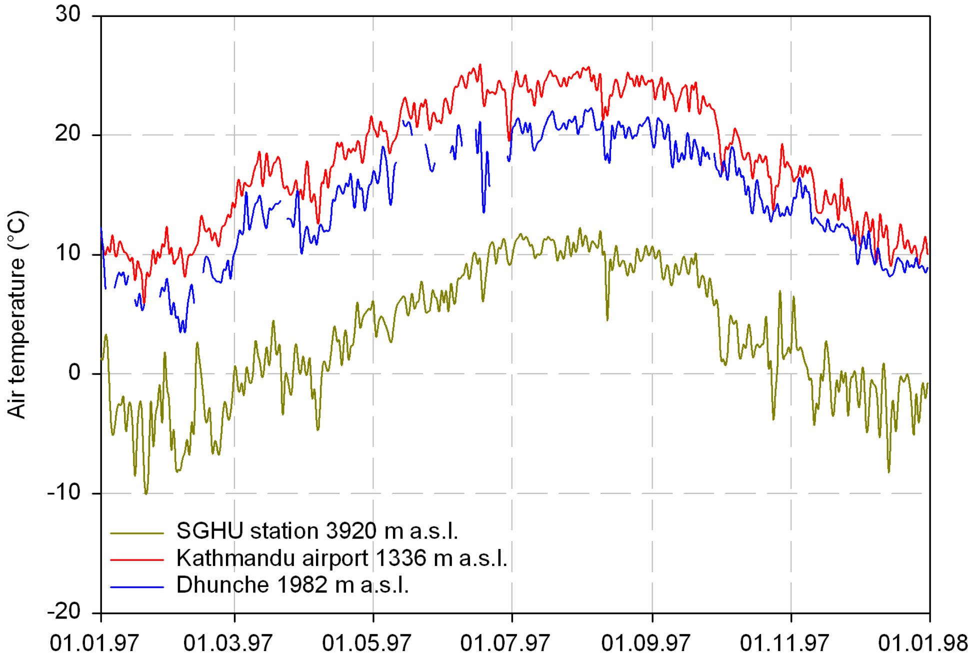

Figure 6.8: Comparison of daily air temperature at Kathmandu airport (1336m), Dhunche (1982m) and SGHU station (3920m) in Langtang region, 1997

Dhunche is located at an altitude of 1982 m around 6 km down valley from the SGHU station. It is situated on a plateau in a west oriented slope of a steep valley. Kathmandu is about 60 km south of the Langtang catchment at an altitude of 1336 m and surrounded by mountains up to 2000 m. Both reference stations show nearly the same structure in their air temperature variations with a balanced variance all around the year. A reason for this fact could be equal terrain properties of both reference stations. The day to day variability of air temperature increases with altitude (SGHU station) due to the rough climate at higher elevations. Weber 1997 explains the increasing variance with the influences of surface and orography. The variance becomes more pronounced during dry season (October to May) at SGHU station. In Figure 6.9 daily air temperature values of reference stations are ploted linearly versus SGHU data. 85 % respectively 87 % of the temperature information of SGHU station can be explained with the data of Dhunche or Kathmandu. The reference stations have a higher correlation among each other with $R^2 = 0.93$. The slope of the regression line is below 1.0 due to the high variance of the air temperature data of SGHU station. The y-axis section of the regression line corresponds well with the mean temperature differences between SGHU station and reference stations and therefore with the mean vertical temperature gradients shown in Table 6.2.

Table 6.2: Mean air temperature differences between SGHU station and reference stations and the y-axis section of the regression line of Figure 6.9 for the year 1997

	Mean temperature difference (°C)	**Mean vertical temperature gradient (K/100m)**	**y-axis section of the regression line (-)**
SGHU – Kathmandu	14.8	- 0.57	15.0
SGHU – Dhunche	11.6	-0.59	12.2

Furthermore, scattering around the regression line is larger at low temperatures (0 and below at SGHU station) than at higher temperatures, which can be explained with the higher variance of SGHU data during dry season.

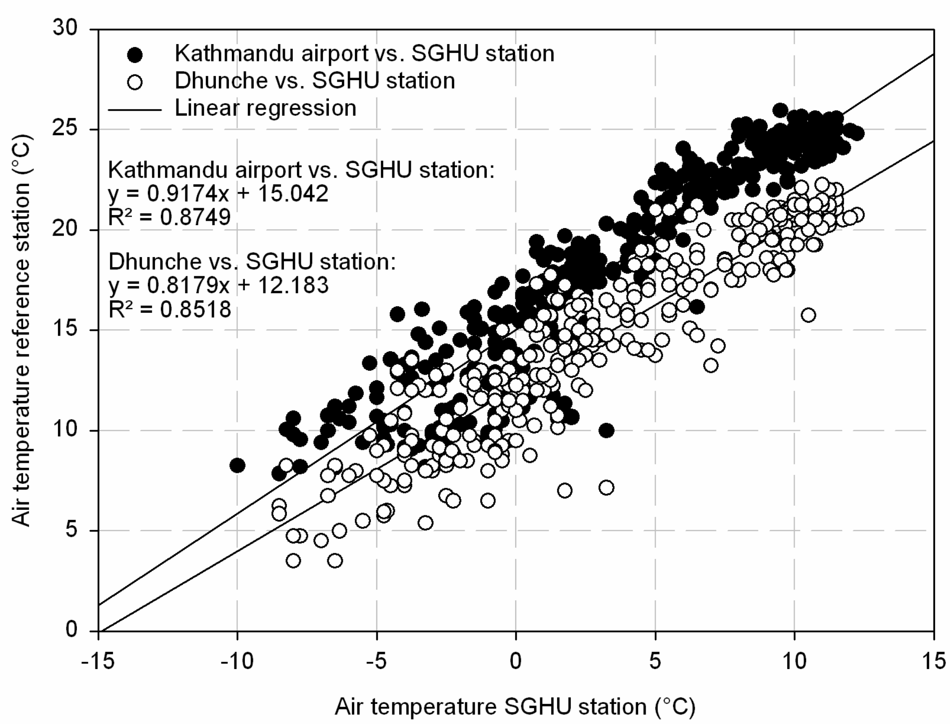

Figure 6.9: Comparison of daily mean air temperature values of SGHU station (3920m) with Kathmandu (1336m) and Dhunche (1982m) meteorological station, 1997

6.3.2.2 Procedure of extrapolation of daily mean air temperature values

Literature (e.g. Hormann, 1994) provides various methods of temperature regionalization in high alpine regions, most of them being regressive approaches. These methods mostly require a remarkable station density which is not available in the Nepal Himalayas. Therefore, the regionalisation method applied here is derived from the vertical gradient as follows:

$T_{SGHU} = T_{Ref} + grad \cdot \Delta z$ (Eq. 6.2)

T_{SGHU}:	Temperature at SGHU station (°C)
T_{Ref}:	Temperature at reference station (°C)
grad:	Vertical temperature gradient (K/100m)
Δz:	Altitude difference (m)

Not taking into account the horizontal information can be justified with the use of daily mean temperature values which make the specific synoptic impacts at the stations neglectable in such a small area under investigation. More arguments can be found in Weber (1997). A linear regression like Equation 6.2 does not consider seasonal variation of regression parameters. However, Figure 6.10 shows a significant difference of the vertical air temperature gradients between monsoon and dry period.

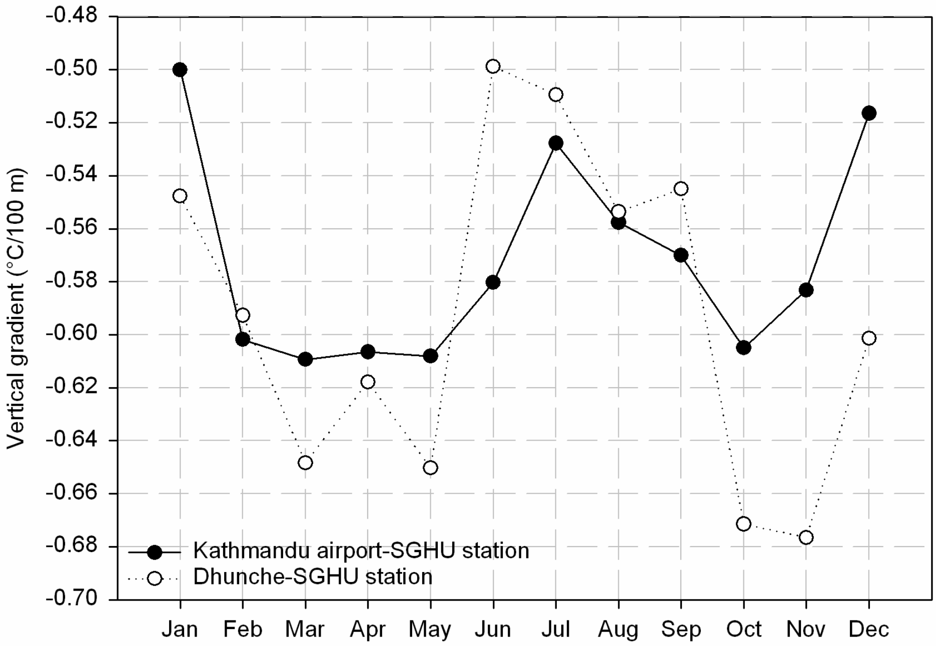

Figure 6.10: Vertical monthly air temperature gradients between SGHU station and Kathmandu and between SGHU station and Dhunche, 1997

As a conclusion of the analysis of temperature gradients it can be stated that a constant mean gradient would overestimate the air temperature at SGHU station in winter and underestimate the air temperature in summer.

Figure 6.9 shows, that an extrapolation of air temperature data of SGHU station with a temperature dependent linear regression with the data of either Kathmandu or Dhunche is more accurate for higher temperatures than for temperature at freezing level. In the precipitation-runoff model high temperatures are responsible for snow- and icemelting, while temperatures around freezing are responsible for distinction of melting or refreezing of water in the snowpack and for distinction between snowfall or rain. Thus, air temperature around freezing level is of great importance for the simulation of the snowpack.

Temperature values only show gaps of a few days of the respective years (Table A1, Appendix) except October and November 1987. Therefore, it is useful to derive air temperature values with a method based on annual data and not on average values of the entire period. This takes into account the specific synoptic situation of each year.

For the extrapolation of temperature values a universal regression method is useful, analogue to the linear regression, which depends only on temperature values of the reference stations. Weber (1997) suggests a second order polynomial function:

$$T_{Ref} = A \cdot T^2_{SGHU} + B \cdot T_{SGHU} + C \qquad \text{(Eq. 6.3)}$$

A,B,C: Coefficients (-)

The coefficients A, B, C are regressively determined from mean monthly air temperature values as shown in Figure 6.11.

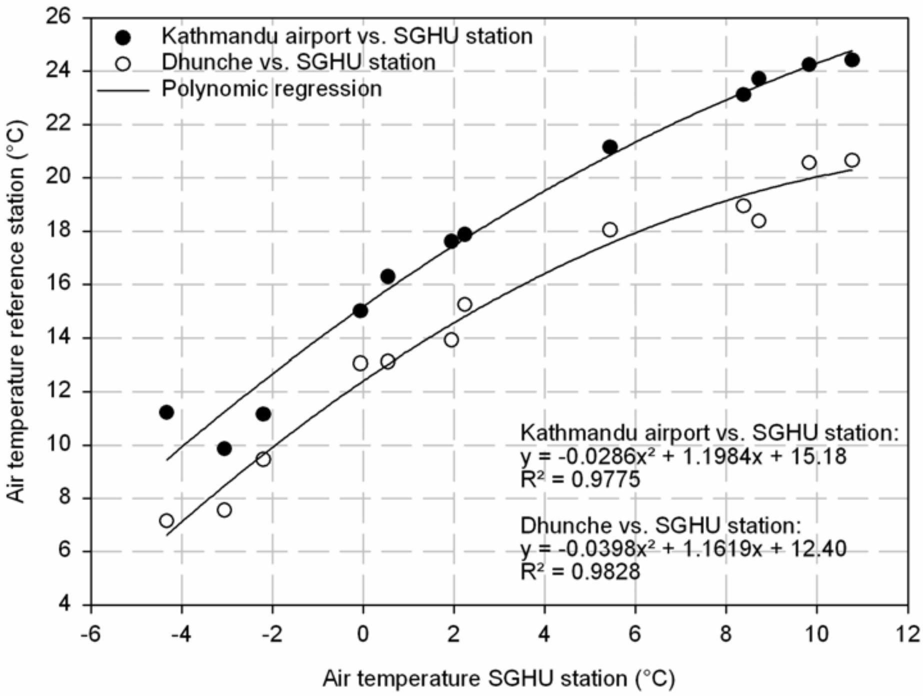

Figure 6.11: Empirical relation between reference stations and SGHU station with a second-order polynomial function, 1997

Weber (1997) states that the value of C gives approximately the mean annual temperature difference between the stations. The B value should be near 1 and A describes mainly the impact of atmospheric stratification. Usually this value is negative with a magnitude of around -0.03. If the coefficients differ significantly from these values the simulation might be unrealistic. Furthermore it is essential that the regression is performed with the values of the reference station as the independent variable to cover the entire range of values of the SGHU station. Only within the range of values of the SGHU station the curve has the appropriate curvature. If the curvature increases above A = |0.05| (Weber 1997) the range of values of the function for T_{Ref} will be limited unrealistically for higher temperature values. A larger curvature could be the result of a wrong representation of parts of the range of values of the stations due to many missing data in a specific period, e.g. in the monsoon season. This is not a problem in the Langtang Khola catchment because of good data availability. The application of the second order polynomial function improves the fit as compared to a linear function (Table 6.3).

Table 6.3: Comparison of regression analysis between monthly mean air temperature values of the SGHU station and reference stations with different regression models

Reference station	R^2-value for polynomial function	R^2-value for linear function
Kathmandu	0.9775	0.9656
Dhunche	0.9828	0.9539

This finding corresponds well with the results of temperature extrapolation at Vernagtferner, Austria (Schulz, 1999). The curvature lies within the intended magnitude for all years. The only exception is the year 1987 where October and November shows greater gaps of more than 10 days. The curvature is A = -0.0466 in that year. Weber (1997) and Schulz (1999) found for the Annapurna region (Nepal) and the Vernagtferner (Austria), respectively, that the coefficients only vary slightly from year to year and can be considered as nearly constant for a station. The same can be stated for the Langtang Khola catchment in periods when data availability is appropriate. Therefore an average of each coefficient (A, B, C) was calculated for the period 1988 to 1998 and applied for extrapolation of the air temperature values of the year 1987 where the number of missing data is to large to derive representative coefficients. The reference station Kathmandu is a station at an airport and therefore complete data sets are available from 1987 to 1998. Thus, for data extrapolation Kathmandu was taken as reference station to derive the required coefficients.

6.4 Daily precipitation data

Daily sums of precipitation are available for 93 % of the investigation period. Most of the gaps occur during the dry season (Table A1, Appendix). Low level reference stations in the vicinity of the SGHU station (Table 6.1) are used for extrapolation to bridge the gaps. The filling of data gaps is necessary if observations are missing or only sums over several days were recorded instead of daily readings (Braun et al. 1998). These sums had to be redistributed over the previous days. The analyses described here were processed for all years within the investigation period.

6.4.1 General remarks

Nepal's precipitation regime is of a continental type and predominantly convective (Chapter 3.2.2). There are distinctive dry seasons and rainy seasons where precipitation events are short but very intensive. In the dry season precipitation is quite rare as well as days without precipitation in rainy season. These characteristics enable an approach to reconstruct daily values of precipitation at a SGHU station with adequate reliability.

If precipitation is solid it will be assigned to the snow storage of TAC^d and contributes to runoff maybe weeks or months later when the snow cover is melting. Therefore, it is more important to get the total amount of snowfall rather than the correct temporal distribution. Stricter rules must be set in case of rainfall. If storages are filled, liquid precipitation contributes to runoff directly, therefore it is important to get the correct timing of daily rain events.

The TAC^d model considers numerous processes which are important for runoff calculation, and the exact assignment of amount and time of precipitation is only one factor. Also important for runoff calculation is the correct timing of meltwater production, which is, however, directly related to temperature. In any case, it is important to derive representative time series of precipitation and air temperature to simulate short term fluctuation in runoff.

6.4.2 Procedure of extrapolation of daily sums of precipitation

The procedure of extrapolation of daily sums of precipitation is a statistical based method, developed by Weber (1997), which takes different reference stations of the corresponding region into account. An intensive statistical analysis of the time series of the SGHU station and the reference stations revealed that none of the seven reference stations in the Langtang region corresponds well with the SGHU station.

Precipitation data of SGHU station and the reference stations were analyzed after following criteria:

a) Determination of the occurrence probability of precipitation events for each station for each month;
b) Determination of the joint probability of precipitation occurrence at the SGHU station and the DHM reference stations;
c) Determination of the mean ratio of monthly sums of precipitation at the SGHU station and the DHM reference stations;
d) Determination or estimation of the “true” monthly sums of precipitation at the SGHU station.

The criterion for a) is the number of days per month with more precipitation than the 1 mm. The number of days with or without joint precipitation at SGHU and reference stations is the criterion for b). The ratio of c) delivers a dimension of the amount of precipitation which can be expected during a precipitation event at the target station (SGHU station). In high alpine regions an increasing amount of precipitation with altitude like in low lands gets less pronounced. Local upwind-downwind effects are dominant and the theoretically possible amount of precipitation cannot increase constantly with altitude due to the declining water holding capacity of air because of decreasing air temperature. The value of d) is used to match the synthetic precipitation data to a more realistic value. This point is quite delicate because of data gaps in SGHU time series. If no data are available this value must be estimated subjectively.

There is no reference station, which shows similar precipitation patterns as the SGHU station. Therefore, extrapolation methods like the one for temperature extrapolation can not be applied. Thus, all reference stations are considered to derive event probability and amount of precipitation at the SGHU stations. The daily amount of precipitation at the SGHU station is calculated based on this information with following equation (Weber 1997):

$$P_{SGHU} = \frac{1}{N} \cdot \sum_{r=1}^{N} \left(P_r \cdot F_{r,m} \cdot W_{r,m} \right) \qquad \text{(Eq. 6.4)}$$

P_{SGHU}: Daily sum of precipitation at SGHU station (mm/day)
P_r : Measured precipitation at reference station r (mm/day)
$F_{r,m}$: Mean ratio of amount of precipitation between station r and SGHU station of the month m (-)
$W_{r,m}$: Weighting of station r according to the joint occurrence probability of precipitation at target station and reference stations for the month m (-)
N: Number of reference stations

The matrix of the mean ratio of monthly sums of precipitation at reference stations and SGHU station is derived from mean monthly sums of precipitation of the period from 1988 to 1998 as shown in Figure 6.12. Table 6.4 shows the $F_{r,m}$ values of Equation 6.4.

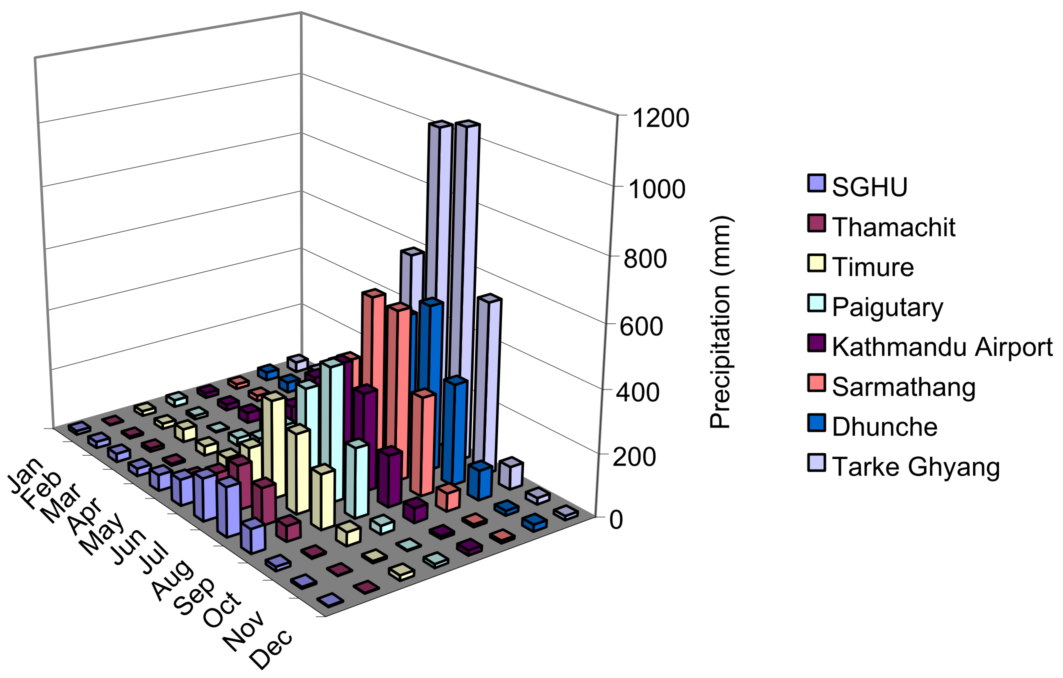

Figure 6.12: Mean monthly sums of precipitation at SGHU station and reference stations from 1988 to 1998

Tabel 6.4: Mean ratio of amount of precipitation between reference station r and SGHU station of the month m ($F_{r,m}$) from January to December

SGHU	Timure	Thamachit	Paigutary	Dhunche	Tarke Ghyang	Sarmathang	Kathmandu Airport
1.00	0.80	2.00	0.59	0.47	0.38	0.82	0.84
1.00	1.19	2.00	1.77	0.61	0.49	1.13	1.07
1.00	0.62	2.00	2.00	0.43	0.43	0.91	0.79
1.00	0.83	2.00	1.00	0.41	0.37	0.67	0.45
1.00	1.34	2.00	0.72	0.34	0.32	0.49	0.35
1.00	0.72	1.22	0.54	0.32	0.14	0.27	0.30
1.00	0.43	0.96	0.42	0.29	0.13	0.25	0.37
1.00	0.62	1.33	0.37	0.30	0.15	0.29	0.50
1.00	0.45	1.57	0.35	0.24	0.14	0.25	0.47
1.00	0.29	2.00	0.47	0.14	0.18	0.22	0.28
1.00	0.87	2.00	1.82	0.37	0.28	0.66	0.63
1.00	0.19	1.57	0.26	0.14	0.25	0.37	0.19

Variation of $F_{r,m}$ is low during monsoon season while it increases during winter season and the factors become more uncertain. However, occurrence probability of precipitation is small and therefore $F_{r,m}$ plays a minor role in Equation 6.4 during winter season. Dhunche, Tarke Ghyang, Sarmathang and Kathmandu airport receive much more precipitation than the SGHU station. In case of Tarke Ghyang the mean annual precipitation amount is approximately six times the amount of the SGHU station. These stations are located at the south-west flank of the Himalaya where condensation of moisture laden air starts due to orographic lifting. This is also the reason for higher precipitation intensities at these stations. Figure 6.13 shows the number of days with precipitation sums greater than 1.0 mm, 5.0 mm, 10.0 mm, 20.0 mm and 50.0 mm for the example year 1997. Days with precipitation sums of more than 50.0 mm only occur at Dhunche, Tarke Ghyang, Sarmathang and Kathmandu airport.

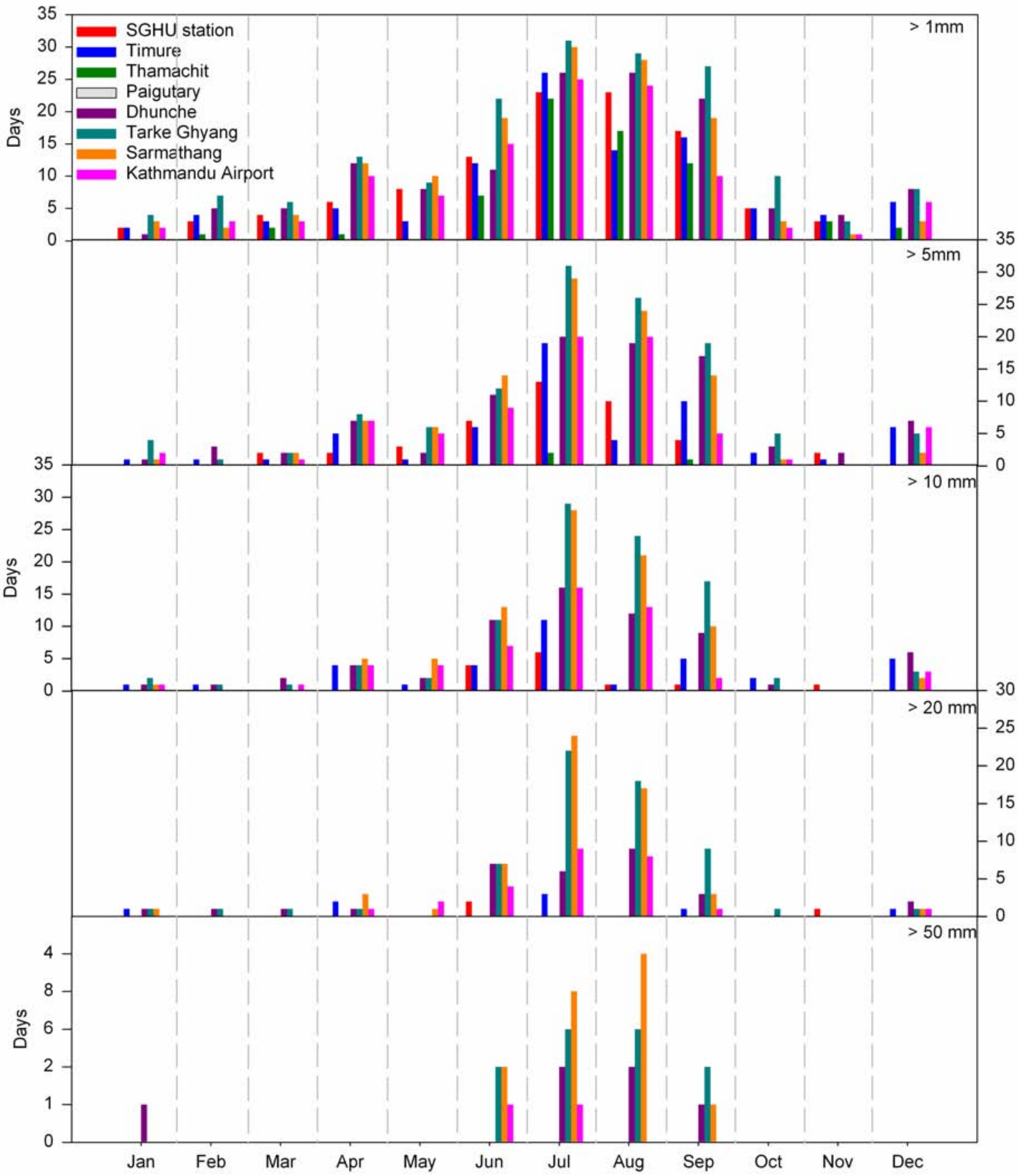

Figure 6.13: Number of days with precipitation amount of more than 1.0 mm, 5.0 mm, 10.0 mm, 20.0 mm and 50.0 mm at SGHU station and reference stations, 1997

Timure and Thamachit correspond better with the SGHU station, but Thamachit usually receives half the precipitation of the SGHU station while Timure gets about 1.5 times more precipitation than the SGHU station in a year. Thamachit is located in the inner Himalayan region in a lee position and therefore receives the smallest precipitation amount of all reference stations.

Figure 6.14 shows the mean daily occurrence probability of precipitation in the Langtang region. The occurrence probability is given in %. It can also be interpreted as percentage of days with precipitation per month. Thus, it is raining nearly every day at Tarke Ghyang in July and August while the SGHU station receives rain at 22 of 31 days. The highest occurrence probabilities of precipitation can be found in July for all reference stations with more than 75 %. At the SGHU station, however, occurrence probability is higher in August with 80 % for the investigation period from 1988 to 2000. Generally, the occurrence probabilities of precipitation are high during monsoon season and small during winter. Precipitation disposition during dry season is higher from February to April than from November to January. Tarke Ghyang receives most precipitation with the highest occurrence probability.

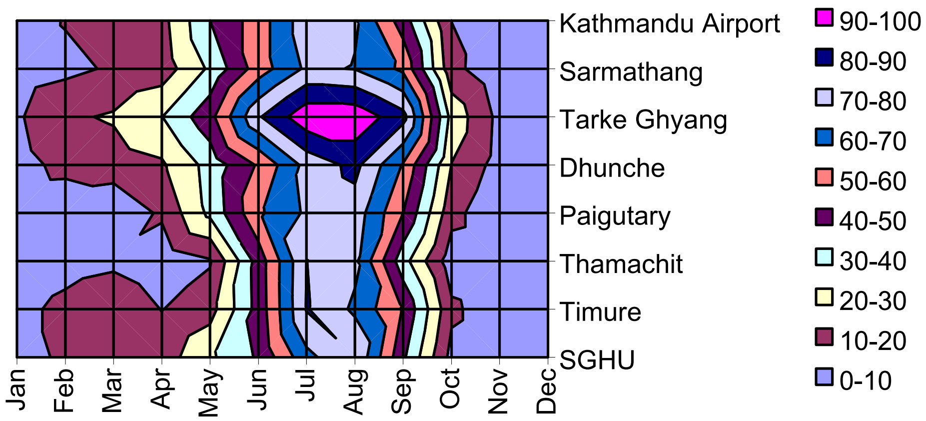

Figure 6.14: Mean daily occurrence probability of precipitation (in %) of SGHU station and reference stations in the Langtang region (1988-1998)

Figure 6.15 illustrates the probability of joint occurrence of precipitation events at the SGHU station and the reference stations in percent. The matrix values of the joint occurrence probability of precipitation (given in absolute numbers) serve as weights ($W_{r,m}$) in Equation 6.4. None of the reference stations reflects the situation at the SGHU station adequately for the whole year. Good correspondence can be found only in August (Tarke Ghyang) and during dry season especially in November and December where nearly no precipitation events occur. For the rest of the year corresponding events can only be expected every second or third day. In most of the years Dhunche, Tarke Ghyang, Sarmathang and Kathmandu airport show a slightly higher joint probability than Timure and Thamachit.

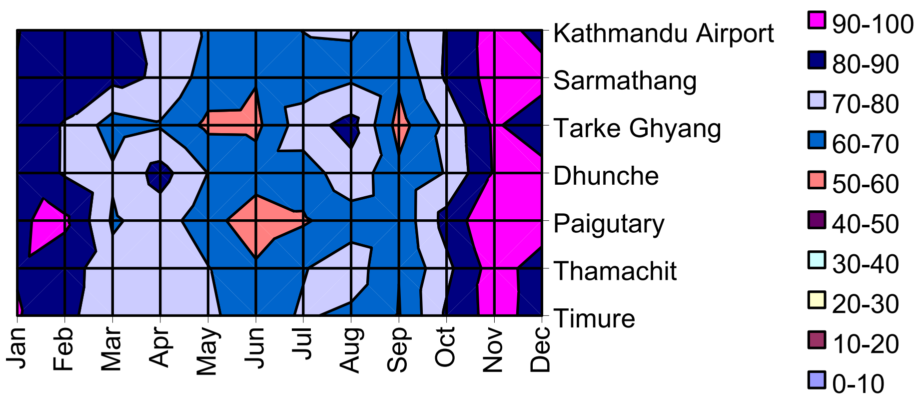

Figure 6.15: Probability of joint occurrence of precipitation events (precipitation yes or no) in % at the SGHU station and at reference stations situated in the Langtang region (1988-1998)

With all these information synthetic daily sums of precipitation can be calculated. Equation 6.4 usually overestimates the real sums of precipitation at the SGHU station. If only a few days are missing the determination or estimation of the “true” monthly sums of precipitation at the SGHU station is possible for the respective month. The ratio of measured monthly sums of precipitation and extrapolated values is taken for the adjustment of the synthetic daily values to the current meteorological situation at the SGHU station. If too many days of a month are missing, mean monthly sums of precipitation of measured values of months without gaps are taken for the adjustment. In that case a mean ratio is calculated for the respective month as shown in Table 6.5.

Table 6.5: Extrapolated and measured monthly sums of precipitation and their ratio of years without gaps in March at the SGHU station

Year	Extrapolated	Measured	Ratio
1988	130.7	56.2	2.3
1989	81.7	31.0	2.6
1992	47.1	14.0	3.4
1993	50.3	27.4	1.8
1994	50.5	13.2	3.8
1997	37.0	21.5	1.7
1998	184.5	40.8	4.5
1999	5.0	21.8	0.2
Mean ratio			2.6

In case of March 1991 there are 30 days without measurements and therefore it is impossible to estimate the “true” monthly sum of precipitation based on measurements. Thus, the mean ratio of Table 6.5 is taken. A subjective criterion to check the reliability of the ratio is the percentage deviation of monthly sums of precipitation of SGHU station and reference stations from the long-term mean. These deviations show whether the respective month is wetter or dryer than the long-term mean. Table 6.6 and Figure 6.16 show that in March 1991 some stations are wetter (Timure, Dhunche, Kathmandu Airport) than the long-term mean and others are dryer (Tarke Ghyang, Sarmathang, Paigutary). Months with gaps in the daily time series are not considered in this statistical analysis. These months deliver no deviation values in Table 6.6. Timure and Paigutary are close to the SGHU station and both stations are located in the inner Himalayan region like the SGHU station. Timure receives about twice as much (102 % more) precipitation in March 1991 compared to the long-term mean, while Paigutary gets no precipitation at all. March 1991 is therefore considered as a month with balanced precipitation patterns compared to the long-term mean. An example for a dryer month than the long-term mean is October 1991 where all stations show a negative deviation. Therefore, the long-term mean ratio for March (2.6) seems to be quite reliable because it delivers a modified extrapolated sum of 27 mm which is exactly the same as the long-term mean value of March. This criterion is only subjective but it gives some support to judge the reliability of the ratio and thus the reliability of the extrapolated values. The ratio is now used to adjust the daily precipitation data.

Table 6.6: Deviation of monthly sums of precipitation from long-term mean of precipitation in 1991 at SGHU station and reference stations in Langtang region

month	SGHU	Timure	Thamachit	Paigutary	Dhunche	Tarke Ghyang	Sarmathang	Kathmandu Airport
Jan	-	-	0	-100	-	-12	25	31
Feb	-	-	83	-100	-18	-	-83	-42
Mar	-	102	-	-100	2	-47	-97	32
May	48	-	-33	-100	-32	-26	-97	89
Apr	29	13	-	-11	-	-	-69	-
Jun	-	42	-	71	-	-	-84	-
Jul	-45	-	-31	40	-	-22	-94	-49
Aug	-	-	-3	37	-	-14	-62	-11
Sep	-	-	-	8	-	3	-45	-
Oct	-77	-93	-60	-100	-	-	-64	-100
Nov	50	-57	-100	233	-	-	-89	-100
Dec	400	0	100	92	-	38	-	56

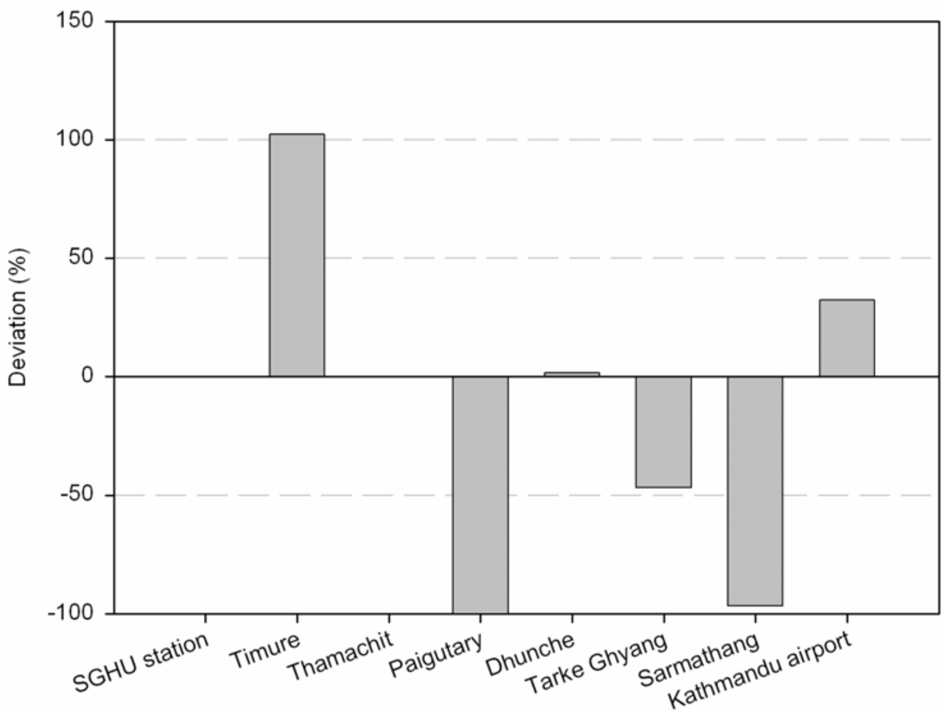

Figure 6.16: Deviation of sums of precipitation in March 1991 from mean monthly sums of precipitation (period 1988-1998) at reference stations and SGHU station in the Langtang region

Data of the extrapolated time series are only used to fill gaps in the original time series of the SGHU station or to redistribute cumulated values over the previous days. Figure 6.17 summarizes the steps of the extrapolation method.

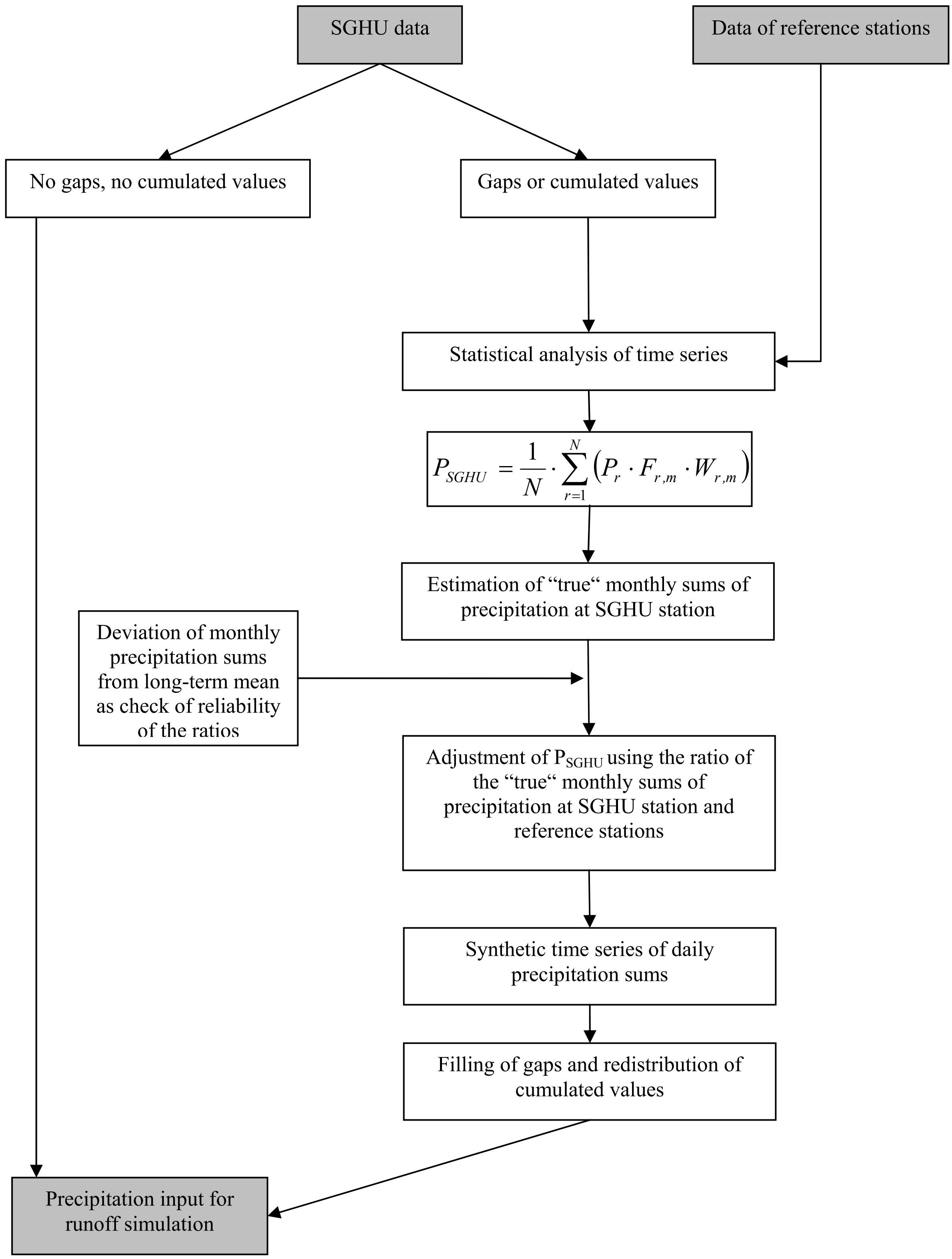

Figure 6.17: Steps of the extrapolation method for daily sums of precipitation

6.5 Spatial data

6.5.1 Data base

Areal information were derived from digital maps of the Survey Department of His Majesty's Government of Nepal. The glacier covered area was taken from maps published in ICIMOD's glacier inventory (ICIMOD 2002). The digital maps were produced by the Survey Department in co-operation with the government of Finland. Table 6.7 shows the digital maps, which were used in the study. They contain GIS layers with altitude, landuse, river system and glacier information as vector based polygons or lines.

Table 6.7: Digital maps of the Survey Department used to derive area information

Sheet No.	Date of aerial photography	Date of field verification	Scale
2885 11	1992	1996	1:50,000
2885 15	1992	1996	1:50,000
2885 16	1992	1996	1:50,000

In the case of Langtang catchment digital maps of the Survey Department do not cover the whole catchment area. The north-western part is located in China therefore the map of the German Alpine Club (DAV) is used to complete the digital maps. The following Table 6.8 gives the data of the additional DAV map called "Langthang Himal-Ost".

Table 6.8: Additional topographic map, which covers the Chinese part of the Langtang catchment

Sheet No.	Date of aerial photography	Date of field verification	Scale
DAV 0/11	1973	-	1:50,000

The glacier distribution is derived from the digital maps of ICIMOD's glacier and glacier lake inventory. This inventory was realised in co-operation with the United Nations Environmental Program (UNEP) (ICIMOD 2002). Digital data sets of the Land Observation Satellite (LANDSAT)-5 Thematic Mapper (TM) and of the Indian Remote Sensing Satellite Series 1D (IRS1D) were used mostly for the inventory. Some data sets of Système Probatoire d'Observation de la Terre (SPOT) Multi-Spectral (XS) and SPOT Panchromatic (PAN) were also used. The topographic maps were published by the Survey of India in the period from the 1950s to the 1970s on a scale of 1 inch to 1 mile (i.e. 1:63,360) and by the Survey Department of His Majesty's Government of Nepal in 1996 on a scale of 1:50,000. The topographic maps of the Survey Department were based on aerial photographs from 1992 and field verification in 1996. The aerial photographs (1:50,000 scale) used for ICIMOD's glacier inventory were taken in 1992 for eastern Nepal and in 1996 for western Nepal. Prints of the satellite images in the form of planimetric maps on a scale of 1:250,000 published by the Remote Sensing Centre of Nepal in 1984 have been used for the inventory of glaciers and glacial lakes. Landsat MSS data in digital format from March–April 1994, resampled in 50 m pixel size, are available at ICIMOD in Kathmandu, Nepal.

6.5.2 Spatial discretization and transformation of vector based maps into raster maps

As described above the Survey Department provides vector maps of landuse, contour lines and river systems. These vector maps have to be converted into raster maps. A cell size of 200 x 200 m² is considered to be appropriate in view of computation time and temporal discretization. Larger cell sizes are not appropriate in relief dominated areas like mountain valleys when applying process-oriented modeling. Ott (2002) found a significant information loss with increasing cell size which is especially problematic in mountainous catchments. Various methods to derive the raster maps out of the vector based maps were tested. The first method (method I) is the conversion of the vector map into a 10 x 10 m² grid. This grid is aggregated to a 50 x 50 m² grid and then to the final 200 x 200 m² raster map using average values. Aggregation from a 10 x 10 m² to a 200 x 200 m² raster map is the second method (method II). The third method (method III) is the direct conversion from the vector map to the 200 x 200 m² raster map without aggregation. Results of method I to III are evaluated using the deviation of the area distribution of each altitude belt (400 m) of the 200 x 200 m² raster map from the 10 x 10 m² raster map (Figure 6.18, upper graphic). The 10 x 10 m² raster map is considered to provide the most reliable area distribution. Figure 6.18 (upper graphic) shows that the area distribution of altitude belts of raster maps calculated by method III deviates the least from the area distribution of the 10 x 10 m² raster map. Methods I and II overestimate the area of the higher altitude belts significantly whereas method I delivers no values for the altitude belt from 6800 to 7200 m. Method III underestimates the area of the highest altitude belt. 0.23 % of the catchment area is located in this altitude belt this are 0.84 km² of 360 km². Method III delivers 0.64 km² for this altitude belt.

Another evaluation criterion is the deviation of the area distribution of slope classes (10°) of the 200 x 200 m² raster map from the 10 x 10 m² raster map (Figure 6.18, lower graphic). Slopes were derived from the 200 x 200 m² digital elevation models which were calculated using methods I-III. The differences between the results of the three methods are not as significant as in Figure 6.18 (upper graphic). The area distribution of slope class 51°-60° is highly underestimated by all three methods. This effect is caused by the dominance of flat areas in raster maps with low resolution (200 x 200 m²) and is therefore independent from the method applied to derive the 200 x 200 m² raster map. Method III is taken to calculate the raster maps out of the vector maps.

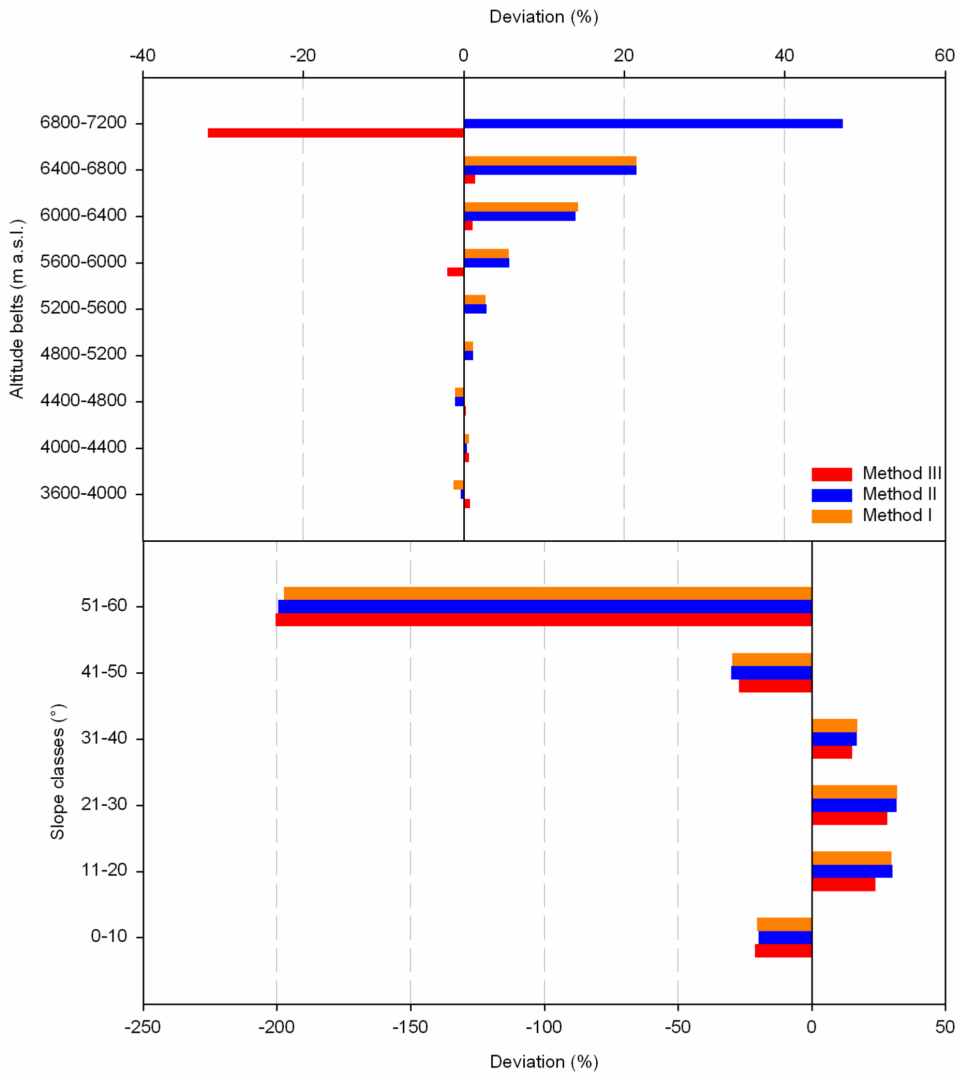

Figure 6.18: Deviation of area distribution of altitude belts (400 m) and of area distribution of slope classes (10°) of the 200 x 200 m² raster maps calculated using methods I-III from the 10 x 10 m² map

6.5.3 Digital elevation model

The digital elevation model was derived from the digital topographic vector map of the Survey Department with contour intervals of 40 m. A triangular irregular network (TIN) was used to convert the contour lines into a 3D elevation model on vector basis. This elevation model consists of polygons which can be converted into raster cells using method III. The 200 x 200 m² digital elevation model serves as fundamental map for spatial modeling.

6.5.4 River network

The river network was digitized from the DAV topographic map (Table 6.8) and converted into the raster format. The river network layer of the digital maps of the Survey Department clearly overestimates the stream density and the river network shows many gaps. Field visits revealed that in this digital map water-free channels in the flanks of the mountains are defined as rivers.
Meandering of the streams in the catchment causes an overestimation of stream cells in the raster format. This was also observed in the Dreisam- or Brugga catchment (Roser 2001, Ott

2002). The unrealistic accumulation of stream cells in the area of meanders was corrected manually to achieve a more realistic river network. The river network covers the glacier free part of the catchment and all streams end at the glacier tongues (Figure 6.19, left).

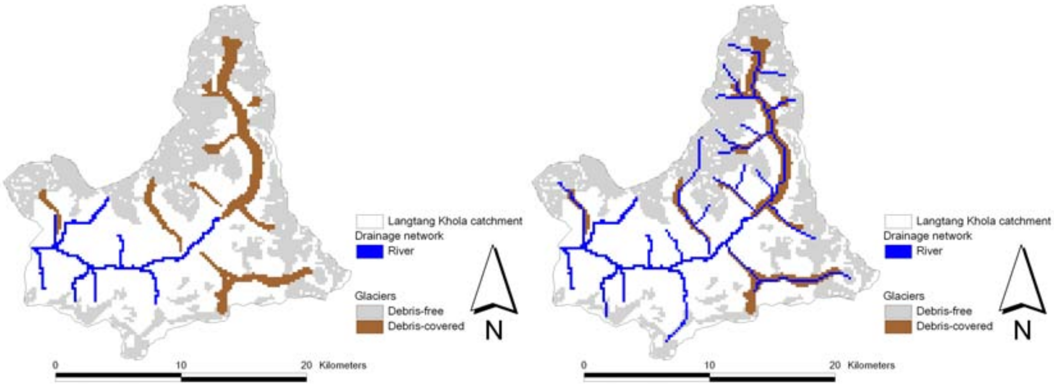

Figure 6.19: River network derived form DAV topographic map (left) and revised river network (right)

It can be assumed that a subglacial channel network exists (Chapter 5.5). Field visits have substantiated this assumption (Figure 6.20).

Figure 6.20: Stream beneath the debris-covered Lirung glacier

Therefore the river network was extended below glaciers manually as shown in Figure 6.19 (right). Subglacial channel networks exist mainly in the ablation area of valley glaciers, therefore the channel network was extended only in the areas of these glaciers. The range of the extension is hard to define but actually no liquid water is produced in the model in the higher altitudes of the catchment, and thus no lateral fluxes occur in these areas. An overestimation of the river network in the higher altitudes therefore causes no significant error in the simulation. It is much more important to get a realistic river network in the ablation area of the glaciers where liquid precipitation and meltwater occurs. The extension of the river network is necessary to get a more realistic simulation of the discharge dynamics. Water in the river network is directed to the outlet of the catchment during one time step (here taken to be 1 day) while lateral fluxes are only directed from one cell to the next downstream cell during one time step. With the river network derived from the DAV map unrealistic residence times of water in the glacier covered parts of the catchment would cause wrong simulations of discharge dynamics. The obtained river network (Figure 6.19, right) was not concordant with the local drainage direction network (ldd), which was derived from the DEM (Chapter 4.2.3). Thus, it was necessary to “burn” the revised river system into the DEM to match the ldd to the river network. All river network cells of the DEM were deepened by 100 m, and the ldd was calculated using the revised DEM. This DEM is not used for spatial regionalization of meteorological data because it would yield wrong information at the revised cells due to the altitude dependence of the regionalization methods. No sinks or pits were observed while creating the ldd.

6.5.5 Land use

The land use 200 x 200 m² raster map was derived from the land use map of the Survey Department, the DAV map and from the glacier map of ICIMOD. Three units were distinguished (Figure 6.21): non-glacier covered parts (Survey Department), glacier covered areas (ICIMOD) and debris-covered glaciers (DAV).

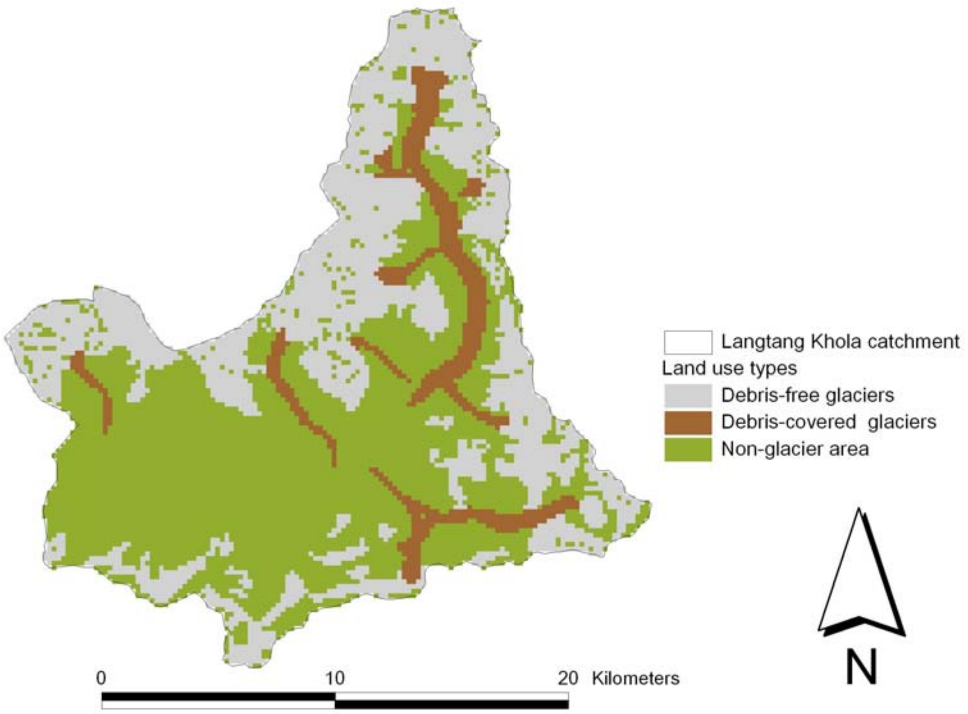

Figure 6.21: Land use map of the Langtang Khola catchment

6.5.6 Runoff generation type units

As described in Chapter 5.5 four runoff generation type units were identified on the basis of topographic maps and field surveys. The units are (Figure 6.22): non-glacier covered parts (nRGType 1), glacier covered areas (nRGType 2), glacier tongues with an inclination of less than 3° and debris cover (nRGType 3), and the valley bottom with an inclination of less than 8° (nRGType 4). A more detailed differentiation was not possible on the available data base.

NRGType 1 and 2 are dominating in the catchment while nRGType 3 and 4 together only cover 2 % of the catchment area (Table 6.9).

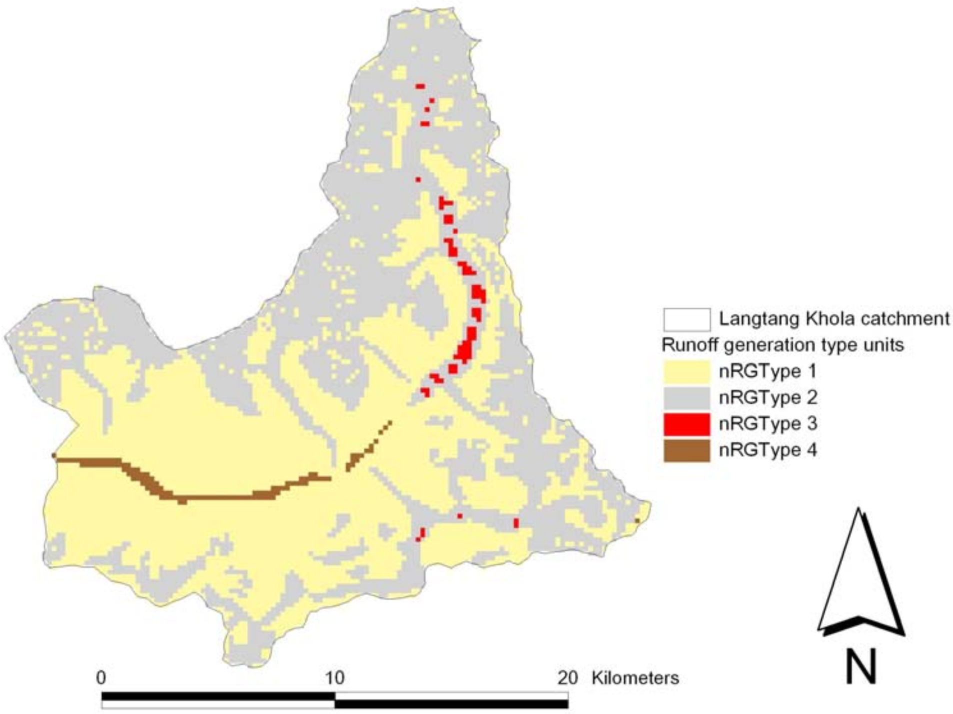

Figure 6.22: Runoff generation type units of the Langtang Khola catchment

Table 6.9: Area of the runoff generation type units

nRGType	Area (km²)	Area (%)
1	189.7	53
2	162.1	45
3	3.2	1
4	4.8	1

6.6 Conclusions

The quality of the meteorological input data is considered to be appropriate for discharge simulation in daily resolution after the described corrections and extrapolations whereas the quality of the measured discharge data strongly varies between the hydrological years. It is therefore proposed to take the visual inspection of the simulated hydrograph as an important evaluation criterion beside the objective evaluation criteria for the calibration of the model.
Various ways to transfer the vector maps into raster maps were tested and the method with the smallest information loss was taken. The spatial resolution of 200 x 200 m² seems to be quite high compared to the temporal resolution of daily time steps regarding lateral flow simulations. However, the extension of the river network partly compensates these errors and the spatial resolution of 200 x 200 m² is essential for realistic melt simulations.
The runoff generation type units are derived subjectively from the digital elevation model and from the available land use maps and topographical maps under consideration of observations during field trips.

7 Processing

The processing section contains details of the model application. The available input data set was subdivided into a calibration- and a verification period. The model was tested in the verification period 1987-1993 with the optimal parameter set obtained in the calibration period 1993-1998.

7.1 Model evaluation

In addition to the visual inspection of the simulated hydrograph in comparison with the measured one four different objective evaluation criteria were used. The most common criterion is the model efficiency according to Nash and Sutcliffe (1970):

$$R_{eff} = 1 - \frac{\sum_{i=1}^{n}(Q_{i,obs} - Q_{i,sim})^2}{\sum_{i=1}^{n}(Q_{i,obs} - \overline{Q_{obs}})^2} \qquad \text{(Eq. 7.1)}$$

R_{eff}: Model efficiency (-)
$Q_{i,obs}$: Observed runoff at time step i (mm/time step)
$Q_{i,sim}$: Simulated runoff at time step i (mm/time step)
$\overline{Q_{obs}}$: Mean observed runoff for the whole observation period (mm/time step)
i: Time step
n: Duration of simulation period (number of time steps)

Model efficiency is dimensionless and ranges from -∞ to 1. A perfect fit is achieved if the value is 1. The logarithmic model efficiency emphasizes the weighting of low discharges and therefore can be used to evaluate the simulated low flows (Uhlenbrook 1999):

$$R_{log\,eff} = 1 - \frac{\sum_{i=1}^{n}(log(Q_{i,obs}) - log(Q_{i,sim}))^2}{\sum_{i=1}^{n}(log(Q_{i,obs}) - \overline{log(Q_{obs})})^2} \qquad \text{(Eq. 7.2)}$$

R_{logeff}: Logarithmic model efficiency (-)
$\overline{log(Q_{obs})}$: Mean logarithmic observed runoff for the whole observation period (mm/time step)

Another criterion is the coefficient of determination which is defined as the ratio of explained sum of squares and total sum of squares (Yamane 1964):

$$R^2 = \frac{\left(\sum_{i=1}^{n}((Q_{i,obs} - \overline{Q_{obs}})(Q_{i,sim} - \overline{Q_{sim}}))\right)^2}{\sum_{i=1}^{n}(Q_{i,sim} - \overline{Q_{sim}})^2 \cdot \sum_{i=1}^{n}(Q_{i,obs} - \overline{Q_{obs}})^2} \qquad \text{(Eq. 7.3)}$$

R^2: Coefficient of determination (-)
$\overline{Q_{sim}}$: Mean simulated discharge for the whole observation period (mm/time step)

The coefficient of determination ranges from 0 to 1 where 1 is the optimal correlation between measured and simulated discharge. The fourth criterion is the volume error, which is the standardized cumulated difference between simulated and measured discharge of a defined period:

$$VE = \sum_{i=1}^{n}(Q_{i,obs} - Q_{i,sim}) \qquad \text{(Eq. 7.4)}$$

VE: Volume error (mm)

In the present work the volume error is calculated for each hydrological year (mm/a).

The evaluation criteria were calculated in an external statistics program. Missing values in the measured discharge data were considered, and only complete data pairs of simulated and measured discharge of a time step were used for the calculation of the evaluation criteria.

7.2 Initialization

The initialization of storage values is of great importance for realistic simulations of discharge and other components of the hydrological cycle. Initial storage levels have to be adjusted to the conditions at the beginning of the simulation by initialization runs (Chapter 5.8). Wissmeier (2005) found that simulations with TAC^d are extremely sensitive to their initial conditions. Thus climatic input data of the validation period (1987-93) were taken to calculate the initialization maps containing storage levels of the beginning of the calibration period (1993-98). These maps have to be calculated during initialization runs of TAC^d with given starting values for storage levels for the first initialization run. Depending on parameterization, initialization maps are produced at the end of each initialization run. The calculated storage values are used as new starting values for storage levels. This procedure has to be repeated until constant storage levels are achieved (Figure 7.1).

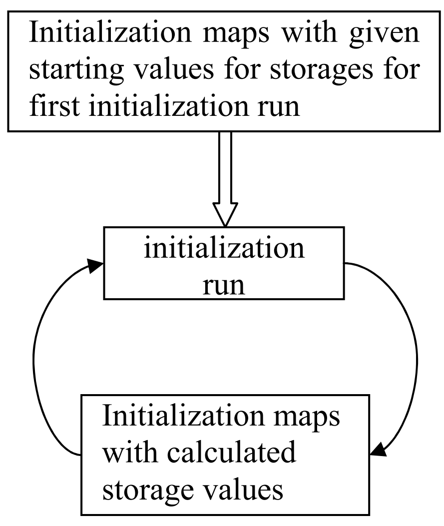

Figure 7.1: Initialization procedure

Six initialization runs were performed to achieve stable storage levels. Wissmeier (2005) recommended repeating the initialization procedure for each calibration run. This is not applicable due to long computation time. Here, the initialization procedure has been repeated if significant changes in the objective evaluation criteria occurred or if storage parameters of the runoff generation routine were calibrated. These parameters mainly determine the storage characteristics and therefore they have the greatest impact on the initialization maps. If, for example, the upper limit of the storages is reduced during a calibration run and therefore the initial storage levels are higher than the upper limit, fast drainage would occur and discharge would be highly overestimated at the beginning of the simulation period. Figure 7.2 shows a section of an initialization map of the upper storage levels (US_box) with the ldd. Highest storage levels occur at convergent points like valley bottoms or nodes of the ldd.

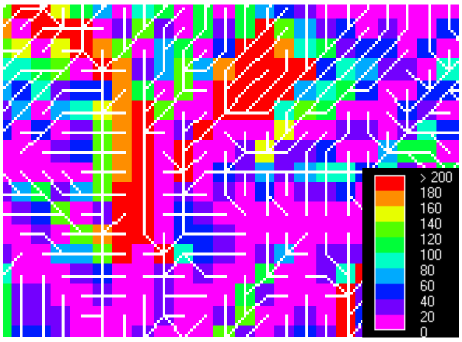

Figure 7.2: Section of the initialization map for upper storage levels (US_box) with ldd

The verification period was initialized with the same initialization maps as used for the calibration period. These maps represent the situation at the end of the verification period therefore the levels are not the realistic values of the beginning of the verification period. The simulation error caused by this assumption affects only the first year of the verification period until the storage levels have adjusted to the situation at the beginning of the verification period. This adjustment takes place quickly because the magnitude of the storage levels does not vary that much from one post-monsoon season to the other.

7.3 Calibration of the model

The aim of the calibration procedure is the optimal adaptation of model parameters to achieve best simulation results. Optimization of parameters of TAC^d was realized by a so-called inverse modeling technique where simulated values were compared with measurements and the results were evaluated by visual inspection of the hydrographs and by statistic evaluation criteria (Chapter 7.1). Good simulation of measured discharge was the main optimization criterion, additionally, glacier mass balances or water equivalents of snow cover can be taken for the optimization of the model parameters. Snow water equivalent measurements were not available in the Langtang Khola catchment. Sporadic measurements of glacier mass balances were used as an additional calibration criterion.
Due to the long computation time, sophisticated parameter estimation techniques cannot be applied. However, a systematic approach consisting of three phases was chosen to yield the optimal parameter set. The first parameter set was created in phase I using guide numbers from the literature. Braun et al. (1993) and Hagg (2003) applied the HBV-ETH model in various highly glacierized catchments in Central Asia. Parameters of the snow and glacier

routine were derived from this study because the snow and glacier routine of TAC^d is comparable to the HBV-ETH model.
The magnitudes of the parameters of the soil and runoff generation routine of the different HRUs are intended to reflect the different hydrological responses of each HRU. Thus, mainly the expected relations between the HRUs were considered in the parameterization of these routines. NRGType 3, for example, was expected to have the highest storage capacity of all HRUs and therefore the parameter GlacierLS_H was assumed to be at least 10 times higher than US_H2 of nRGType 2. Retardation of the upper storage is generally considered to be lower than retardation of the lower storage. This relation can be expressed with higher K-values of the upper storages. The parameters of the soil and runoff generation routine were chosen based on calibration experiences with TAC^d in other catchments and on process understanding as shown in the examples above (Uhlenbrook 2005, personal conversation).
The values of this parameter set deliver magnitudes of the parameters for further calibration. Parameters were varied by a manual trial-and-error technique in phase II. Mainly, parameters of the snow and glacier routine and the precipitation correction factors were changed during this phase. The ratios between the storage parameters of the soil- and runoff generation routine were not changed in this phase. If GlacierLS_H was reduced, all other upper limits of storages had to be reduced proportunately. The manual trial-and-error technique revealed the principle behavior of the parameters and showed the occurrence of optima after only a few calibration runs. Based on this experience, pair wise calibration of the most sensitive parameters was performed in calibration phase III. This phase is often referred to as fine-tuning. Parameters of the soil and runoff generation routine remained untouched in this phase. The following pairs of model parameters were selected, based on previous modeling exercises with HBV-ETH by Renner et al. (1990):

1.) PCF-SFCF
2.) Cfmax-TT
3.) Cfmax-Rexp
4.) Cfmax-CRFR
5.) Cfmax-SFCF
6.) SFCF-TT

The 5x5 Matrix of R_{eff} identifies the optimal constellation of the parameter pairs (Figure 7.3). The pair wise optimization runs were repeated until simulation results could not be improved any more.

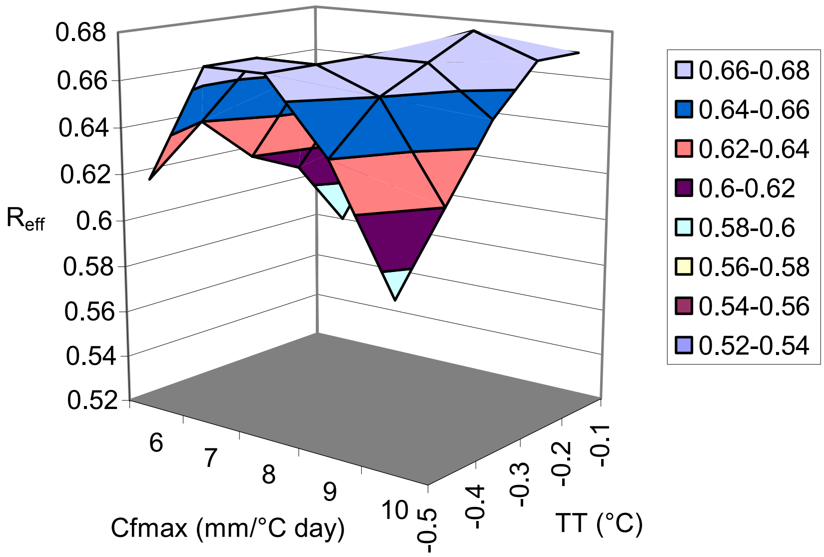

Figure 7.3: Example of 3D visualization of the results of pair wise (TT vs. Cfmax) calibration of TAC[d]

Calibration of conceptual rainfall-runoff models in highly glacierized catchments is quite tricky. Glaciers are sources of water whose contribution to runoff generation is hard to estimate from discharge data. An overestimation of meltwater production can for instance, compensate for underestimated basin precipitation or vice versa. In this way, good simulation results can occur for the wrong reasons. In order to improve the process simulation a multi criteria calibration can be applied instead of a single criteria calibration (Hottelet et al. 1994, Seibert 2000). Information about the glacier mass balances in addition to discharge were considered in the calibration procedure to find the optimal parameters of the snow and glacier routine. Table 7.1 shows the available measurements of glacier mass balances in the Langtang Khola catchment.

Table 7.1: Glacier mass balances in the Langtang Khola catchment

Glacier	Altitude of point measurement (m a.s.l.)	Mass balance (mm)	Observation period	Study
Yala	5150	-2300	May-October 1996	Fujita et al. (1998)
	5190	-2100	May-October 1996	Fujita et al. (1998)
	5230	-1700	May-October 1996	Fujita et al. (1998)
	5280	-1500	May-October 1996	Fujita et al. (1998)
	5350	-300	May-October 1996	Fujita et al. (1998)
	5380	300	May-October 1996	Fujita et al. (1998)
	5390	900	May-October 1996	Fujita et al. (1998)
	Areal average	-357	May-October 1996	Fujita et al. (1998)
Yala	5240	-2240	March 1991-March 1992	Braun et al. (1993)

5580	510	March 1991-March 1992	Braun et al. (1993)

This second optimization criterion enables a more realistic simulation of glaciermelt and therefore a more realistic discharge simulation.
The optimal parameter set is shown in Table 7.2. Approximately 350 model runs were performed in the calibration procedure.

Table 7.2: Optimized parameter set of TAC[d] for the Langtang Khola catchment

Parameter	Description	Determination	Value	Unit
Precipitation correction and regionalization				
PCF	"Precipitation correction factor" for rain	Calibration	1.05	(-)
PGrad	Vertical precipitation gradient	Calibration (Externally set from values in the literature)	0.04	((%/100m)/100)
PHorizGrad	Horizontal precipitation gradient	Calibration (Externally set from values in the literature)	-0.03	((%/1000m)/100)
SFCF	"Snowfall correction factor"	Calibration	1.2	(-)
Temperature regionalization				
TGrad	Vertical temperature gradient	Calibration (Externally set from values in the literature)	-0.5	(°C/100m)
Potential evaporation calculation and regionalization				
ETmax	Maximum of potential evapotranspiration	Calibration (Externally set from values in the literature)	2.2	(mm/day)
ETGrad	Vertical evapotranspiration gradient	Calibration (Externally set from values in the literature)	-0.01	((%/100m)/100)
Snow and glacier routine				
TT	Threshold value of temperature for snowfall also general temperature correction	Calibration (Externally set from values in the literature)	-0.2	(°C)
Cfmax	Degree-day factor	Calibration	7.0	(mm/°C day)
CWH	Water holding capacity of snow	Literature (Bergström 1992)	0.1	(-)
CFR	Coefficient of refreezing	Literature (Bergström 1992)	0.05	(-)
Rexp	Correction factor for	Calibration	1.3	(-)

	cells with maximum potential sunshine duration			
Rmult	Multiplicative factor to account for accelerated melt over ice as compared to snow	Calibration	1.4	(-)
Rmultd	Reduction factor of glaciermelt over debris-covered parts of the glacier	Calibration (Externally set from values in the literature)	0.3	(-)
Soil routine				
LP	Reduction parameter of field capacity	Literature (Menzel 1997)	0.6	(-)
Non-glacier area (nRGType 1)				
FC1	Maximum soil moisture storage (field capacity)	Calibration	20	(mm)
BETA1	Empirical parameter	Calibration	2.0	(-)
Glacier area (nRGType 2)				
FC2	Maximum soil moisture storage (field capacity)	Calibration	20	(mm)
BETA2	Empirical parameter	Calibration	1.5	(-)
Glacier area with inclination less 3° and debris cover (nRGType 3)				
FC3	Maximum soil moisture storage (field capacity)	Calibration	40	(mm)
BETA3	Empirical parameter	Calibration	1.5	(-)
Valley bottom with inclination less 8° (nRGType 4)				
FC4	Maximum soil moisture storage (field capacity)	Calibration	120	(mm)
BETA4	Empirical parameter	Calibration	2.5	(-)
Runoff generation routine				
Non-glacier area (nRGType 1)				
US_K1	Storage coefficient of upper storage	Calibration	0.13	(1/day)
LS_K1	Storage coefficient of lower storage	Calibration	0.005	(1/day)
US_P1	Percolation capacity	Calibration	1	(mm/day)
US_H1	Limit of upper storage	Calibration	100	(mm)
Glacier area (nRGType 2)				
US_K2	Storage coefficient of upper storage	Calibration	0.1	(1/day)
LS_K2	Storage coefficient of lower storage	Calibration	0.02	(1/day)
US_P2	Percolation capacity	Calibration	3	(mm/day)
US_H2	Limit of upper	Calibration	200	(mm)

	storage			
Glacier area with inclination less 3° and debris cover (nRGType 3)				
GlacierLS_K	Storage coefficient of glacier storage	Calibration	0.01	(1/day)
GlacierLS_H	Limit of glacier storage	Calibration	3000	(mm)
Valley bottom with inclination less 8° (nRGType 4)				
ValleyLS_K	Storage coefficient of valley storage	Calibration	0.01	(1/day)
ValleyLS_H	Limit of valley storage	Calibration	1000	(mm)
Routing routine				
MaxBas	Empirical parameter	Set a priori	1	(-)

7.4 Results of the calibration period

Comparative studies of conceptual precipitation-runoff models (Rango 1992) have shown that for the simulation of daily values of discharge in high alpine catchments R_{eff}-values over 0.8 can be assessed as good. The first two hydrological years of the calibration period show a good adaptation of the simulated to the measured discharge. The dynamics of the hydrograph is reproduced satisfactorily in these years. From the hydrological year 1995/96 onwards the discharge is consistently overestimated by the model. In these years the measured discharge data show many gaps and inconsistencies which seem to be measuring errors. Measured discharge in the monsoon period in 1996/97 varies between 14.08 m^3/s and 16.69 m^3/s and remains on the same level for several days. Further, measured discharge values in the post-monsoon season 1997 show unrealistic high values until the beginning of November. In 1997/98 many data gaps occur and again, unrealistic plateaus of the discharge values can be observed. Due to these inconsistencies the hydrological years 1996/97 and 1997/98 were not considered for calibration. Table 7.3 summarizes the evaluation criteria.

Table 7.3: Evaluation criteria of the calibration period

Hydrological year	R_{eff} (-)	log R_{eff} (-)	R^2 (-)	VE (mm/a)
1993/94	0.85	0.75	0.89	57
1994/95	0.87	0.80	0.88	-8
1995/96	0.53	0.31	0.72	92
1996/97	0.46	0.84	0.76	-8
1997/98	0.28	0.49	0.83	-43

The winter discharge is simulated well in the years 1993/94, 1994/95 and 1996/97 with logarithmic model efficiencies (log R_{eff}) from 0.75 to 0.84. The years 1995/96 and 1997/98 show unreliable equal values in the low flow season which could be reading errors or errors in digitizing the handwritten data.

Generally, the calculated onset of discharge in May and June is delayed by some 10 days or more, and consequently, discharge is underestimated at the beginning of the melt/monsoon period. On the other hand, discharge is generally overestimated in the second half of the melt/monsoon period. This causes an underestimation of measured annual discharge of 57 mm in 1993/94 and 92 mm in 1995/96. In 1994/95 there is a significant overestimation of the discharge in the pre-monsoon season. This overestimation is compensated over the year and the volume error is minimal in this year. Figure 7.4 compares the simulated discharge with the measured discharge of the calibration period.

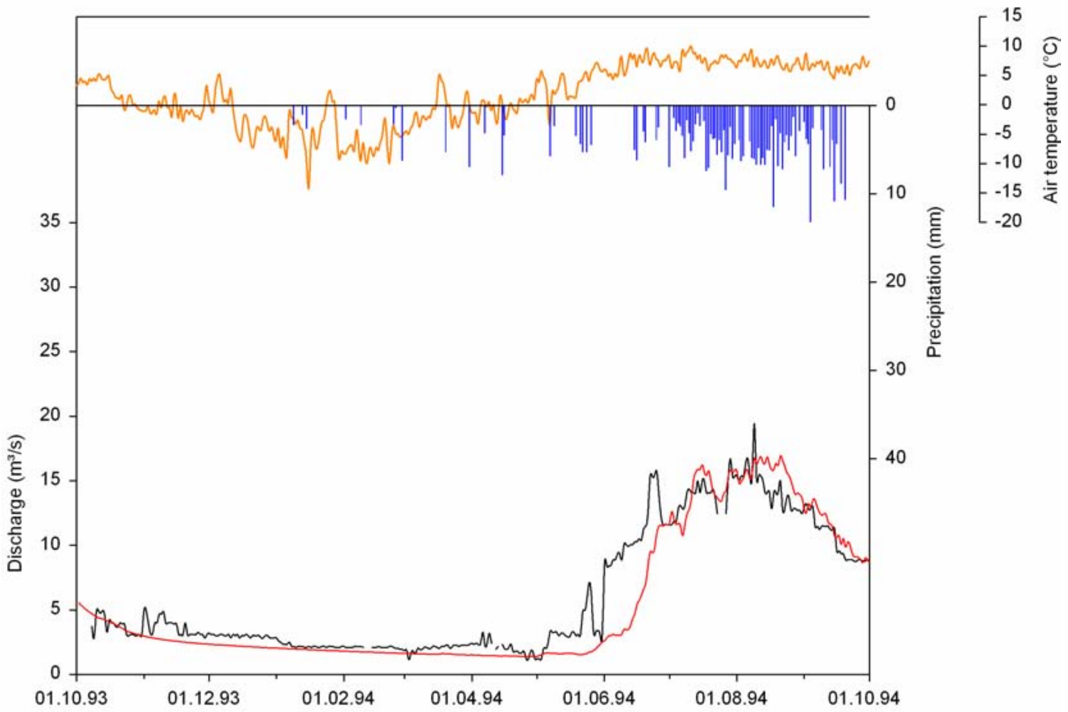

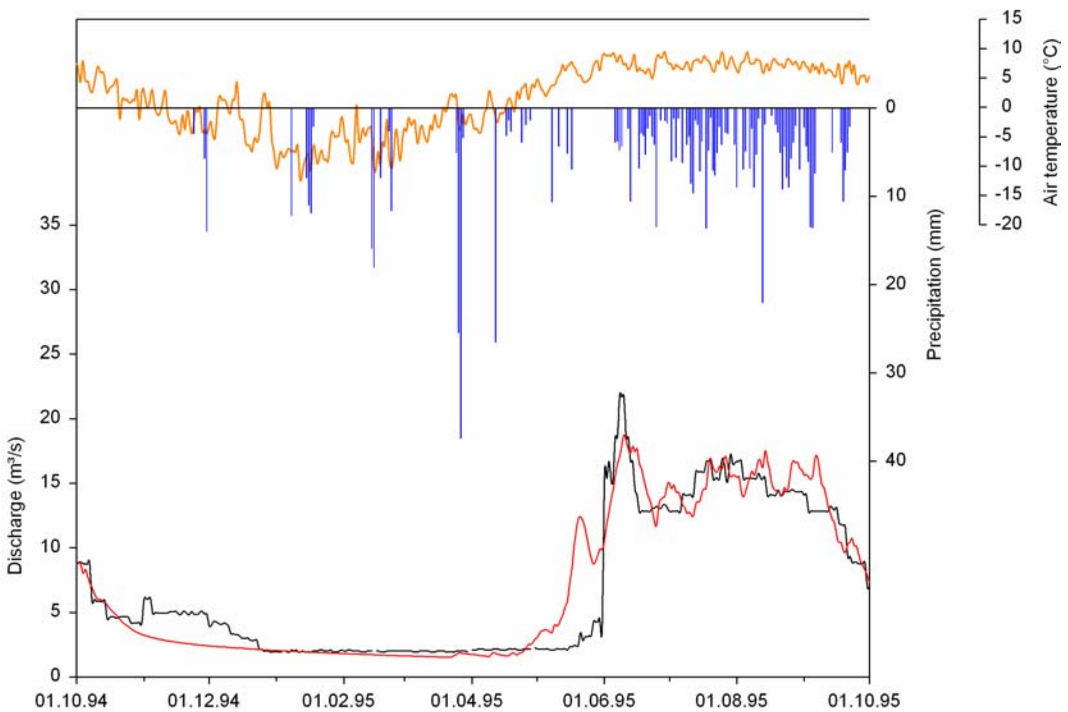

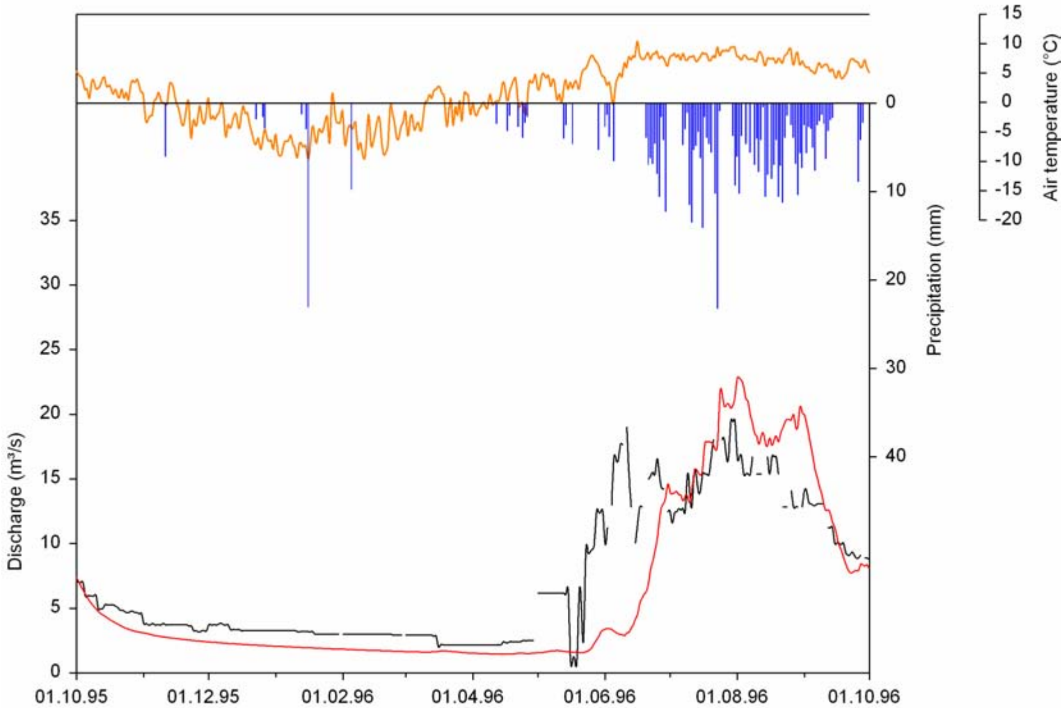
Discharge (m³/s)
Precipitation (mm)
Air temperature (°C)
01.10.95
01.12.95
01.02.96
01.04.96
01.06.96
01.08.96
01.10.96

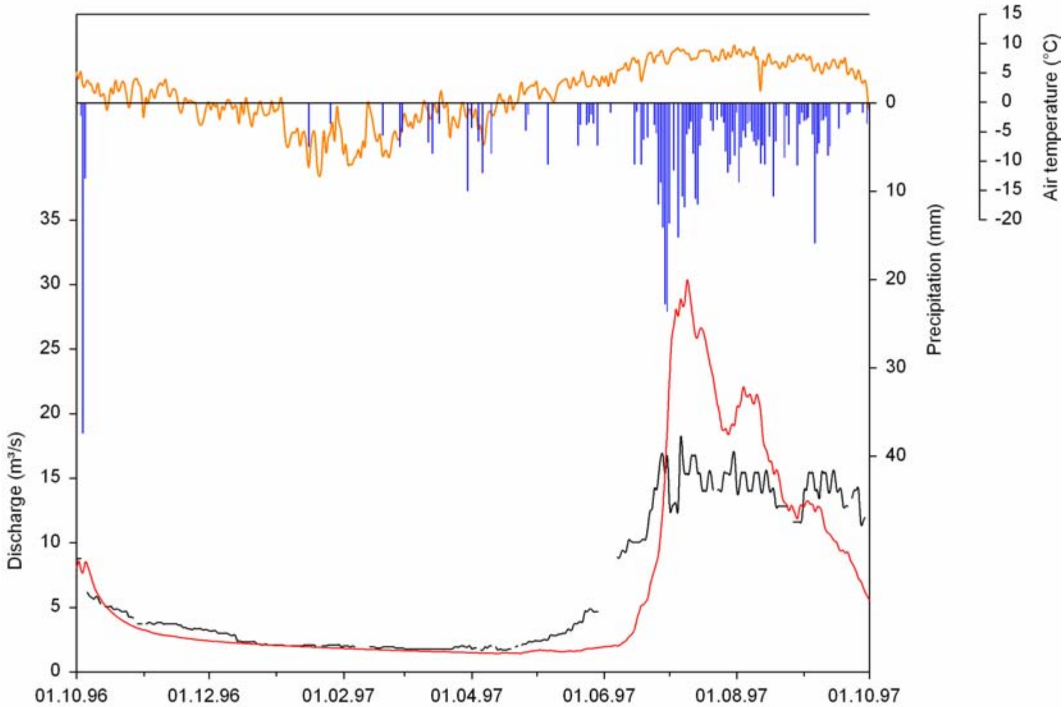
Discharge (m³/s)
Precipitation (mm)
Air temperature (°C)
01.10.96
01.12.96
01.02.97
01.04.97
01.06.97
01.08.97
01.10.97

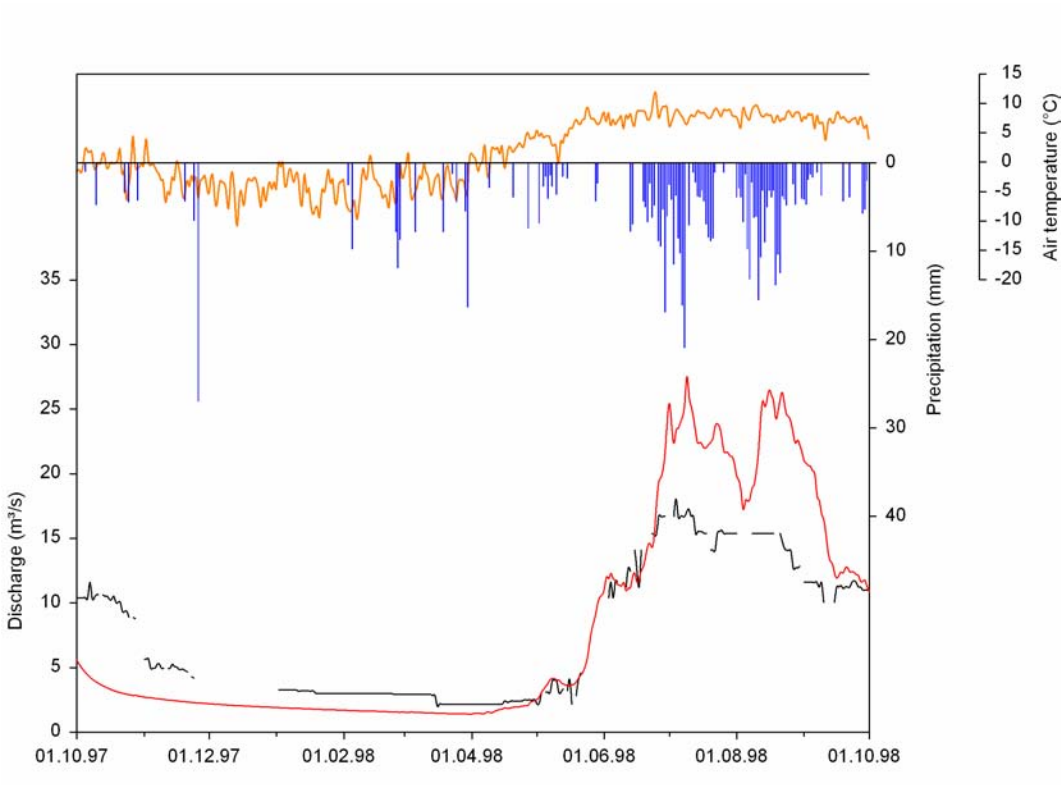

Figure 7.4: Comparison of measured (black) and simulated (red) discharge of the calibration period (1993-1998) with measured air temperature (orange) at the SGHU station and calculated basin precipitation (blue)

Glacier mass balances were observed from 19.5.1996 to 6.10.1996 by Fujita et al. (1998) in altitudes from 5150 m a.s.l. to 5390 m a.s.l. on Yala glacier (Table 7.1). The mass balances are calculated for the cells in which the point measurements took place. Figure 7.5 shows that the balances generally are underestimated either in the ablation area or in the accumulation area. However, the magnitudes are in the right order of magnitude. A reason for the differences of the simulated and measured balances is the cell size of 200 x 200 m². That means that point measurements are compared with simulated mass balances of an area of 40000 m². The altitudes of the cells and of the point measurements differ and therefore different meteorological conditions prevail at the cells and at the observation points. Further, microbial production on the surface of Yala glacier was observed by Kohshima et al. (1993). The surface of the ablation area was covered with a dark colored mud-like material which mainly consisted of algae and bacteria. This thin layer reduces the surface albedo of the glacier and accelerates glacier melting (Figure 5.5 in Chapter 5.3.3). The study revealed that the melting rates at the covered surface were about 3 times larger than at uncovered surface. This could be a reason for the underestimation of the ablation.

Fujita et al. (1998) determined the areal average mass balance of Yala glacier for the investigation period as -357 mm the simulated mass balance for entire Yala glacier is -332 mm for the same period, which compares favorably.

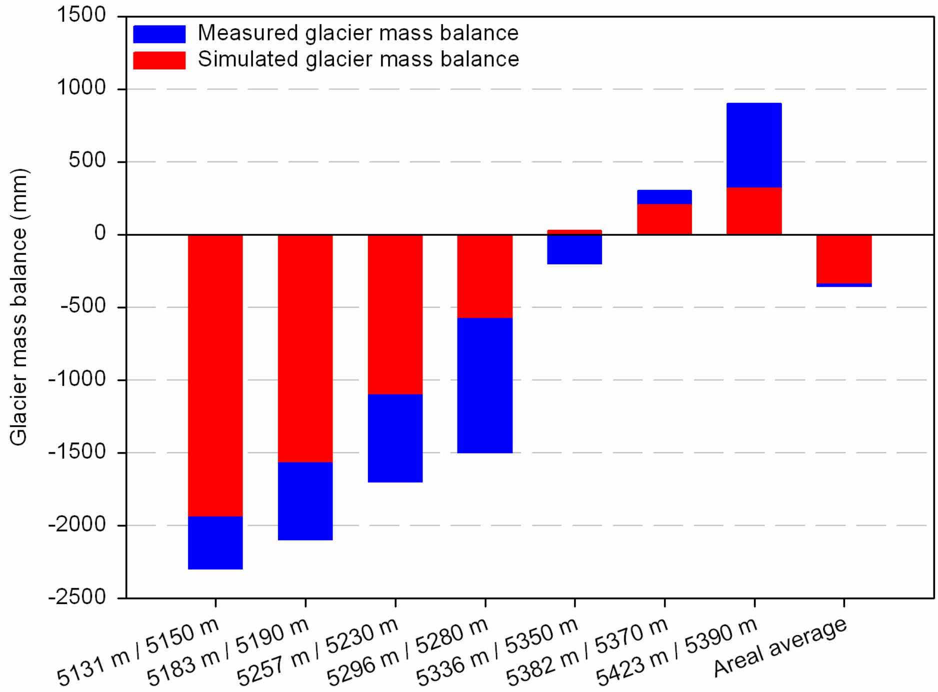

Figure 7.5: Comparison of simulated and measured glacier mass balances at different altitudes on Yala glacier from 19.05.1996 to 6.10.1996. The blue bars are behind the red bars and both start at 0.00 mm. First numbers of x-axis are the altitudes of the 200 x 200 m² cells in which the balance was measured. Second numbers show the altitudes of the observation points

7.4.1 Water balance of the Langtang Khola catchment for the calibration period

The results of the individual components of the annual water balance are presented in this chapter.

7.4.1.1 Annual basin precipitation

The aggregational state of precipitation was determined at each cell using the extrapolated air temperature at the given cell and the threshold air temperature (TT). The basin precipitation was derived from the daily precipitation sums at the SGHU station using vertical and horizontal gradients (Chapter 5.1.1). About 47 % of the basin precipitation falls as snow and 53 % as rain (Table 7.4). This result shows the important role of snow and ice storage in the controlling of the water balance.

Table 7.4: Annual basin precipitation (mm/a) and its aggregational state for the calibration period calculated with the TAC^{d} model

	1993/94	1994/95	1995/96	1996/97	1997/98
Solid precipitation	184	384	212	267	278
Liquid precipitation	248	284	309	309	350
Total over catchment	432	668	520	576	628
Measured precipitation at SGHU station	461	689	551	611	656

7.4.1.2 Annual water balance

The following main components of the annual water balance can be distinguished:

$$Q = P_b + G_{melt} - ET - \Delta S \qquad \text{(Eq. 7.5)}$$

Q: Discharge (mm/a)
P_b: Basin precipitation (mm/a)
G_{melt}: Glaciermelt (mm/a)
ΔS: Changes in storages, here primarily in form of snow accumulation which feeds the glaciers (mm/a)

Table 7.5 and Figure 7.6 show the values of the individual terms as calculated by the model. Basin precipitation (432 to 668 mm/a) and discharge (470 to 694 mm/a) are by far the largest components, followed by glaciermelt (274 to 422 mm/a). Basin precipitation and glaciermelt are the input into the system. The storage term summarizes water storage in groundwater, snowpack and soil. Actual evapotranspiration accounts for 12 to 17 % of the Input.

Table 7.5: The main terms of the water balance of Langtang Khola catchment as assessed by the TAC[d] model for the calibration period in mm/a

	1993/94	1994/95	1995/96	1996/97	1997/98
Discharge	470	605	532	556	694
Actual ET	122	134	126	112	127
Glaciermelt	295	313	316	274	422
Precipitation	432	668	520	576	628
Storage change	135	242	179	182	229
Balance	0	0	0	0	0

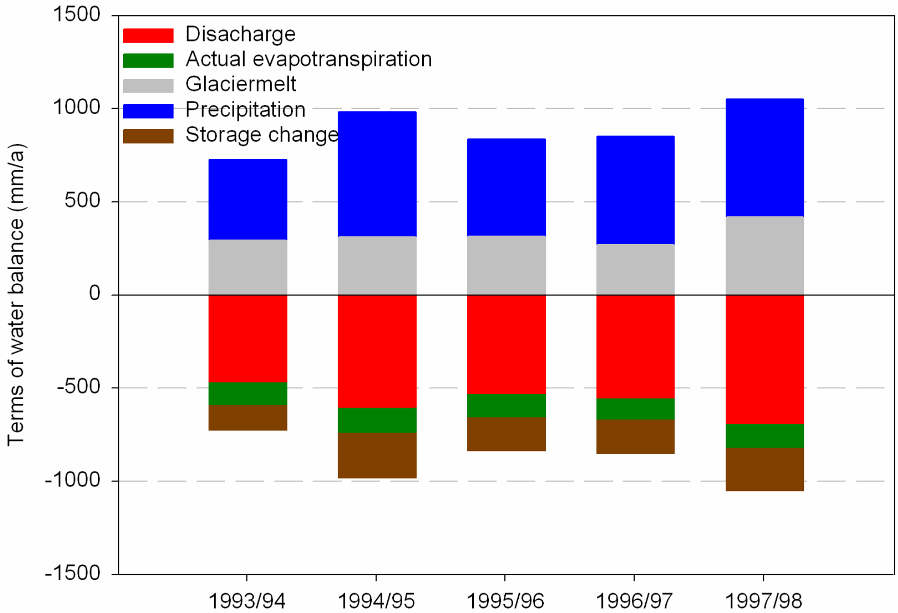

Figure 7.6: Main terms of the water balance of the calibration period of Langtang Khola catchment. Added components with a positive sign are the input into the system, whereas the added values with a negative sign are the output of the system and the storage change

7.5 Results of the verification period

The hydrological years from 1987/88 to 1992/93 were simulated for model verification with the optimal parameter set shown in Table 7.2. There are gaps in the measured discharge data in this period which partly complicates the interpretation of the results (Table A1, Appendix). Nearly no reliable data are available for June 1989 and September 1991. This was considered in the calculation of the evaluation criteria. The evaluation criteria are shown in Table 7.6.

Table 7.6: Evaluation criteria of the verification period

Hydrological year	R_{eff} (-)	log R_{eff} (-)	R^2 (-)	VE (mm/a)
1987/88	0.58	0.05	0.87	97
1988/89	0.72	0.32	0.90	40
1989/90	0.68	0.45	0.84	50
1990/91	0.20	0.40	0.88	-30
1991/92	0.30	0.59	0.82	-9
1992/93	0.76	0.68	0.91	37

Measured winter discharge is higher in this period, with an average from November to the end of April of 3.35 m³/s compared to the average of 2.73 m³/s in the calibration period. TAC^d systematically underestimates the winter discharge in all hydrological years of the verification period and overestimates discharge in the melt/monsoon period (Figure 7.7). These compensating effects are the reason for the relatively small volume errors (Table 7.6). R_{eff} and log R_{eff}, however, show a drop in performance compared to the calibration period, whereas the coefficient of determination implies a strong connection between measured and simulated hydrograph.

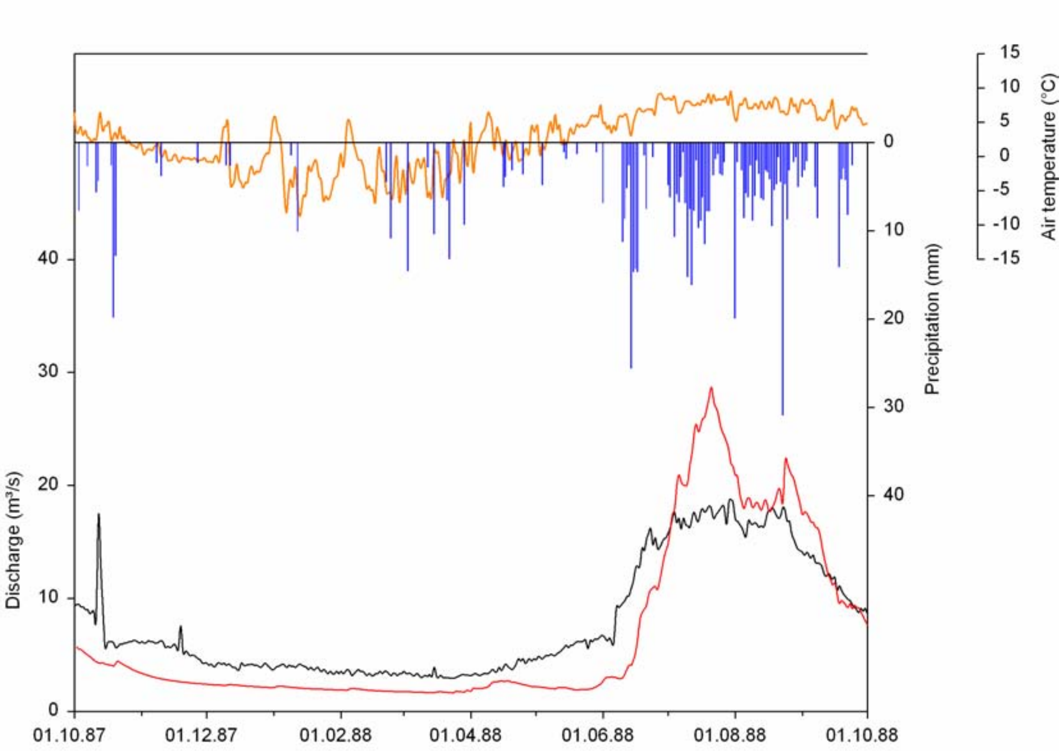

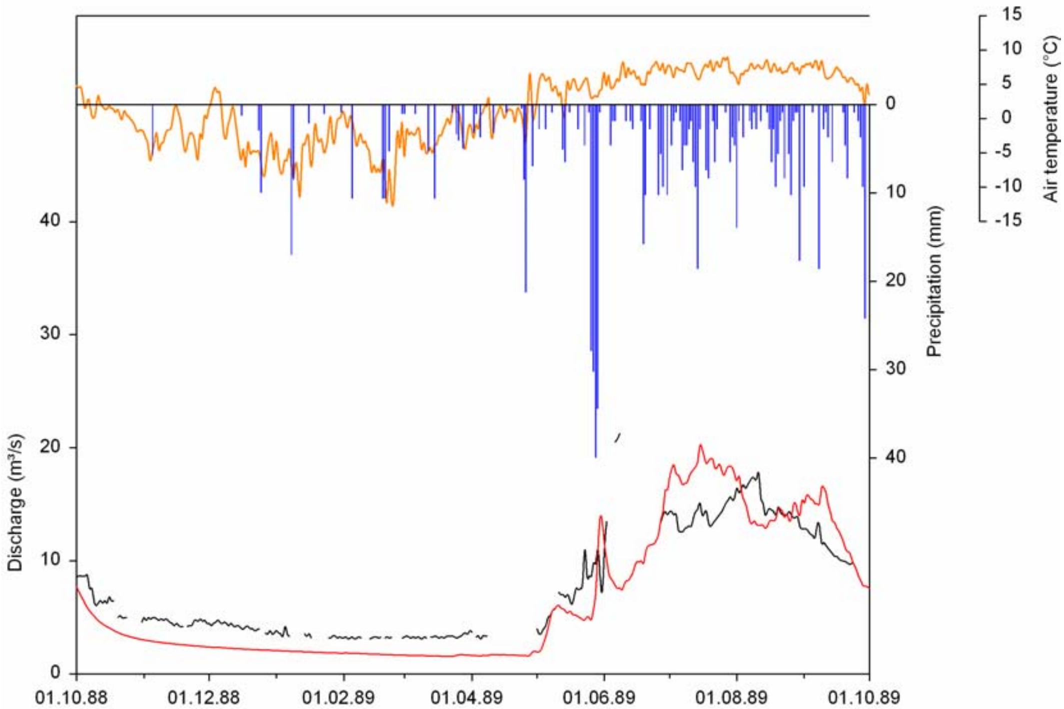

Discharge (m³/s)
0
10
20
30
40
Precipitation (mm)
0
10
20
30
40
Air temperature (°C)
15
10
5
0
-5
-10
-15
01.10.88
01.12.88
01.02.89
01.04.89
01.06.89
01.08.89
01.10.89

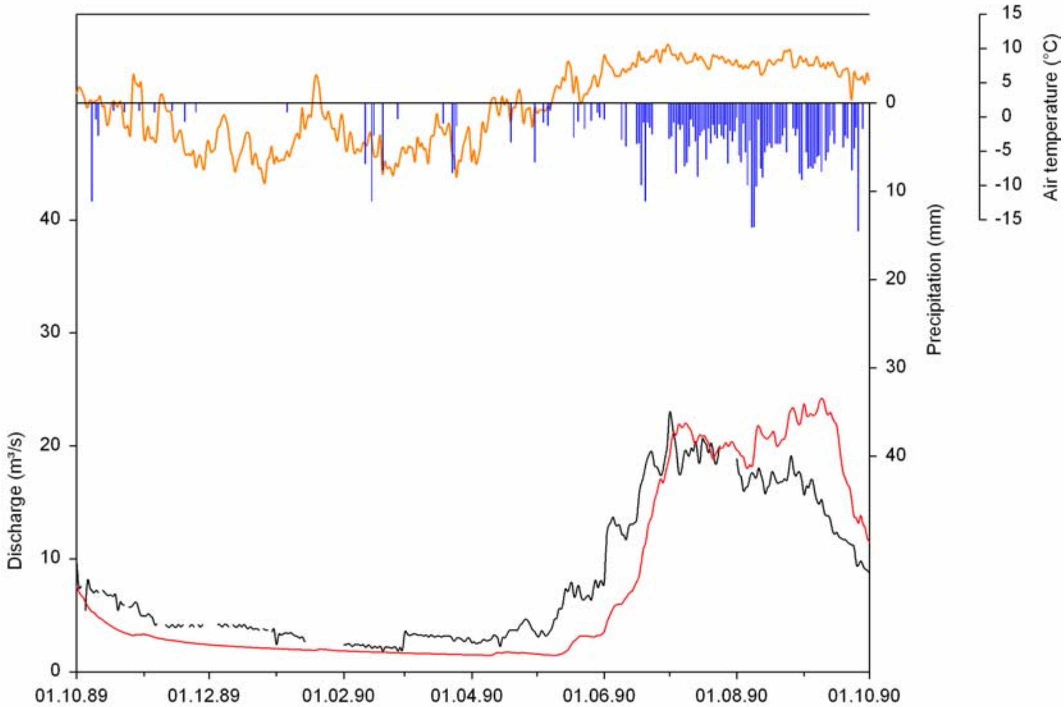

Discharge (m³/s)
0
10
20
30
40
Precipitation (mm)
0
10
20
30
40
Air temperature (°C)
15
10
5
0
-5
-10
-15
01.10.89
01.12.89
01.02.90
01.04.90
01.06.90
01.08.90
01.10.90

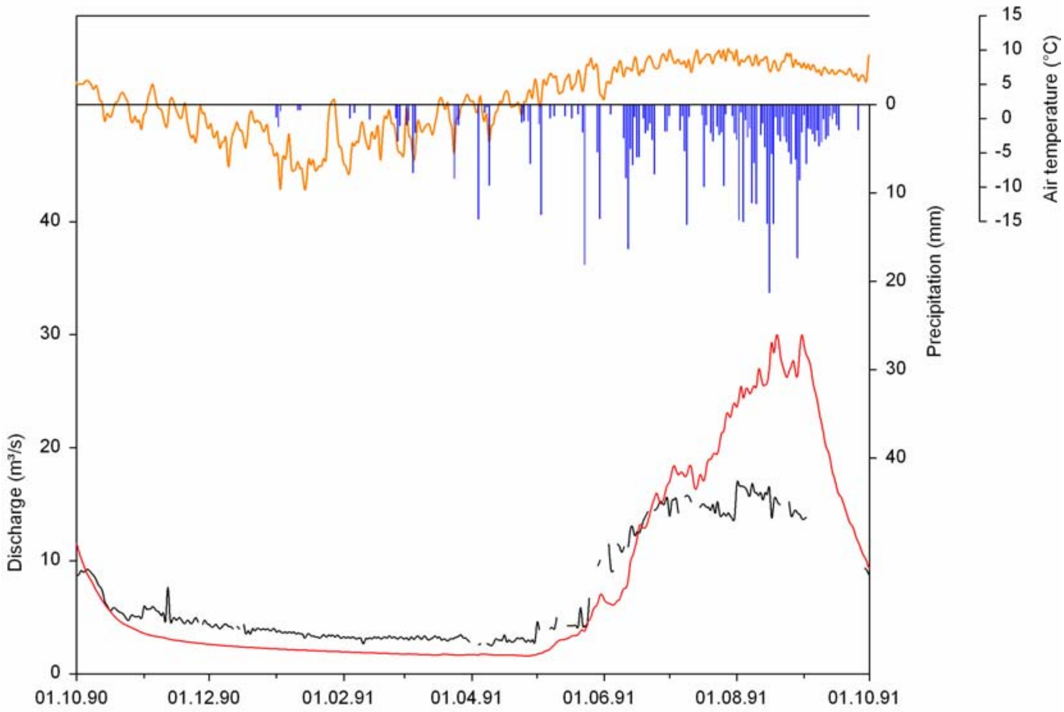

15
10
5
0
-5
-10
-15
Air temperature (°C)
0
10
20
30
40
Precipitation (mm)
0
10
20
30
40
Discharge (m³/s)
01.10.90
01.12.90
01.02.91
01.04.91
01.06.91
01.08.91
01.10.91

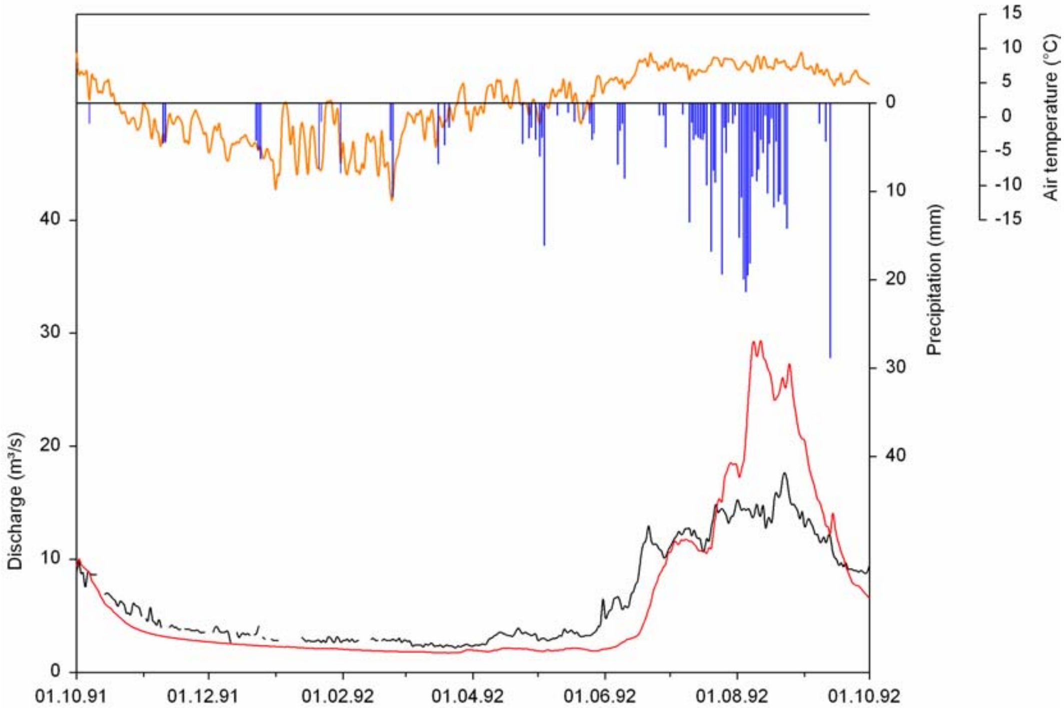

15
10
5
0
-5
-10
-15
Air temperature (°C)
0
10
20
30
40
Precipitation (mm)
0
10
20
30
40
Discharge (m³/s)
01.10.91
01.12.91
01.02.92
01.04.92
01.06.92
01.08.92
01.10.92

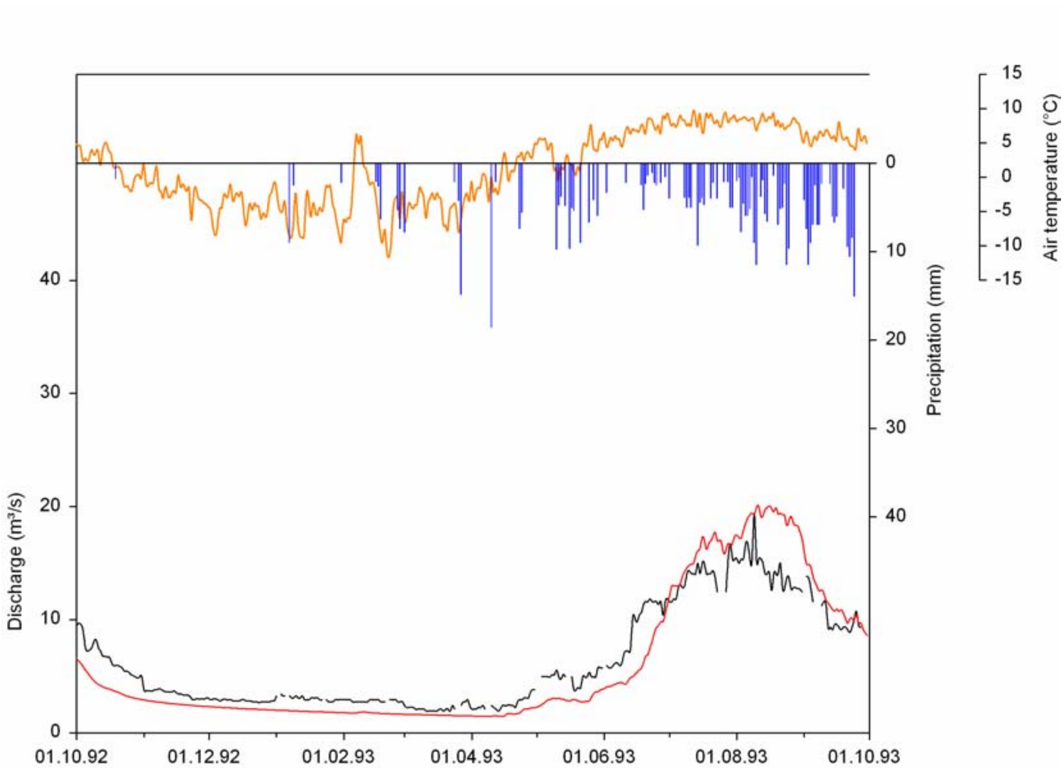

Figure 7.7: Comparison of measured (black) and simulated (red) discharge of the verification period (1987-1993) with measured air temperature (orange) at the SGHU station and calculated basin precipitation (blue)

In the verification period there is one glacier mass balance observation available from 28.03.1991 to 17.03.1992 (Braun et al. 1993). This observation is again a point measurement which causes the same problems as described for the comparison of measured and simulated mass balances of the calibration period. However, the agreement is satisfactory and shows that the parameterization of the snow and glacier routine is representative for the entire simulation period (Figure 7.8).

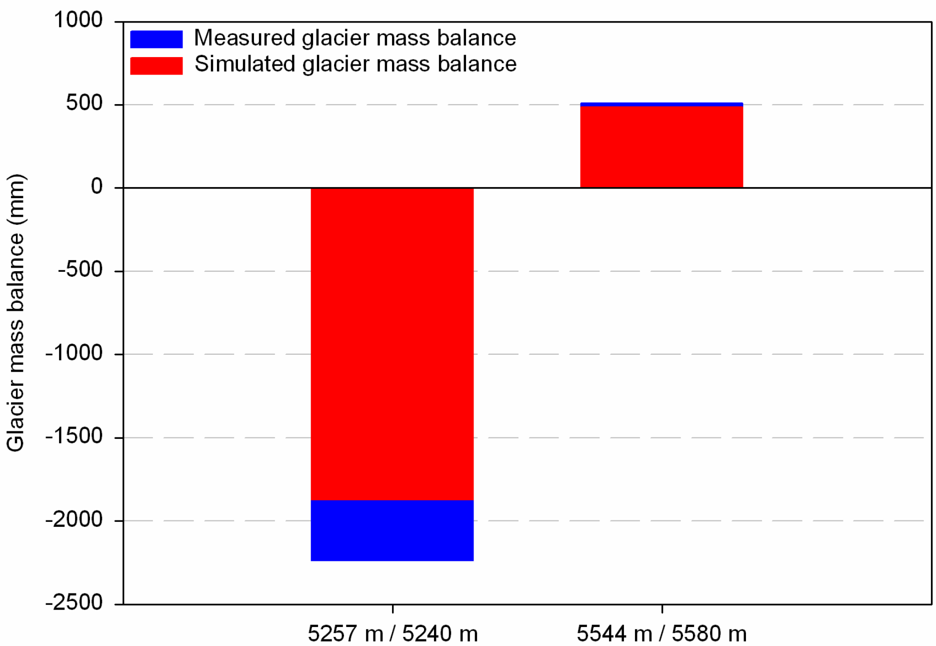

Figure 7.8: Comparison of simulated and measured glacier mass balances at different altitudes on Yala glacier from 28.03.1991 to 17.03.1992. The blue bars are behind the red bars and both start at 0.00 mm. First numbers of x-axis are the altitudes of the 200 x 200 m² cells in which the balance was measured. Second numbers show the altitudes of the observation points

7.5.1 Water balance of the Langtang Khola catchment for the verification period

7.5.1.1 Annual basin precipitation

In the verification period approximately 50 % of precipitation is solid. Table 7.7 summarizes the results of the single hydrological years.

Table 7.7: Annual basin precipitation (mm/a) and its aggregational state for the verification period calculated with the TAC^d model

	1987/88	1988/89	1989/90	1990/91	1991/92	1992/93
Solid precipitation	355	469	222	213	254	280
Liquid precipitation	337	265	353	337	284	229
Total over catchment	691	734	575	551	539	509
Measured precipitation at SGHU station	733	769	609	585	569	537

7.5.1.2 Annual water balance

The water balances (Equation 7.5) of the verification period show nearly the same patterns as the water balances of the calibration period. However, discharge and precipitation is higher in the validation period, with an average annual discharge of 602 mm compared to 571 mm in the calibration period, an average annual precipitation of 600 mm in the validation period and 565 mm in the calibration period. Again the balance is 0 for all years. Table 7.8 and Figure 7.9 summarize the components of the water balance.

Table 7.8: The main terms of the water balance of Langtang Khola catchment as assessed by the TAC^d model for the validation period in mm/a

	1987/88	1988/89	1989/90	1990/91	1991/92	1992/93
Discharge	593	567	656	715	559	522
Actual ET	117	109	136	141	110	112
Glaciermelt	255	222	412	445	291	317
Precipitation	691	734	575	551	539	509
Storage change	236	279	195	140	160	192
Balance	0	0	0	0	0	0

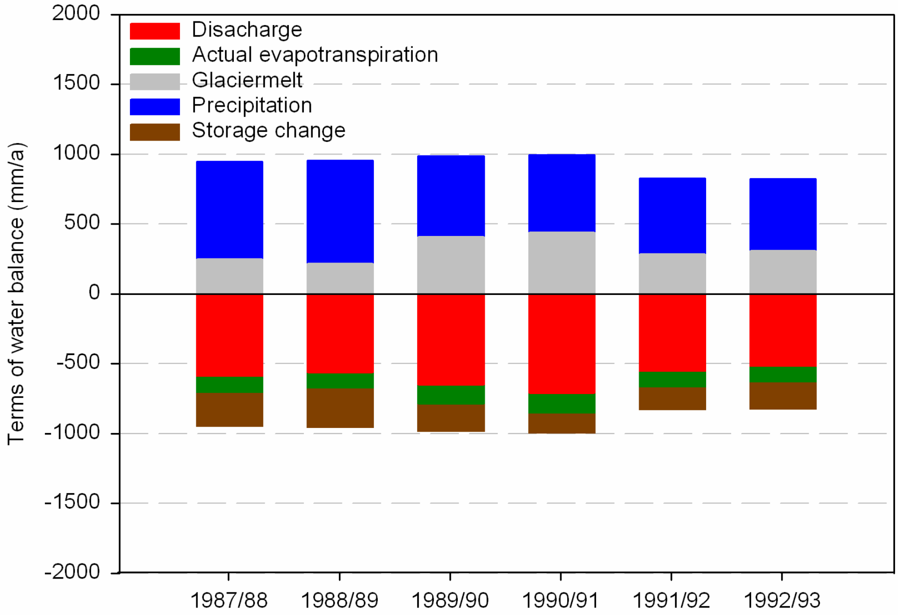

Figure 7.9: Main terms of the water balance of the verification period of Langtang Khola catchment. Added components with a positive sign are the input into the system, whereas the added values with a negative sign are the output of the system and the storage change

7.6 Conclusions

The application of TAC[d] in the Langtang Khola catchment was successful in most of the simulated years with model efficiencies from 0.20 to 0.87. The dynamics of the hydrograph can be reproduced satisfactorily considering the reliability of the measured discharge and climatological data. Not only discharge but also glacier mass balances can be simulated well. However, the simulation of the onset of discharge in the pre-monsoon season is delayed in most of the simulated hydrological years. The soundness of the model code is proven by a balanced water balance.

The calibration procedure is still subjective compared to automatic calibration techniques, but the advantage of using this method is that the modeler becomes familiar with the sensitivity of the parameters. The compliance of the fixed ratios between the storage parameters of the soil and runoff generation routine in particular, as well as the decoupling of these parameters from the calibration procedure in phase three reduce the risk of over-parameterization. The multi criteria calibration with additional mass balance data as a further calibration criterion in addition to discharge enables a more realistic discharge simulation, to be carried out.

8 Model analysis and discussion

8.1 Extrapolation of input data

Complete time series of daily mean air temperature and daily precipitation sums are the prerequisite for the simulation of daily discharge with TAC^d. Statistical methods were used to bridge gaps in the time series and to redistribute cumulated precipitation sums. The extrapolation results and their impacts on discharge simulation are discussed in the following chapters.

8.1.1 Temperature extrapolation

The comparison of measured and extrapolated air temperature is shown in Figure 8.1 for the sample year 1997. The annual measured temperature course was reproduced well by the extrapolation and even single structures were modeled realistically. The simulation of the monsoon season is generally better than the simulation of the dry season. The R_{eff} is 0.88 for the year 1997.

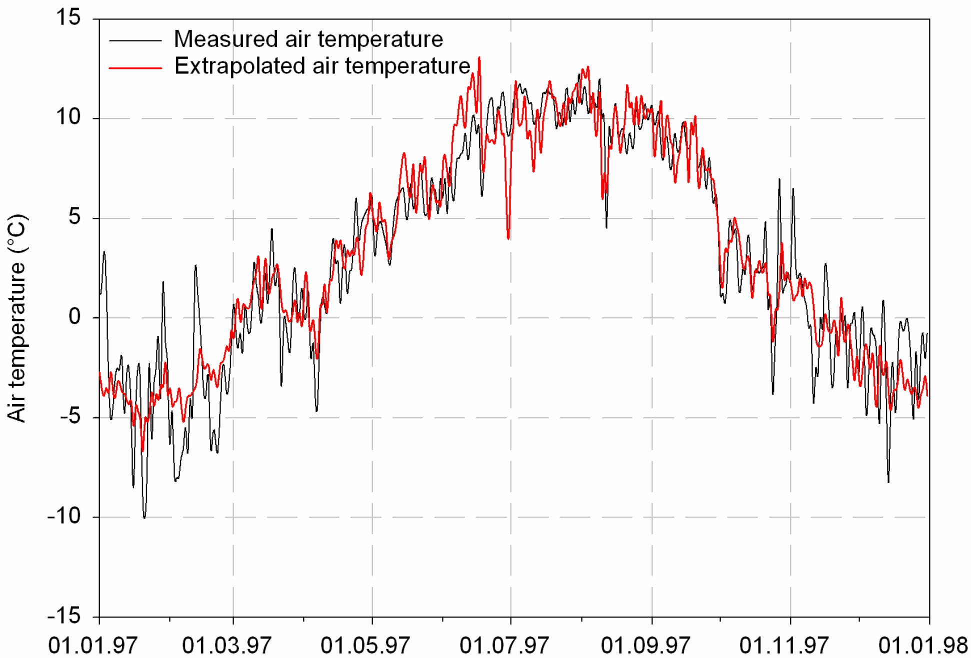

Figure 8.1: Comparison of measured and extrapolated air temperature, 1997

A more objective visualization is shown in the scatter plot in Figure 8.2 (left). The parameters of the linear regression line still deviate from a 1:1 relation and errors of several °C occur in the isolated case. However, an improvement compared to the simple linear regression as extrapolation method can be observed (Figure 8.2, right). 90 % of the observed daily mean air temperature can be explained with the extrapolation using the second order polynomial function, while only 87 % can be explained with the simple linear regression in 1997.

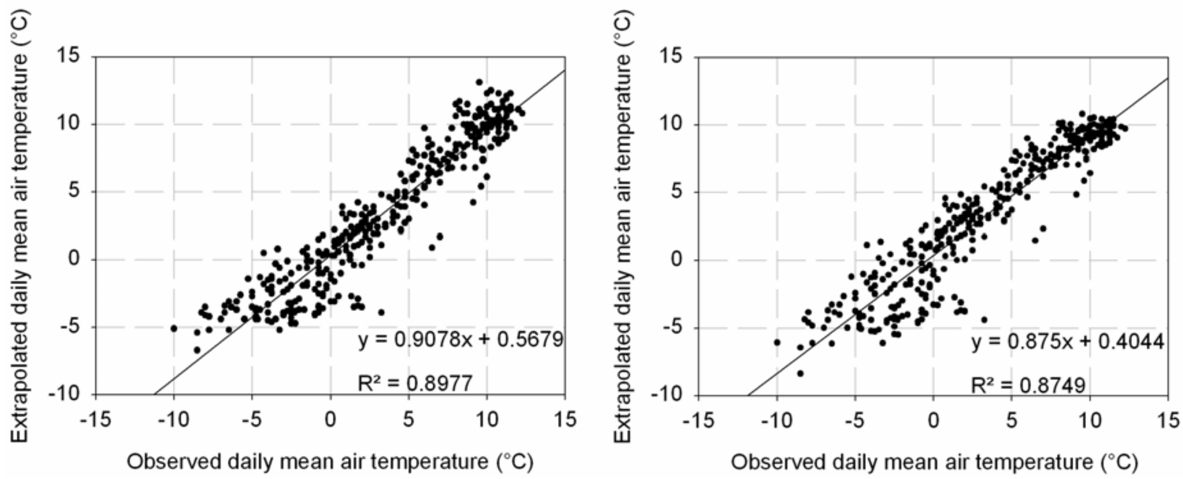

Figure 8.2: Scatter plots of observed and simulated daily mean air temperature. Extrapolation with second order polynomial function (left) and simple linear regression (right), 1997

Table 8.1 summarizes the R^2 values of the years in which the extrapolation method was applied.

Table 8.1: Coefficients of determination for the years in which the gaps in air temperature time series were filled using the extrapolation method

Year	**R^2**
1987 (18.6. to 31.12.)	0.70
1988	0.75
1989	0.86
1991	0.91
1997	0.90
1998	0.85

The extrapolated values were used only to bridge the gaps in the time series. For 98 % of the time, measured values were available and therefore only single values of the extrapolated time series were used. The extrapolated values are considered as "first guess" of the order of magnitude of the values which were used for bridging the gaps. The final values have to fit in the course of the measured values and can be adjusted subjectively if the calculated values seem to be unreliable and do not fit in the course of the measured time series. Thus, the course of the inserted values is determined by the course of the extrapolated values as well as by the course of the measured values. Figure 8.3 shows an example for the mode of operation where extrapolated values were used to bridge the gaps in the time series.

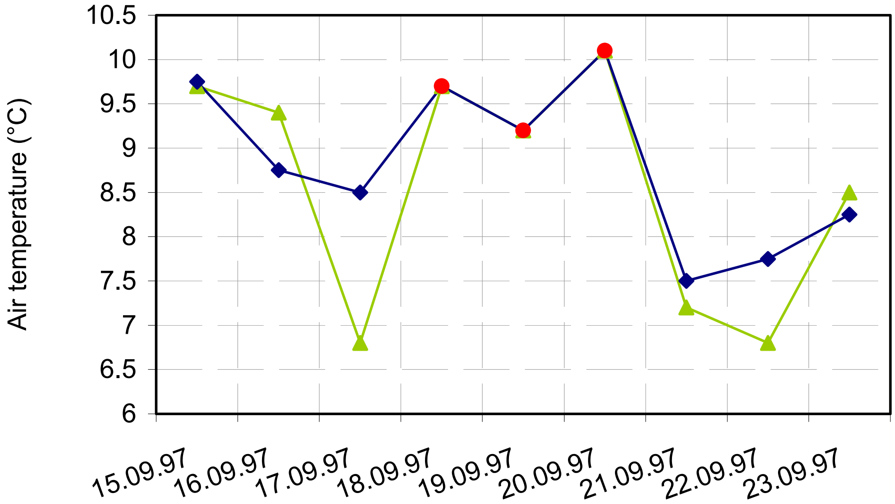

Figure 8.3: Example for the mode of operation of data extrapolation of air temperature time series, 1997. Red points are the values inserted to bridge the gaps in the time series, blue squares are the measured values and the green triangles are the extrapolated values

The combination of extrapolation and subjective evaluation of the extrapolated values in relation to the course of the measured time series reduces the error of the inserted value. The error is not zero but should be below 1 °C in most cases. Further, most of the gaps are single missing days or, at the most, series of 3 to 4 days during periods where air temperature is above the threshold temperature for melting (TT). This simplifies the adjustment of the extrapolated values to the course of the measured values and the error of the inserted values becomes minimal. Longer series of missing values occur mainly in November and December when air temperature is below TT. If air temperature is clearly below TT, the impact of possible extrapolation errors on the discharge simulation results is minimal because no meltwater production occurs. Correct extrapolation results are therefore most important for temperature levels above and around TT. Figure 8.1 shows that extrapolation results of air temperature above TT (in the monsoon season) are much better than of air temperature below TT.

8.1.2 Precipitation extrapolation

The measured precipitation values are compared with the synthetic values of June and July 1997 in Figure 8.4 for the visualization of the precipitation extrapolation results. Some of the precipitation sums are reproduced well, e.g. around 27th July, 1997; others are redistributed over several days, e.g. around 29th June, 1997. However, there are some significant deviations between the measured and the simulated precipitation sums. The reconstruction of the precipitation sums is based on probabilities and it is not an extrapolation like the temperature extrapolation where reliable correlations between SGHU station and reference stations are a prerequisite (Chapter 6.4.2). Nevertheless, the synthetic time series are able to describe the actual situation adequately. Figure 8.4 shows that the main patterns of the measured precipitation sums are reproduced well by the algorithm.

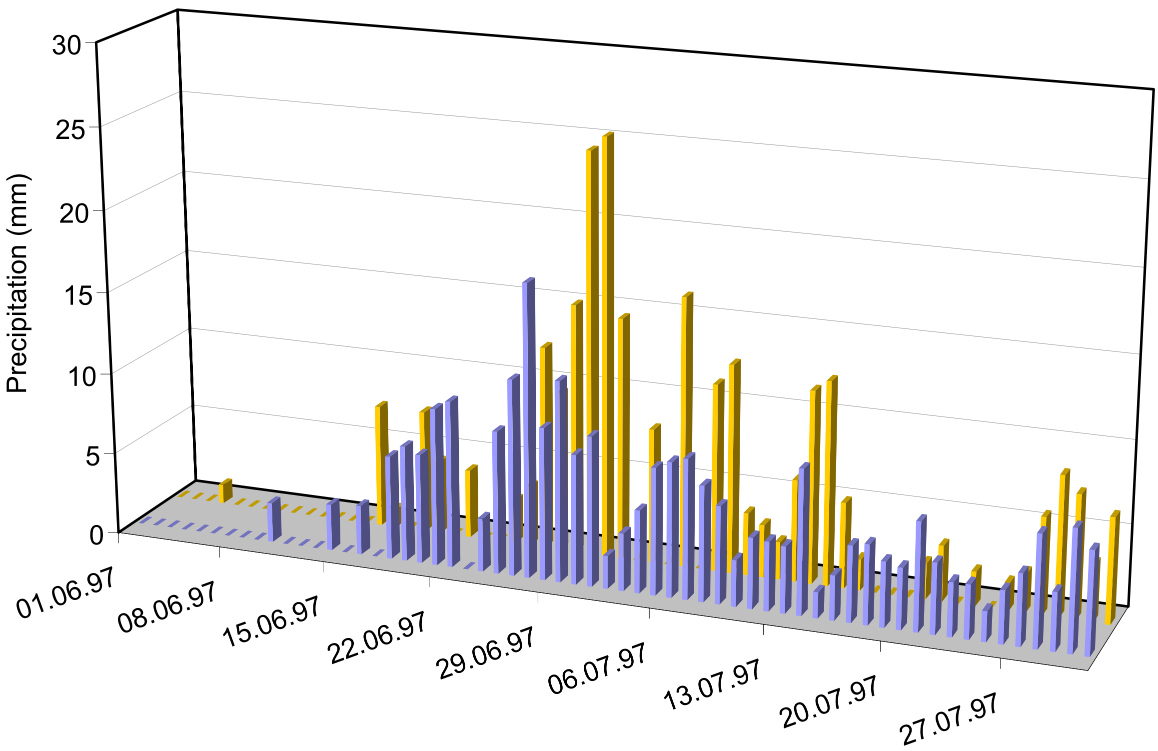

Figure 8.4: Comparison of measured daily precipitation sums (yellow bars) and simulated daily precipitation sums (blue bars)

The simulated daily precipitation sums were adjusted to the actual precipitation sums and therefore the deviations of the monthly amounts of precipitation are not significant. The temporal shift of the simulated precipitation sums does not necessarily influence the discharge simulation. If the storage capacities of soil, snowpack or of the storages of the runoff generation routine are not exceeded, additional water is added to these storages and contributes to runoff generation with retardation. These retardation effects allow errors in temporal assignment in the magnitude of the errors of the simulated precipitation sums. It must be considered further that precipitation events in the same region do not always occur at the same time or are stationary throughout the event. An event which was observed at several reference stations in the region can occur at the SGHU station earlier or later. If precipitation occurs at a reference station in the evening the algorithm implies that there is rain- or snowfall at the SGHU station on the same evening, whereas the precipitation event occurred in reality on the following morning at the SGHU station. This causes temporal shifts of the simulated precipitation sums even if there is a strong coupling of the climatological conditions between the region and the target station (SGHU station).

The artificial coupling of the local conditions to the regional conditions might not necessarily be a disadvantage. There is only one station in the Langtang Khola catchment which is meant to represent the entire meteorological situation of the catchment and the absence of further data makes the evaluation of the representativity of this station impossible. It is possible that the more regionalized information of the simulated precipitation sums are even more representative for the catchment than the measured values of a single station at the valley bottom.

A comparison of the simulated hydrographs calculated based on measured daily precipitation sums and extrapolated daily precipitation sums in Figure 8.5 shows that the differences are minimal. The hydrological year 1995/96 was chosen for the comparison because this year

shows neither gaps nor cumulated values and is therefore the most suitable for showing the influences of different precipitation inputs on the simulated hydrograph. The measured precipitation event of 25th July, 1996 accounts for 25 mm while the extrapolation algorithm distributes this amount over previous days. The discharge peak calculated with the measured precipitation sums is therefore not found in the simulated discharge with extrapolated precipitation input.
The extrapolated values are used only to fill gaps and to redistribute cumulated values. Plausible values of the measured time series were taken over unchanged in the newly generated time series. The new time series does not represents the real conditions for 100 % but can be seen as an appropriate input for the simulation of daily discharge with TAC^d.

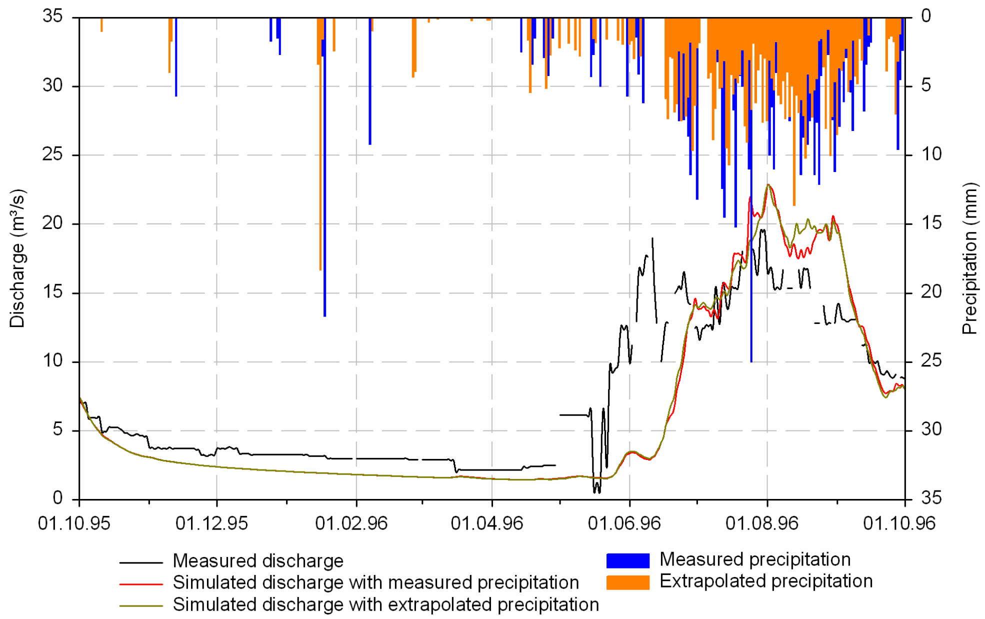

Figure 8.5: Comparison of the influences of different precipitation inputs on the discharge simulation. The hydrological year 1995/96 was chosen because there are no missing values or cumulated sums of precipitation in the measured time series

8.2 Regionalization of input data

Two studies were found in the literature which provide spatial distributed information about air temperature and precipitation for the evaluation of the regionalization of climatological input data. Figure 8.6 shows the location of the meteorological stations and the sites where precipitation, air temperature and maximum snow depth were measured. Shiraiwa et al. (1992) provide mean monthly air temperature data from June 1989 to March 1991 and precipitation data from June 1990 to April 1991 with maximum snow accumulation data from December 1989 to June 1990. Their stations were located in altitudes from 3920 m a.s.l. to 5300 m a.s.l. . Sakai et al. (2004) measured precipitation and air temperature at Lirung glacier (4190 m a.s.l.) from 15th July to 29th August, 1996. Table 8.2 summarizes information on the meteorological stations and the conducted measurements.

Table 8.2: Meteorological stations in the Langtang valley and the measurements from Shiraiwa et al. (1992), Steinegger et al. (1993) and Sakai et al. (2004)

Station	Altitude (m a.s.l.)	Measurement	Observation period
1	5090	Precipitation	June 1990-September 1990
		Air temperature	June 1989-March 1991
2	3920	Precipitation	June 1990-September 1990
(SGHU		Maximum snow depth	December 1989-June 1990
station)		Air temperature	June 1989-March 1991
3	5090	Precipitation	June 1990-September 1990
		Maximum snow depth	December 1989-June 1990
		Air temperature	June 1989-March 1991
4	4677	Maximum snow depth	December 1989-June 1990
5	5013	Maximum snow depth	December 1989-June 1990
6	4942	Maximum snow depth	December 1989-June 1990
7	5300	Precipitation	June 1990-September 1990
		Air temperature	June 1989-March 1991
8	4190	Precipitation	July 1996-August 1996
		Air temperature	July 1996-August 1996
9	5580	Snow accumulation	1980/81-1988/89
10	5350	Snow accumulation	1980/81-1988/89
11	5800	Snow accumulation	1980/81-1988/89

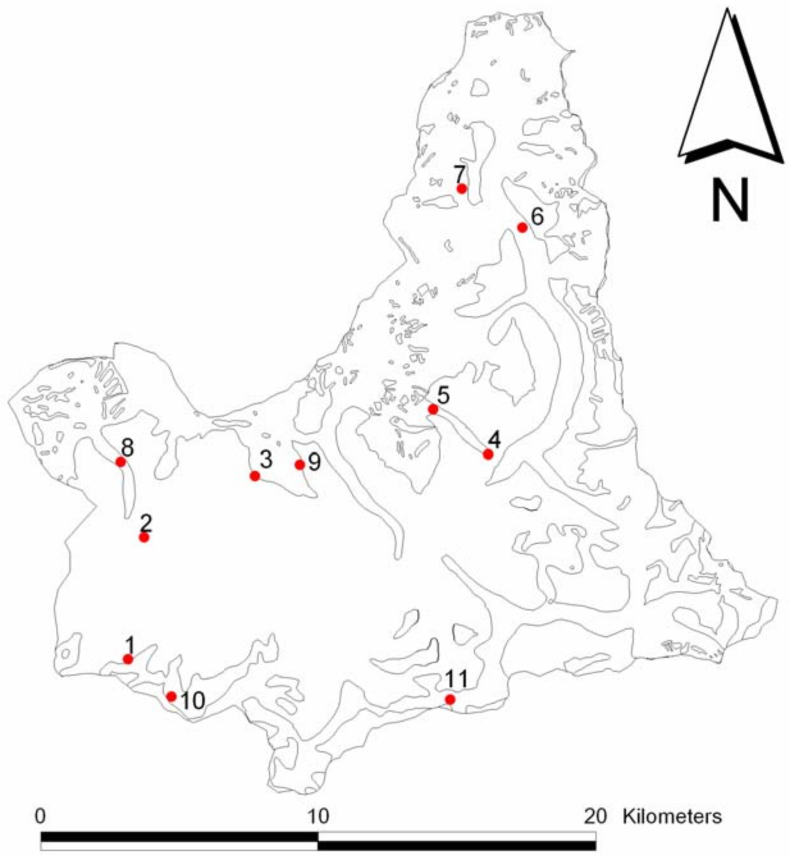

Figure 8.6: Langtang valley and the observation sites of the studies conducted by Shiraiwa et al. (1992), Steinegger et al. (1993) and Sakai et al. (2004)

8.2.1 Regionalization of air temperature

The air temperature regionalization is achieved using a fixed lapse rate as described in Chapter 5.1.2. Calculated mean monthly air temperature values are compared with measurements at the stations described in Chapter 8.2 for evaluation of the regionalization method (Figure 8.7). Table 8.3 shows the coefficients of determination for the period from June 1989 to March 1991.

Table 8.3: Coefficients of determination for the comparison of simulated and measured mean monthly air temperature at different stations in the Langtang valley for the period from June 1989 to March 1991

Station	Altitude (m a.s.l.)	R^2
1	5090	0.94
3	5090	0.92

The R^2-values show a good simulation of the measured mean monthly air temperature for both stations with the fixed lapse rate of -0.5 °C/100 m. Visual inspection reveals, however, that air temperature during monsoon season is underestimated at both stations. The mean air temperature at Station 8 from July to August 1996 (8.8 °C) is also underestimated with 6.6 °C as simulated mean air temperature for that period.

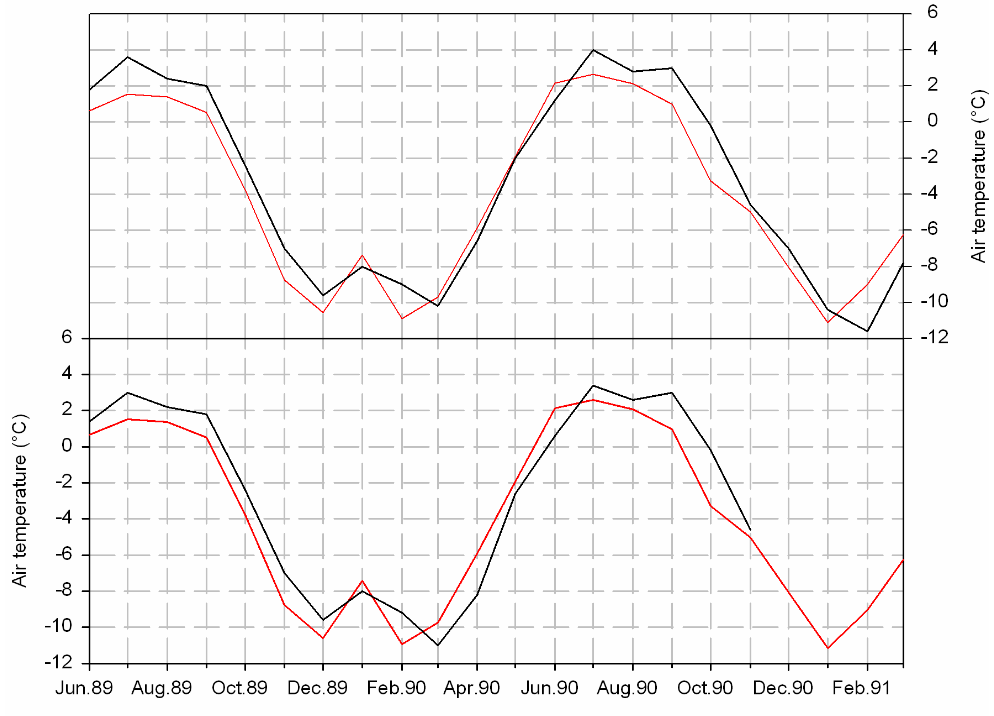

Figure 8.7: Comparison of simulated and measured air temperature at Station 1 (upper graphic) and Station 3 (lower graphic)

The decline of air temperature with altitude during monsoon season is less than the fixed rate. The seasonal variation in the vertical air temperature gradient between SGHU station and Station 1 is shown in Figure 8.8 from June 1989 to March 1991.

Figure 8.8: Seasonal variation in the vertical air temperature gradient between SGHU station (3920 m a.s.l.) and Station 1 (5090 m a.s.l.)

The mean lapse rate from November to May is -0.54 °C/100 m while it is -0.38 °C/100 m from June to October. This seasonal change of the lapse rate cannot be considered using a fixed lapse rate. In addition to that, the temperature gradient used in the model must be seen as an average value which has to be applicable to all simulated years and the measured air temperature at the SGHU station is considered to be representative for the entire catchment.
Air temperature is used for the calculation of snow- and icemelt in the temperature-index method. The threshold temperature TT in Equations 5.8, 5.9, 5.10 (Chapter 5.3.3) is also a correction for the simulated temperature at the respective cell. TT is negative (-0.2 °C, Table 7.2) in this application which means that the daily air temperature is increased by the value of TT for the calculation of snow- and icemelt. This correction reduces the errors during monsoon season caused by the fixed lapse rate. The regionalization method does not consider the spatial variability of air temperature due to topographical shading effects. Shading effects are considered in the calculation of snow- and icemelt by the correction factor RexpMap (Chapter 5.3.1). It is not necessary to include this information in the regionalized temperature values in order to obtain a realistic simulation of melt. The regionalization of air temperature with a fixed gradient is considered to be an appropriate method for the available data base.

8.2.2 Regionalization of precipitation

Horizontal and vertical gradients were used for the regionalization of daily precipitation sums. The horizontal gradient was introduced based on the observations by Shiraiwa et al. (1992). Figure 8.9 compares the measured and simulated precipitation sums from June to September 1990 at Stations 1, 3 and 7. The sums over the 4 months were calculated with and without the horizontal gradient. The measured sums are generally underestimated at Stations 1 and 3. By contrast, simulation without the horizontal gradient overestimates the precipitation sum at Station 7, and the calculated sum is even higher than the calculated sums at Stations 1 and 3. The altitudes of the stations provide the reason for this: Station 7 is the highest station. The measured precipitation sums at Stations 1 and 3 are even more underestimated if the horizontal gradient is used for the simulation. However, the basic patterns of spatial distribution of basin precipitation are described more realistically. Station 7 receives less precipitation than Stations 1 and 3 (Chapter 3.2.2).

Figure 8.10 shows the influence of the horizontal gradient on annual precipitation distribution. Most of the annual precipitation falls in the upper reaches of the valley due to the higher elevations if the simulation is conducted without the horizontal gradient.
The measurements of maximum snow depth also show the declining amounts of solid precipitation in the upper reaches of the catchment. They cannot be compared with the simulated water equivalents because no snow density measurements were carried out.
Either the horizontal or the vertical gradient was determined from the measurements of Shiraiwa et al. (1992) as a magnitude for these parameters, but had to be changed slightly during the calibration procedure. The gradients in Table 7.2 are average values which were used for the entire simulation period. Deviations from measured events must therefore be expected.

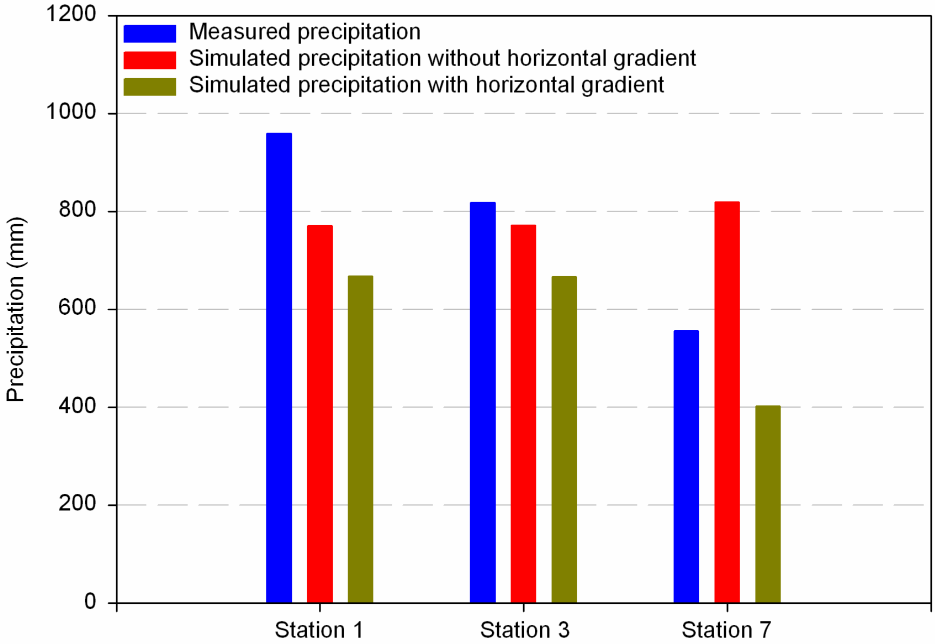

Figure 8.9: Comparison of measured and simulated precipitation sums from June to September 1990 at three stations in the Langtang valley. The precipitation sums were calculated with and without the horizontal gradient

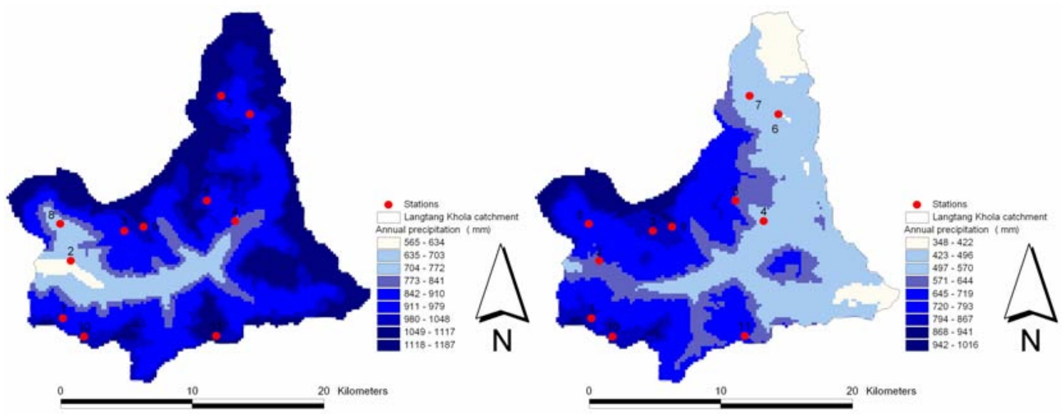

Figure 8.10: Distribution of annual precipitation sums calculated without (left) and with (right) the horizontal gradient

8.3 Evapotranspiration

Actual evapotranspiration was measured at Stations 2 and 8 by Sakai et al. (2004) and given as an average from 15th July to 29th August, 1996. The average value from Station 8 amounts to 1.99 mm/day and compares favorably with the simulated average value of 2.10 mm/day.

The actual evapotranspiration at Station 2 is underestimated by the model with a simulated average of 2.01 mm/day compared to the measured average value of 4.5 mm/day.
The spatial distribution of the mean annual accumulated actual evapotranspiration from 1993 to 1998 in Figure 8.11 shows that the highest values occur at the valley bottom and at places where water is stored, e.g. glaciers.

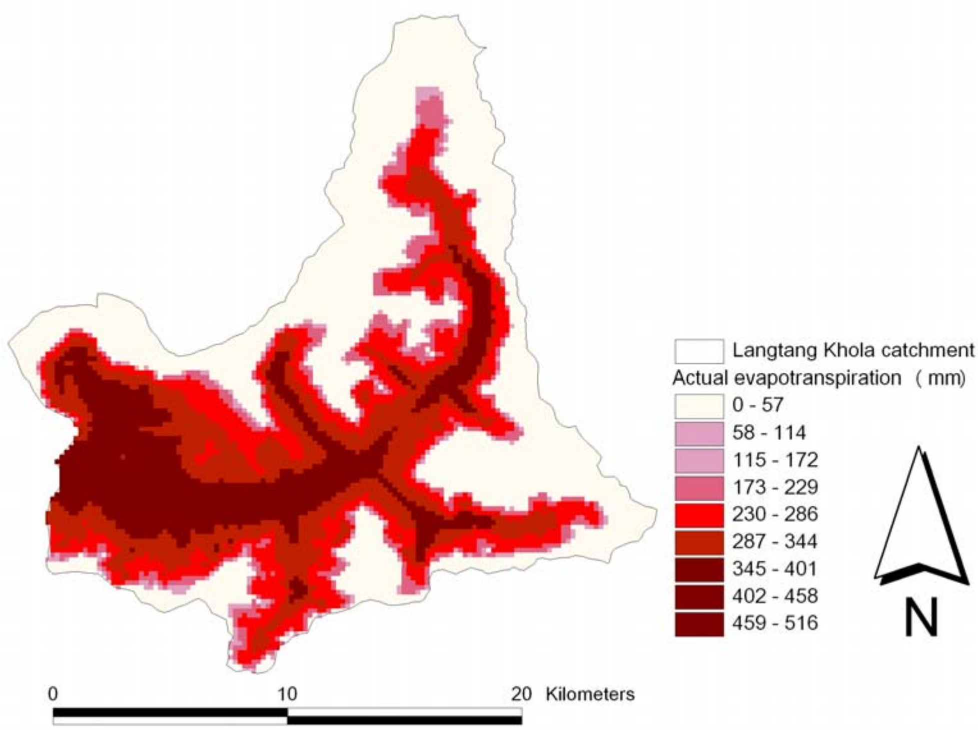

Figure 8.11: Spatial distribution of the mean annual accumulated actual evapotranspiration from 1993 to 1998

Evapotranspiration can be an important factor, energy-wise, over a short period but as a water balance component the amount of evapotranspiration is small compared to, for example, precipitation in high alpine areas (Lang 1981). Thus, the simple sinusoidal approach for the calculation of potential evapotranspiration with a vertical gradient for regionalization is considered to be appropriate for the available data base and the climatological conditions of the Langtang Khola catchment.

8.4 Snow and glacier routine

As Figure 8.12 shows, the integration of the algorithms for the calculation of glaciermelt brought the expected improvement in discharge simulation. There is a significant drop in performance if glaciermelt is neglected. The R_{eff}-values for the sample year 1994/95 are 0.88 for simulation including glaciermelt, and 0.03 for simulation without glaciermelt. In general, the simulations without the extensions for glaciermelt greatly underestimate the observed runoff (VE is 297 mm/yr in 1994/95). Therefore, it is not possible to make reliable assumptions of the water balance of the catchment, mainly in monsoon season, where a large amount of runoff originates from glaciermelt if glaciermelt is neglected.
TAC^d is able to reproduce the glacier mass balances satisfactorily as already shown in Chapters 7.4 and 7.5.

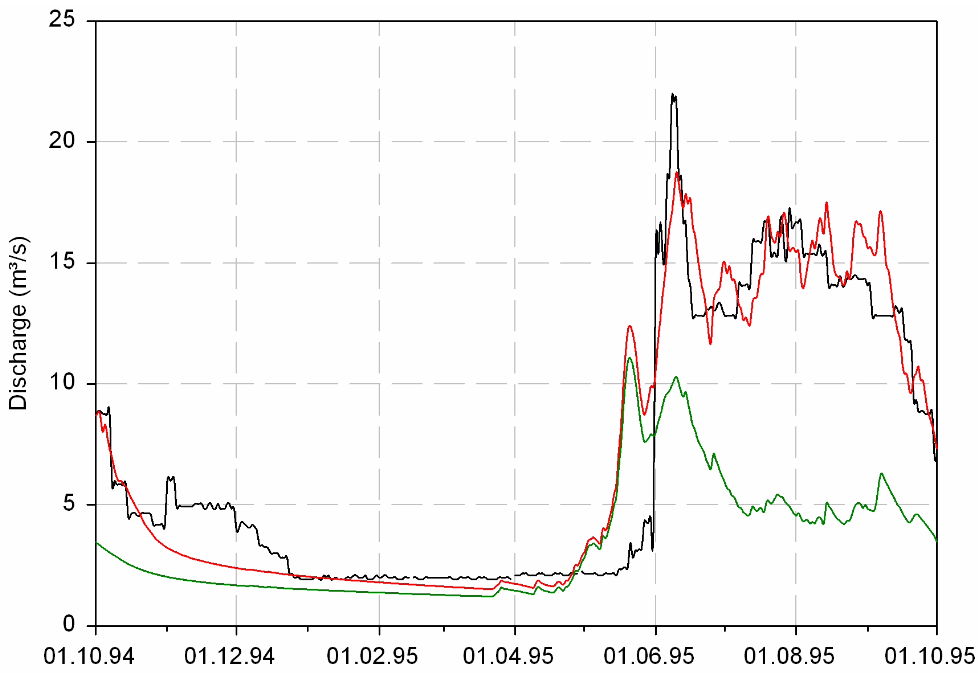

Figure 8.12: Comparison between observed discharge (black line) and simulated discharge (red line: with contribution of glaciermelt; green line: without contribution of glaciermelt)

The effects of the implemented extensions of the snow and glacier routine will be discussed in the following chapters and evaluated as far as possible on the basis of measurements.

8.4.1 Seasonally and spatially distributed modeling of snow- and icemelt

The correction factor for the degree-day method (RexpMap) accounts for seasonal and spatial variations in the degree-day factor. Figure 8.13 shows the spatial distribution of RexpMap for the winter and the summer solstice as it is visualized in PCRaster.

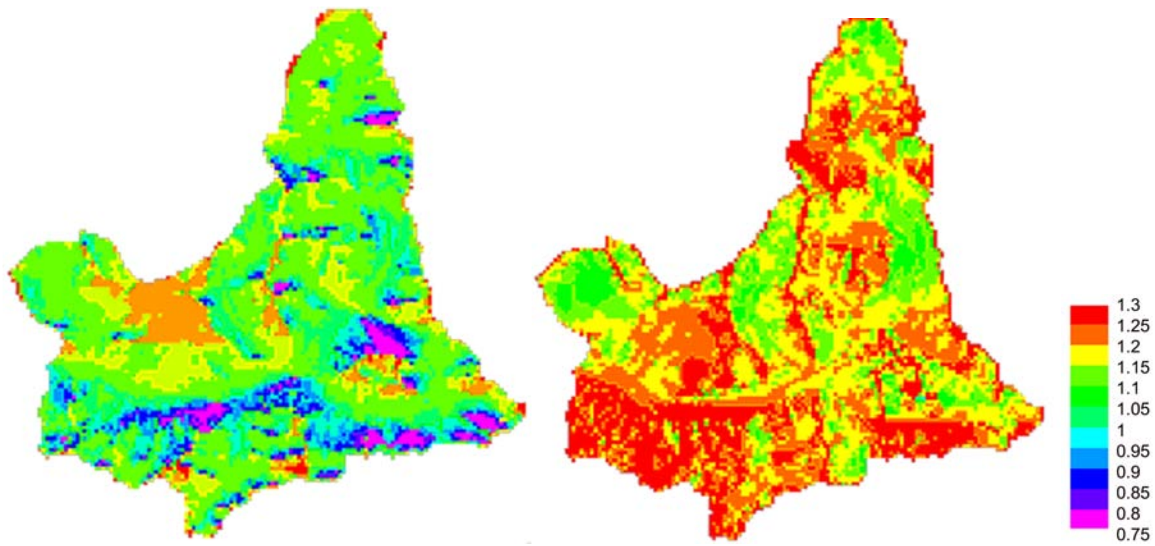

Figure 8.13: Spatial distribution of the correction factor for the degree-day method (RexpMap) at the winter solstice (21^{st} December (left)) and the summer solstice (21^{st} June (right))

The spatial distribution of RexpMap shows realistic patterns. On the 21st December the lowest values of RexpMap can be found at the north-oriented slopes at the valley bottom, whereas the highest values occur at the peaks and at highly elevated south-oriented plateaus. The zenith angle of the sun is close to 0° in the Langtang valley at the summer solstice due to its location close to the Tropic of Cancer (23.5° N). Thus, the map of the 21st June shows the highest values at cells with northern and southern orientation and at the peaks or ridges. The lowest values are at east- or west-oriented slopes.
The temporal distribution of RexpMap follows a sinusoidal course with its maximum on the 21st June and its minimum on the 21st December. Figure 8.14 shows the average values of RexpMap of the Langtang valley for a hydrological year. The values are not less than 1.0, which indicates the dominance of cells with high RexpMap values in the catchment.

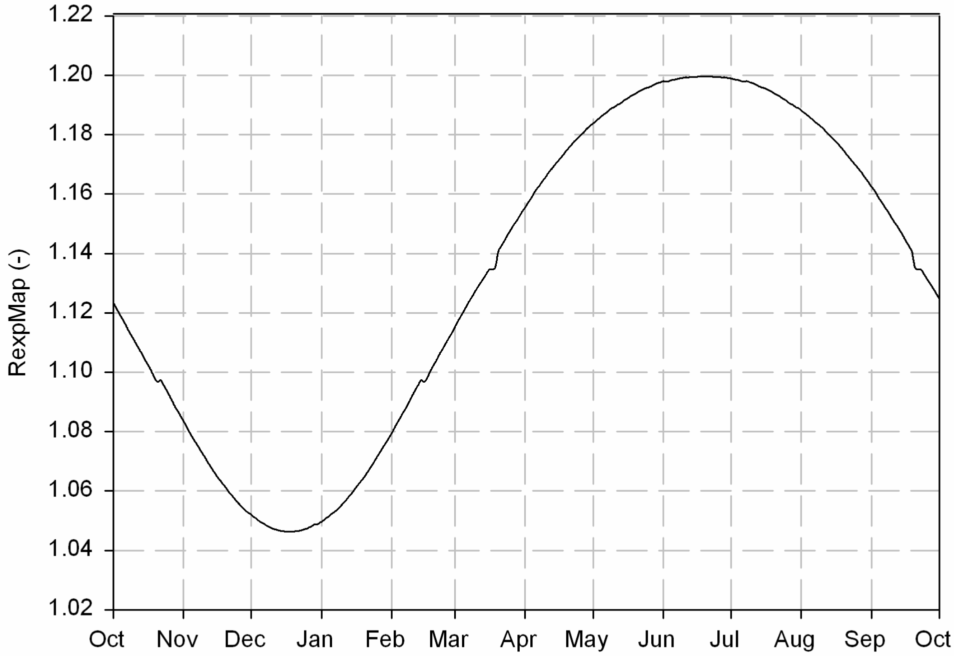

Figure 8.14: Sinusoidal course of the average correction factor for the degree-day method (RexpMap) of the Langtang valley for a hydrological year

A sinusoidal annual course of the degree-day factor is proposed by Braun et al. (1993). They determined the sinusoidal oscillation of the degree-day factor with two parameters for the minimum and maximum of the curve. In this thesis the sinusoidal course of the degree-day factor is derived from astronomic and topographic information for each cell. This enables a more realistic temporal and spatial distributed simulation of melting processes.
This regionalization method for meltwater calculation is linked with the potential sunshine duration and not with the actual sunshine duration. Thick clouds reduce the sunshine duration, especially during the monsoon season. The clouds are mainly convective, characterized by a large temporal and spatial variation (Kappenberger et al. 1993). For the most part, the sky is clear in the morning and clouds develop at the slopes during the day. Correction of the potential sunshine duration using measurements of actual sunshine duration was not possible due to the lack of measurements.

The degree-day factor is about twice as large as in alpine applications (Braun et al. 1990). Motoyama et al. (1989) observed surface glaciermelt rates of 12.7 mm/(°C day) for Yala Glacier at 5100 m a.s.l. for the period from 23rd August to 3rd September, 1987. Further measurements of surface glaciermelt rates on Khumbu glacier (Everest region) were even larger, with 16.9 mm/(°C day) for bare ice (Kayastha et al. 2000). The simulated degree-day factor for the area where the measurements at Yala glacier were conducted amounts to 11.9

mm/(°C day). This value for bare ice is the product of Cfmax, RexpMap and the correction factor for accelerated melt of ice compared to snow (Rmult) (Equation 5.9). It can be considered as constant for the same period in different years because Cfmax and Rmult are constant values and the course of RexpMap is similar for all hydrological years. The simulated value can therefore be compared with the measured value of Motoyama et al. (1989) although their observation period does not lie within the simulation period. The values compare favorably.
The observed value at 5300 m a.s.l. at Yala glacier, however, shows a very large difference as compared with the simulated degree-day factor. The value observed by Motoyama et al. (1989) for the period from 23rd September to 3rd October, 1987 amounted to 19.2 mm/(°C day) and is more than twice as large as the simulated value of 8.5 mm/(°C day). When air temperature is measured over snow and ice surfaces as done by Motoyama et al. (1989), its information content with respect to energy availability for melt is greatly reduced. Air temperature measurements taken outside the glacierized area are considered to be more representative for the use of index methods in calculating snow- and icemelt (Chapter 5.3.1).
Figure 8.15 shows the spatial distribution of the snow cover at the end of the calibration period. The regions above 5500 m a.s.l. have a massive snow cover.

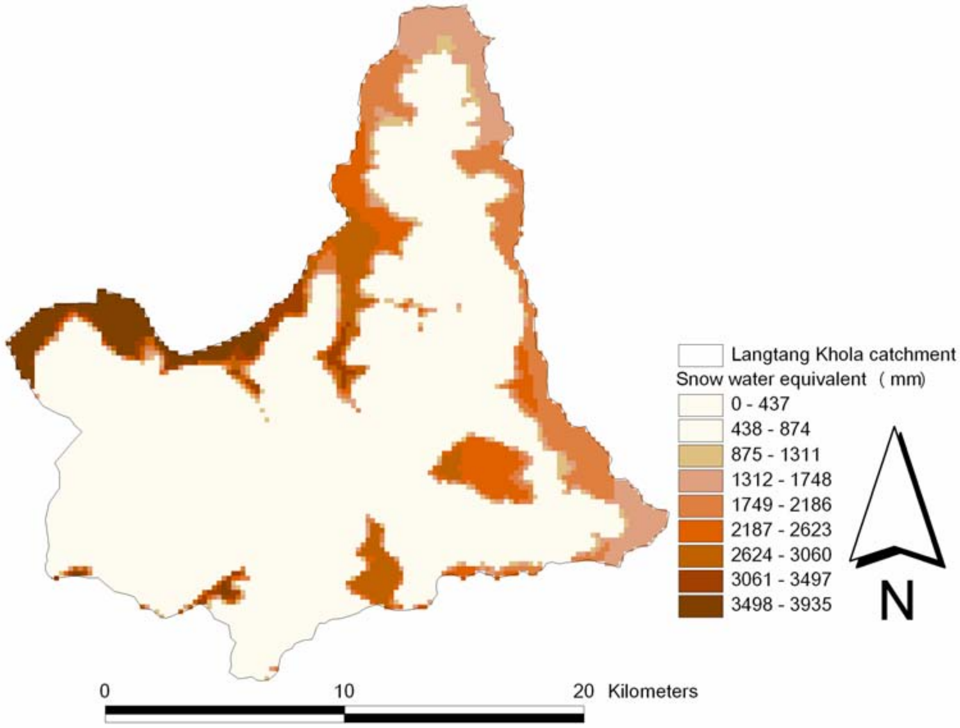

Figure 8.15: Spatial distribution of the snow cover at the end of the calibration period (30th September, 1998)

Ablation in TAC^d is simulated as snow- or icemelt, whereas redistribution of snow via avalanches or wind is not considered by the model. Thus, no ablation is simulated for the areas above the altitude shown in Figure 8.16 where the air temperature is below the threshold temperature (TT).

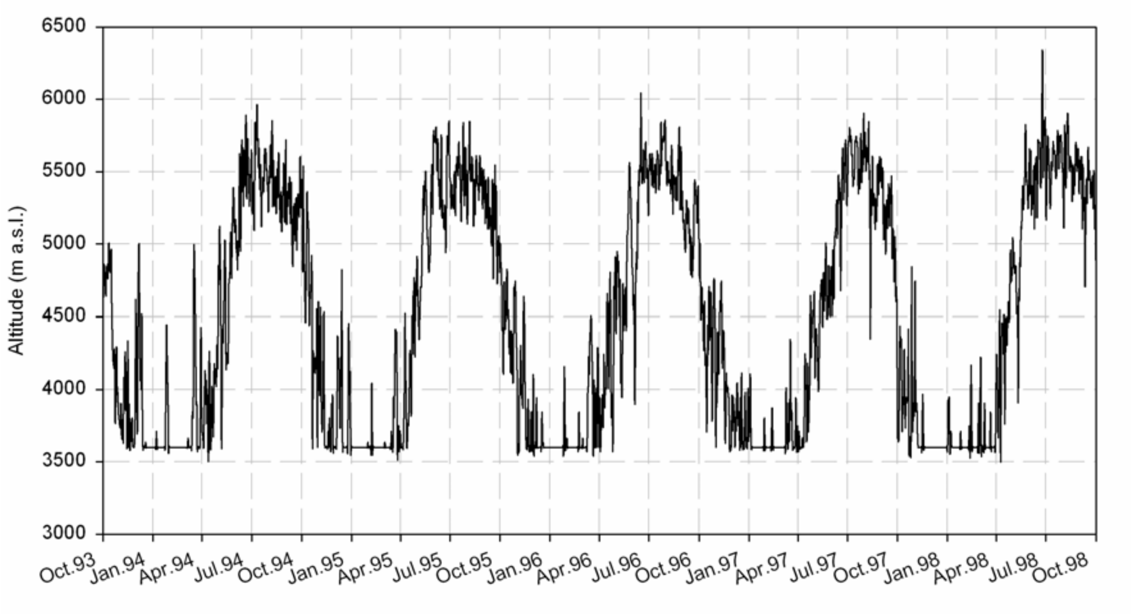

Figure 8.16: Altitude at which the air temperature equals TT

This leads to an unrealistic snow cover simulation at the peaks and at steep slopes where snow is, in reality, redistributed via avalanches or wind, or where sublimation plays a significant role in the ablation process. Steinegger et al. (1993) measured stored precipitation in accumulation areas of glaciers from 1980/81 to 1988/89 and assessed the water equivalent of the individual snow layers. The variation in the annual accumulation is in the range of 600 to 1300 mm of water equivalent. For the assessment of the simulated snow accumulation the measured values are compared with the simulated ones in Table 8.4.

Table 8.4: Comparison of measured and simulated annual snow accumulation rates

	Measured accumulation			**Simulated accumulation**		
	Station 9	Station 10	Station 11	Station 9	Station 10	Station 11
1987/88	638	133	723	847	490	700
1988/89	614	128	596	1219	947	743

Annual accumulation rates are overestimated at all stations except Station 11 in 1987/88. The impacts on the runoff generation are discussed in Chapter 8.5.3.

Generally, the temperature-index method performs well if the air temperature is above TT, because the air temperature is a representative diagnostic variable for the three major energy sources which determine snow- and icemelt, namely incoming long-wave radiation, absorbed global radiation and sensible heat flux (Chapter 5.3.1). If the air temperature is below TT no ablation can be calculated by this method. This leads to an overestimation of accumulation rates in high altitudes where sublimation in addition to mechanical redistribution of snow contributes to ablation. Zappa et al. (2003) compared different approaches for snowmelt modeling. They found that the temperature-index-based methods are suitable if the interest is limited to simulations in daily resolution. Further, the classical temperature-index method as used in TAC^d performs very well compared to more sophisticated approaches, due to its robustness. The conceptual structure of the temperature-index method is less sensitive to the quality of the meteorological input than the physical-based approaches since the index method allow the calibration of more free parameters. This is a very important point for model applications in the Nepalese Himalayas.

8.4.2 Melt over debris-covered parts of the glaciers

About 19 % of the glaciers in the Langtang Khola catchment are covered by debris, most of which lie in the lowest parts of the basin. Generally, glacier surfaces at these low elevations experience high melt rates and therefore constitute a strong water yield (Braun et al. 1993). However, the thickness of this debris layer may be up to several meters, and as mentioned in Chapter 5.3.3, melt rates as a function of the current meteorological situation are reduced. The parameter Rmultd was introduced to account for this reduction. Rmultd ranges from 0.0 to 1.0. Rmultd = 0.0 means that melt is suppressed totally over the debris-covered parts of the glacier whereas melt rates are calculated as over clean ice if Rmultd is set at 1.0. Figure 8.17 shows the sensitivity of this parameter.

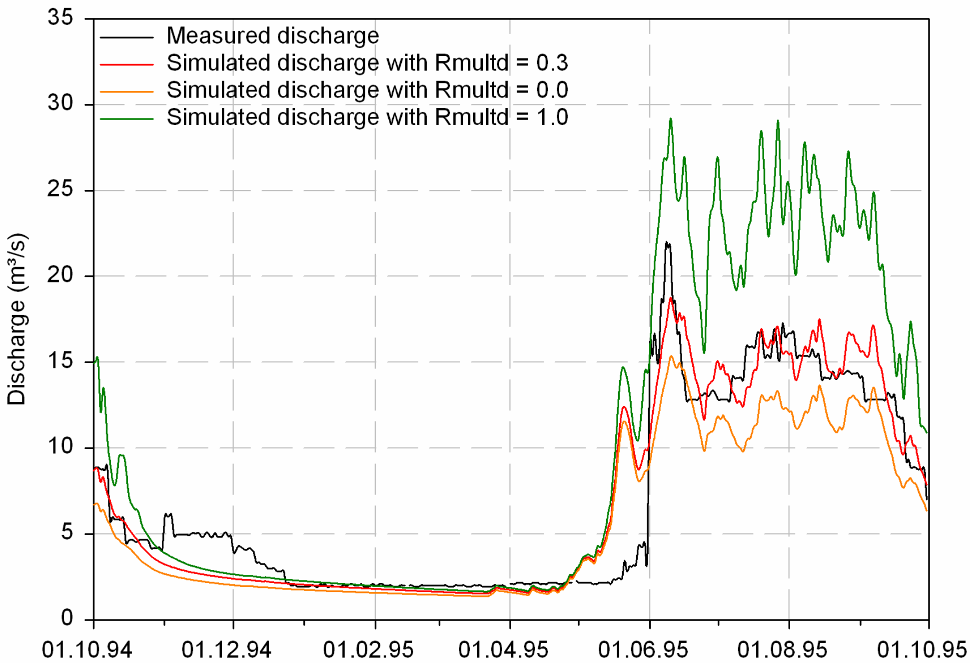

Figure 8.17: Sensitivity of the parameter Rmultd

Discharge is generally underestimated if melt is suppressed totally and overestimated if debris-covered glaciers are treated the same way as clean glaciers. In the sample year 1994/95 volume losses of 100 mm/a occur when setting Rmultd = 0.0, discharge is overestimated by about 269 mm/a if Rmultd = 1.0.

Sub-catchments of the Langtang Khola catchment are delineated for a scale-dependent analysis of the effects of Rmultd on discharge (Figure 8.18). Table 8.5 summarizes the characteristics of the sub catchments.

Table 8.5: The main characteristics of sub catchments in the Langtang Khola catchment

	Area (km² / %*[1])	Glacier area (km² / %*[2])	Debris-covered glacier area (km² / %*[3])	Altitude range of debris-covered glaciers (m a.s.l.)
Lirung glacier	17.5 / 4.9	11.5 / 65.7	1.6 / 13.9	4000-4435
Langtang glacier	116.4 / 32.3	79.4 / 68.2	19.8 / 24.9	4477-5431
Langtang Khola	360.0 / 100.0	164.4 / 45.7	32.12 / 19.5	4000-5431

*[1] % of the Langtang Khola area, *[2] % of sub catchment area, *[3] % of glacier area of the sub catchment

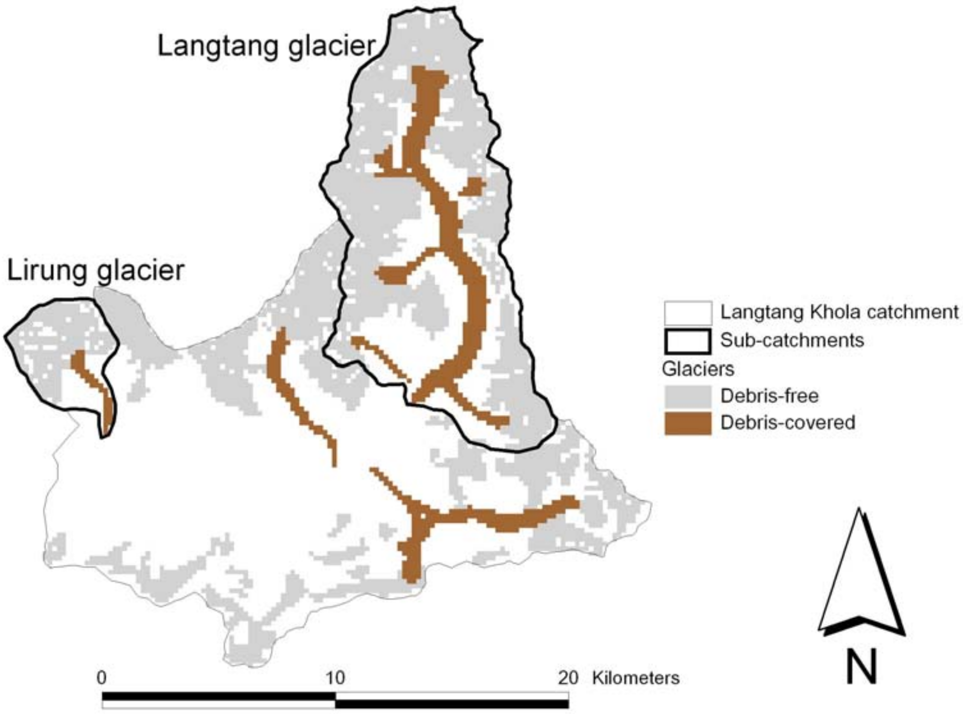

Figure 8.18: The Langtang Khola catchment with Lirung glacier and Langtang glacier sub catchments

The same two scenarios were calculated for the sub catchments, and the deviation from the discharge simulated with the calibrated parameter value (Rmultd = 0.3) was taken to show the consequences on the simulation results (Figure 8.19).

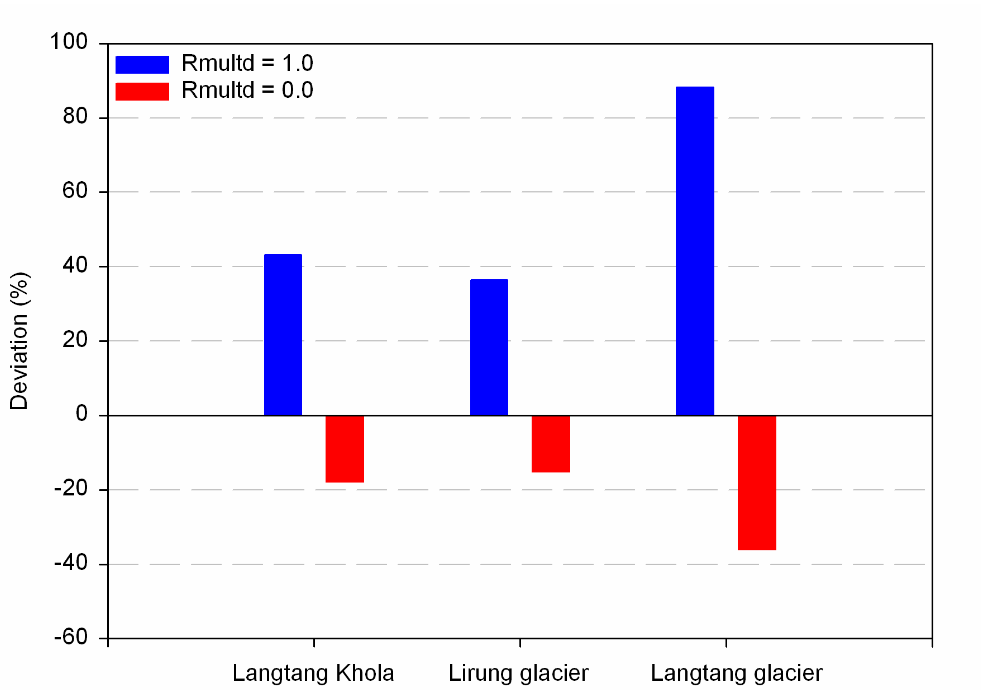

Figure 8.19: Deviation of scenarios results from discharge simulated with calibrated value of Rmultd = 0.3 for the entire Langtang Khola catchment and the sub catchments in the calibration period

The Langtang glacier sub catchment has the highest percentage of debris-covered glaciers and therefore shows the strongest reactions to changes in Rmultd. If Rmultd = 1.0, discharge in

this subcatchment increased by about 88 % compared to the discharge simulated with the calibrated value of Rmultd. If Rmultd = 0.0, discharge is reduced by about 36 %.
The Langtang Khola catchment and the Lirung glacier sub catchment show nearly similar reactions to changes in Rmultd although the difference in the debris-covered area between both catchments (5.6 %) is the same as the difference between the Langtang Khola catchment and the Langtang glacier sub catchment (5.4 %). The debris-covered glacier tongue of the Lirung glacier ranges from 4000 m to 4435 m a.s.l. and is the lowest ice-covered area in the Langtang Khola catchment. Melting rates are therefore higher compared to the other debris-covered glacier tongues due to higher air temperatures at lower altitudes. The generally higher melting conditions compensate for the effects of a smaller debris-covered area of the Lirung glacier sub catchment if Rmultd = 1.0.
If melt is suppressed over debris-covered glaciers, the altitudinal distribution of the clean glaciers of the respective sub catchment is important for the assessment of the impact of suppression of melt on runoff generation. Figure 8.20 shows this altitudinal distribution of the clean glaciers in percent of the entire sub catchment area. These glaciers constitute the water yield if there is no melt at the debris-covered glaciers. The absolute area of clean glaciers is much larger in the Langtang Khola catchment (132.28 km²) than in the Lirung glacier sub catchment (9.9 km²). However, a larger proportion of the clean glaciers of the Lirung glacier sub catchment is below 5000 m a.s.l. and experiences higher air temperatures. Thus, the deviations of the simulation results with Rmultd = 0.0 are quite similar for both catchments.

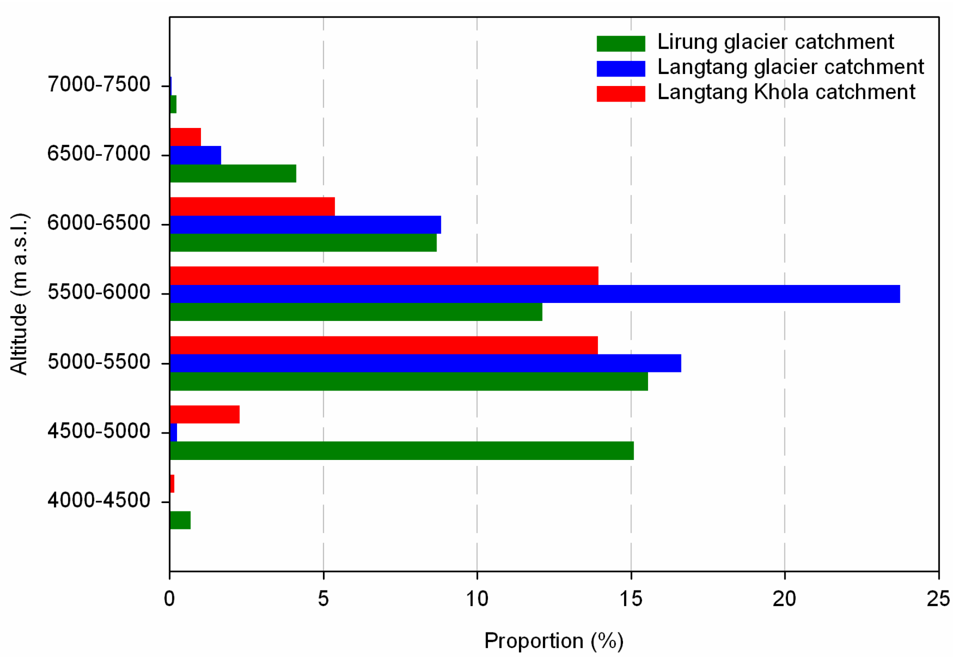

Figure 8.20: Altitudinal distribution of clean glaciers as a percentage of the entire sub catchment area

The value of Rmultd must lie between the two extremes, as shown above. Rmultd = 0.3 was chosen due to the experiences of Popovnin et al. (2002) at Djankuat glacier, Caucasus. They found a reduction of melt under debris layers of 50 to 70 cm of approximately 70 % (Figure 5.5 in Chapter 5.3.3) compared to the melt rate of bare ice.
These observations show that the impact of the debris-covered glaciers on icemelt mainly depends on the area of the debris layer within a catchment. The altitude of the glacier tongues and the spatial distribution of the clean glaciers, however, can cause compensating effects which complicates a general prediction of the scale-dependent impacts of debris-covered glaciers on meltwater production. The analysis has shown that Rmultd is a very sensitive parameter and the approach supports the idea of distributed modeling to include different glacier surfaces

8.5 The runoff generation routine

8.5.1 Composition of runoff in the river network

The composition of runoff shows seasonal variation (Figure 8.21). The high flow season is dominated by the outflow from the upper storages. The low flow is mainly a superposition of runoff of the lower storages of nRGType 1 and 2 and of the storages of nRGTypes 3 and 4. Outflow from the storages of nRGTypes 3 and 4 are important components for the maintenance of winter discharge although the area of these HRUs is small compared to the contribution areas of nRGType 1 or 2 (Chapter 6.5.6, Table 6.9).

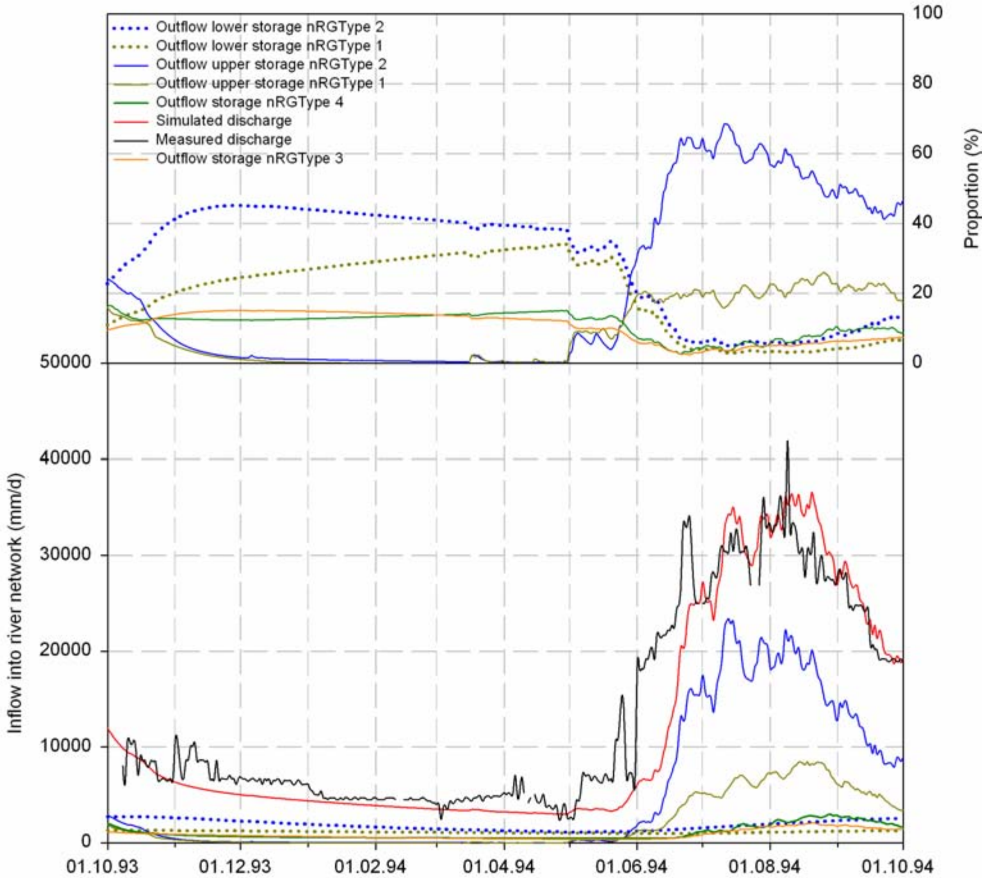

Figure 8.21: Contribution of each runoff component to the entire runoff in percent of the entire runoff (upper graphic) and as absolute values (lower graphic) for the hydrological year 1993/94

8.5.2 Impact of the river network on the simulated discharge

The river network was derived from the DAV topographical map and had to be extended as described in Chapter 6.5.4. The runoff composition of the simulated discharge with the unrevised river network is shown in Figure 8.22. A strongly reduced dynamic in the monsoon season can be observed as well as a temporal shift of the simulated discharge in the monsoon season. The onset of the simulated discharge at the beginning of the monsoon season is much more delayed than the simulated discharge with the revised river network (Figure 8.20). The recession of the simulated discharge at the end of the monsoon season is also delayed by nearly one month.

It is noticeable that the outflow from the upper storage of nRGType 1 contributes more to the maintenance of the winter discharge than in the simulation with the revised river network. This can be explained with conceptualization of the lateral fluxes. The cells which represent the glaciers are generally not directly connected to the unrevised river network and therefore do not directly contribute to the inflow into the river network. Figure 5.11 (Chapter 5.6), however, shows that the outflow from the storage of nRGType 3 is directed to the upper storages of either nRGTypes 1 or 2, which are also connected laterally. Therefore, the outflows from nRGTypes 2 and 3 fill the upper storage of nRGType 1 and contribute to the maintenance of the winter discharge in that way.

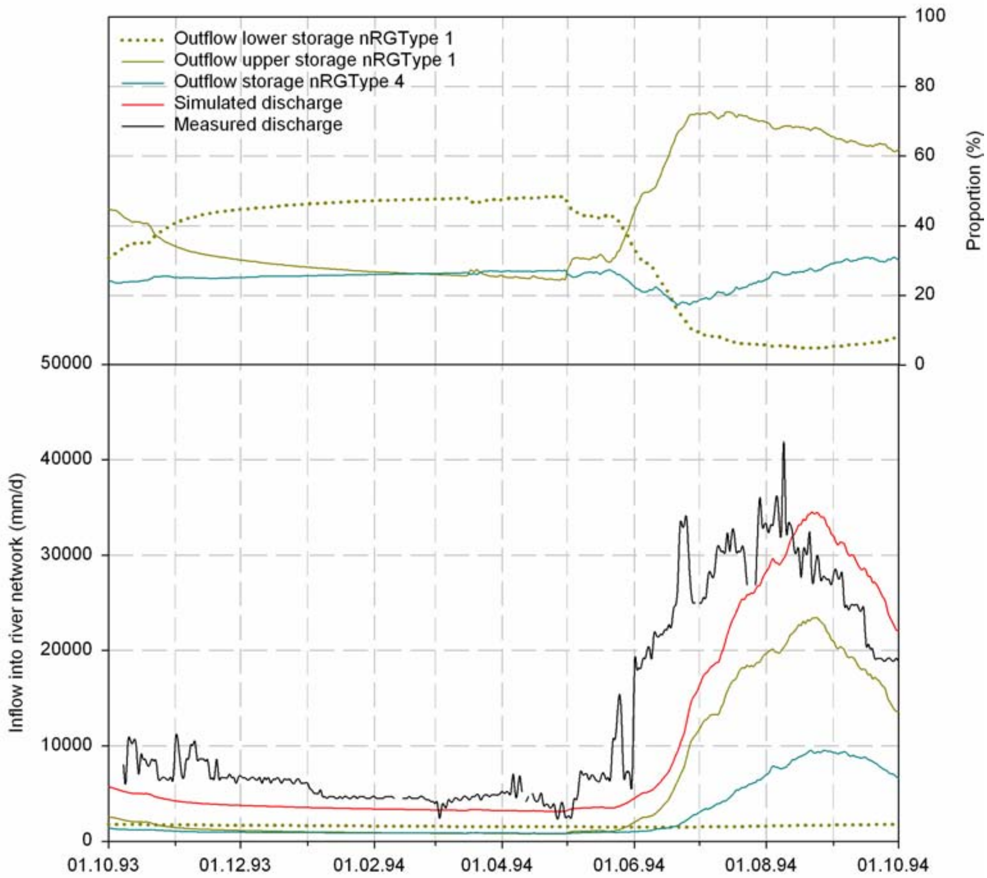

Figure 8.22: Contribution of each runoff component to the entire runoff in percent of the entire runoff (upper graphic) and as absolute values (lower graphic) for the hydrological year 1993/94 calculated with the unrevised river network

The simulation results in Figure 8.22 show the importance of the modification of the river network. The subglacial drainage networks play an important role in the runoff generation but were not considered in the unrevised river network. The unrevised river network ended at the glacier tongues and therefore did not drain the upper reaches of the catchment which are covered mainly by glaciers. Runoff from a raster cell can flow through only one cell per time step if the cell is not defined as river network. This means that runoff which is generated in the upper reaches of the catchment needs many time steps until the unrevised river network is reached and therefore a delay of the simulated discharge is the result. The revised river network includes the glaciers and therefore accounts for the important role of the subglacial drainage network.

8.5.3 Simulation of the onset of discharge at the beginning of the monsoon season

The onset of discharge at the beginning of the monsoon season is delayed by some ten days or more in most of the simulated hydrological years. An exception is the year 1994/95 for which discharge at this time is overestimated by the model. A comparative analysis of the transformation of the output from the snow and glacier routine to discharge in the years 1993/94 and 1994/95 will show the reasons for these simulation errors (Figures 8.23 and 8.24).

For the comparison of the reactions of the outflows from the storages and of the storage levels on the input from the snow and glacier routine, all values were standardized on the catchment area. This means for instance that the storage levels of each cell of the same storage unit (e.g. GlacierLS_box, see Chapter 5.5) were added and divided by the number of cells of the entire catchment (8996 cells). This standardization allows the comparison of the sizes with respect to their importance to the turnover of water in the entire catchment.

Figures 8.23 and 8.24 show that the output from the snow and glacier routine of both years is directed to the runoff generation routine without retardation in the soil routine. In 1993/94 this input to the runoff generation routine fills the upper storages of the glacier and the non-glacier area (nRGType 1 and 2) until the end of June (Figure 8.23). The outflow from the storages is controlled by the respective storage levels and thus a constant rise of the outflow from both the upper storage of the glacier area (nRGType 2) and the upper storage of the non-glacier area (nRGType 1) can be observed in this period. Both outflows are responsible for the high flow simulation. The fluctuations in the input into the runoff generation routine are suppressed in the storages of the runoff generation routine which causes a strongly reduced dynamic of the outflow from the storages compared to the input.
At the end of June the upper storages are filled and the storage contents remain on nearly constant levels. Due to the conceptualization of the upper storages, all additional water is directed to the next cell without retardation if the storages are filled completely. The dynamic of the outflow from both upper storages increases strongly from the end of June onwards. The fluctuations in the input are directly converted into fluctuations in the outflow. This fast reaction of the storages causes an improved discharge simulation during this period. In general, the dynamic of the output from the snow and glacier routine or the output from the soil routine agrees well with the dynamic of the measured discharge which proves that the underestimation of the measured discharge at the beginning of the monsoon season is caused by continuous saturation of the upper storages, ending in the suppression of the outflow dynamic.

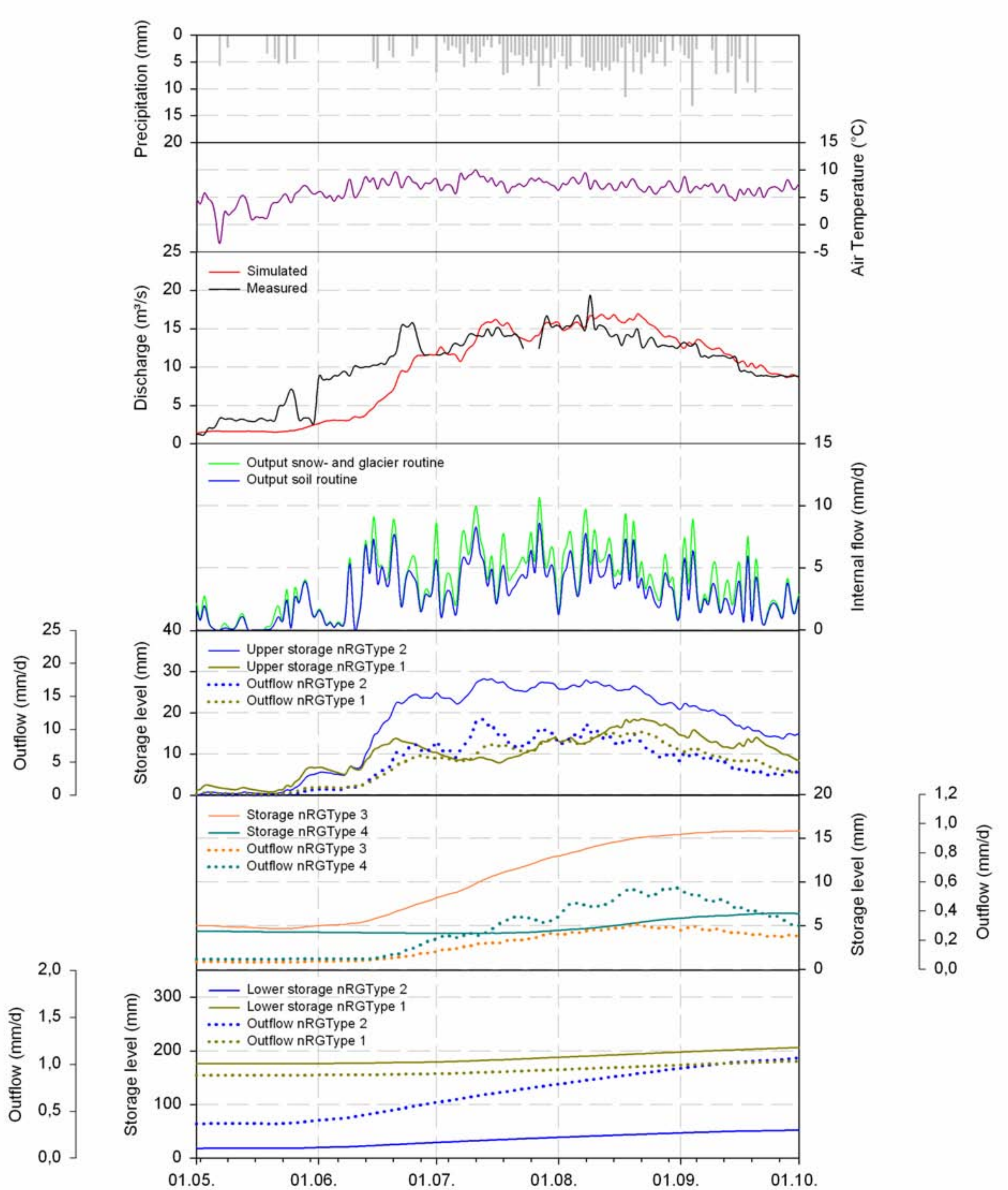

Figure 8.23: Transformation of snow- and glaciermelt and precipitation into discharge (hydrological year 1993/94), intermediate results are average values per cell related to the entire catchment area

In 1994/95 discharge is overestimated by the model at the beginning of the monsoon season. Figure 8.24 shows that this is caused by snowmelt. Solid precipitation from October 1994 to May 1995 amounts to 235 mm (water equivalent) compared to 44 mm during the same period in the previous year. This unusual snow cover causes a meltwater wave which quickly saturates the upper storages, especially of the non-glacier area. As Figure 3.4 in Chapter 3.1 shows, only a small part of the area below 4400 m a.s.l. is covered by glaciers. Therefore, snowmelt at the beginning of the monsoon season mainly affects the storage levels of the non-glacier area in lower altitudes due to higher snowmelt rates.

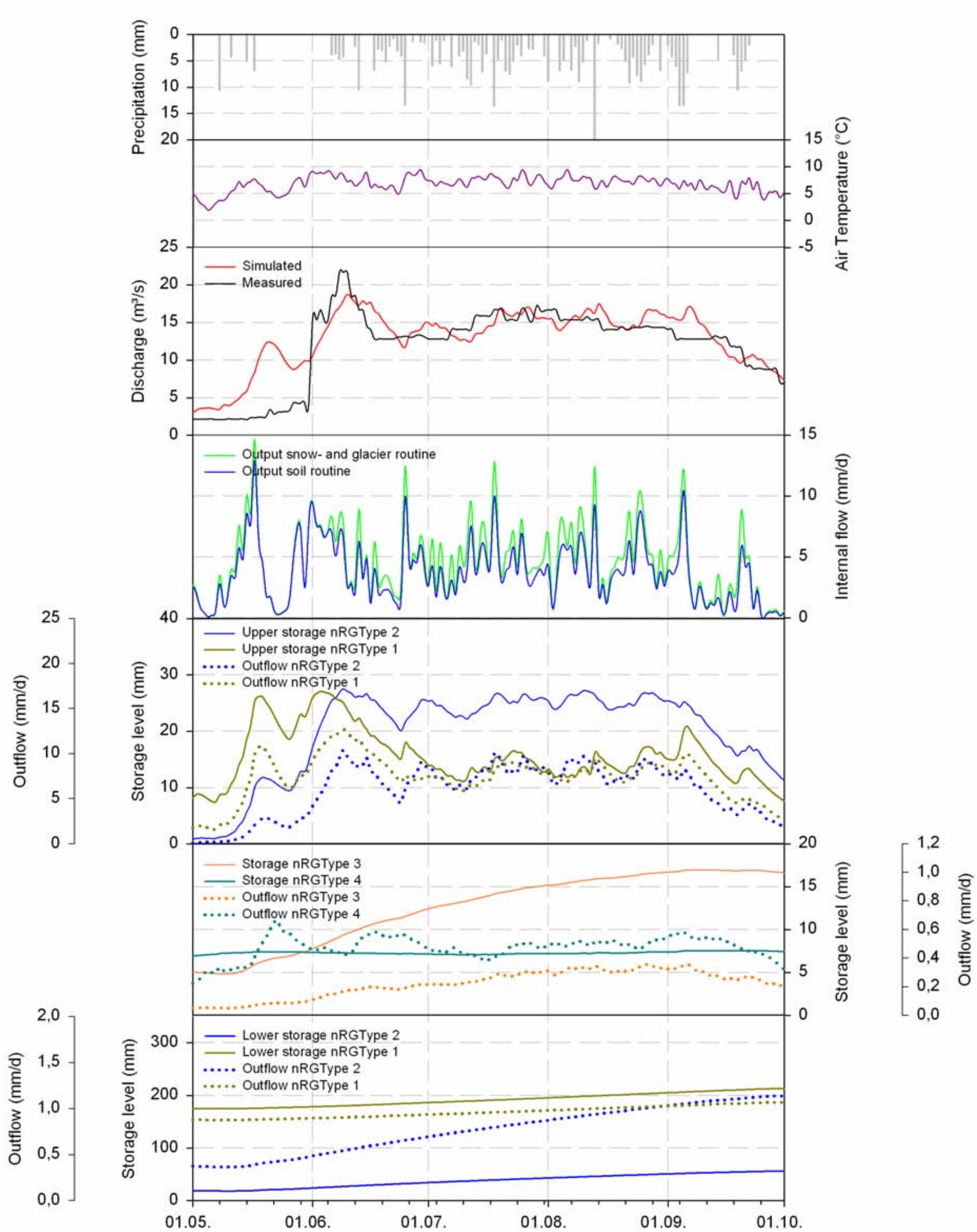

Figure 8.24: Transformation of snow- and glaciermelt and precipitation into discharge (hydrological year 1994/95), intermediate results are average values per cell related to the entire catchment area

Figure 8.25 shows the spatial distribution of the output of the snow and glacier routine as cumulated values from 1st October, 1994 to 17th May, 1995 when the output of the snow and glacier routine peaks.

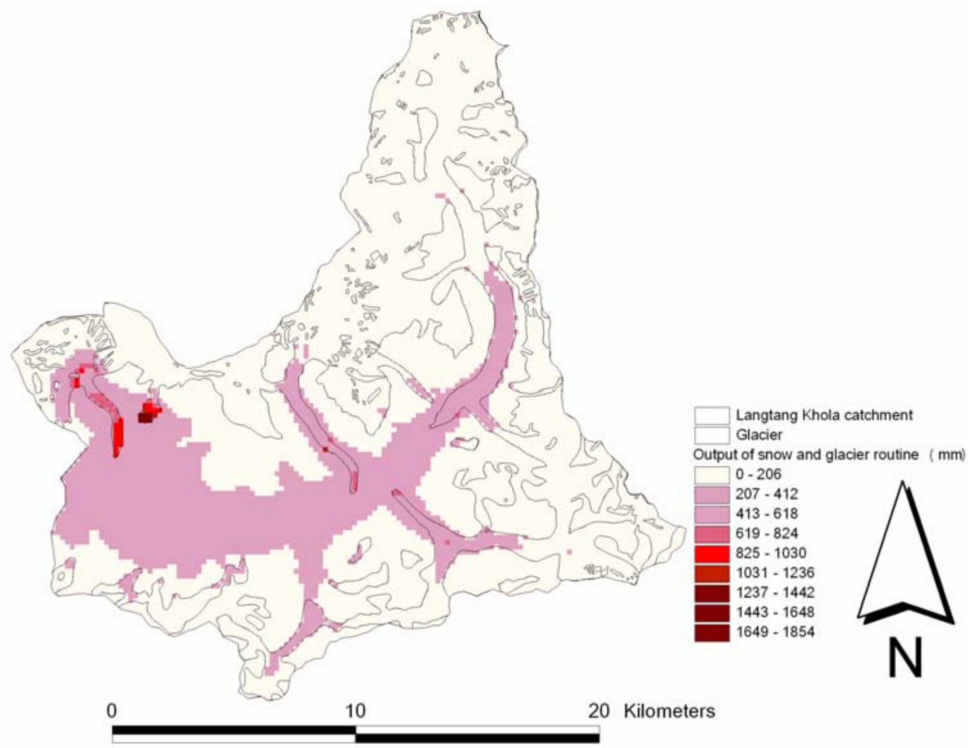

Figure 8.25: Spatial distribution of cumulated output of the snow and glacier routine from 1st of October, 1994 to 17th of May, 1995

The storages of the non-glacier area are filled faster than the storages of the glacier area due to that spatial distribution and thus dominate the runoff generation at the beginning of the monsoon season in 1995. This fast saturation of the upper storages in May 1995 causes the same effects as observed at the end of June, 1994. The dynamic of the outflow of the snow and glacier routine is directly represented in the outflow of the upper storage of nRGType 1 whereas the outflow dynamic of the upper storages of the nRGType 2 is suppressed until mid-June, 1995 compared to the outflow of the upper storage of nRGType 1.

The hydrograph is generally simulated well at the end of the monsoon season which proves that the parameterization of the k-values of the upper storages is in order. The k-values control the drainage of the storages (Chapter 4.2.3).
The comparison of the simulation results from these two monsoon seasons shows that the simulation of the onset of discharge strongly depends on the filling level of the upper storages. Meltwater mainly contributes to the saturation of the upper storages in the pre-monsoon season. The following could be the cause of the simulation problems at the beginning of the monsoon season:

- Wrong determination of solid precipitation, either measured or simulated. The distinction between solid and liquid precipitation is achieved by the TT parameter in the model.
- Measured air temperature is not representative for the energy input in the pre-monsoon season. A snow cover at the SGHU station could be the cause of cooling effects. The temperature-index method strongly depends on representative air temperature values for correct calculation of melt (Chapter 5.3.1).
- Wrong storage concepts or parameterization. It takes a long time until the upper storages are saturated due to nearly complete emptying during the winter season. This suppresses the dynamic of the outflow of the upper storages.

- Discharge was measured only once a day in the early afternoon. Discharge in glacierized catchments shows pronounced diurnal fluctuations especially if there is no further precipitation input. Discharge peaks in the early afternoon.
- Mass distribution due to avalanches causes an increased snow cover in the lower altitudes and thus an increase in meltwater production at the beginning of the monsoon season which cannot be calculated by the model.
- Temporal and spatial resolution does not fit. Water can flow only 200 m per day with a spatial resolution of 200 x 200 m². The residence times of fast runoff components are therefore unrealistically high.

8.6 Simulation results of the verification period

Winter discharge is underestimated in the verification period whereas discharge in the monsoon season is overestimated (Chapter 7.5). A possible explanation could be that the storage capacity of the glaciers (of nRGType 2 and 3) was higher in the verification period. In the conceptualization of the runoff generation routine these glaciers are considered to store most of the water during monsoon season and maintain discharge in dry season. The glacier map of the Langtang Khola catchment was derived from aerial photography shots taken between 1992 and 1996. Kappenberger et al. (1993) revealed with terrestrial photogrammetry that only small fluctuations in the glacier tongues occurred on south-facing glaciers from 1980 to 1991. Meanwhile, glaciers on north-facing slopes advanced in the same period. This observation was confirmed by measurements of annual surface lowering rates of Lirung and Yala glaciers (Yamada et al. 1992, Fujita et al. 1998). The surface lowering has accelerated since the late 1980s on Lirung glacier as well as on Yala glacier (Asahi 1998, Fujita et al. 1998, Naito et al. 2002). This means that the glacier map is representative for the calibration period but not necessarily for the verification period. If the storage capacity of the glaciers was higher in the verification period more water could be retained during melt/monsoon season and released during the winter season. This would reduce the discharge peaks in melt/monsoon season and increase discharge in the winter season.
The model was calibrated to the situation of the calibration period. The comparison of glacier mass balances in Figure 7.8 (Chapter 7.5) shows that the parameterization of the snow and glacier routine is representative for the entire simulation period (1987-1998). In Figure 8.26 only the upper storage limits of the glacier storages were increased and discharge was calculated using the same glacier map as for the calibration period. The simulated discharge with the revised optimal parameter set shows the expected tendencies. Discharge in melt/monsoon season declined while winter discharge increased, especially in the post-monsoon season (September to October). The effect would be more pronounced if an increased glacier area were also used for the simulation of the verification period.

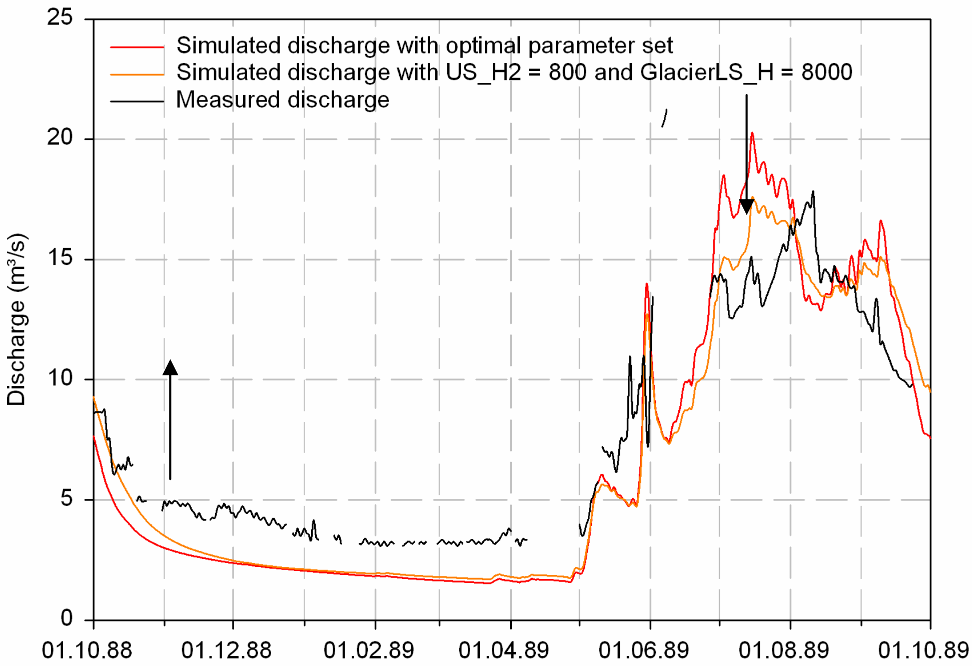

Figure 8.26: Simulation of the hydrological year 1988/89 with different parameter sets. The arrows indicate the tendency of the simulated hydrograph with the revised parameter set

8.7 Multi criteria calibration

The importance of a further calibration criterion beside measured discharge will be presented in the following example.
Table 8.6 shows the optimal parameter set obtained from calibration (Table 7.2 in Chapter 7.3) and another parameter set (parameter set 2) which mainly differs from the optimal parameter set in the parameters of the snow and glacier routine and the parameters which control the calculation of the basin precipitation.

Table 8.6: Differences between the optimal parameter set and parameter set 2

	Optimal parameter set	Parameter set 2
PCF	1.05	1.3
PGrad	0.04	0.045
PHorizGrad	-0.03	-0.02
TGrad	-0.5	-0.55
SFCF	1.2	1.4
Cfmax	7.0	4.0
Rmult	1.4	1.2
Rmultd	0.3	0.5

Both parameter sets deliver nearly the same simulation results as shown in Figure 8.27 and Table 8.7. The simulation using the optimal parameter set shows slightly better objective evaluation criteria but a visual inspection of the simulated curves reveals that the differences between the two simulation results are minimal for all hydrological years.

Table 8.7: R_{eff}-values of simulation results with different parameter sets

	R_{eff} of optimal parameter set	R_{eff} of parameter set 2
1993/94	0.85	0.72
1994/95	0.87	0.87
1995/96	0.53	0.48
1996/97	0.46	0.24

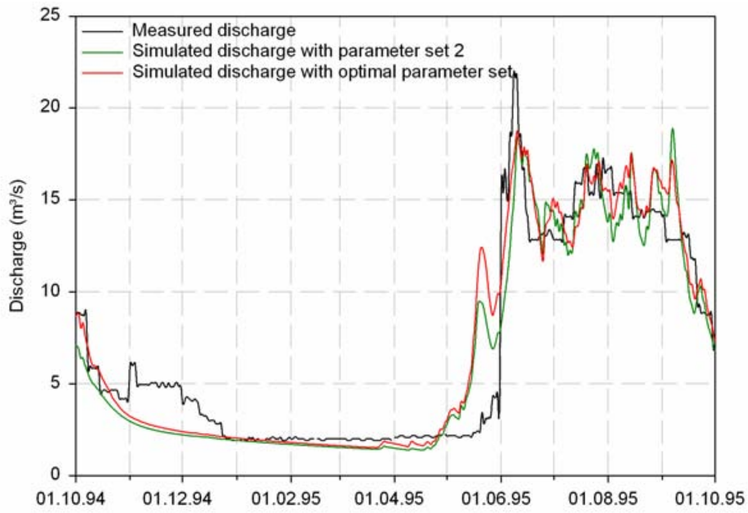

Figure 8.27: Comparison between measured and simulated discharge calculated using the optimal parameter set and parameter set 2

However, the comparison of simulated glacier mass balances in Figure 8.28 shows significant differences. It becomes obvious that ablation is underestimated, but this error is compensated for by an overestimation of basin precipitation and thus the differences in the simulated discharge are minimal.

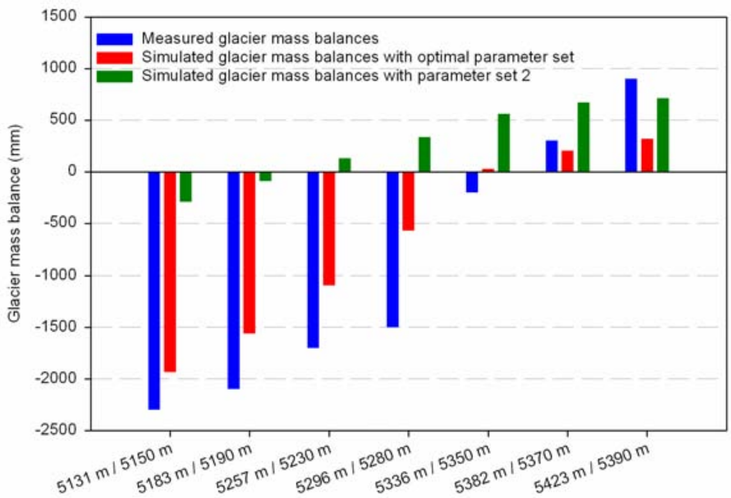

Figure 8.28: Comparison between measured and simulated glacier mass balances calculated using the optimal parameter set and parameter set 2

8.8 Comparison with the HBV-ETH model

The simulation results of TAC^d are compared with the results of the HBV-ETH model for further evaluation of TAC^d. The HBV-ETH precipitation-runoff model is a version of the widely used HBV model with special features to calculate the runoff of glacierized catchments. Development of the HBV model began in 1973 at the SMHI (Swedish Meteorological and Hydrological Institute) (Bergström 1976, 1992) and was further refined at the ETH Zurich (Braun und Renner 1992; Hottelet et al. 1993). Altitude belts and orientation classes (North, South, East, West) are used for spatial discretization of the snow and glacier routine. The glacier area is considered as a percentage of the area of each altitude belt and orientation class. A temperature-index method is used for the calculation of melt as in TAC^d, whereas debris-covered glaciers are not considered specifically in the version of the HBV-ETH model applied here.

The soil routine and the runoff generation routine are not spatially distributed. An upper and a lower storage simulates the runoff generation. Detailed information about the HBV-ETH model can be found in Konz (2003). Table 8.8 compares selected features of TAC^d with those from the HBV-ETH model.

Table 8.8: Comparison of TAC^d with the HBV-ETH model

	TAC^d	HBV-ETH
Regionalization of meteorological input data	Horizontal and vertical gradients	Vertical gradients
Calculation of potential evapotranspiration	Calibrated sinusoidal course	Calibrated sinusoidal course
Calculation of snow- and icemelt	Temperature-index method	Temperature-index method
Spatial distribution of snow and glacier routine	Raster-based	Altitude belts and orientation classes
Debris-covered glaciers	Considered	Not considered
Spatial distribution of soil routine	Raster based, HRUs	lumped
Spatial distribution of runoff generation routine	Raster based, HRUs	lumped

HBV-ETH has been successfully applied in various Alpine and Himalayan catchments (Braun et al. 2000). For the comparison of TAC^d and HBV-ETH the same calibration and validation period was used as for the application of TAC^d. Table 8.9 summarizes the simulation results. The parameter set of the HBV-ETH model can be found in Table A2 (Appendix) and Figure A1 (Appendix) contains the simulation results of the HBV-ETH model from 1987 to 1997.

Table 8.9: Comparison of evaluation criteria of simulations with TAC^d and HBV-ETH

	TAC^d				HBV-ETH			
	R_{eff}	Log R_{eff}	R^2	VE	R_{eff}	Log R_{eff}	R^2	VE
1987/88	0.58	0.05	0.87	97	0.26	-2.83	0.78	258
1988/89	0.72	0.32	0.90	40	0.37	-1.45	0.81	161
1989/90	0.68	0.45	0.84	50	0.37	-0.49	0.77	20
1990/91	0.20	0.40	0.88	-30	-0.33	-0.38	0.80	-136
1991/92	0.30	0.59	0.82	-9	-0.05	-0.44	0.68	80
1992/93	0.76	0.68	0.91	37	0.40	-0.60	0.76	107
1993/94	0.85	0.75	0.89	57	0.59	0.07	0.75	123
1994/95	0.87	0.80	0.88	-8	0.83	0.63	0.91	126
1995/96	0.53	0.31	0.72	92	0.29	-0.38	0.62	81
1996/97	0.46	0.84	0.76	-8	0.18	0.15	0.63	46

The comparison of the evaluation criteria shows that TAC[d] generally delivers better simulation results. Figure 8.29 shows that the monsoon season in July and August, 1994 is simulated well by both models.

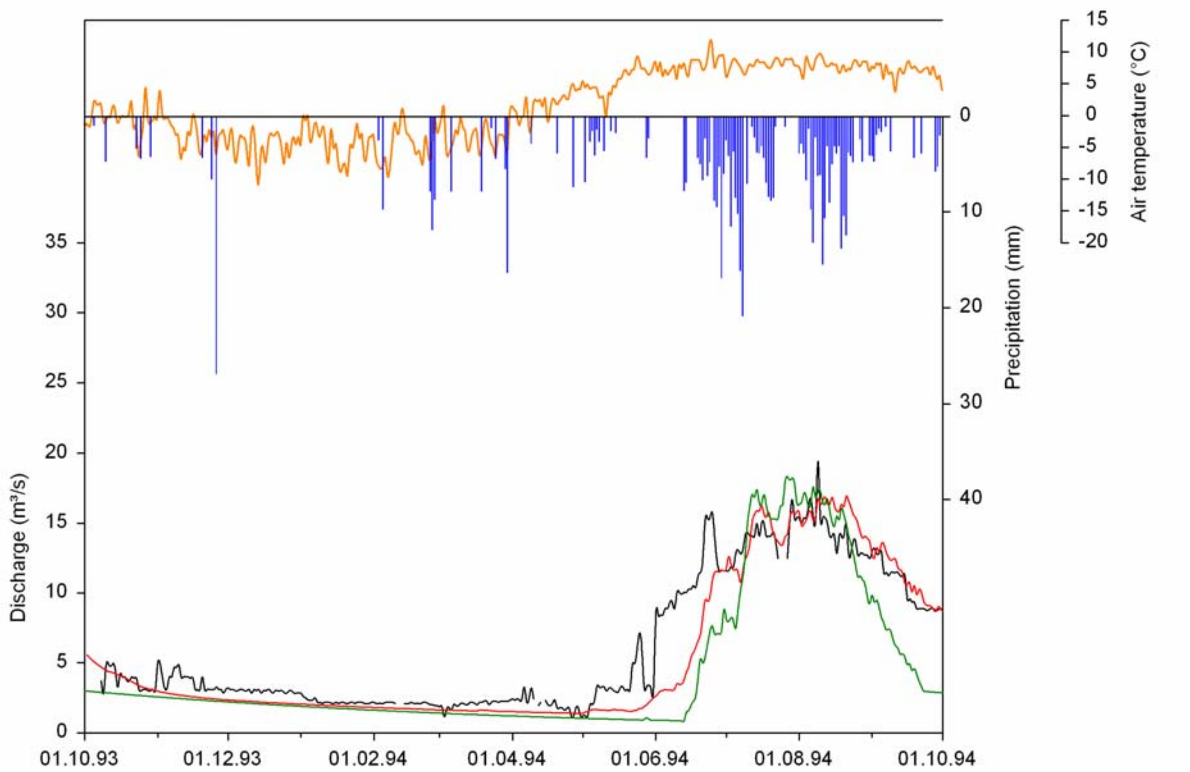

Figure 8.29: Comparison between measured (black) and simulated discharge with TAC[d] (red) and HBV-ETH (green), 1993/94

However, the HBV-ETH model underestimates the discharge both at the beginning of the monsoon season and during the post-monsoon season. These observations are typical for all simulated hydrological years. The great correspondence between the two models can be expressed by the large R^2-values as shown in Table 8.10.

Table 8.10: R^2-values of the comparison between the simulation results of TAC[d] and HBV-ETH

	R^2
1987/88	0.94
1988/89	0.86
1989/90	0.94
1990/91	0.93
1991/92	0.93
1992/93	0.91
1993/94	0.87
1994/95	0.89
1995/96	0.94
1996/97	0.96

It is difficult to compare the models due to their different spatial discretization. Therefore, Figure 8.30 shows the output from the snow and glacier routine and the input into the runoff generation routine of TAC[d] as an average value of all HRUs and the storage levels related to the entire catchment for summer 1994. The output from the snow and glacier routine shows only minor differences between the two models. HBV-ETH delivers higher values if precipitation contributes significantly to the composition of the output of the snow and glacier routine because there is no negative horizontal gradient for the calculation of basin precipitation. At the beginning and at the end of the monsoon season more water is retained in the soil routine in the HBV-ETH model than in the TAC^d model. The input into the runoff generation routine does not contribute to the filling of the upper storage of the HBV-ETH model until the middle of June, 1994. The water is directed to the lower storage because the input into the upper storage is smaller than the fixed percolation rate (CPERC) of 1.5 mm/day. Therefore, the onset of discharge of the monsoon season simulated by the HBV-ETH model is delayed more than the simulated discharge of the TAC^d model. The upper storage of the HBV-ETH model is emptying continously from the middle of August until the end of September, 1994, whereas the upper storages of the TAC^d model remain at the same level. This causes the fast decline of discharge at the end of the monsoon season as simulated by the HBV-ETH model. The lower storage outflow of HBV-ETH maintains the winter discharge and the storage is filled during the monsoon season. A more detailed comparison of both models is not attempted here as it would be beyond the scope of this thesis. Nevertheless, it can be stated that the TAC^d model and the HBV-ETH model are applicable to the Langtang Khola catchment. Both models are able to simulate the melting of ice and snow appropriately. The advantage of the TAC^d model is the better redistribution of the water stored during monsoon season. During calibration of the HBV-ETH model it got obvious that the model can either be calibrated to simulate the high flow season well or the low flow season in winter. It was not possible to get a good simulation of the entire hydrological year.

The more sophisticated and distributed runoff generation routine of TAC^d enables the storage of water for maintaining the rather high level of winter discharge and at the same time simulates well the discharge conditions of the monsoon season.

A more detailed comparison of both models is not attempted here as it would be beyond the scope of this thesis. Nevertheless, it can be stated that the TAC^d model and the HBV-ETH model are applicable to the Langtang Khola catchment. Both models are able to simulate the melting of ice and snow appropriately. The advantage of the TAC^d model is the better redistribution of the water stored during monsoon season. During calibration of the HBV-ETH model it became clear that the model can be calibrated to simulate either the high flow season well, or the low flow season in winter. It was not possible to get a good simulation of the entire hydrological year.

The more sophisticated and distributed runoff generation routine of TAC^d enables the storage of water for the maintaining the rather high level of winter discharge, and at the same time it delivers a good simulation of discharge conditions in the monsoon season.

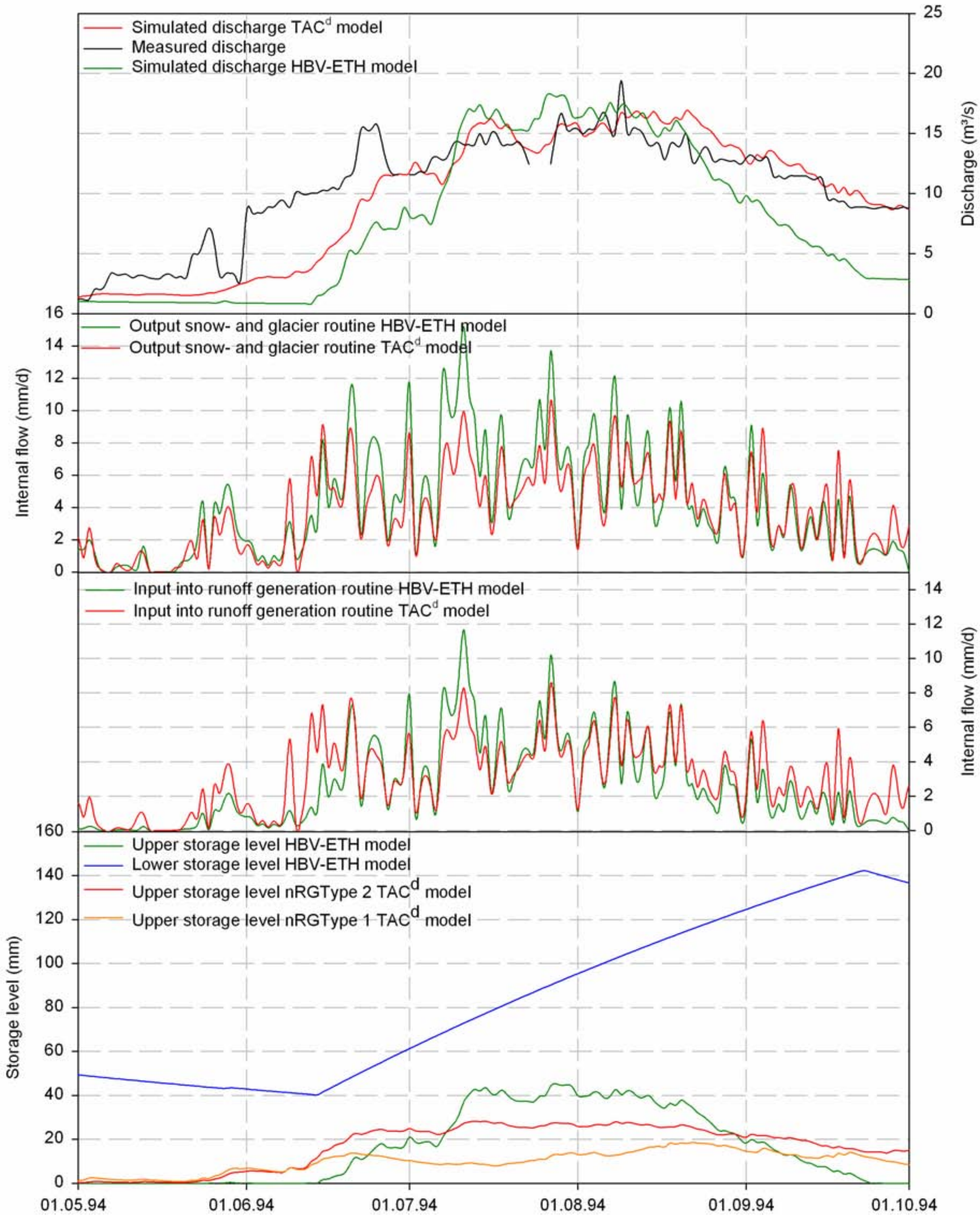

Figure 8.30: Comparison of HBV-ETH model and TAC^d model for summer 1994

8.9 Conclusions

The extrapolation methods for temperature and precipitation data are appropriate tools for bridging gaps in the time series or for redistributing cumulated precipitation sums. The regionalization of air temperature and precipitation with fixed vertical and horizontal gradients is problematic because the seasonal variation of the gradients is not considered. Precipitation and air temperature measurements are provided at only one station in the catchment for the entire simulation period. Thus it is not possible to use the advantages of a distributed model to apply sophisticated regionalization methods for the climatological input data. The introduction of the horizontal gradient, however, enables a more realistic simulation of the basin precipitation. For the calculation of the potential evapotranspiration a simple sinusoidal approach was chosen, which is justified due to the minor importance of evapotranspiration with regard to the annual water balance of high alpine head watersheds.

The main advantage of the temperature-index method, the importance of which cannot be overestimated when working in alpine environments, is that data requirements may be limited to just average daily air temperatures. However, this is also potentially their biggest drawback, as factors other than air temperature control ablation rates. Ablation processes in cases where the air temperature is below the threshold temperature for melting (TT), e.g. sublimation, cannot be treated by the method. The introduction of the correction factor for the degree-day factor (RexpMap) enables spatial and temporal distributed modeling of snow- and icemelt based on physiographic characteristics of the catchment. The approach seems to deliver realistic melt rates for final evaluation; however, aerial photos of the snow cover distribution would still be required. The inclusion of debris-covered glacier surfaces supports the idea of distributed hydrological modeling and the parameter which controls melting over debris-covered glaciers turns out to be highly sensitive.

Mapped river networks of glacierized catchments generally end up at the glacier tongues and have to be extended to include subglacial drainage networks. This brought the expected improvement of the discharge simulation with TAC^d.

Inner annual distribution of water with spatial distributed storage concepts delivers good simulation results as expressed by the objective evaluation criteria. However, the simulation of the onset of discharge at the beginning of the monsoon period is not satisfactory. Simple conceptual storage approaches to describe the hydrological situation of the Langtang Khola catchment can be considered as sufficient for the simulation of the runoff generation. The comparison with the HBV-ETH model in particular justifies the conceptualization of the runoff generation routine of TAC^d. However, detailed experimental analyses of the discharge composition, especially of the low flow season, are essential for the evaluation of the conceptualization of the runoff generation routine.

Spatial and temporal resolution of 200 x 200 m² and daily time steps, causes a delay of the fast runoff components. The lowering of the time step from daily to hourly intervals is not possible because measurements are available only in daily resolution. A smaller spatial resolution would improve the simulation of fast runoff components. This is, however, problematic for the simulation of snow- and icemelt because detailed physiographic information gets lost with a smaller spatial resolution. Meltwater is an important component of the water balance and thus it is necessary to simulate these processes in as detailed a way as possible. Calibration of the snow and glacier routine was improved by using a multi criteria calibration.

9 Final remarks and outlook

Satisfactory simulation results of daily discharge could be achieved using the modified version of TAC^d in the highly glacierized Langtang Khola catchment. It further reproduces some basic glaciological features such as the total annual glacier mass balance. Calibrated rainfall-runoff models can give good estimates of discharge even when either spatial distribution of precipitation or melt processes are poorly simulated. Errors related to parameter uncertainties can be compensated for, especially when meltwater of glaciers is an additional input to the model beside precipitation. Additional glacier mass balance measurements enable a multi criteria calibration which helps to reduce parameter uncertainties of the snow and glacier routine and of parameters controlling regionalization of climatic data. The simple conceptualization of the routines of TAC^d requires a rather modest amount of input data and the model can therefore be applied to Himalayan head watersheds. A snow- and icemelt routine can be simple, due to the implicit relevance of air temperature in the surface layer for the computation of the seasonal course of snowpack (Zappa 2003). The robustness of the temperature-index method is the most important factor related to the quality of input data. Hydrological processes, especially melt processes, in alpine catchments are strongly varied, spatially and temporally. A distributed simulation of snow- and icemelt is therefore necessary and can be achieved by incorporating potential sunshine duration without any further input data other than information derived from digital elevation models. Within the scope of this work, a detailed evaluation of the snow and glacier routine was not possible and must be the subject of future investigation. The conceptualization of the runoff generation routine is kept as simple as possible and it is designed to represent exclusively the most important runoff generation processes. Given the simplicity of the model structure and its effectiveness for discharge and glacier mass balance simulations, the model offers a useful tool for water resources management in remote high alpine regions.

The model does not account for seasonal variations of the subglacial drainage system. This evolution of the internal drainage system can be assumed to have a notable influence on discharge. Schaefli et al. (2005) suggest investigations of the time-dependency of parameters of the snow and glacier routine, considering potential links between the parameters and climate variables. In that context, not only the fluctuations in hydraulic conditions of subglacial drainage systems must be considered, but also the fact that changing storage capacities of glaciers are crucial for a realistic discharge simulation, as revealed by the simulation results from the early simulation period. Detailed experimental investigations of runoff composition in both monsoon and winter seasons is necessary to verify the conceptualization of the runoff generation routine. If water is actually stored in the glacier tongues during monsoon season, as the current conceptualization implies, then the retreat of glaciers will have impacts on the hydrological cycle in two ways:

- Less meltwater can be produced during monsoon season due to declining ice masses.
- Less water can be stored in the glacier tongues due to declining storage capacities.

This would result in a remarkable decline in winter discharge when no precipitation maintains the runoff generation. The author considers research on the following topics, beside those already mentioned, to be most important with regard to long-term studies, e.g., on the impacts of climate change:

- Volumes of glacier tongues need to be investigated via aerial photography and geodetic measurements combined with geophysical measurements (e.g., ground radar or seismic) to determine the storage capacities.
- Continuous glacier mass balance measurements and snow surveys are necessary for calibration of the model.
- Detailed observations of avalanche activity during monsoon and winter season would be helpful for estimating their impact on meltwater production at lower altitudes. Again aerial photography could be used to determine the spatial distribution of avalanche cones.
- Demarcation of debris-covered glaciers from debris-covered moraines, e.g., by means of thermal images.
- Estimation of sublimation amounts in high altitudes via measurements of the terms of the energy balance in altitudes where the air temperature is below zero all year round.
- Estimation of ablation rates through wind erosion via parallel measurements of snow accumulation (e.g., by ultrasound) and wind speed at exposed ridges.
- Application of TAC^d to head watersheds in the Khumbu and Annapurna region to investigate the possibilities for regionalization of model parameters.

The impact of climate change on regional water resources in terms of energy production and water supply can be determined based on these investigations. For sustainable water resources management hydrological investigations must be coupled with socio-economic studies to develop a comprehensive plan of action for managing the effects of global change in these climatically highly sensitive regions.

References

Ambach, W. (1972): Floods caused by the melting of snow and ice. Piene: Loro previsione e difesa del suolo, Accademia Nazionale Dei Lincei, Quaderno N. 169. 121-136.

Asahi, K. (1998): Recent glacier fluctuations and their factors of eastern part of Nepal Himalaya. Master thesis, Tokyo Meteropolitan University, 143pp. (In Japanese with English abstract).

Becker, A. (1992): Methodische Aspekte der Regionalisierung. Mitteilung Nr. XI der Senatskommission für Wasserforschung, Regionalisierung in der Hydrologie, Deutsche Forschungsgemeinschaft.

Beek, T. aus der (2004): The further development of the process-based catchment model TAC^d and its application to the H.J. Andrews Experimental Forest, Oregon, USA. Diploma thesis at the Institute of Hydrology, Albert-Ludwigs-University Freiburg, Germany, (unpublished).

Bergström, S. (1976): Development and application of a conceptual runoff model for Scandinavian catchments. PhD. Thesis SMHI Reports RH, No. 7, Norrköping.

Bergström, S. (1992): The HBV-model - its structure and applications. SMHI Reports RH, No. 4, Norrköping.

Braun, L.N. (1985): Simulation of snow melt-runoff in lowland and lower alpine regions of Switzerland. Züricher Geographische Schriften 21, Geographisches Institut ETH, Zurich.

Braun, L.N.; Aellen, M. (1990): Modeling discharge of glacierized basins assisted by direct measurements of glacier mass balance. IAHS Publication No.193, 99-106.

Braun, L.N.; Renner, C.B. (1992): Application of a conceptual runoff model in different physiographic regions of Switzerland. Hydrological Sciences-Journal 37, 3, 217-231.

Braun, L.N.; Grabs, W. and Rana, B. (1993): Application of a conceptual precipitation runoff model in the Langtang Khola basin, Nepal Himalaya. IAHS Publication No. 218, 221-237.

Braun, L. N.; Hottelet, Ch.; Weber, M.; Grabs, W. (1998): Measurement and simulation of runoff from Nepalese head watersheds. IAHS Publication No. 248, 9-18.

Braun, L.N.; Schulz, M.; Weber, M. (2000): Consequences of climate change for runoff from Alpine regions. Annals of Glaciology 31, 19-25.

Brubaker, K.; Rango, A.; Kustas, W (1996): Incorporating radiation inputs into the snowmelt runoff model. Hydrological Processes, 10, 1329-1343.

Cazorzi, F; Fontana, D. G. (1996): Snowmelt modeling by combining air temperature and a distributed radiation index. Journal of Hydrology, 181, 169-187.

Chen, J.; Ohmura, A. (1990): On the influence of alpine glaciers on runoff. IAHS Publication No. 193, 117-125.

Colebeck, S.C. (1972): A theory of water percolation in snow. Journal of Glaciology, 11 (63), 369-385.

Demuth, S. (2001): Regionalisierungsverfahren in der Hydrologie. Script of university course Albert-Ludwigs-University, Freiburg i. Br..

Dyck, S.; Peschke, G. (1995): Grundlagen der Hydrologie. Verl. f. Bauwesen, Berlin.

Escher-Vetter, H. (1980): Der Strahlungshaushalt des Vernagtferners als Basis der Energiehaushaltsberechnung zur Bestimmung der Schmelzwasserproduktion eines Alpengletschers. Wissenschaftliche Mitteilungen, Meteorologisches Institut, München, 39.

Escher-Vetter, H. (2000): Modelling meltwater production with distributed energy balance method and runoff using a linear reservoir approach-results from Vernagtferner, Oetztal Alps, for the ablation seasons 1992 to 1995. Zeitschrift für Gletscherkunde und Glazialgeologie, 36, 119-150.

Ferguson, R. I. (1999). Snowmelt runoff models. Progress in Physical Geography 23 (2): 205-227.

Fox, A. (2003): A distributed, physically based snow melt and runoff model for alpine glaciers. PhD Thesis St. Catherine' s College.

Fujita, K.; Takeuchi, N.; Seko, K. (1998): Glaciological observations of Yala Glacier in the Langtang Valley, Nepal Himalayas, 1994 and 1996. Bulletin of Glacier Research, 16, 75-81.

Grabs, W. and Pokhrel, A.P. (1993): Establishment of a measuring service for snow and glacier hydrology in Nepal – conceptual and operational aspects. IAHS Publication No. 218, 3-16.

Gronowski, T.V. (1992): Die natürliche Grundwasserneubildung in einem urban beeinflussten Einzugsgebiet im Voralpenraum. Züricher Geographische Schriften 50, Geographisches Institut ETH, Zurich.

Hagg, W. (2003): Auswirkungen von Gletscherschwund auf die Wasserspende hochalpiner Gebiete, Vergleich Alpen-Zentralasien. Münchener geographische Abhandlungen, Reihe A, Band A 53, Department für Geo- und Umweltwissenschaften der Universität München, Sektion Geographie.

Heuberger, H.; Masch, L.; Preuss, E.; Schrocker, A. (1984):Quaternary landslides and rock fusion in Central Nepal and in the Tyrolean Alps. Mountain Research and Development, 4, 345-362.

Hock, R. (1998): Modeling of glaciermelt discharge. Züricher Geographische Schriften 70, Geographisches Institut ETH, Zurich.

Hock, R. (1999): A distributed temperature-index ice- and snowmelt model including potential direct solar radiation. Journal of Glaciology 45 (149), 101-111.

Hock, R. (2003): Temperature-index melt modeling in mountain areas. Journal of Hydrology 282 (1-4), 104-115.

Hooke, R. (1989): Englacial and subglacial hydrology: a qualitative review. Arctic and Alpine Research 21 (3), 221-233.

Hormann, K., 1994: Computer-based Climatological Maps for High Mountain Areas – New Methods and Theirs Application, with Examples from the Himalayas. ICIMOD, MEM Series No. 12.

Hottelet et al., 1994: Application of the ETH snow model to three basins of different character in central Europe. Nordic Hydrology 25, 113-128.

Hottelet, Ch.; Braun, L.N.; Leibundgut, Ch. und Rieg, A. (1993): Simulation of Snowpack and Discharge in an Alpine Karst Basin. IAHS Publication No. 218, 249-260.

ICIMOD and UNEP (2002): Inventory of glaciers, glacier lakes and glacier lake outburst floods monitoring and early warning systems in the Hindu Kush – Himalayan region. CD-ROM. ISBN 92 9115 359 1.

Iida, H.; Watanaba, O.; Takikawa, M. (1984): First results from Himalayan glacier boring project in 1981-1982, Part II. Studies on internal structure and transformation process from snow and ice of Yala Glacier, Langtang Himal, Nepal. Glacial Studies in Langtang Valley, Data Center for Glacial Research, Japanese Society of Snow and Ice. Publication No. 2, 25-34.

Jansson, P.; Hock, R.; Schneider; T. (2002): The concept of glacier storage: a review. Journal of Hydrology 282 (1-4), 116-129.

Jauk, G. (2003): Gletscherschwund im Himalaya. Spektrum der Wissenschaft. Spektrum der Wissenschaft, August 2003, Verlagsgesellschaft mbH, Heidelberg, ISSN 0170-2971.

Johst, M. (2003): Die Weiterentwicklung und Anwendung des prozessorientierten Einzugsgebietsmodells TAC^d im Löhnersbach-Einzugsgebiet, Kitzbüheler Alpen, Österreich. Diploma thesis at the Institute of Hydrology, Albert-Ludwigs-University Freiburg, Germany, (unpublished).

Kappenberger, G.; Steinegger, U.; Braun, L.N.; Kostka, R. (1993): Recent changes in Glacier tongues in the Langtang Khola basin, Nepal, determined by terrestrial photogrammetry. IAHS Publication No. 218, 95-101.

Kattelmann, R. (1993): Role of snowmelt in generating streamflow during spring in east Nepal. IAHS Publication No. 218, 103-111.

Kayasta, R. B.; Takeuchi, Y.; Nakawo, M.; Ageta, Y. (2000): Practical prediction of ice melting beneath various thickness of debris cover on Khumbu Glacier, Nepal, using a positive degree-day factor. IAHS Publication No. 264, 71-81.

Kohler, J. (1995): Determining the extent of pressurized flow beneath Storglaciären, Sweden, using results of tracer experiments and measurements of input and output discharge. Journal of Glaciology 41 (138), 217-231.

Kohshima, S.; Seko, K.; Yoshimura, Y. (1993): Biotic acceleration of glaciermelting in Yala glacier, Langtang region, Nepal Himalaya. IAHS Publication No. 218, 309-316.

Konz, M. (2003): HBV3-ETH9 User's manual. Internal report Bavarian Academy of Sciences, Commission of Glaciology, Munich.

Kraus, H. (1966): Wie entsteht der Tagesgang der Lufttemperatur? Zeitschrift für Meteorologie. Band 17 Heft 9-12, 339-342.

Kraus, H. (1966): Das Klima von Nepal. The series Khumbu Himal, Bd.1/4, 301-321.

Lang, H. (1968): Relation between glacier runoff and meteorological factors observed on and outside the glacier. IUGG Ge. Ass. 1967, Berne, IAHS Publication No. 79, 429-439.

Lang, H. (1981): Is evaporation an important component in high alpine hydrology? Nordic Hydrology 12 (4/5), 217-224.

Mader, H. (1992): Observations of the water-vein system in polycrystallinic ice. Journal of Glaciology 38, 333-347.

Male, D.H. (1980): The seasonal snow cover. In : Colebeck, S. : Dynamics of snow and ice masses. Academic Press, New York.

Martinec, J. (1989): Hour-to-hour snowmelt rates and lysimeter outflow during an entire ablation period. IAHS Publication No. 183, 19-28.

Melloh, R. A. (1999). A Synopsis and Comparison of Selected Snowmelt Algorithms. Hanover, New Hampshire, US Army Corps of Engineers, Cold Regions Research and Engineering Laboratory. CRREL Report 99-8

Menzel, L. (1997): Modellierung der Evapotranspiration im System Boden-Pflanze-Atmosphäre. Züricher Geographische Schriften 67, Geographisches Institut ETH, Zurich.

Menzies, J. (2002): Modern & past glacial environments. Butterworth-Heinemann Ltd., Oxford.

Messerli, B. (1997): Mountains of the world: a global priority; a contribution to Chapter 13 of Agenda 21. Parthenon Publications XIV.

Moribayashi, S. (1974): On the characteristics of Nepal Himalayan glaciers and their recent variation, Seppyo 36, 11-21. (In Japanese with English abstract).

Morris, E. M. (1985). Snow and Ice. Hydrological forecasting. M. G. Anderson and T. P. Burt. Chichester, UK, John Wiley and Sons: 153-182.

Moser, H; Escher-Vetter, H.; Oerter, H.; Reinwarth, O.; Zunke, D. (1986): Abfluss in und von Gletschern. GSF-Bericht 41/86, Teil 1.

Motoyama, H. ; Yamada, T. (1989): Hydrological observations in the Langtang Valley, Nepal Himalayas during 1987 monsoon – postmonsoon season. Bulletin of Glacier Research 7, 195-201.

Motoyama, H.; Ohta, T.; Yamada, T. (1987): Winter runoff in the glacialized drainage basin in Langtang Valley, Nepal Himalayas. Bulletin of Glacier Research 5, 29-33.

Naito, N.; Kadota, T.; Fujita, K.; Sakai, A.; Nakawo, M. (2002): Surface lowering over the ablation area of Lirung glacier, Nepal Himalayas. Bulletin of Glacier Research 19, 41-46.

Nakawo, M.; Takahashi, S. (1982): A simplified model for estimating glacier ablation under a debris layer. IAHS Publication No. 138, 137-145.

Nakawo, M.; Young, G.J. (1981): Field experiments to determine the effect of a debris layer on ablation of glacier ice. Annals of Glaciology 2, 85-91.

Nash, J.E.; Sutcliffe (1970): River flow forecasting through conceptual models, Part I – a discussion of principles. Journal of Hydrology 10, 282-290.

Nesje, A.; Dahl, S.O. (2000): Glaciers and environmental change. Oxford University Press Inc., New York.

Nye, J.F. (1976): Water flow in glaciers; Jökulhlaups, tunnels and veins. Journal of Glaciology 17, 181-201.

Ohmura, A. (2001): Physical basis fort he temperature-based melt-index method. Journal of Applied Meteorology 40, 753-761.

Ono, Y. (1986): glacial fluctuations in the Langtang Valley, Nepal Himalaya. Göttinger Geographische Abhandlungen 81, 31-38.

Östling, M.; Hooke, R. (1986): Water storage in Storglaciären, Kebnekaise, Sweden. Geografiska Annaler 68A (4), 279-290.

Ott, B. (2002): Weiterentwicklung des Einzugsgebietsmodells TAC^d und Anwendung im Dreisameinzugsgebiet. Diploma thesis at the Institute of Hydrology, Albert-Ludwigs-University Freiburg, Germany, (unpublished).

Paterson, W. S. B. (1969): The physics of glaciers. 1st edition. Pergamon Press, Oxford.

Paterson, W. S. B. (1994): The physics of glaciers. 4th edition. Pergamon Press, Oxford.

PCRaster (2004): Faculty of Geographical Sciences, Utrecht University. Internet: URL: http://www.pcraster.geog.uu.nl/index.html (access date: 24.04.2005).

Popovnin, V. V.; Rozova, A. V. (2002): Influence of sub-debris thawing on ablation and runoff of the Djankuat glacier in the Caucasus. Nordic Hydrology 33 (1), 75-94.

Ramage, C. S. (1971): Monsoon meteorology. Academic Press.

Rana, B.; Nakawo, M.; Fukushima, Y.; Ageta, Y. (1996): Runoff modelling of a river basin with a debris-covered glacier in Langtang Valley, Nepal Himalaya. Bulletin of Glacier Research 14, 1-6.

Rana, B.; Nakawo, M.; Fukushima, Y.; Ageta, Y. (1997): Application of a conceptual precipitation-runoff model (HYCYMODEL) in a debris-covered glacierized basin in the Langtang Valles, Nepal Himalayas. Annals of Glaciology 25, 226-231.

Rango, A. (1992): Worldwide testing of the snowmelt runoff model with application for predicting the effects of climate change. Nordic Hydrology 23, 155-172.

Renner, C. B.; Braun, L. N. (1990): Die Anwendung des Niederschlag-Anfluss Modells HBV3-ETH (V 3.0) auf verschiedene Einzugsgebiete in der Schweiz. Geographische Institut ETH Zürich. Berichte und Skripten Nr. 40.

Richter, D. (1995): Ergebnisse methodischer Untersuchungen zur Korrektur des systematischen Messfehlers des Hellmann-Niederschlagsmessers. Ber. d. Deutschen Wetterdienstes, 194.

Rohrer, M. B.; Braun, L. N.; Lang, H. (1994): Long term records of snow cover water equivalent in the Swiss Alps: 2. Simulation, Nordic Hydrology, 25, 67-78.

Roser, S. (2001): Flächendetaillierte Weiterentwicklung des prozessorientierten Einzugsgebietsmodells TAC und Visualisierung der Modellergebnisse in einem dynamischen GIS. Diploma thesis at the Institute of Hydrology, Albert-Ludwigs-University Freiburg, Germany, (unpublished).

Röthlisberger, H. (1972): Water pressure in intra- and subglacial channels. Journal of Glaciology 11, 117-203.

Röthlisberger, H.; Lang, H. (1987): Glacial Hydrology. In A.M. Gurnell and M.J. Clark (Ed.), Glacio-Fluvial Sediment Transfer – An Alpine Perspective, pages 207-284. John Wiley and Sons, Chichester, New York, Toronto, Singapore.

Sakai, A.; Fujita, K.; Kubota, J (2004): Evaporation and percolation effect on melting at debris-covered Lirung Glacier, Nepal Himalayas, 1996. Bulletin of Glacier Research, 21, 9-15.

Schaefli, B.; Hingray, B.; Niggli, M.; Musy, A. (2005): A conceptual glacio-hydrological model for high mountainous catchments. Hydrology and Earth System Sciences Discussions 2, 73-117.

Schuler, T. (2002): Investigation of water drainage through an alpine glacier by tracer experiments and numerical modeling. Versuchsanstalt für Wasserbau, Hydrologie und Glaziologie der Eidgenössischen Technischen Hochschule Zürich. Mitteilung 177.

Schulla, J. (1997): Hydrologische Modellierung von Flussgebieten zur Abschätzung der Folge von Klimaänderungen. Züricher Geographische Schriften 69, Geographisches Institut ETH, Zurich.

Schulz, M., 1999: Bestimmung der Wasserhaushaltsgrößen ausgewählter hochalpiner Einzugsgebiete mittels Messung und Simulation. Diploma thesis at the Institute of Geography, Ludwig Maximilians Universität Munich, Germany, (unpublished).

Seibert, J. (2002): HBV light – User's manual. Uppsala University, Department of Earth Sciences, Hydrology.

Seibert, J., 2000: Multi-criteria calibration of a conceptual runoff model using a genetic algorithm. Hydrology and Earth System Sciences 4 (2), 215-224.

Seko, K. (1987): Seasonal variation of altitudinal dependence of precipitation in Langtang Valley, Nepal Himalayas. Bulletin of Glacier Research 5, 41-47.

Sevruk, B. (1985): Systematischer Niederschlagsmessfehler in der Schweiz. In: Der Niederschlag der Schweiz. Beitr. z. Geol. d. Schweiz-Hydrol. 31. 65-86.

Sharma, C. K. (1977): River systems of Nepal. S. Sharma, Kathmandu.

Shiraiwa, T.; Ueno, K.; Yamada, T. (1992): Distribution of mass input on glaciers in the Langtang Valley, Nepal Himalayas. Bulletin of Glacier Research 10, 21-30.

Shrestha, A.; Shrestha, M. (2004): Recent trends and potential climate change impacts and glacier retreat/glacier lakes in Nepal and potential adaptation measures. Global forum on sustainable development: Development and climate change. OECD, Paris, 11-12 November 2004.

Shreve, R.L. (1972): Movement of water in glaciers. Journal of Glaciology 11, 205-215.

Spreafico, M. and Grabs, W. (1993): Determination of discharge with fluorescence tracers in Nepal Himalayas. IAHS Publication No. 218, 17-27.

Steinegger, U.; Braun, L. N.; Kappenberger, G.; Tartari, G. (1993): Assessment of annual snow accumulation over the past 10m years at high elevations in the Langtang region. IAHS Publication No. 218, 155-165.

Tangborn, W.; Rana, B. (2000): Mass balance and runoff of the partially debris-covered Langtang glacier, Nepal. IAHS Publication No. 264, 99-108.

Tarar, R. N. (1982): Water resources investigation in Pakistan with the help of Landsat imagery-snow surveys, 1975-1978. IAHS Publication No. 138, 177-190.

Ueno, K.; Shiraiwa, T.; Yamada, T. (1993): Precipitation environment in the Langtang Khola Valley, Nepal Himalayas. IAHS Publication No. 218, 207-219.

Ueno, K.; Yamada, T. (1990): Diurnal variation of precipitation in Langtang Valley, Nepal Himalayas. Bulletin of Glacier Research 8, 93-101.

Uhlenbrook, S. (1999): Untersuchung und Modellierung der Abflussbildung in einem mesoskaligen Einzugsgebiet. Freiburger Schriften zur Hydrologie Schriften, Band 10, Institut für Hydrologie der Universität Freiburg i. Br.

Uhlenbrook, S. (2005): Personal conversation.

Vallon, M.; Petit, J.R.; Fabre, B. (1976): Study on ice core to bedrock in the accumulation zone of an alpine glacier. Journal of Glaciology 17 (75), 13-28.

Van Dam, O. (2004): Modelling incoming potential radiation on a land surface with PCRaster. From retired internet-Site (05.2005), http://www.geog.uu.nl/fg/ovandam/potrad.htm.

Van Deursen, W.P.A. (1995): Geographical Information Systems and Dynamic Models development and application of a prototype spatial modelling language. Ph.D. thesis, Faculty of Spatial Sciences, University of Utrecht the Netherlands.

Verbunt, M.; Gurtz, J.; Jasper, K.; Lang, H.; Warnerdam, P.; Zappa, M. (2003): The hydrological role of snow and glaciers in alpine river basins and their distributed modeling. Journal of Hydrology 282, 36-55.

Viessmann, W.; Lewis, G. L. (1996): Introduction to hydrology. 4th edition. HarperCollins, New York.

Watanabe, T.; Shiraiwa, T.; Ono, Y. (1989): distribution of periglacial landforms in the Langtang Valley, Nepal Himalaya. Bulletin of Glacier Research 7, 209-220.

Weber, M. (1997): Aspekte zur Extrapolation von Tagesmittelwerten von Temperatur und täglichen Niederschlagssummen an hochgelegenen Gebirgsstationen aus Klimadaten des örtlichen Klimamessnetzes in Nepal. Internal report Bavarian Academy of Sciences, Commission of Glaciology, Munich.

Weber, M. (2004): Mikrometeorologische Prozesse bei der Ablation eines Alpengletschers. PhD-Thesis at the Institut of Meteorology and Geophysics University of Insbruck, Austria.

Wissmeier, L. (2005): Implementation of distributed solute transport into the catchment model TAC^d and event based simulations using oxygen-18. Diploma thesis at the Institute of Hydrology, Albert-Ludwigs-University Freiburg, Germany, (unpublished).

Yamada, T.; Shiraiwa, T.; Iida, H.; Kadota, T.; Watanabe, T.; Rana, B.; Ageta, Y.; Fushimi, H. (1992): Fluctuations of the glaciers from 1970s to 1989 in the Khumbu, Shorong and Langtang regions, Nepal Himalayas. Bulletin of Glacier Research 10, 11-19.

Yamane, T. (1964): Statistics – An Introductory Analysis. Harper & Row, New York.

Zappa, M.; Pos, F.; Strasser, U.; Warmerdam, P.; Gurtz, J. (2003): Seasonal water balance of an alpine catchment as evaluated by different methods for spatial distributed snowmelt modeling. Nordic Hydrology 34 (3), 179-202.

Zingg, Th. (1951): Beziehung zwischen Temperatur und Schmelzwasser und ihre Bedeutung für Niederschlags- und Abflussfragen. IAHS Publication No. 32, 266-269.

Appendix

Table A1: Missing data at the SGHU station in the Langtang Khola catchment

Hydrological year	Air temperature	Precipitation	Stage (waterlevel)
1987/88	Oct.: 14 days	Nov.: 30 days	Oct.: 2 days
	Nov.: 30 days		Nov.: 1 day
	Dec.: 7 days		Dec.: 2 days
	Jan.: 2 days		Mar.: 8 days
	Mar.: 2 days		May: 1 day
	Jun.: 2 days		Jun.: 1 day
	Jul.: 2 days		Jul.: 1 day
	Aug.: 1 day		Aug.: 1 day
			Sep.: 1 day
Sum	**60 days**	**30 days**	**18 days**
1988/89	Jan.: 1 day	0 days	Oct.: 7 days
	Mar.: 1 day		Nov.: 1 day
	Apr.: 2 days		Dec.: 2 days
			Jan.: 13 days
			Feb.: 8 days
			Mar.: 1 day
			Apr.: 17 day
			Jun.: 13 day
			Jul.: 6 days
			Aug.: 7 days
			Sep.: 5 days
Sum	**4 days**	**0 days**	**80 days**
1989/90	0 days	Dec.: 31 days	Oct.: 3 days
		Jul.: 30 days	Nov.: 8 day
			Dec.: 5 days
			Jan.: 17 days
			Jul.: 7 days
Sum	**0 days**	**61 days**	**40 days**
1990/91	Jan.: 2 day	Jan.: 31 days	Nov.: 1 day
		Feb.: 28 days	Dec.: 2 days
		Mar.: 30 days	Apr.: 5 days
		Jun.: 3 days	May: 12 days
		Aug.: 3 days	Jun.: 6 days
		Sep.: 27 days	Jul.: 5 days
			Aug.: 4 days
			Sep.: 26 days
Sum	**2 day**	**122 days**	**61 days**
1991/92	Dec.: 21 days	Oct.: 2 days	Oct.: 3 days
		Nov.: 1 day	Nov.: 5 days
		Jul.: 2 days	Dec.: 7 days
		Aug.: 1 day	Jan.: 10 days
			Feb.: 6 days
Sum	**21 days**	**6 days**	**31 days**
1992/93	0 days	Sep.: 1 day	Jan.: 3 days
			Feb.: 1 day
			Mar.: 2 days
			Apr.: 2 days
			May: 4 days

			Jun.: 1 days
			Jul.: 3 days
			Sep.: 7 days
Sum	**0 days**	**1 day**	**23 days**
1993/94	0 days	Feb.: 1 day	Oct.: 7 days
		Jul.: 28 days	Feb.: 3 days
		Aug.: 1 day	Apr.: 2 days
			Jun.: 1 day
			Jul.: 3 days
Sum	**0 days**	**30 days**	**16 days**
1994/95	0 days	Oct.: 31 days	Feb.: 1 day
		Nov.: 30 days	Mar.: 1 day
		Dec.: 31 days	Apr.: 1 day
Sum	**0 days**	**92 days**	**3 days**
1995/96	Feb.: 1 day	0 days	Feb.: 2 days
			Apr.: 1 day
			Jun.: 6 days
			Jul.: 3 days
			Aug.: 6 days
			Sep.: 2 days
Sum	**1 day**	**0 days**	**20 days**
1996/97	Sep.: 3 days	0 days	Oct.: 4 days
			Nov.: 1 day
			Jan.: 2 days
			Feb.: 6 days
			Mar.: 3 days
			Apr.: 4 days
			May: 3 day
			Jun.: 6 days
			Jul.: 1 day
			Aug.: 2 days
			Sep.: 2 days
Sum	**3 days**	**0 days**	**34 days**
1997/98	Jan.: 1 day	Feb.: 1 day	Oct.: 5 days
	Aug.: 3 days		Nov.: 2 days
			Dec.: 21 days
			Jan.: 2 days
			Feb.: 1 day
			Mar.: 8 days
			Apr.: 2 days
			May: 13 days
			Jun.: 8 days
			Jul.: 2 days
			Aug.: 8 days
			Sep.: 4 days
Sum	**4 days**	**1 day**	**76 days**
1998/99	Dec.: 3 days	0 days	Jan.: 31 days
	May :4 days		Feb.: 28 days
	Jul.: 2 days		Mar.: 31 days
			Apr.: 30 days
			May: 31 days
			Jun.: 30 days
			Jul.: 31 days
			Aug.: 31 days
			Sep.: 30 days
			Oct.: 7 days

							Dec.:	1	day
Sum		**9**	**days**		**0**	**days**		**281**	**days**
1999/00	Oct.:	2	days	Feb.:	1	day	Jan.:	31	days
	Feb.:	1	day	Jul.:	5	days	Feb.:	28	days
	Jul.:	2	days				Mar.:	31	days
	Aug.:	1	day				Apr.:	30	days
							May:	31	days
							Jun.:	30	days
							Jul.:	31	days
							Aug.:	31	days
							Sep.:	30	days
							Oct.:	31	days
							Nov.:	30	days
							Dec.:	31	days
Sum		**6**	**days**		**6**	**days**		**365**	**days**

Table A2: Optimized parameter set of HBV-ETH model for the Langtang Khola catchment

Parameter	Description of parameter	Unit	Value
BETA	Empirical coefficient controlling the outflow from soil moisture	(-)	0.8
CMAX	Maximum of degree-day factor	(mm/°C day)	6.0
CMIN	Minimum of degree-day factor	(mm/°C day)	2.0
CPERC	Percolation capacity into lower zone	(mm/day)	1.5
CRFR	Coefficient of refreezing	(-)	0.05
CROUTE	Parameter of transformation function	(-)	1.0
CWH	Water holding capacity of snow	(-)	0.12
ETMAX	Maximum of potential evapotranspiration	(mm/day)	2.2
FC	Maximum soil moisture storage, field capacity	(mm)	50
K0	Storage coefficient of upper storage, fast component	(1/day)	0.2
K1	Storage coefficient of upper storage, medium component	(1/day)	0.08
K2	Storage coefficient of upper storage, slow component	(1/day)	0.005
LP	Limit of potential evapotranspiration	(mm)	30
LUZ	Limit of upper storage	(mm)	80
PGRAD	Vertical precipitation gradient	(%/100 m)	4.0
RCF	Precipitation correction factor for rain	(-)	0.7
REXP	Increasing of snow-, icemelt depending on orientation of the slope	(-)	1.2
RMULT	Multiplicative factor to account for accelerated melt over ice as compared to snow	(-)	1.3
SCF	Snowfall correction factor	(-)	1.24
T0	Threshold value of temperature for snowfall also general temperature correction	(°C)	0.0
TGRAD	Vertical temperature gradient	(°C/100 m)	-0.5

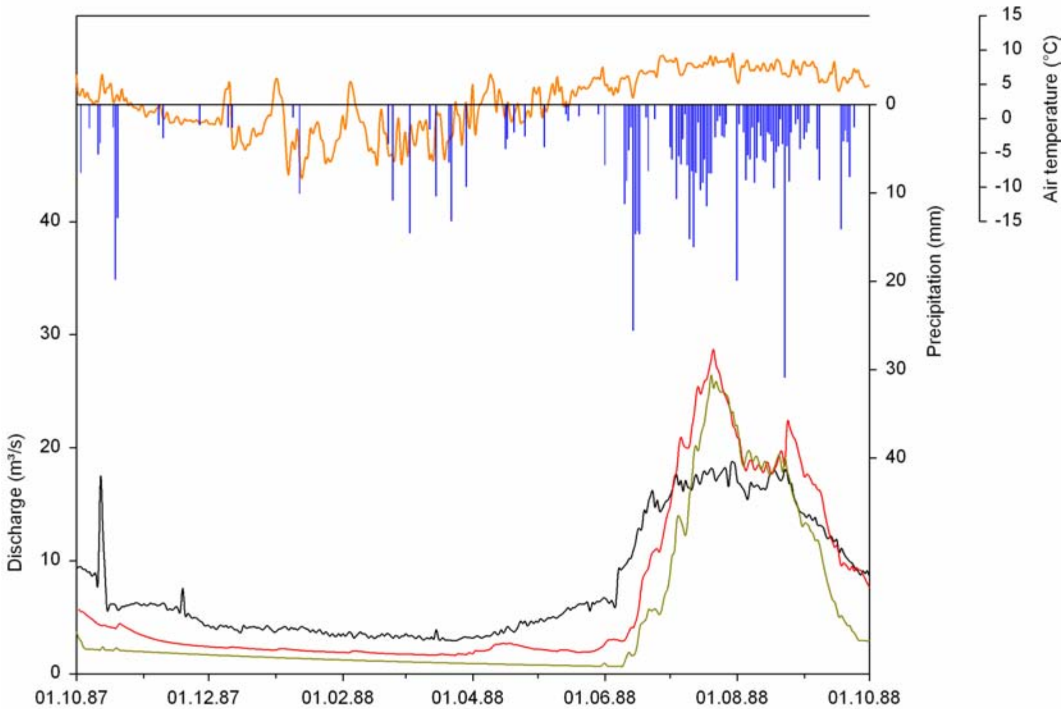

Discharge (m³/s)
Precipitation (mm)
Air temperature (°C)
01.10.87
01.12.87
01.02.88
01.04.88
01.06.88
01.08.88
01.10.88

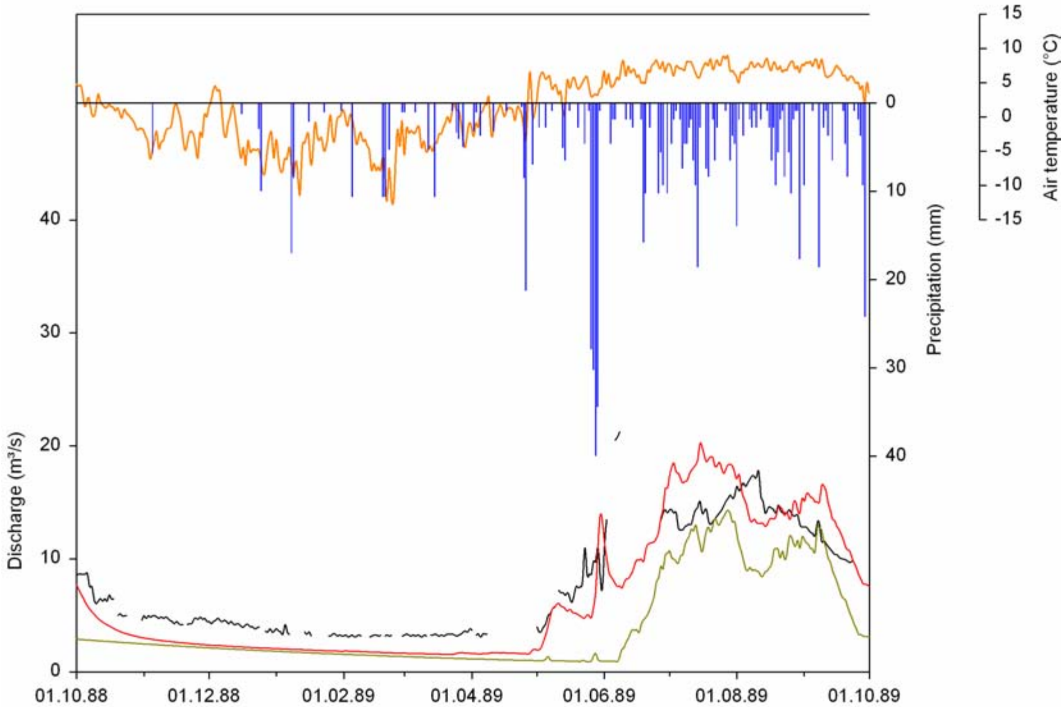

Discharge (m³/s)
Precipitation (mm)
Air temperature (°C)
01.10.88
01.12.88
01.02.89
01.04.89
01.06.89
01.08.89
01.10.89

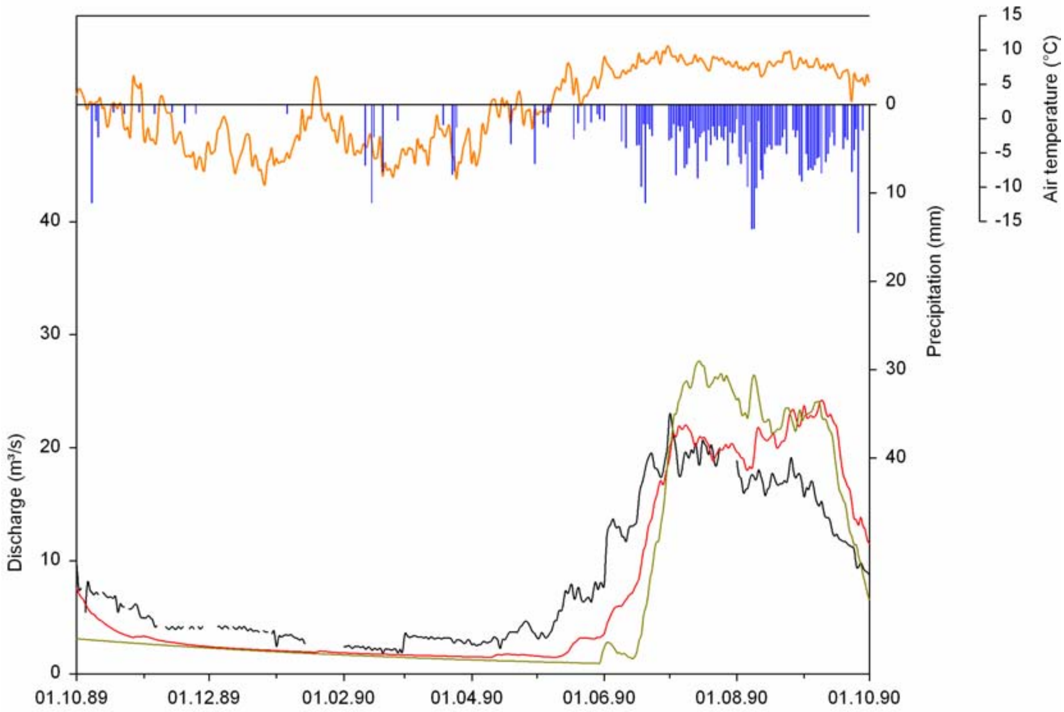
15
10
5
0
-5
-10
-15
Air temperature (°C)
0
10
20
30
40
Precipitation (mm)
0
10
20
30
40
Discharge (m³/s)
01.10.89
01.12.89
01.02.90
01.04.90
01.06.90
01.08.90
01.10.90

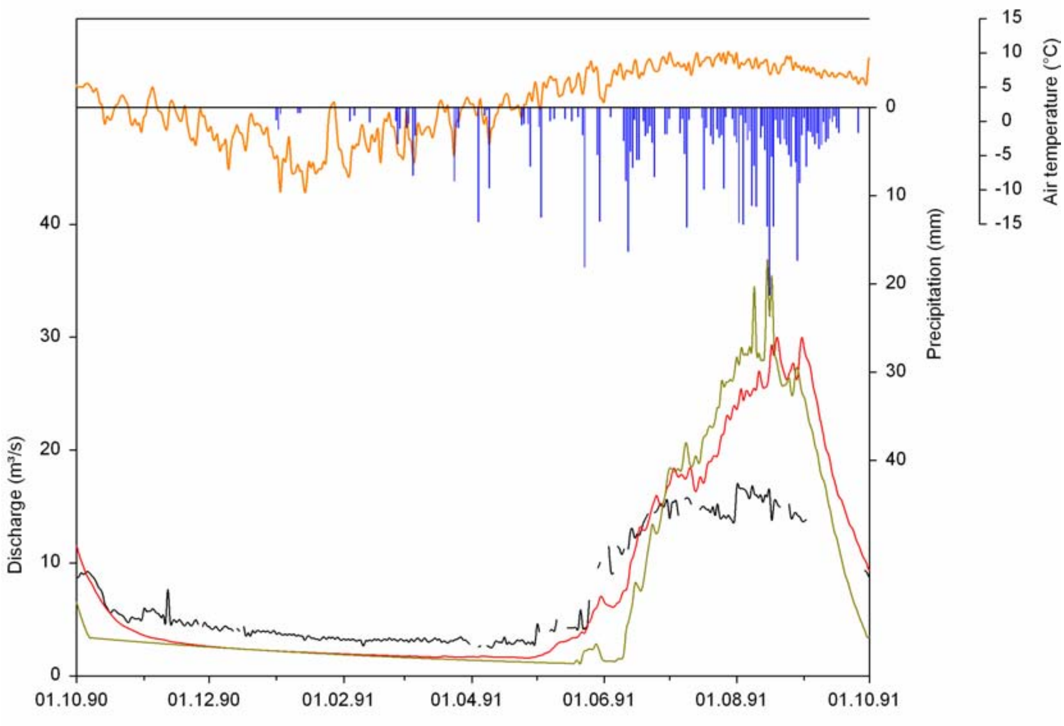
15
10
5
0
-5
-10
-15
Air temperature (°C)
0
10
20
30
40
Precipitation (mm)
0
10
20
30
40
Discharge (m³/s)
01.10.90
01.12.90
01.02.91
01.04.91
01.06.91
01.08.91
01.10.91

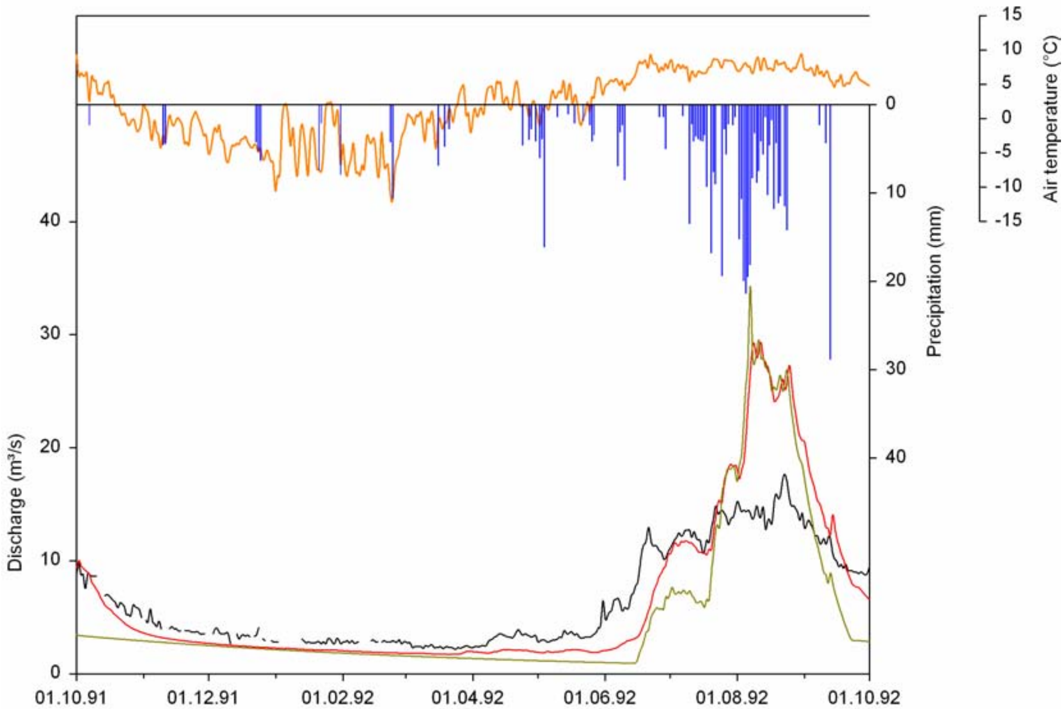
15
10
5
0
-5
-10
-15
Air temperature (°C)
0
10
20
30
40
Precipitation (mm)
40
30
20
10
0
Discharge (m³/s)
01.10.91
01.12.91
01.02.92
01.04.92
01.06.92
01.08.92
01.10.92

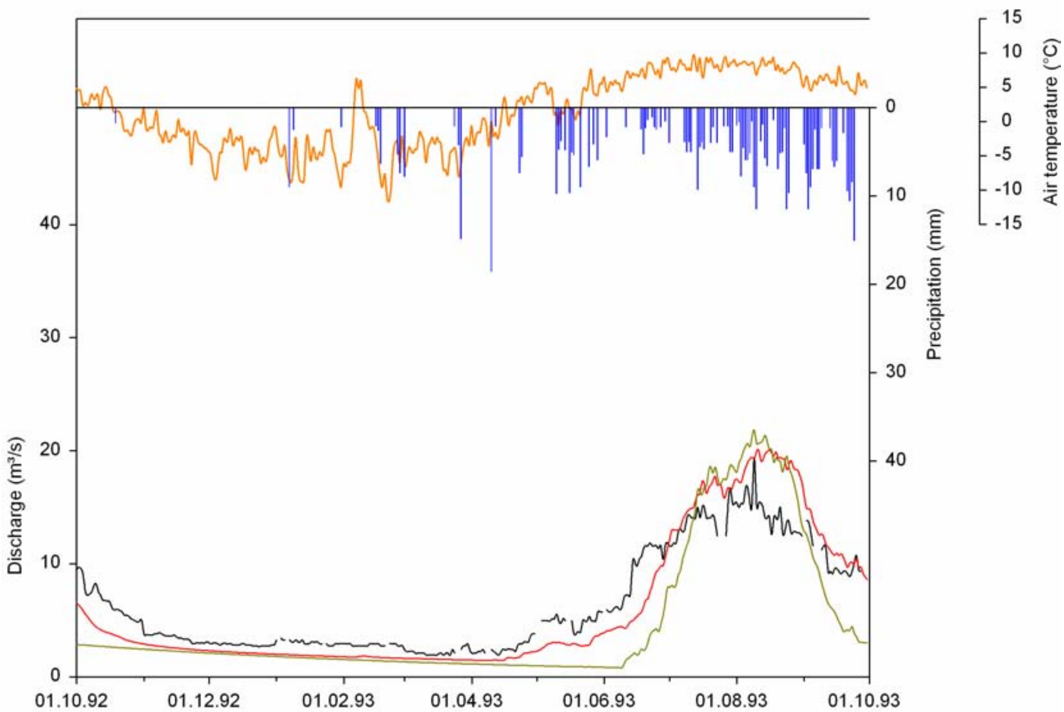
15
10
5
0
-5
-10
-15
Air temperature (°C)
0
10
20
30
40
Precipitation (mm)
40
30
20
10
0
Discharge (m³/s)
01.10.92
01.12.92
01.02.93
01.04.93
01.06.93
01.08.93
01.10.93

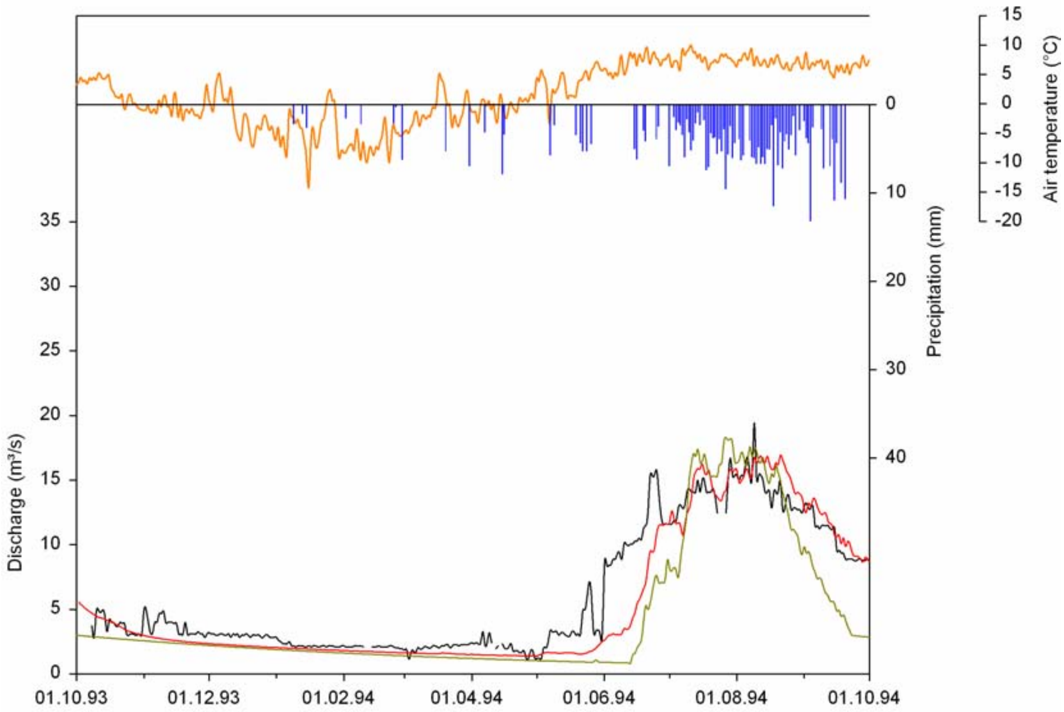

15
10
5
0
-5
-10
-15
-20
Air temperature (°C)
0
10
20
30
40
Precipitation (mm)
35
30
25
20
15
10
5
0
Discharge (m³/s)
01.10.93
01.12.93
01.02.94
01.04.94
01.06.94
01.08.94
01.10.94

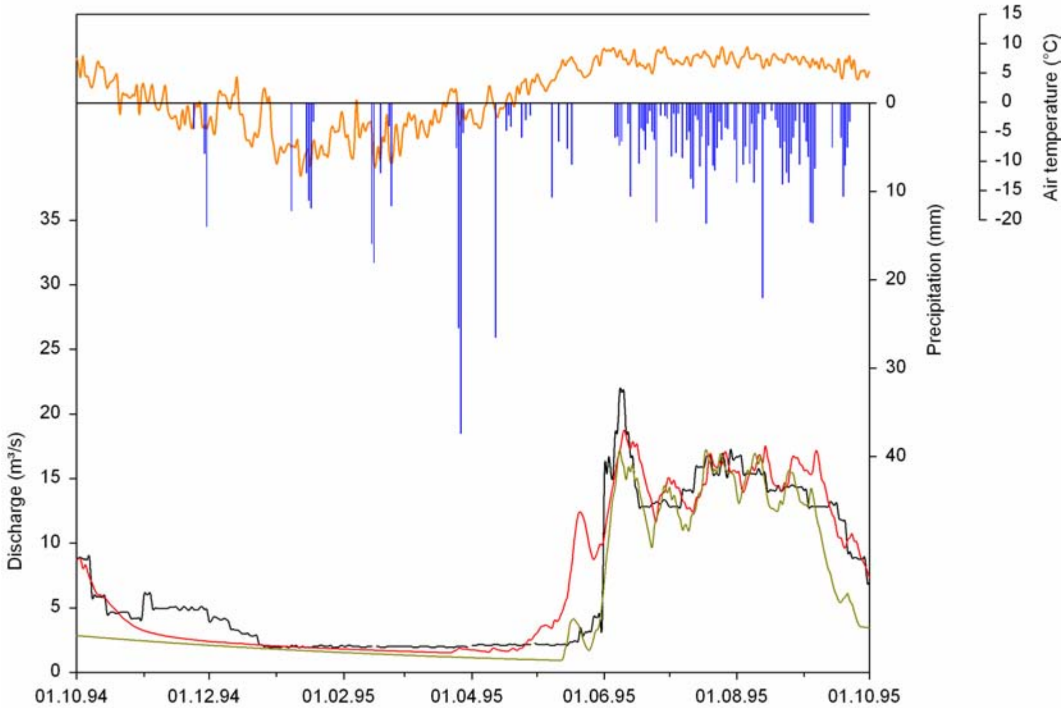

15
10
5
0
-5
-10
-15
-20
Air temperature (°C)
0
10
20
30
40
Precipitation (mm)
35
30
25
20
15
10
5
0
Discharge (m³/s)
01.10.94
01.12.94
01.02.95
01.04.95
01.06.95
01.08.95
01.10.95

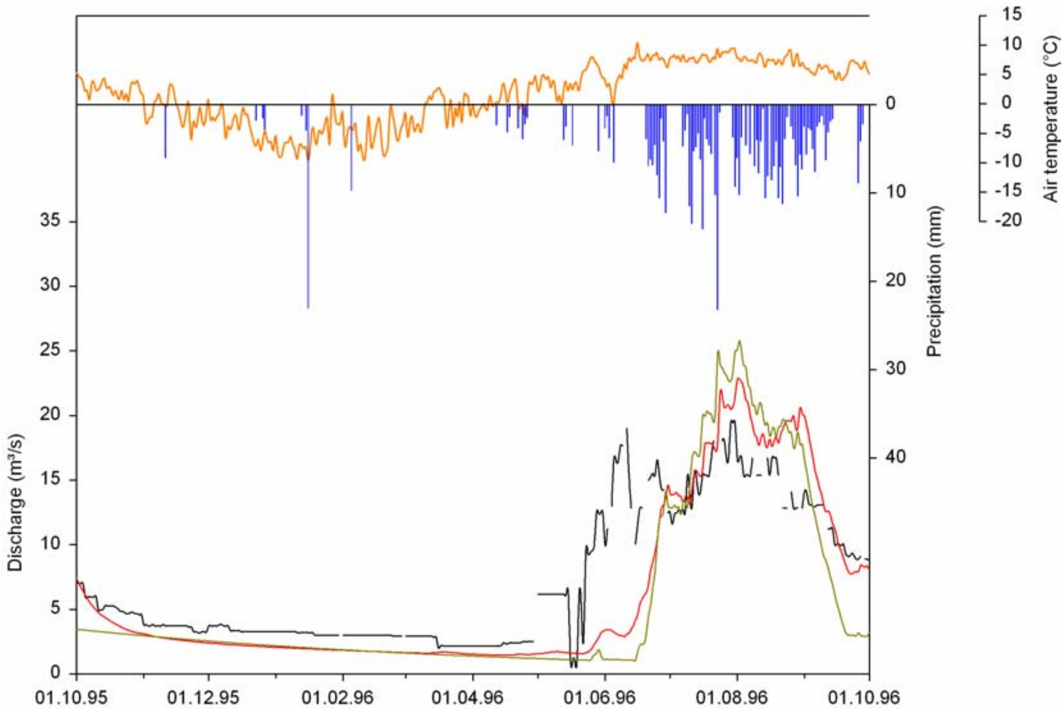

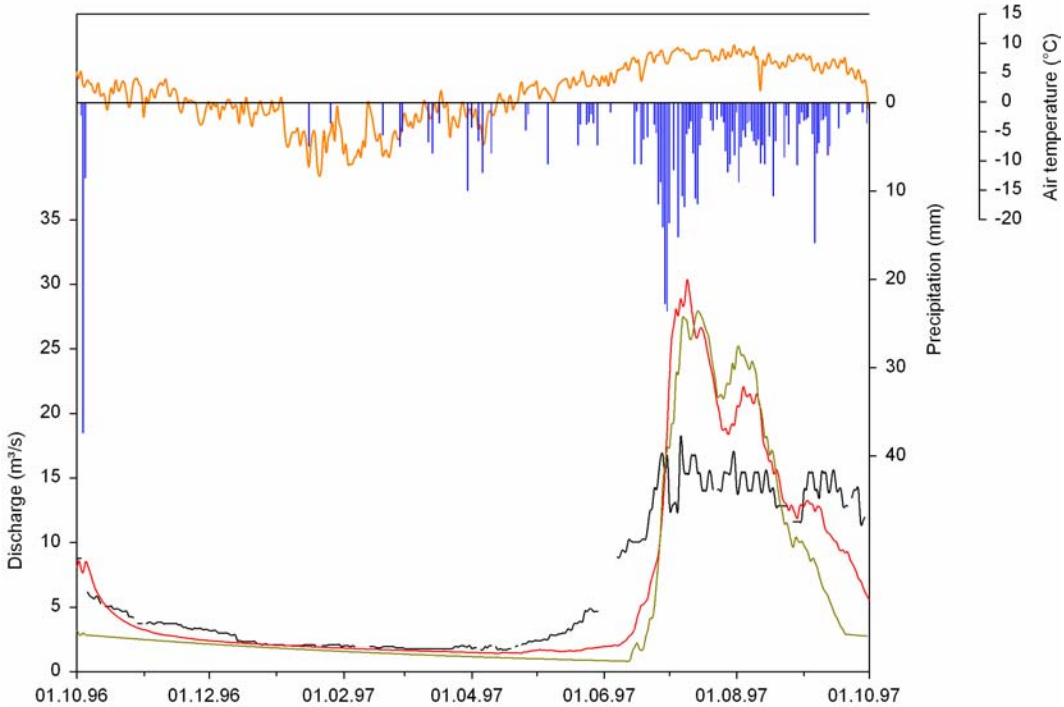

Figure A1: Comparison of measured (black) and simulated discharge (red: TAC^d; green: HBV-ETH) with measured air temperature (orange) at the SGHU station and calculated basin precipitation (blue), 1987-1997

Ehrenwörtliche Erklärung

Hiermit erkläre ich, dass diese Arbeit selbstständig und nur unter Verwendung der angegebenen Hilfsmittel angefertigt wurde.

Freiburg i. Br., Juli 2005